The structure and innervation of sheep extraocular muscles

Harker, D. W.

THE STRUCTURE AND INNERVATION OF SHEEP EXTRAOCULAR MUSCLES.

VOL. II. PLATES.

A thesis presented in candidature for the degree of

Doctor of Philosophy

by

D. W. Harker, B.Sc. (Dunelm),

Department of Zoology, University of Durham.

Durham, October 1974

Figure 1. A dissection of the left orbit of the sheep showing the superior rectus (SR) and levator palpebrae superioris (LP) muscles in situ.

The eyeball has been rotated anteriorly and slightly ventrally and secured with a loop of thread. The zygomatic arch and part of the frontal bone have been removed to enable easier access to the rear of the eyeball. The SR muscle forms a thin, wide sheet of muscle near its tendinous insertion onto the eyeball. The thin, narrow LP muscle overlies the medial edge of SR as it travels anteriorly to insert on the upper eyelid.

1

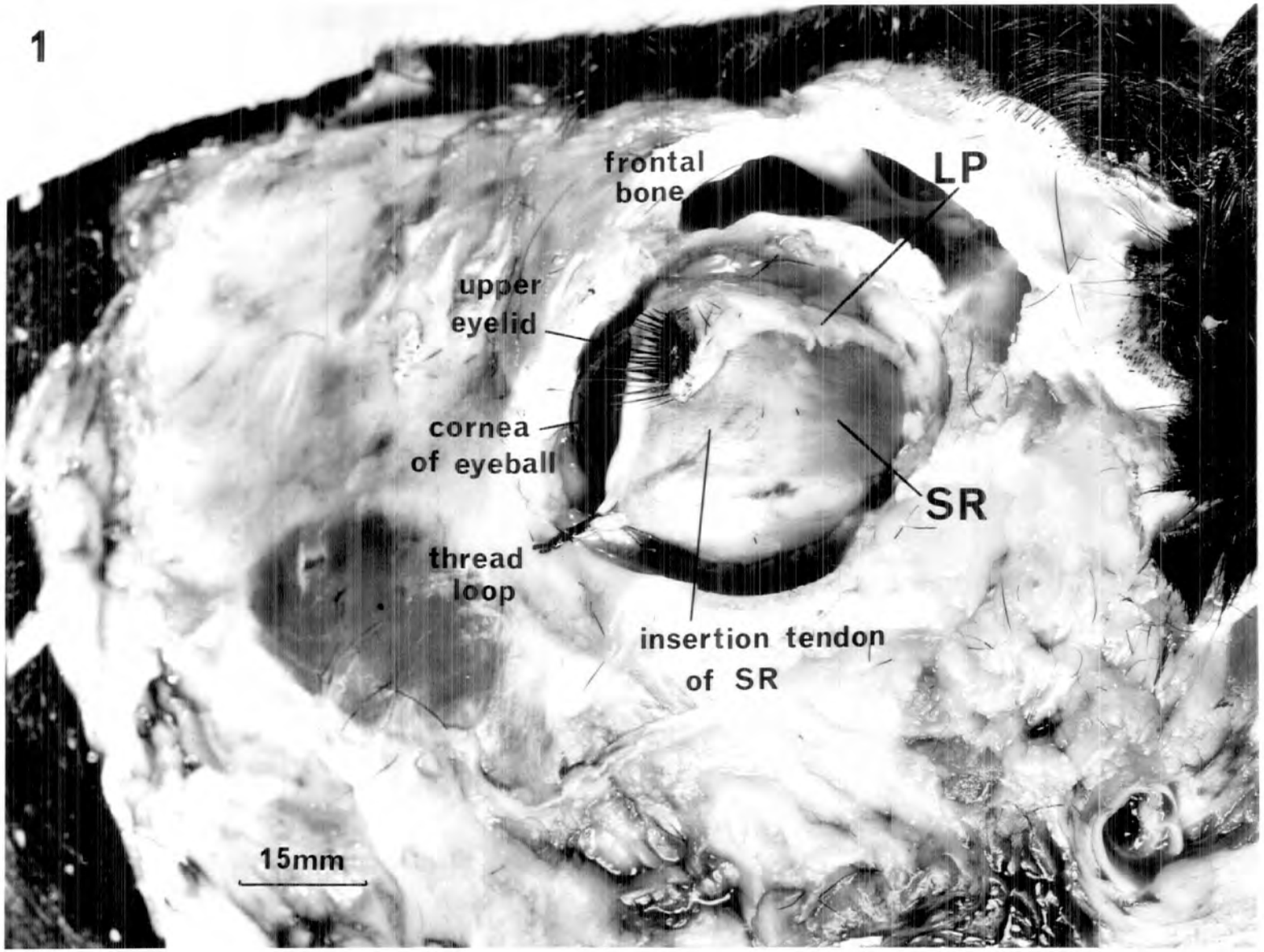
frontal bone
LP
upper eyelid
cornea of eyeball
SR
thread loop
insertion tendon of SR
15mm

Figure 2. A dissection of the left hind foot of the sheep showing the distal portion of peroneus brevis (PB) muscle in situ.

The muscle has been cut through at the hock joint and pinned in place. The unipennate manner of insertion of PB onto the double tendon of the long extensor (Long. ext.) and the medial extensor (Med. ext.) muscles can be seen, together with the tendon of tibialis anterior (Tib. ant.).

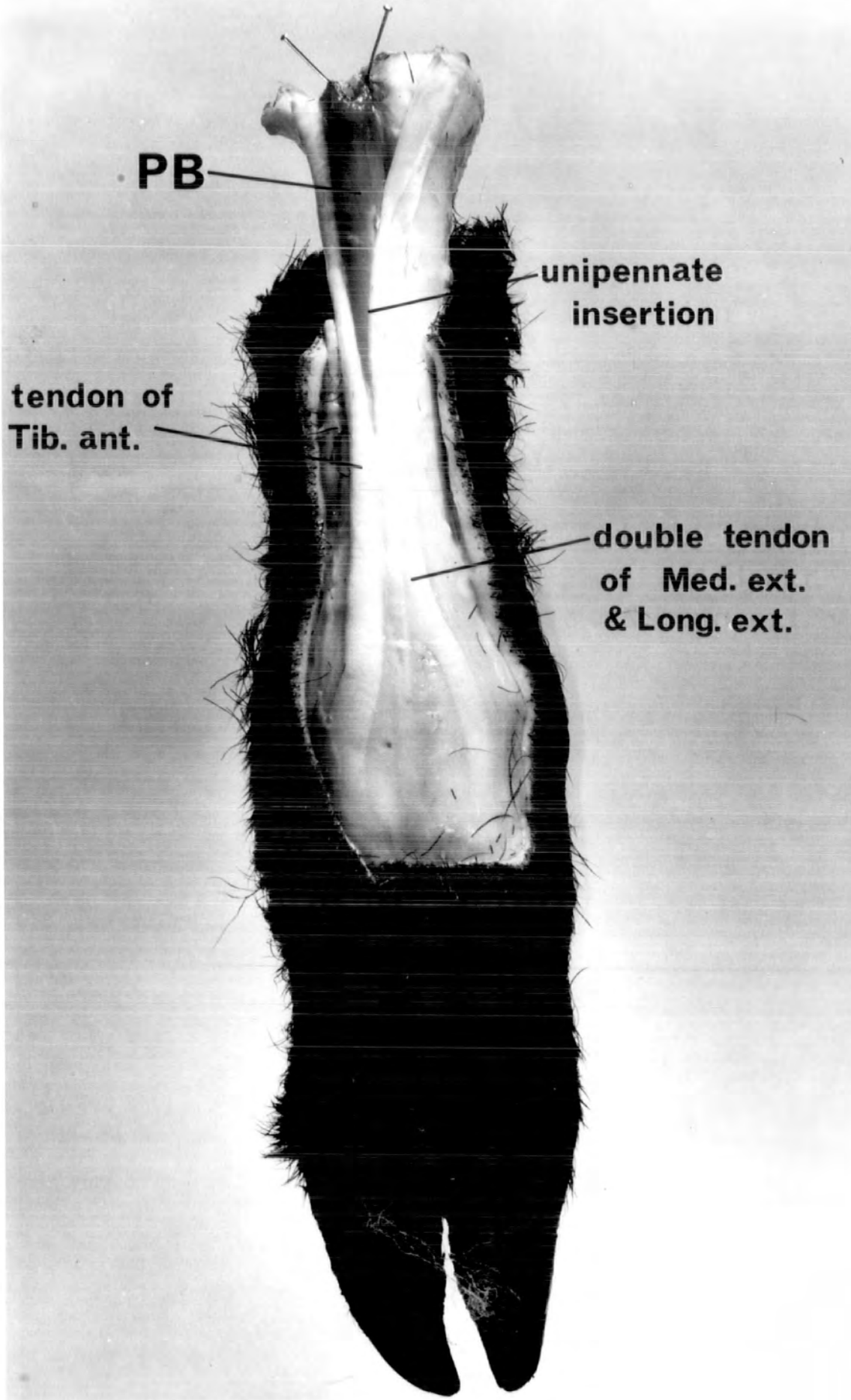
PB
unipennate
insertion
tendon of
Tib. ant.
double tendon
of Med. ext.
& Long. ext.

Figure 3. A schematic representation of the muscle-fibre layers throughout the length of SR.

On the left of the diagram a dorsal view of a right superior rectus muscle shows the entry and major sub-divisions of the branch of the oculomotor nerve. Drawings of transverse sections cut at various points along the muscle are on the right of the figure, with the layered organization indicated. The drawings are based on figs. 4 - 7 & 9 - 11, which show skip-serial transverse sections stained to demonstrate phosphorylase activity.

3

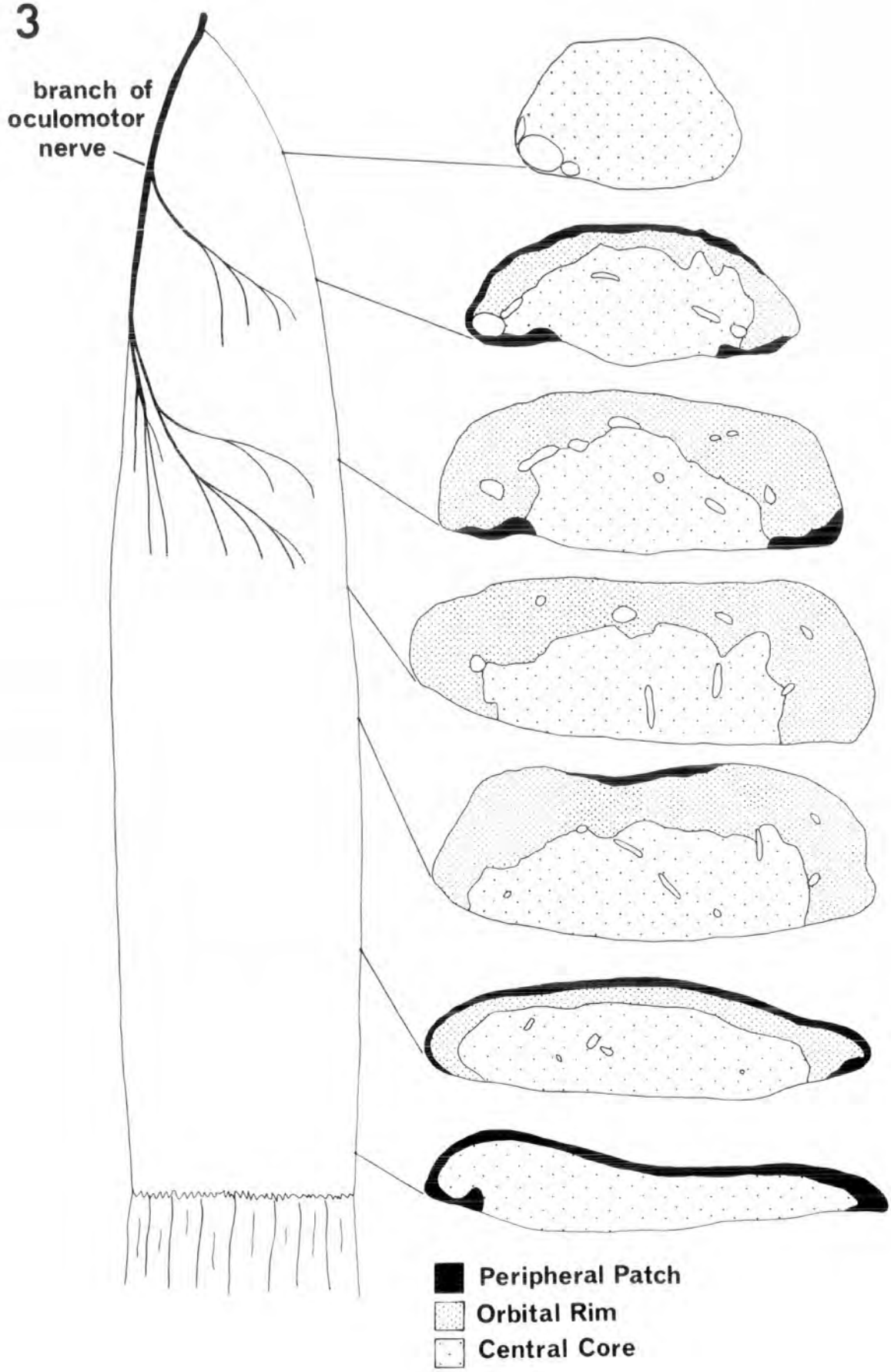
branch of
oculomotor
nerve
Peripheral Patch
Orbital Rim
Central Core

Figures 4 to 11. The layer organization of SR.

Transverse sections sampled at different points along SR to show variation in the distribution and thickness of the central core, orbital rim and peripheral patch layers. The sections sampled at 3.0 mm (fig. 4), 6.5 mm (fig. 5), 11.5 mm (fig. 6), 15.0 mm (fig. 7), 18.5 mm (fig. 9), 25.0 mm (fig. 10) and 31.0 mm (fig. 11) from the origin end of one whole SR muscle have been stained to demonstrate phosphorylase activity.

Fig. 8 is a transverse section taken from the belly of another muscle stained to demonstrate acid-preincubated actomyosin ATPase activity.

Compare with figure 3. Note that the spindles (ringed) are peripherally arranged.

4

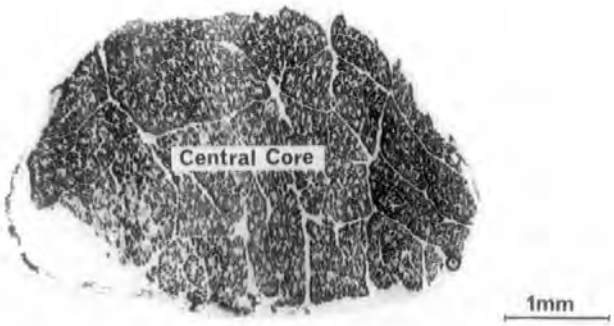
Central Core
1mm

5

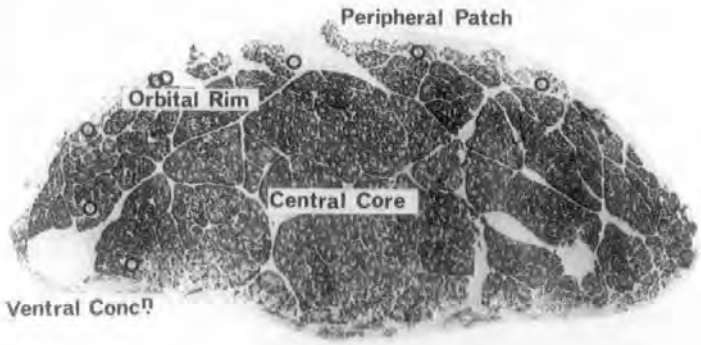
Peripheral Patch
Orbital Rim
Central Core
Ventral Conc^{n}

6

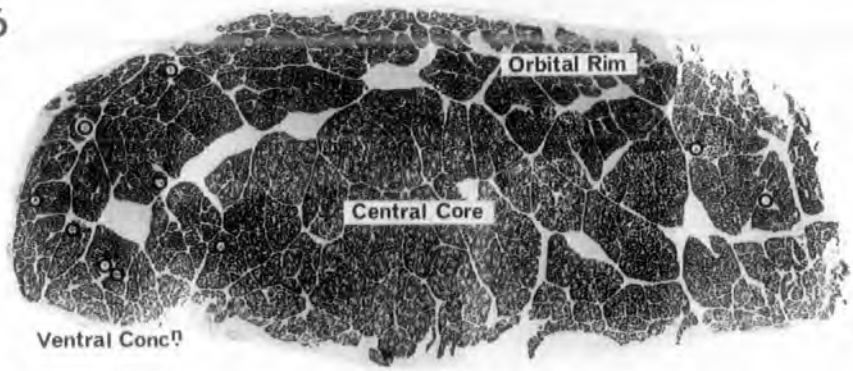
Orbital Rim
Central Core
Ventral Conc^{n}

7

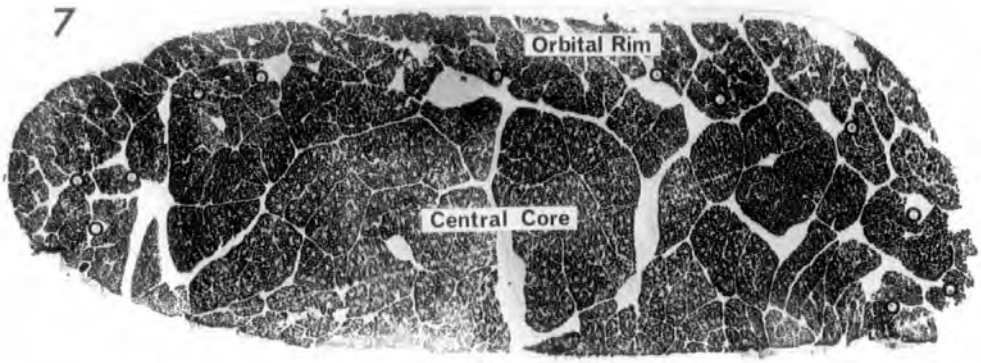
Orbital Rim
Central Core

8

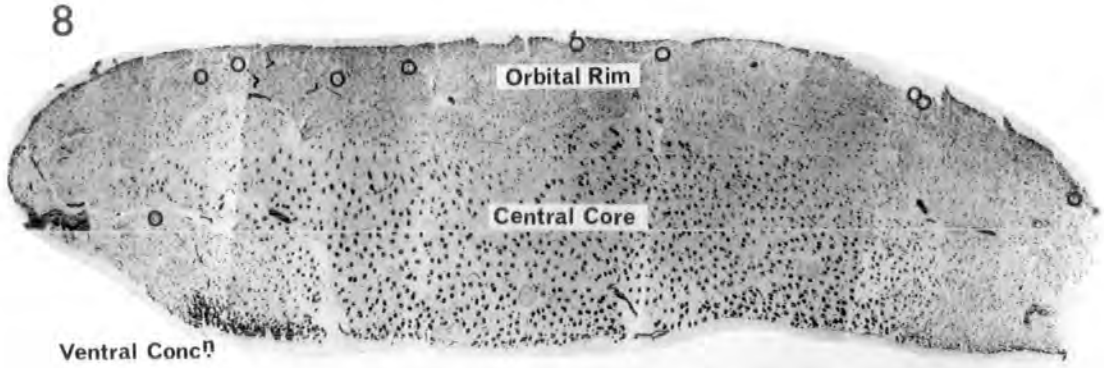
Orbital Rim
Central Core
Ventral Conc?

9

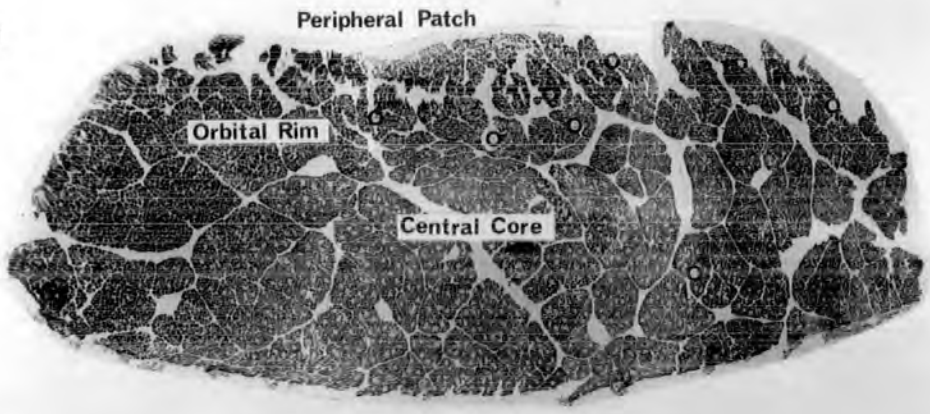
Peripheral Patch
Orbital Rim
Central Core

10


Orbital Rim
Peripheral Patch
Central Core

11

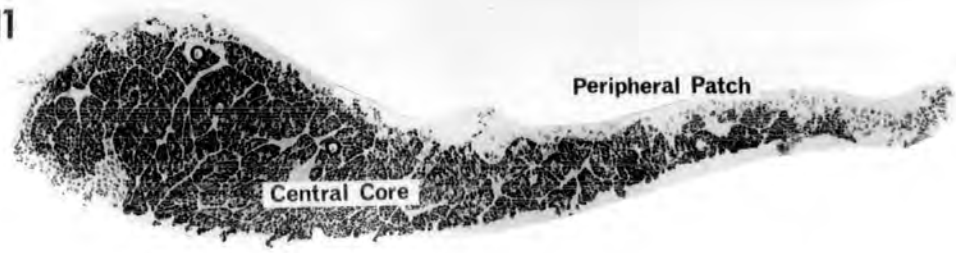
Peripheral Patch
Central Core

Figures 12 to 13. A comparison of the layer organization at the dorsal surface of SR in transverse sections taken from the insertion and belly portions.

Both sections have been stained to demonstrate phosphorylase activity. The dorsal surface of the muscle is at the top of the figure.

Fig. 12. At the insertion (31.0 mm from the origin) there are three distinct layers: a peripheral patch (PP); an orbital rim (OR); and a central core (CC).

Fig. 13. In the belly (15.0 mm from the origin) there are two layers: an orbital rim and a central core. At this particular level these two layers are not well-separated. Note the spindles (arrows) in the orbital rim layer, and also the parasite Sarcocystis in an extrafusal muscle fibre (asterisk).

For clarity, the layers in these two figures are separated by dotted lines. Both figures are the same magnification.

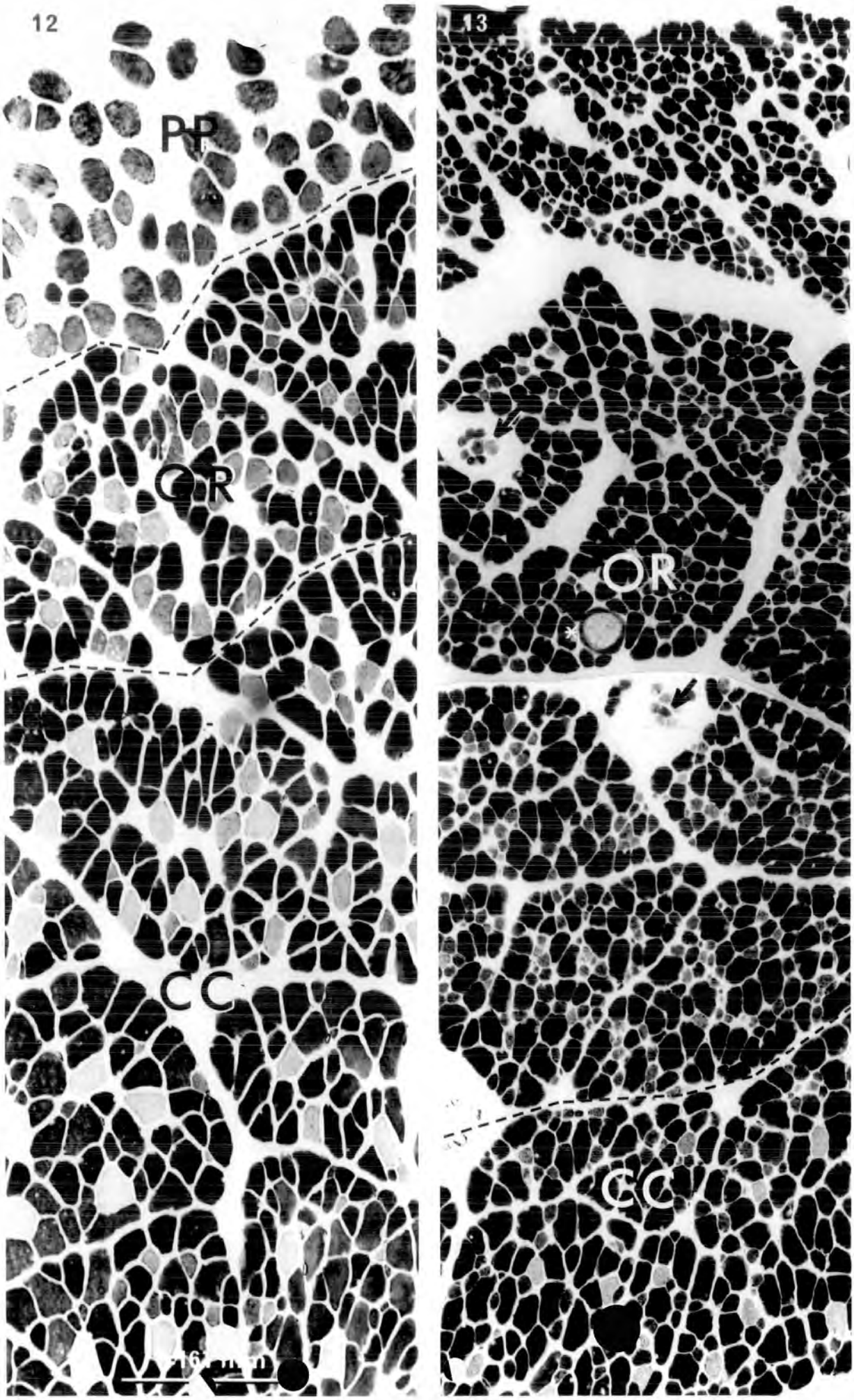
12
PP
OR
CC
13
OR
CC

Figures 14 to 17. Histochemical fibre types in the central core layer of SR.

Serial transverse sections of SR central core layer stained to demonstrate the following enzymes:

Fig. 14. Phosphorylase.

Fig. 15. Succinic dehydrogenase.

Fig. 16. Alkali-preincubated actomyosin ATPase.

Fig. 17. Acid-preincubated actomyosin ATPase.

The central core contains 7% large G (G), 45% large A (A) and 48% intermediate C (C) and small C (c) fibre types.

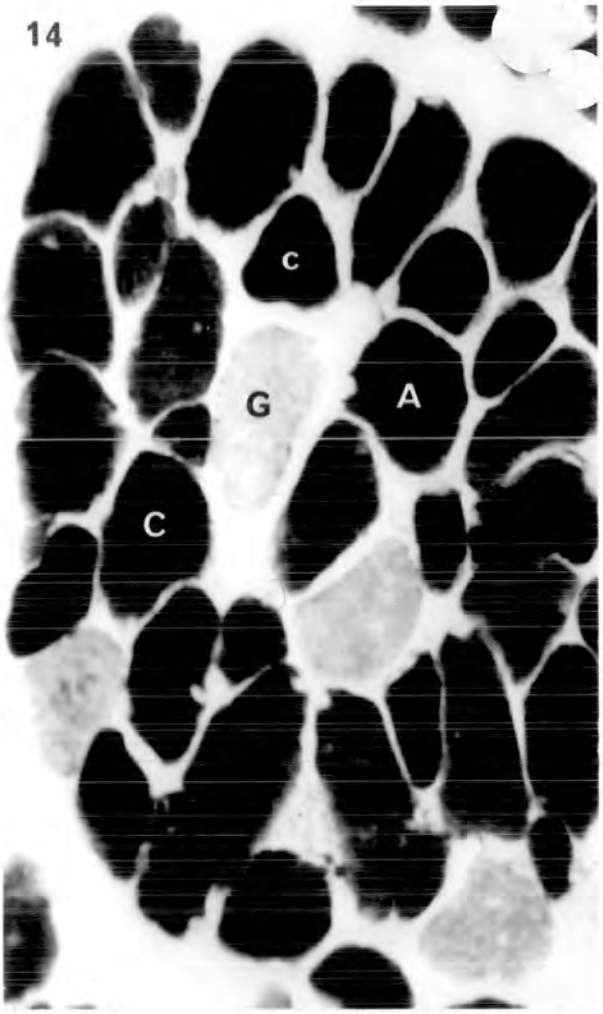
14
c
G
A
C


15
c
G
A
C

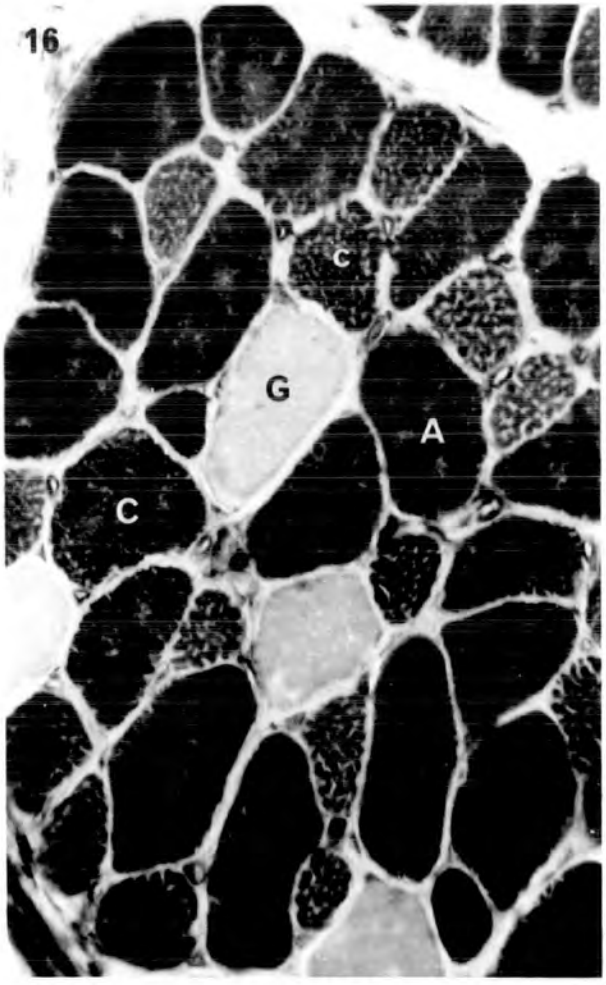
16
c
G
A
C

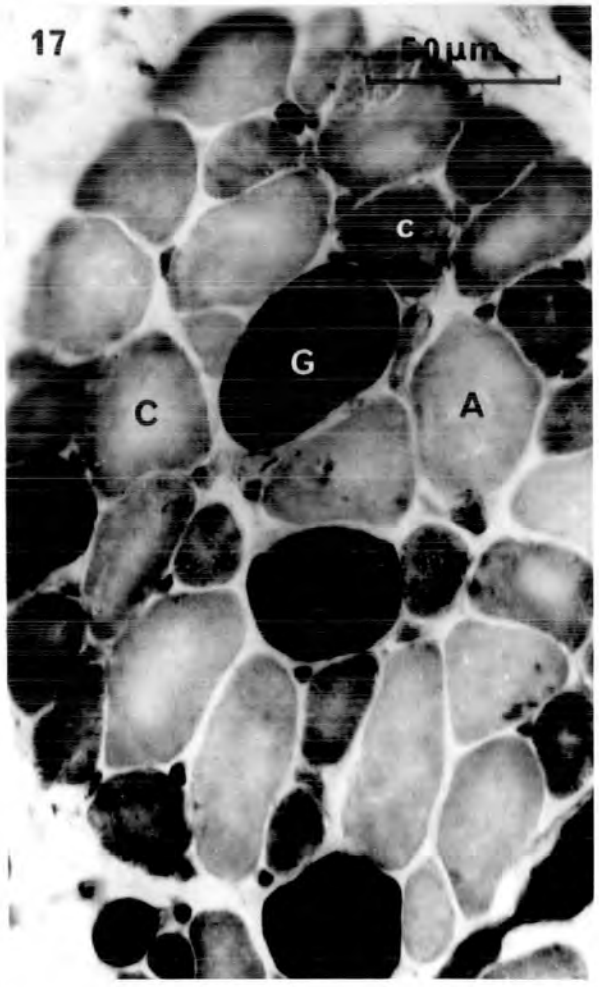
17
50µm
c
G
C
A

Figures 18 to 21. Histochemical fibre types in the orbital rim layer of SR.

A : Belly portion. Serial transverse sections of SR orbital rim layer stained to demonstrate the following:

Fig. 18. Phosphorylase. The small G fibres (arrowed) are relatively low.

Fig. 19. Succinic dehydrogenase. Note the generally higher level of activity of SDH in the orbital rim layer compared to that of the central core, and also the fibres of small-diameter (arrowed) that are relatively low in activity (small G fibres).

Fig. 20. Weigert & van Gieson histological stain. Compare with fig. 19.

Fig. 21. Acid-preincubated actomyosin ATPase. The small G fibres (arrowed) are intensely staining, as are the blood capillaries (star) that are relatively numerous in the orbital rim layer.

In the belly of SR the orbital rim layer contains three histochemical fibre types in roughly equal proportions: the intermediate C (C), small C (c) and small G (arrowed) fibre types.

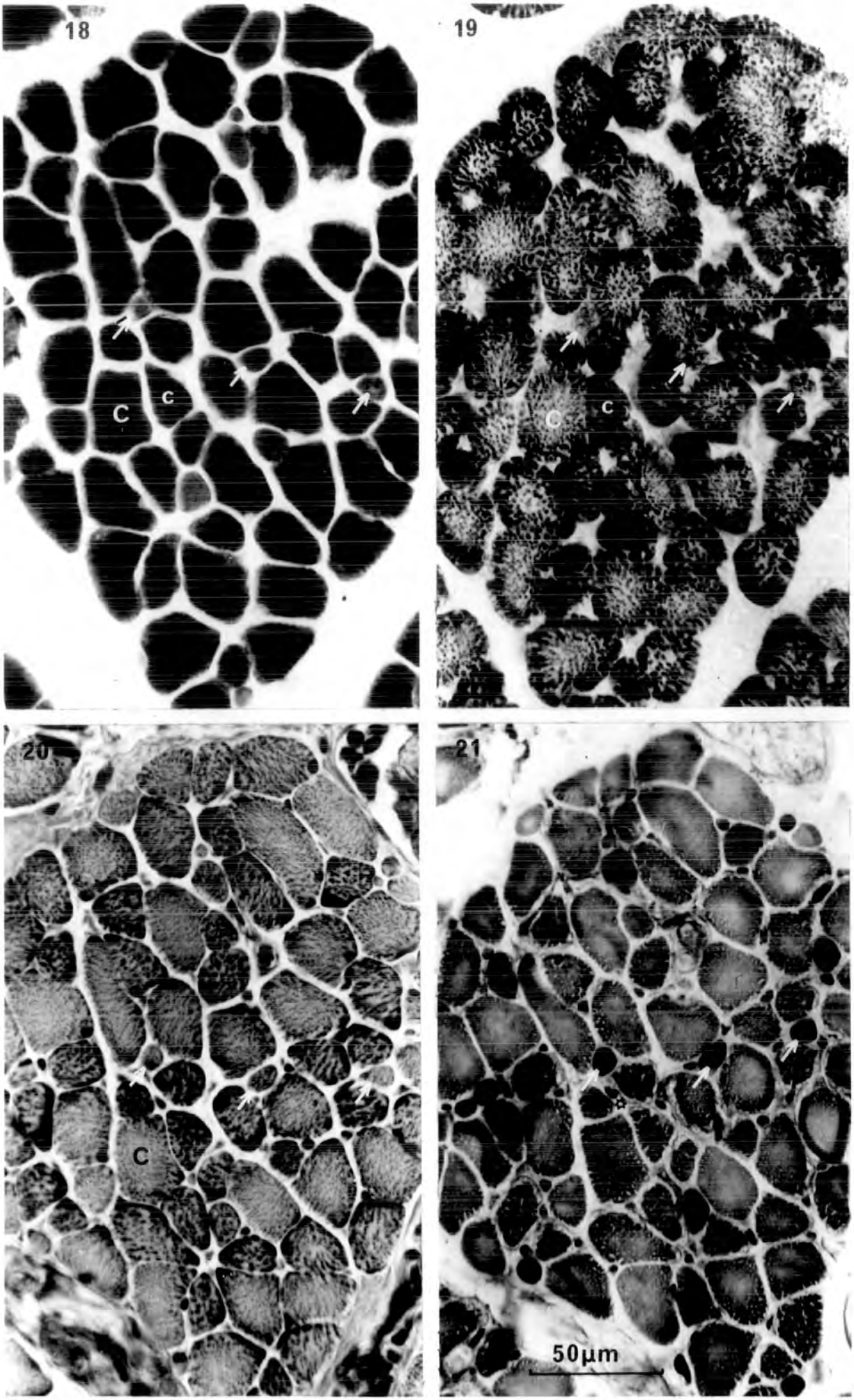
18
19
20
21
C
c
50µm

Figures 22 to 24. Histochemical fibre types in the orbital rim layer of SR.

B : Insertion portion. Serial transverse sections of SR orbital rim layer stained to demonstrate the following:

Fig. 22. Phosphorylase.

Fig. 23. Succinic dehydrogenase.

Fig. 24. Acid-preincubated actomyosin ATPase.

The small G (g) fibres appear larger in diameter than in the belly (figs. 18 - 21) region. In addition to intermediate C (C) and small C (c) fibres that are present in the belly region of the orbital rim, there are also medium to large-diameter type A fibres (A) that are relatively low for SDH activity.

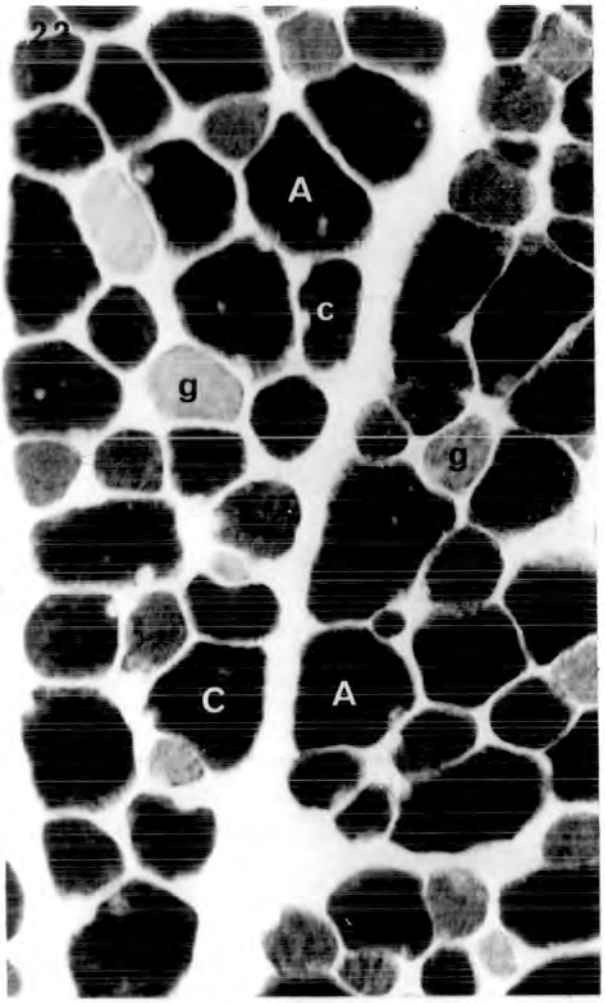
22
A
c
g
g
C
A

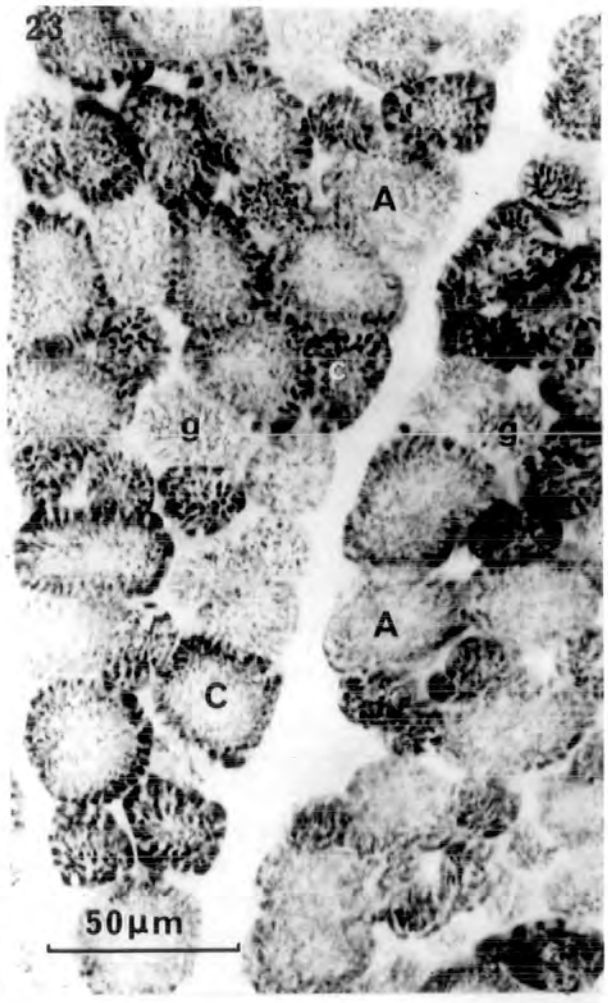
23
A
c
g
A
C
50µm

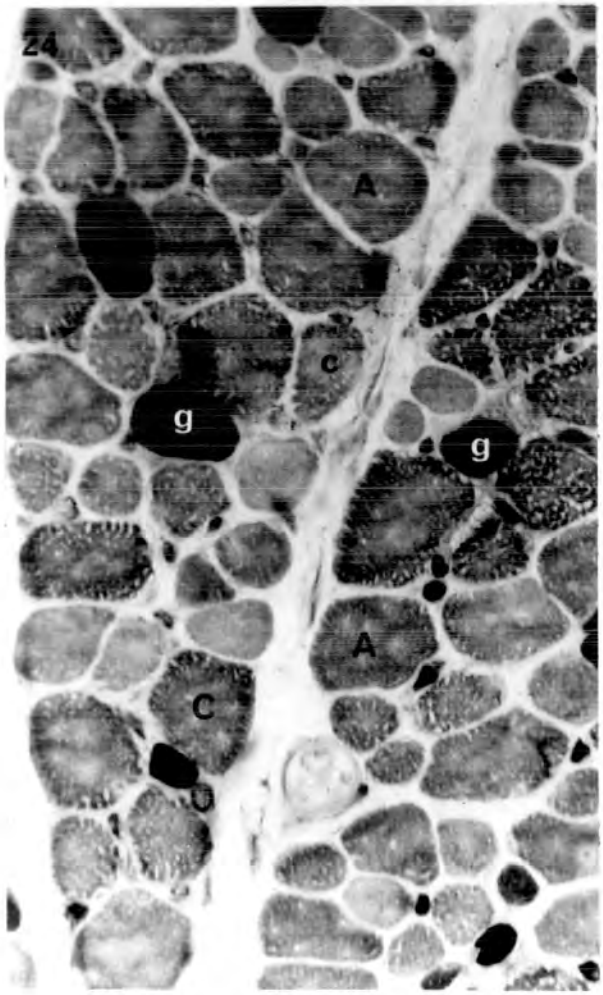
24
A
c
g
g
A
C

Figures 25 to 29. Histochemical fibre types in the peripheral patch layer of SR.

Figs. 25 - 29 show the peripheral patch layer (PP) and the adjacent orbital rim layer (OR) at the extreme insertion end of the muscle.

Figs. 25 - 28 are successive serial transverse sections stained to demonstrate the following:

Fig. 25. Weigert & van Gieson. Note the extensive connective tissue (c.t.) separating the peripheral patch muscle fibres.

Fig. 26. Alkali-preincubated actomyosin ATPase. Note that the blood capillaries (cap.) are intensely stained.

Fig. 27. Phosphorylase.

Fig. 28. Succinic dehydrogenase. Compared to the highly reactive C fibre types (C & c) of the orbital rim, the majority of peripheral patch fibres are relatively low in activity, and are equivalent in staining intensity to the A fibre types (A) in the orbital rim.

Fig. 29. A section in the same series stained to demonstrate Alkali-preincubated actomyosin ATPase. Compare the G fibre types of the peripheral patch (g) and orbital rim (g^1).

At the extreme insertion end of SR the peripheral patch is composed almost entirely of medium to large-diameter G fibres (g).

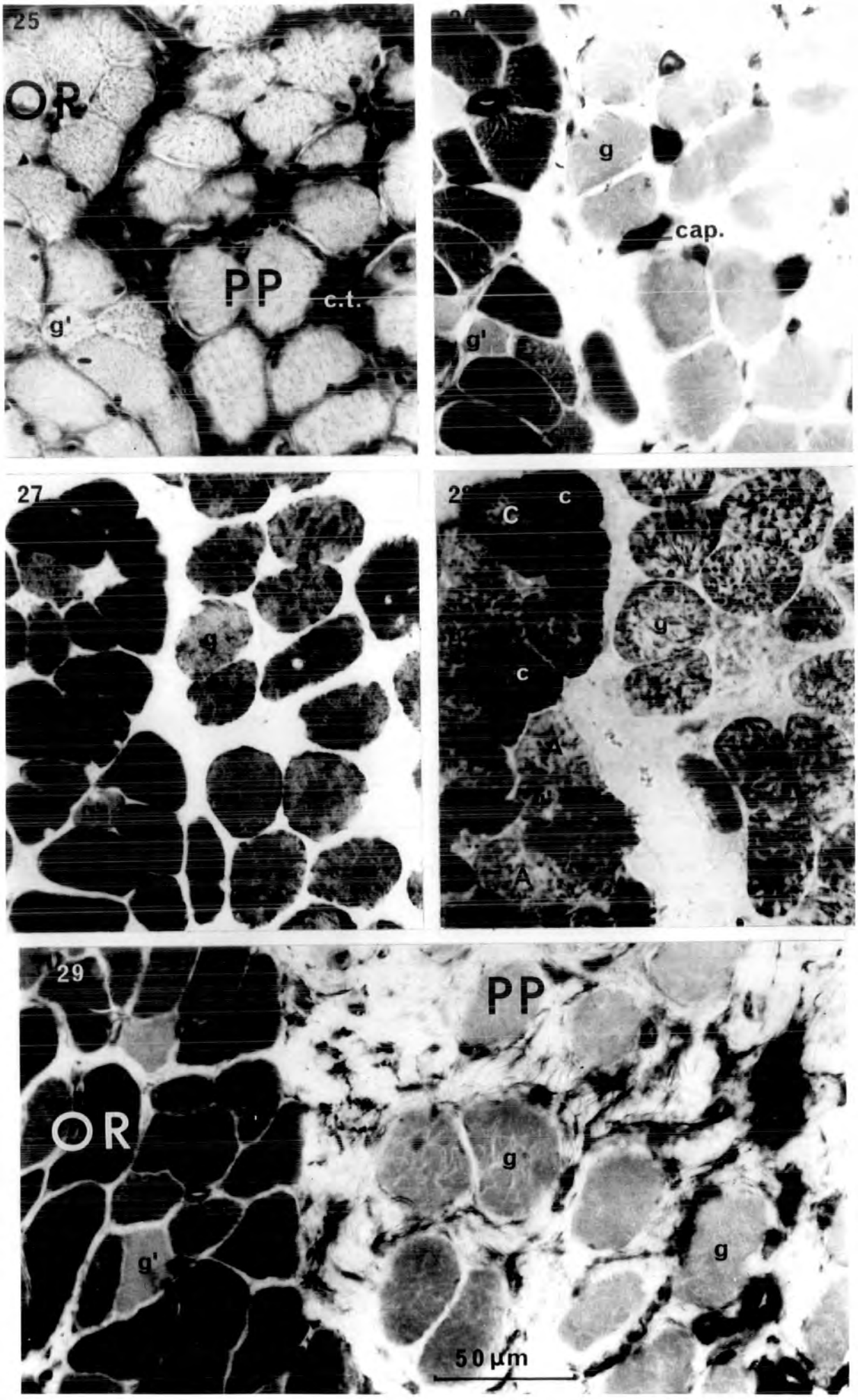
25
OR
PP
c.t.
g'
g
cap.
g'
27
g
C
c
c
g
A
A
29
PP
OR
g
g'
g
50 µm

Figures 30 to 33. Histochemical fibre types of the peripheral patch layer of SR: 'ventral concentrations'.

Figs. 30 - 33 are serial transverse sections illustrating the fibre composition of the peripheral patch 'ventral concentrations'. These are formed where the thin C-shaped peripheral patch rim wraps laterally round the central core layer to form areas that lie adjacent to the globe and which contain a high proportion of type G fibres.

Fig. 30. Phosphorylase.

Fig. 31. Succinic dehydrogenase.

Fig. 32. Acid-preincubated actomyosin ATPase. Note the high proportion of small-diameter fibres of high activity (type G fibres).

Fig. 33. Weigert & van Gieson. Note relatively abundant connective tissue (c.t.) separating the fibres.

The 'ventral concentrations' of the peripheral patch layers are composed of about 50% of small G fibres (g) and about 50% of type C fibres.

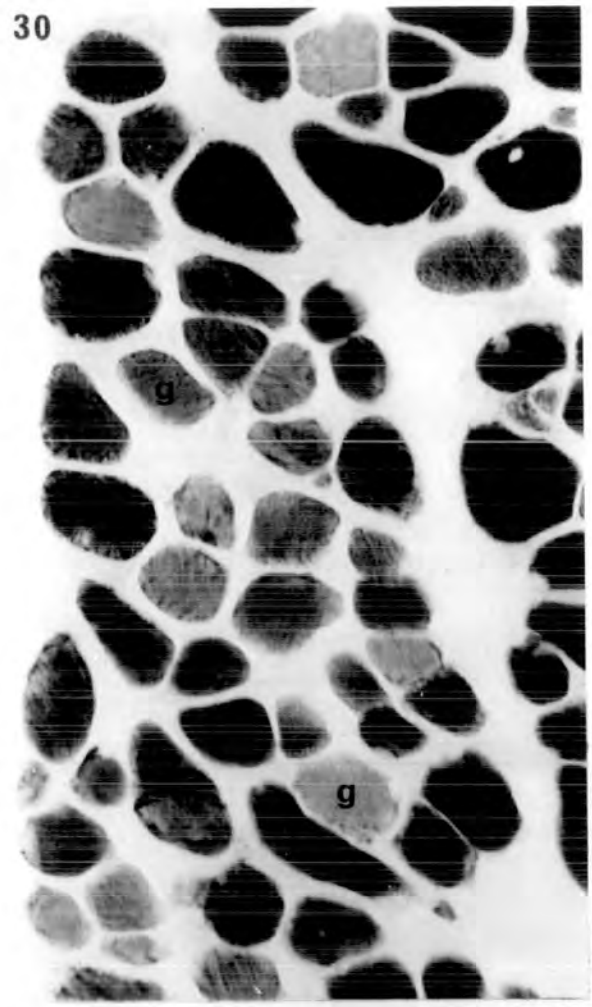
30
g
g

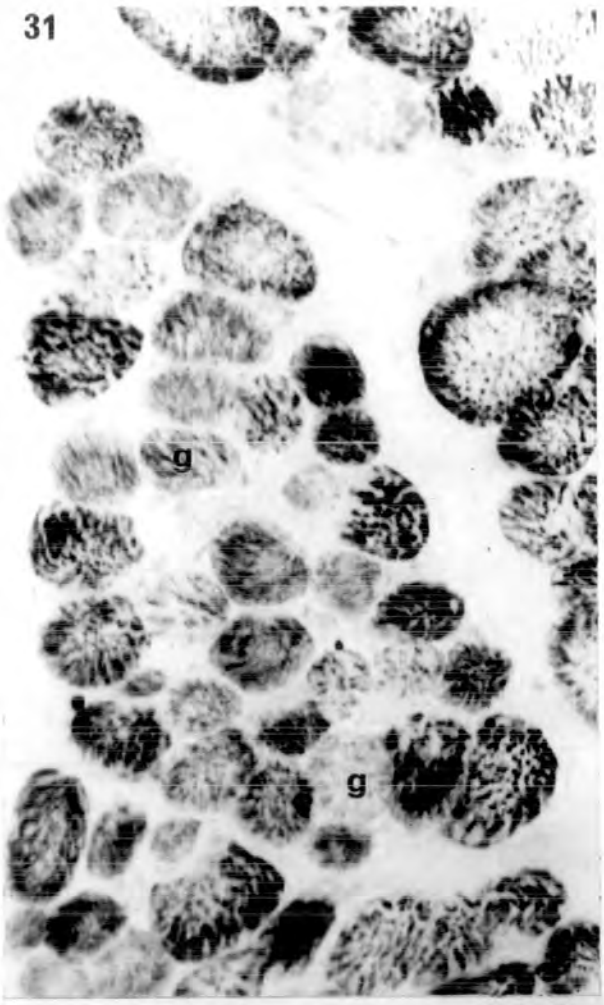
31
g
g

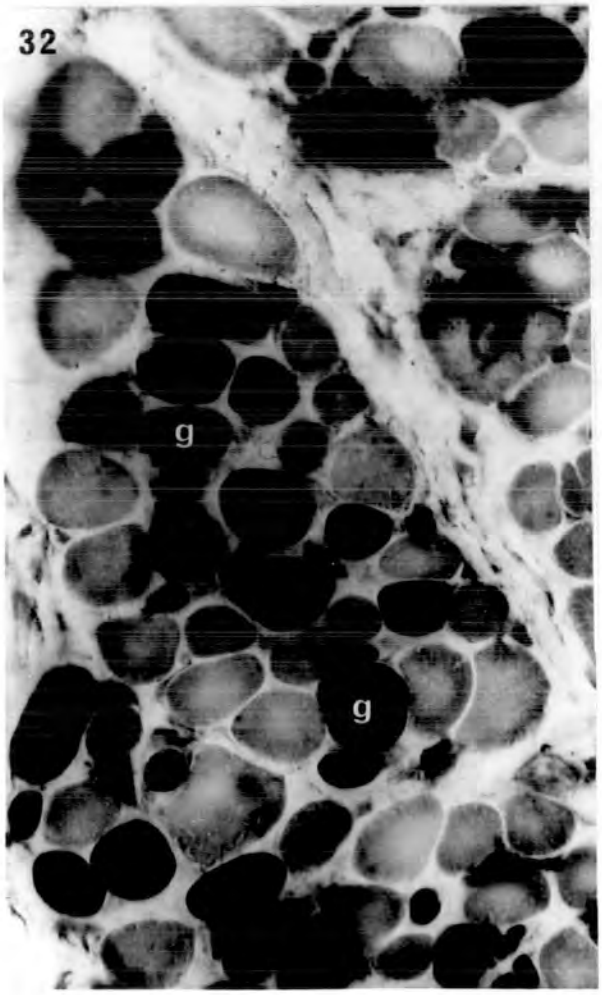
32
g
g

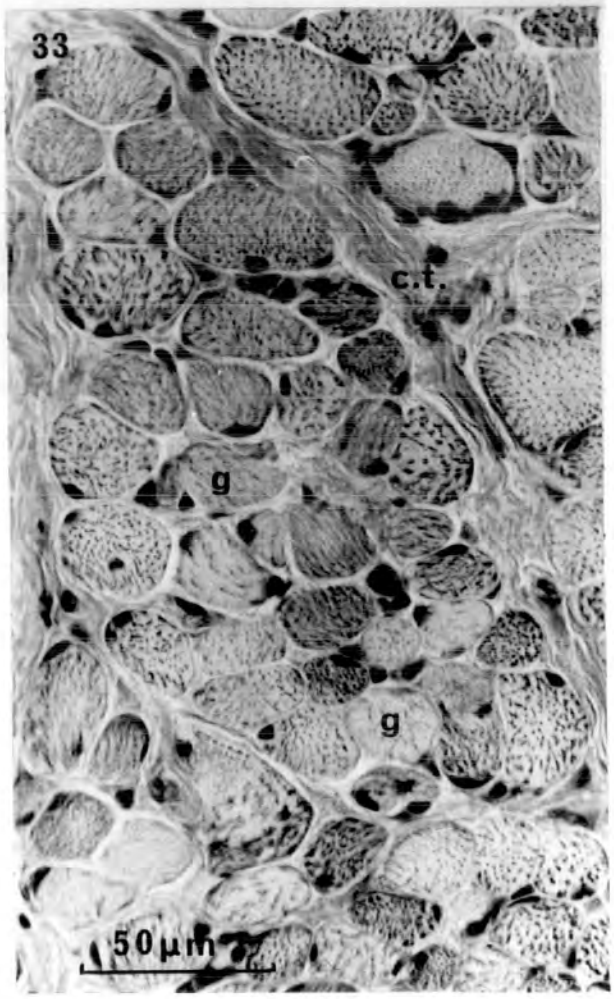
33
c.t.
g
g
50 µm

Figures 34 to 36. Semi-thin (1.5 μm) transverse Epon sections stained with toluidine blue used to identify the extrafusal muscle fibre types in SR for electron microscopy.

Fig. 34. Peripheral patch layer from the insertion end of SR. The layer is composed mainly of intermediate G (g) fibres that possess an intermediate background and have numerous small granulations (mitochondria) and streaks.

Fig. 35. Orbital rim layer from the belly of SR. The layer contains a spectrum of type C fibres ranging from intermediate C (C) to small C (c) types. These have a dark background and large, numerous granulations (mitochondria). The small G (g) fibres have a low background staining intensity with small but relatively numerous granulations (mitochondria).

Fig. 36. The central core layer from the belly of SR. The intermediate C (C) and small C (c) fibre types possess a dark background, large and numerous granulations (mitochondria), and a fibrillar appearance. The large A (A) and large G (G) fibre types both possess relatively low background staining and small, infrequent granulations (mitochondria). The large G fibre, however, is usually larger and isolated, and exhibits an afibrillar myofibril pattern, in contrast to the fibrillar large A fibre.

All figures are the same magnification.

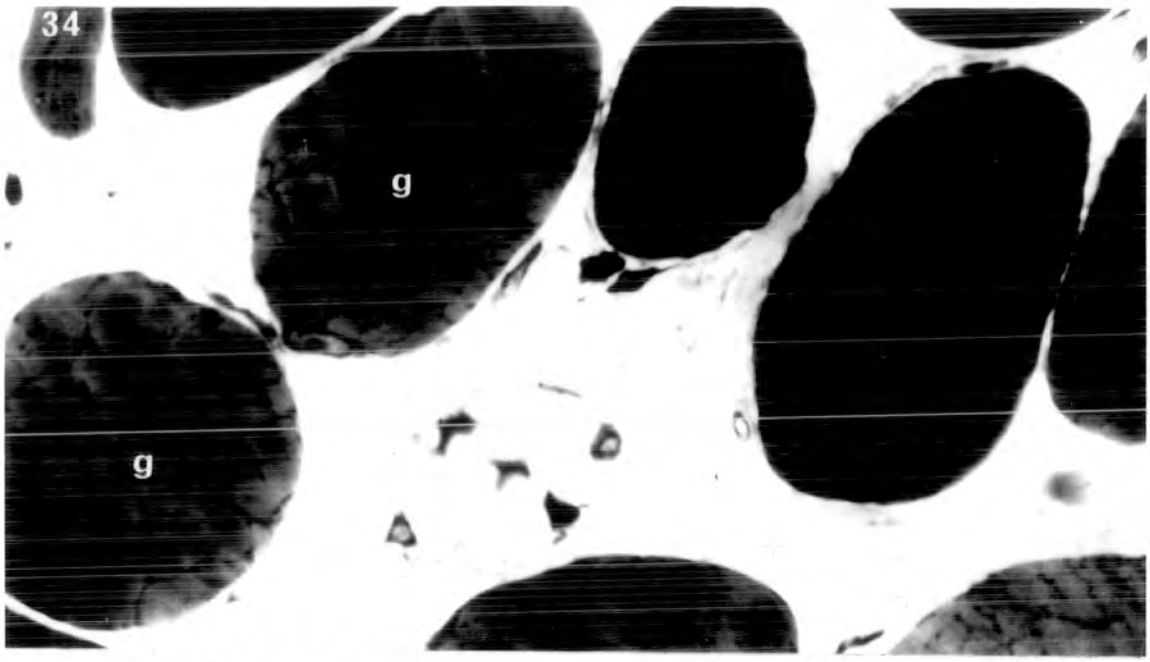
34
g
g

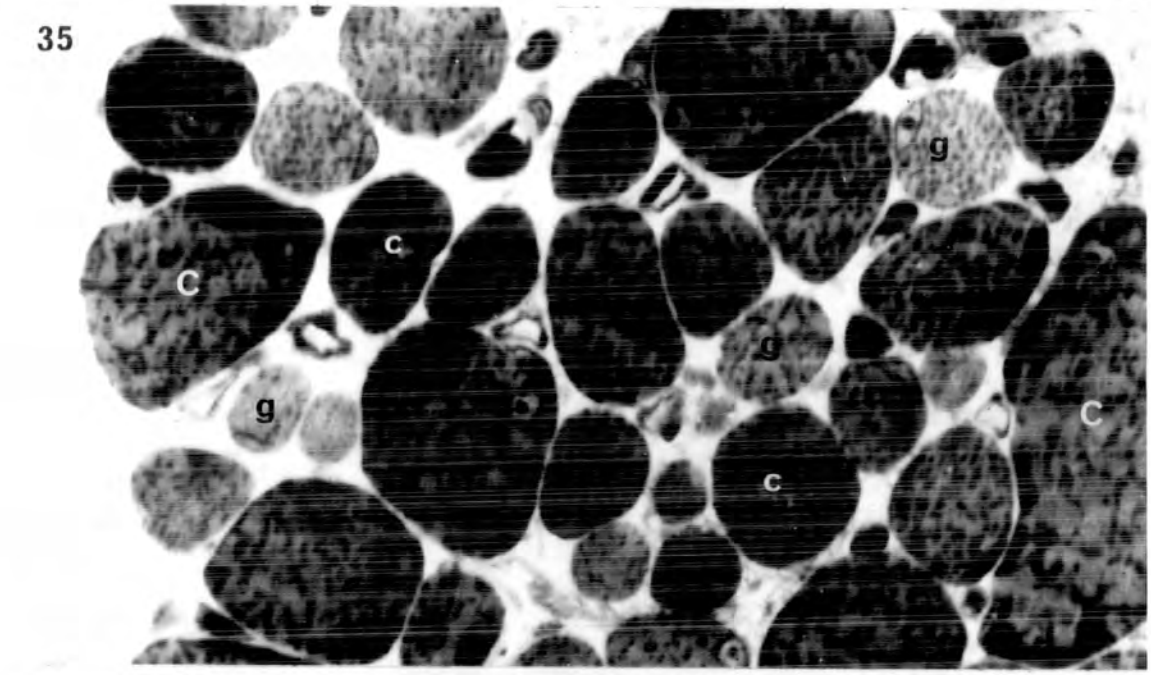
35
g
c
C
g
g
c
C

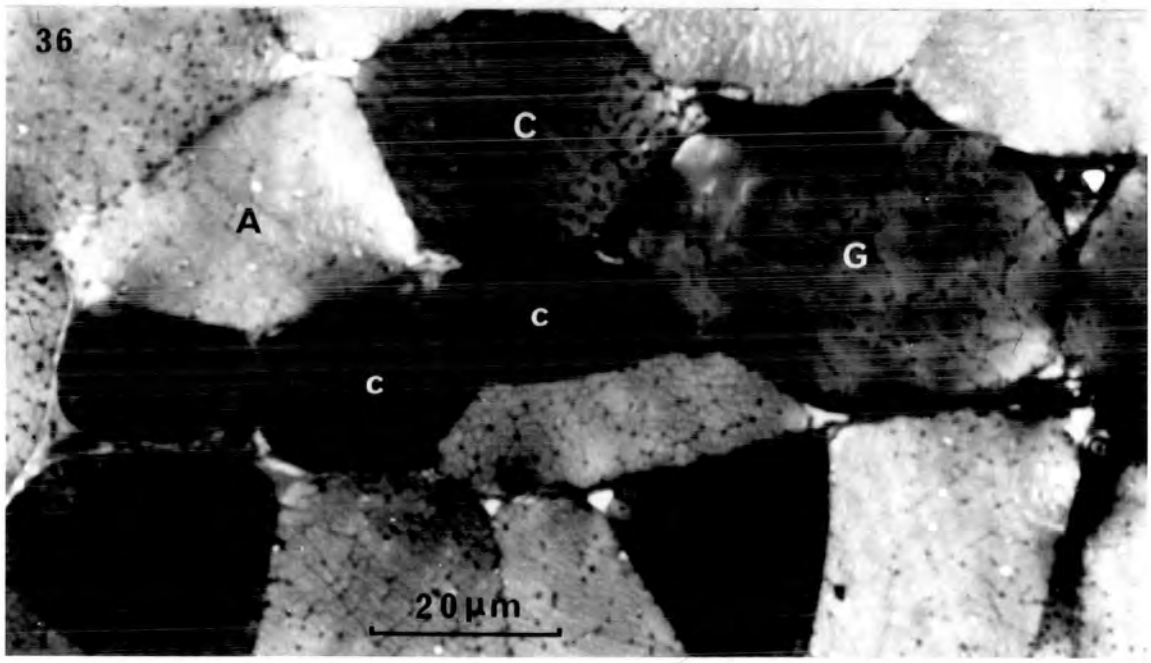
36
C
A
G
c
c
20 µm

Figures 37 to 39. Semi-thin (1.5 μm) Epon transverse sections stained with toluidine blue comparing the type G fibres of each layer of SR at high magnification.

Fig. 37. Peripheral patch layer at the insertion end of SR. The intermediate G fibres (g) have an afibrillar appearance at high power with irregularly-delineated myofibrils that are larger than those of a neighbouring intermediate C (C) fibre.

Fig. 38. Orbital rim layer. Even at high power under the light microscope the pattern of the myofibrils of the small G (g) fibres is difficult to ascertain.

Fig. 39. Central core layer in the belly of SR. The large G (G) fibre possesses an afibrillar pattern of large myofibrils. Compare with an adjoining intermediate C (C) fibre that shows a fibrillar pattern.

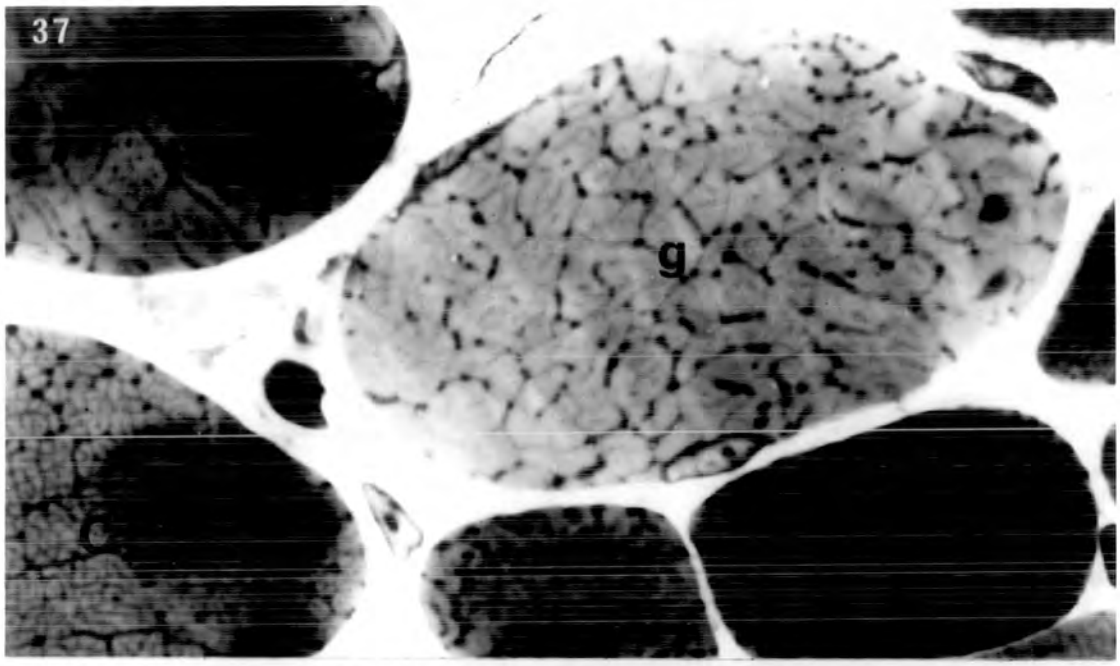
37
g
C

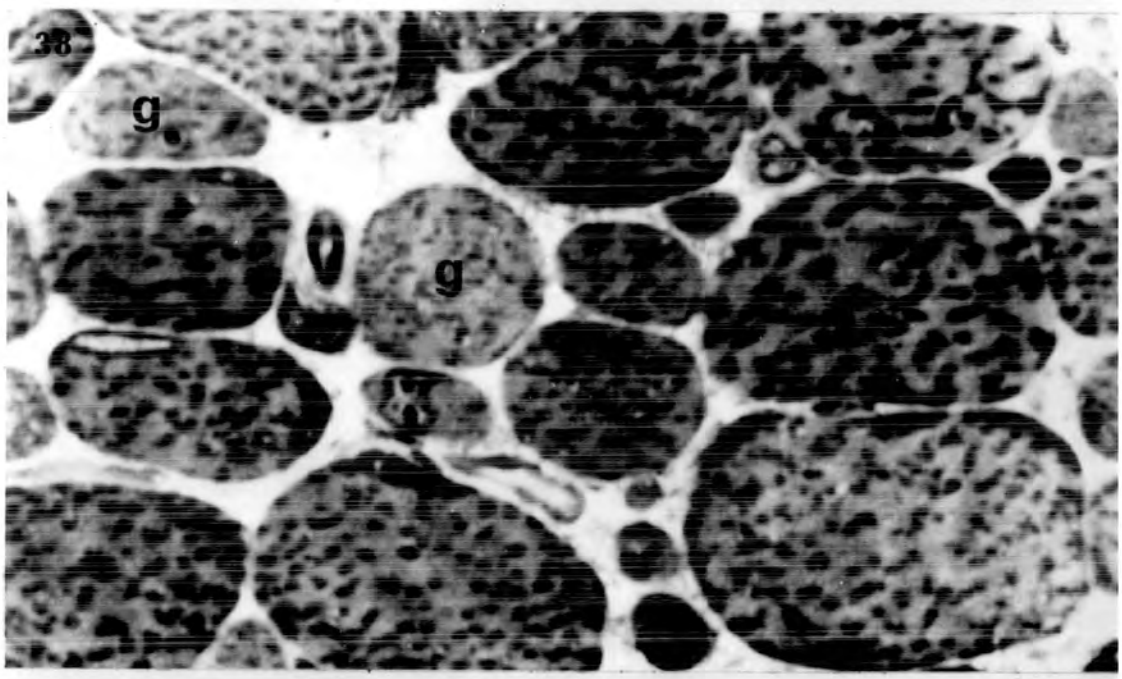
38
g
g

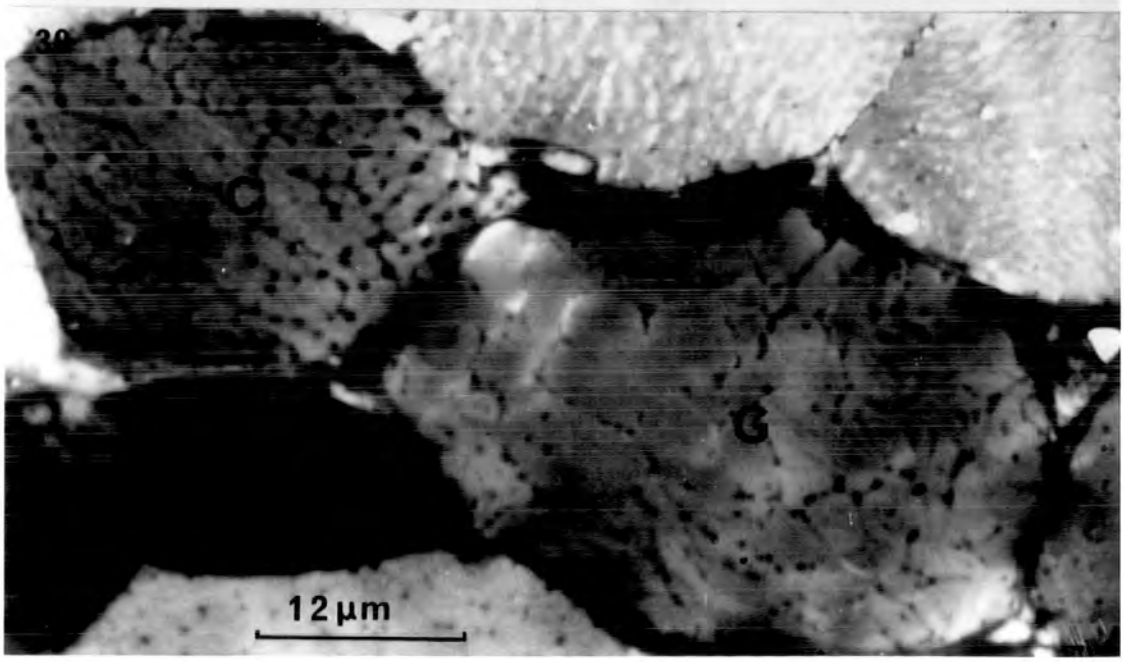
C
C
12 µm

Figures 40 to 41. Electron micrographs of transverse sections of the central core layer of SR.

Fig. 40. An intermediate C (C), a small C (c) and a large A (A) fibre are shown. Note the possession of small, well-delineated myofibrils by all three fibre types, and the differences between the fibres in background staining intensity; and in the size, abundance and distribution of mitochondria.

x 3,200

Fig. 41. A large G (G) fibre appears relatively homogeneous in low-power electron micrographs with large, irregular myofibrils and small, sparse mitochondria.

x 3,200

40

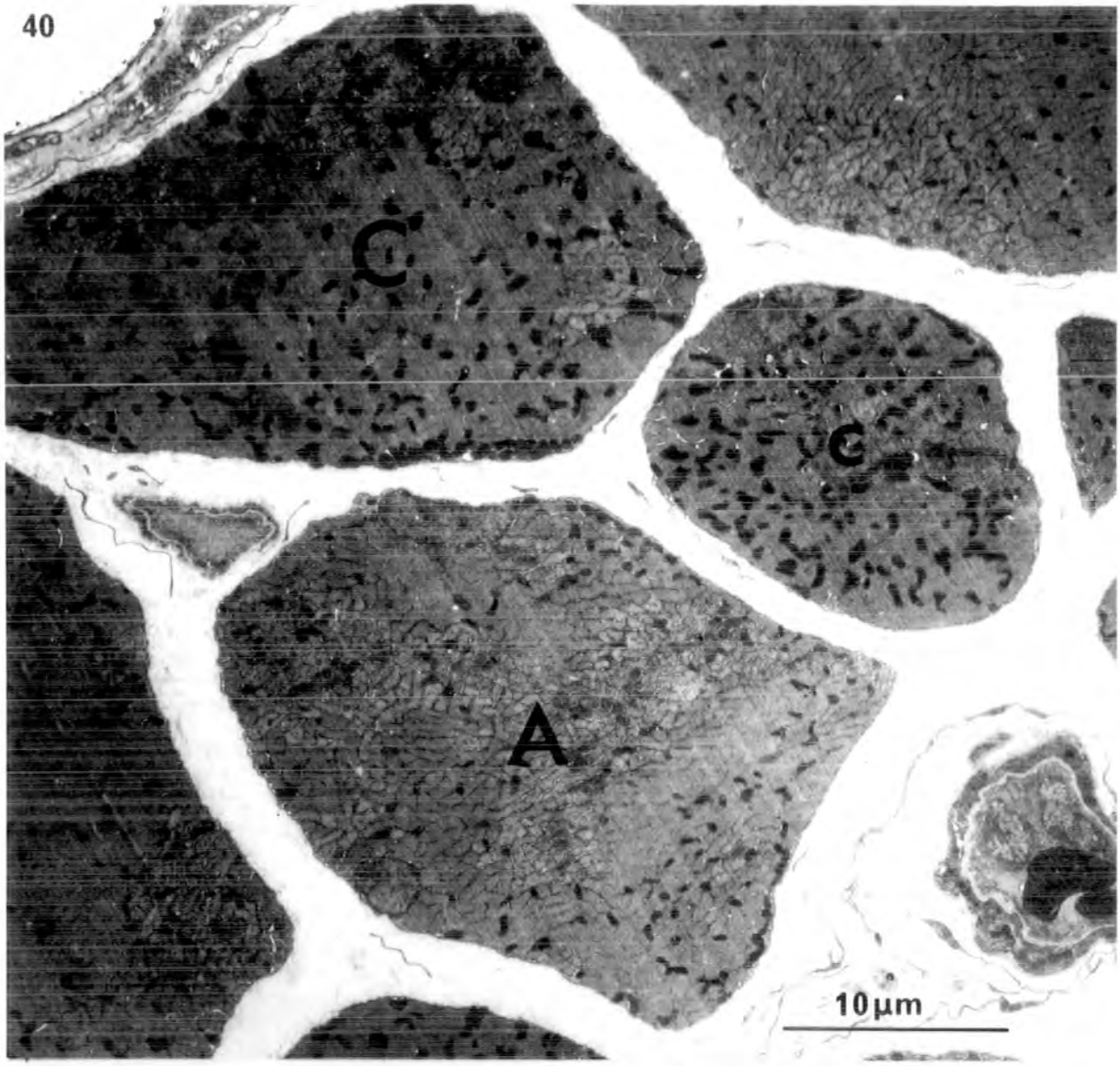

41

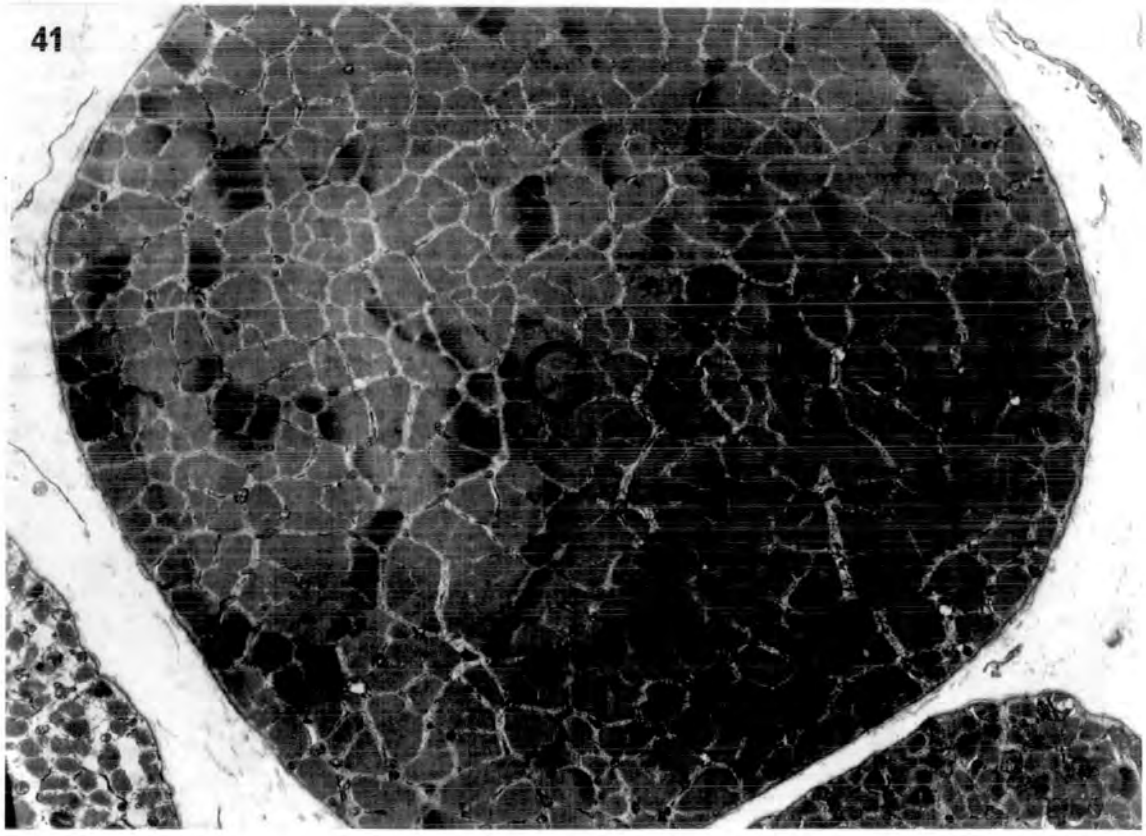

Figures 42 to 45. Electron micrographs of transverse sections comparing the fine structure of the large A and large G fibre types of the central core of SR.

Fig. 42. Large A fibre at the level of the A band/I band junction. Note the small, regular myofibrils (mf) that are particularly well-delineated at this level. The Z line in transverse section (Z) is less dense than in the large G fibre (fig. 44).

x 5,000

Fig. 43. Large A fibre. Higher magnification of part of fig. 42. Note the small, well-delineated myofibrils (mf), extensive transverse tubules (t.t.) and tubules of the sarcoplasmic reticulum (s.r.). The mitochondria (m) are relatively small with few cristae.

x 20,000

Fig. 44. Large G fibre. Note the large, irregular myofibrils (mf) and the dense Z lines (Z).

x 5,000

Fig. 45. Large G fibre. The myofibrils (mf) are separated by sarcoplasm with only poorly-developed sarcoplasmic reticulum (s.r.) and transverse tubules (t.t.). Mitochondria (m) are extremely small and contain only few cristae.

x 20,000

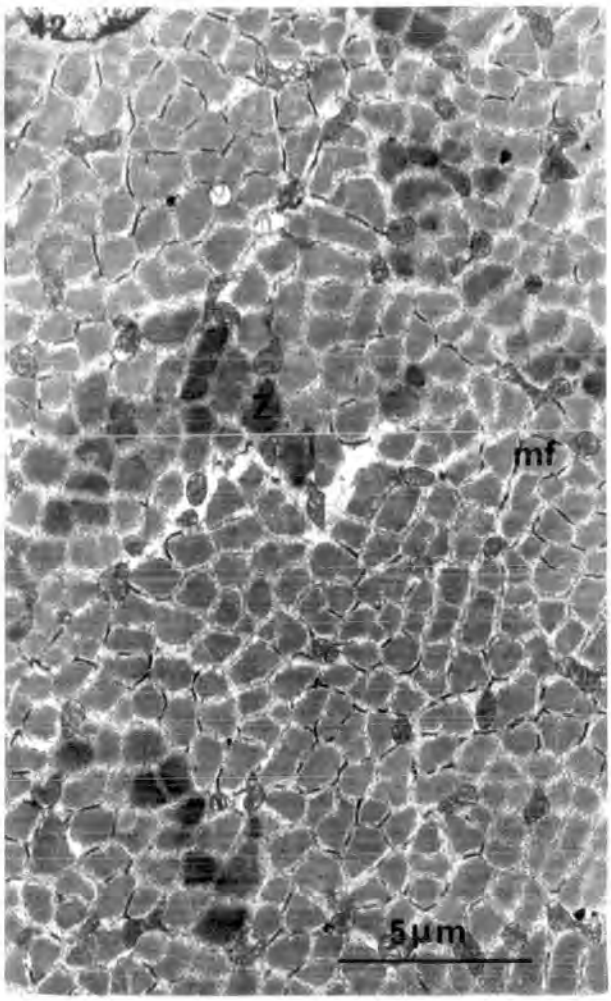
42
Z
mf
5µm

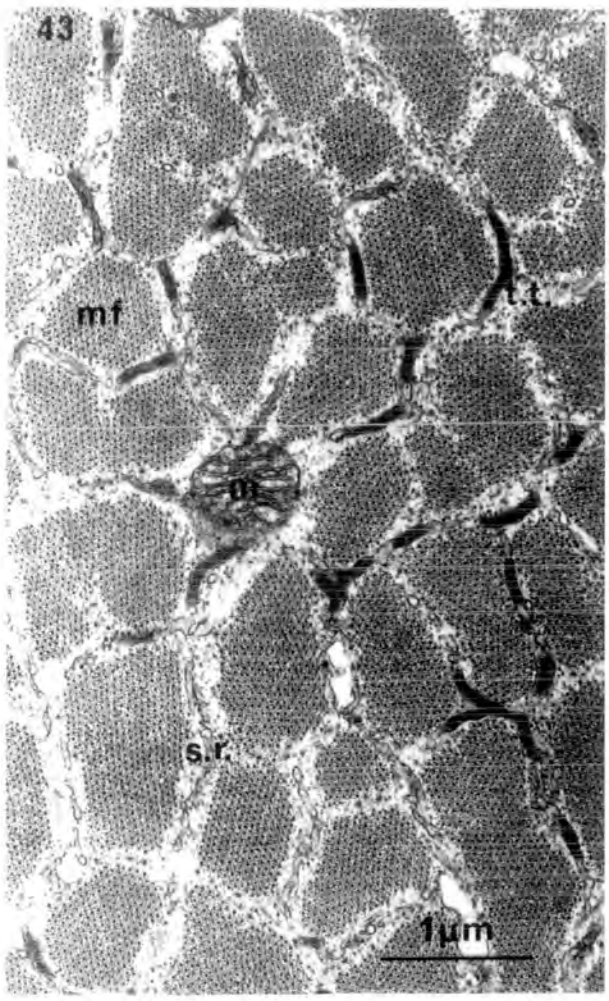
43
mf
t.t.
m
s.r.
1µm

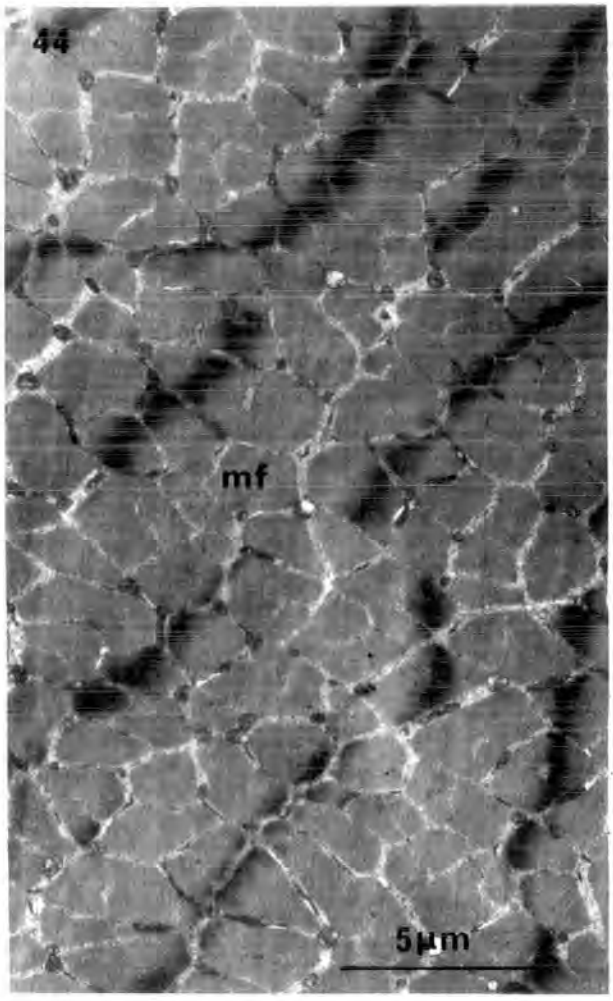
44
mf
5µm

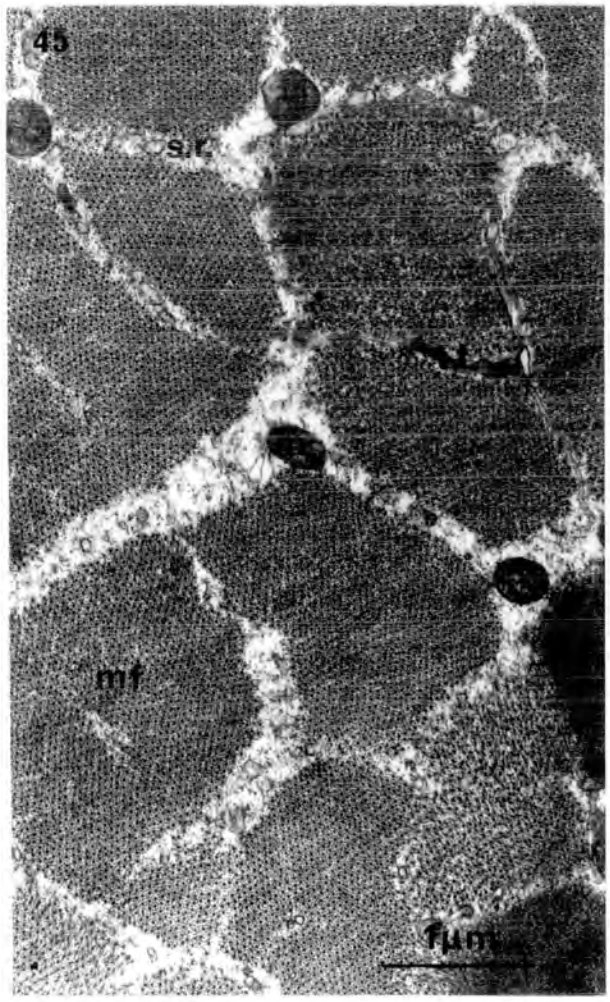
45
s.r.
mf
1µm

Figures 46 to 49. Electron micrographs of transverse sections comparing the fine structure of the small C and intermediate C fibre types of the central core of SR.

Fig. 46. Small C fibre. Note the small diameter of the fibre; the small, well-delineated myofibrils (mf); the numerous, large mitochondria (m) that are scattered evenly throughout the muscle fibre; and the Z line (Z) as it appears in transverse section.

x 5,000

Fig. 47. Small C fibre. Higher magnification of part of fig. 46. The myofibrils are delineated by abundant sarcoplasm, transverse tubules (t.t.) and tubules of sarcoplasmic reticulum (s.r.). The mitochondria (m) are large with tightly-packed cristae. Note the lipid droplet (Li).

x 20,000

Fig. 48. Intermediate C fibre. Note the small, regular myofibrils (mf); the relatively large mitochondria (m) that are especially numerous around the periphery; and the Z line (Z).

x 5,000

Fig. 49. Intermediate C fibre. The myofibrils are delineated by abundant sarcoplasm, transverse tubules (t.t.) and tubules of sarcoplasmic reticulum (s. r.). The mitochondria are relatively large and have tightly-packed cristae.

x 20,000

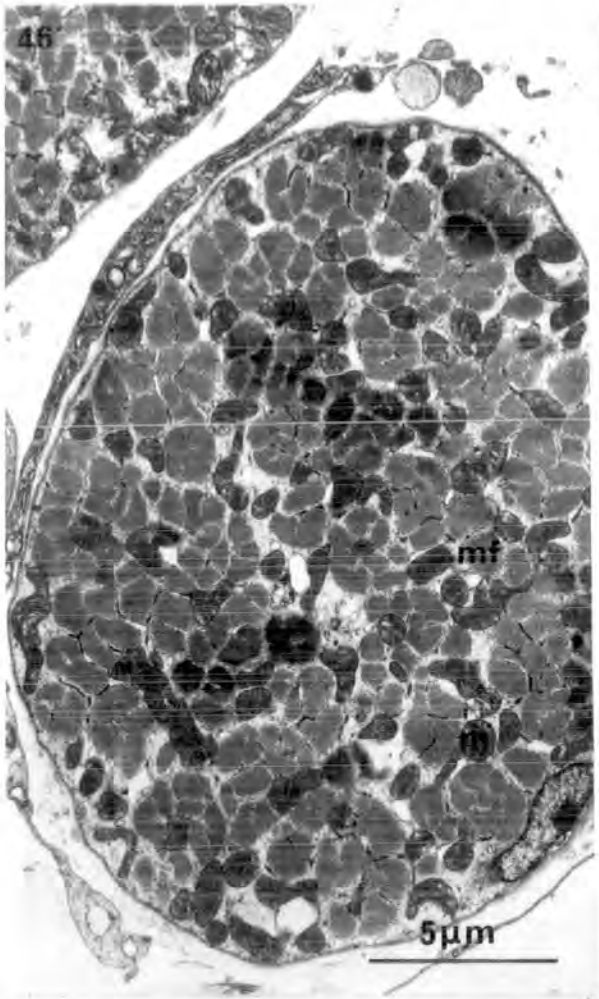
46
mf
m
5µm

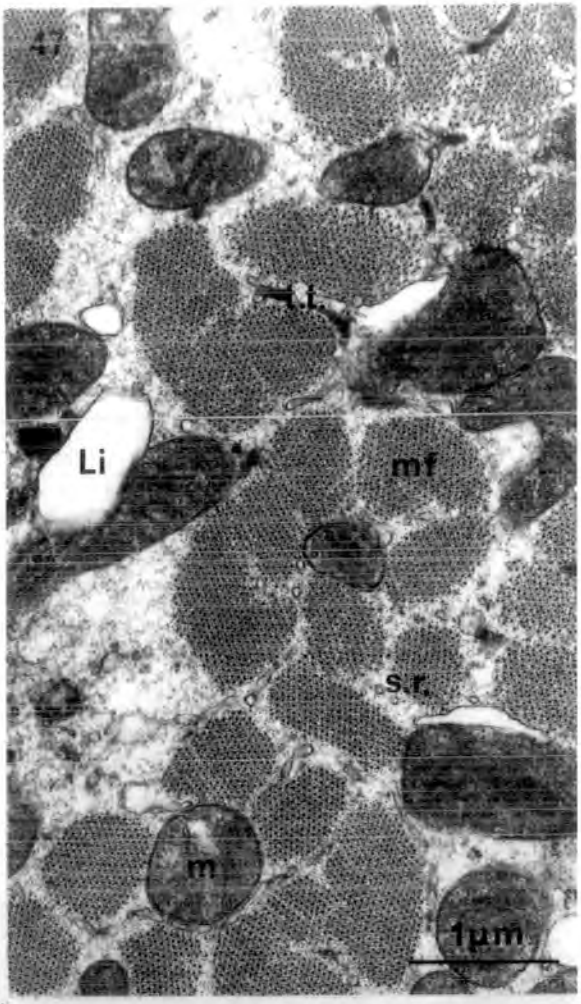
47
t.l.
Li
mf
s.r.
m
1µm

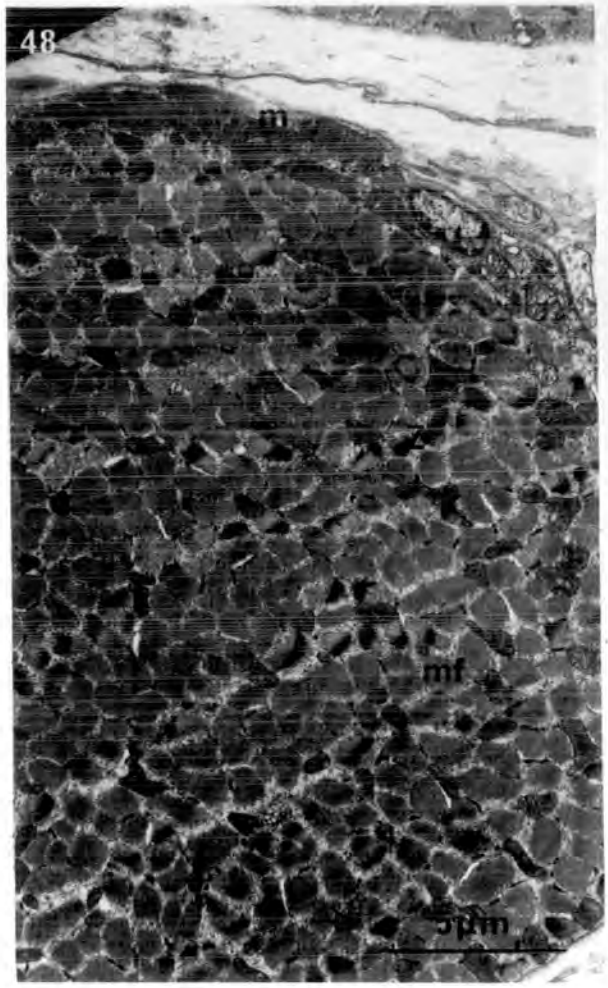
48
m
mf
5µm

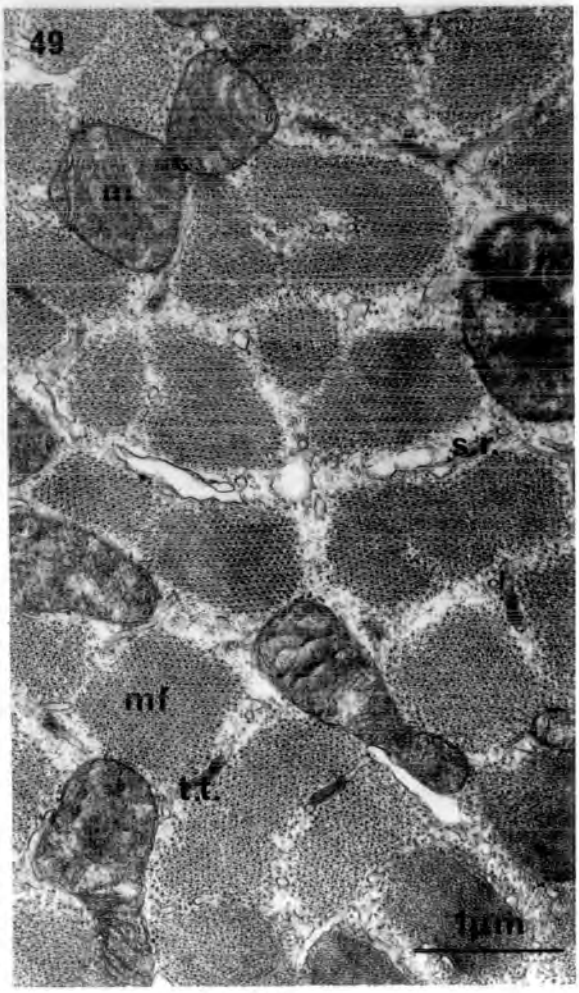
49
m
s.r.
mf
t.t.
1µm

Figures 50 to 52. Electron micrographs of longitudinal sections of the large G fibre type located in the central core layer of SR.

Fig. 50. A low-power view of a large G fibre in L.S. Note the small round mitochondria (m) with few cristae that are usually paired on either side of the straight Z line (Z); the prominent M line (M) in the middle of the A band; the occasional triads (tr) at the A/I band junction; and the sparse sarcoplasmic reticulum (s.r.) with associated glycogen granules (Gl) only in the I band.

x 15,750

Figs. 51 - 52 show two sarcomeres of a large G fibre. Note that the Z lines (Z) have a visible sub-structure of Z filaments; and that the M line (M) lies within a pseudo-H zone (marked by lines) in the middle of the A band.

x 25,000

In fig. 52 the transverse tubules (t.t.) near to the surface of the fibre are seen to be obliquely orientated.

x 30,000

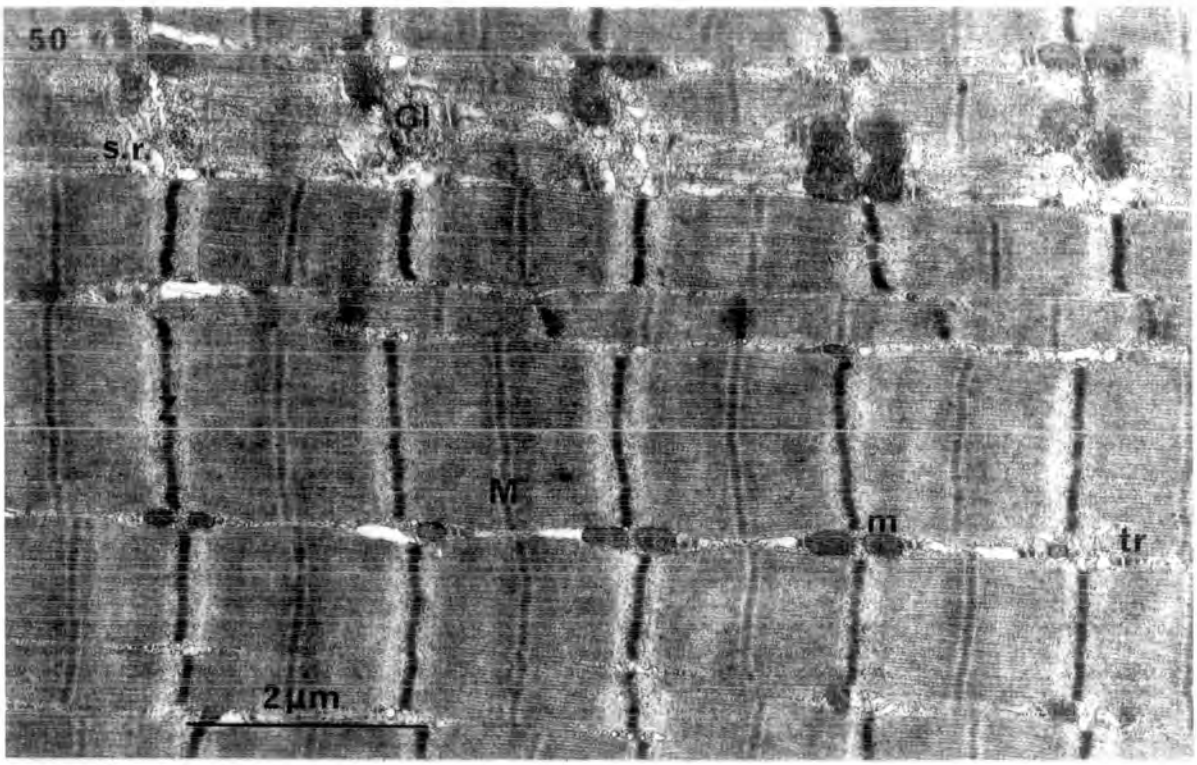
50
s.r.
Cl
M
m
tr
2µm

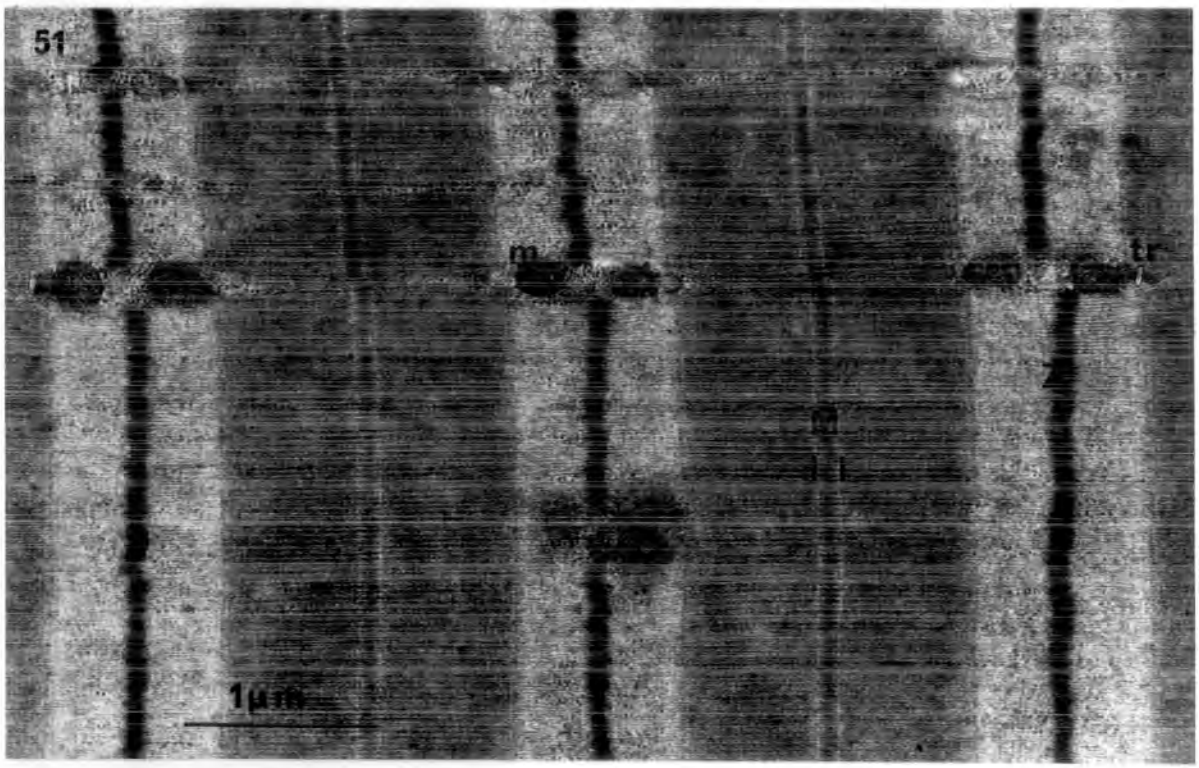
51
m
tr
1µm


52
M
Z
t.t
1µm

Figures 53 to 55. Electron micrographs of longitudinal sections of the large A fibre type located in the central core layer of SR.

Fig. 53. A low-power view of a large A fibre shows the relatively infrequent, small mitochondria (m) that are usually located in pairs on either side of a straight Z line (Z).

x 5,000

Fig. 54. At high magnification note the prominent M line (M) within a pseudo-H zone (marked by lines); the regular triads (tr) at the junction of the A and I bands; and the abundant sarcoplasmic reticulum (s.r.) that separates the myofibrils in the I band.

x 12,600

Fig. 55. Note that the Z line (Z) has a visible substructure of Z filaments, and that large amounts of glycogen granules (Gl) are associated with the sarcoplasmic reticulum.

x 40,000

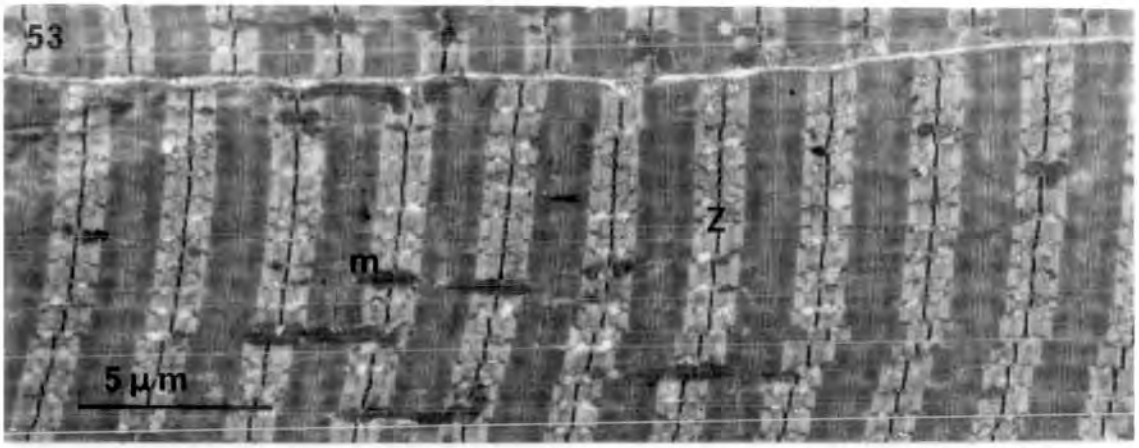
53
m
Z
5 µm

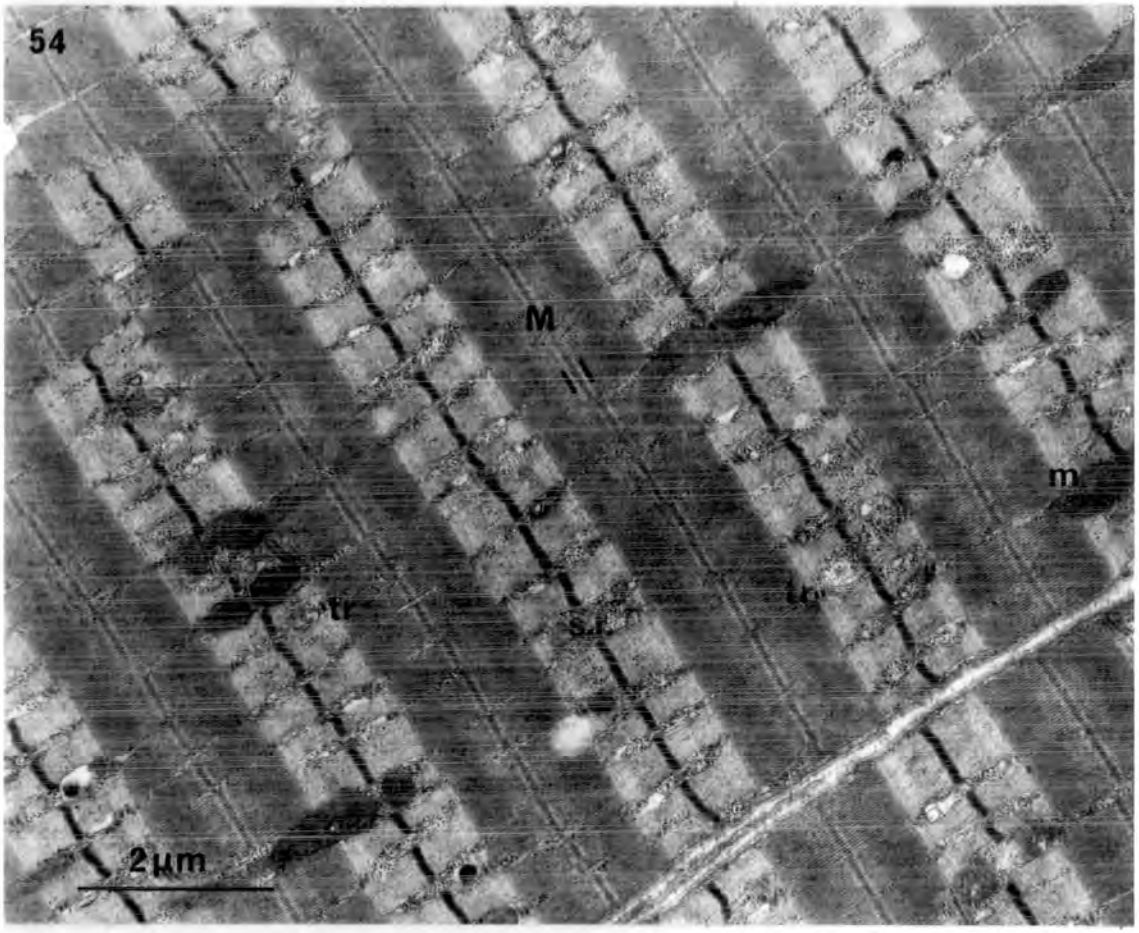
54
M
m
tr
2 µm

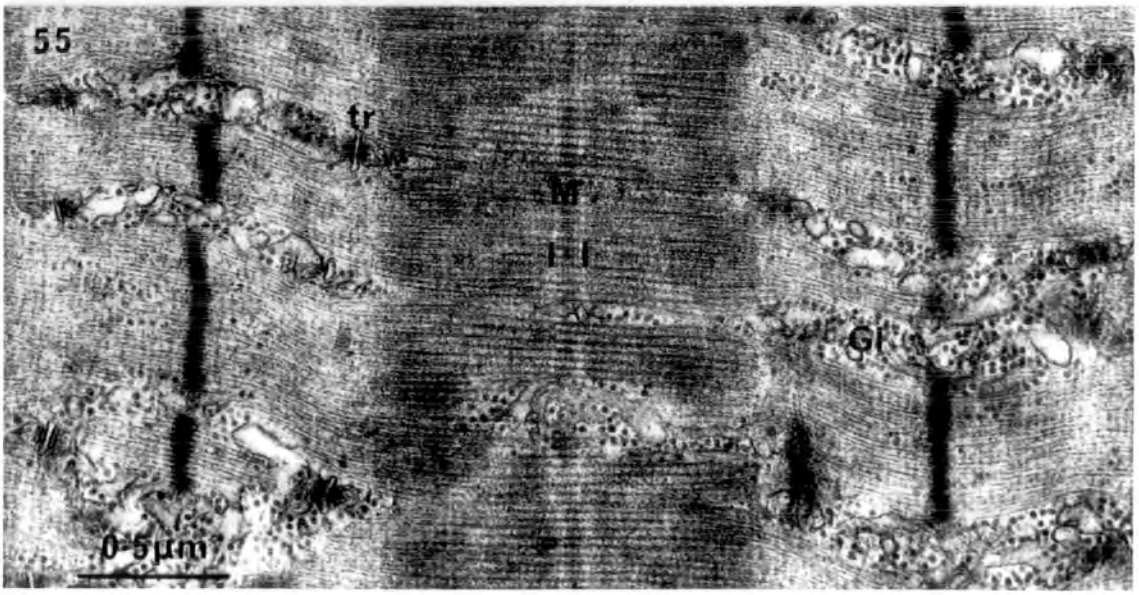
55
tr
M
I
I
GI
0·5 µm

Figures 56 to 58. Electron micrographs of longitudinal sections of the C fibre types in the central core layer of SR.

Fig. 56. A low-power L.S. showing a small C fibre (small C) on the left and an intermediate C fibre (Int C) on the right.

Note in both types of C fibre the small, well-delineated myofibrils; the elongate mitochondria (m) with tightly-packed cristae which form extended chains separating the myofibrils; the lipid droplets (Li) associated with the mitochondria; and the relatively thick Z lines (Z) that appear slightly wavy. The intermediate C fibre is of larger diameter than the small C fibre and shows the characteristic subsarcolemmal accumulations of mitochondria.

x 8,000

Fig. 57. Part of fig. 56 above at higher magnification showing the fine structure of the small C fibre in more detail. Note especially the tightly-packed cristae within the mitochondria (m); the regularity of the triads (tr); the lipid droplet (Li); and the M line (M) within a pseudo-H zone (marked by lines) that is fainter than in the large G and large A fibre types.

x 12,600

Fig. 58. A single sarcomere of an intermediate C fibre. Note that the Z line has Z filaments; the faint M-line (M) within a pseudo-H zone (marked by lines) in the centre of the A band; the extensive sarcoplasmic reticulum (s.r.) in the I band that extends into the A band; and the glycogen granules (Gl) that are associated with the sarcoplasmic reticulum.

x 20,000

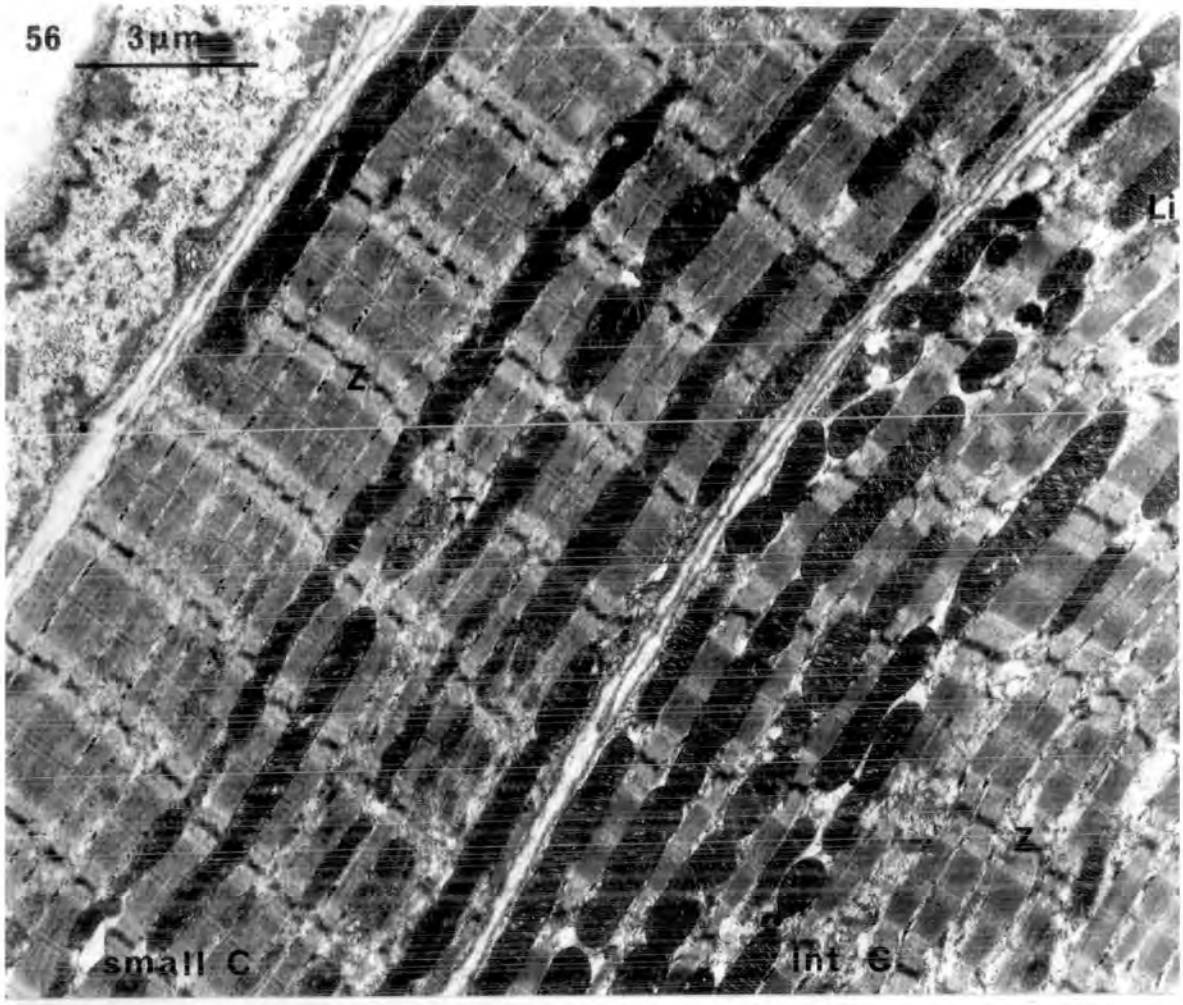
56
3µm
Li
Z
T
Z
small C
Int C

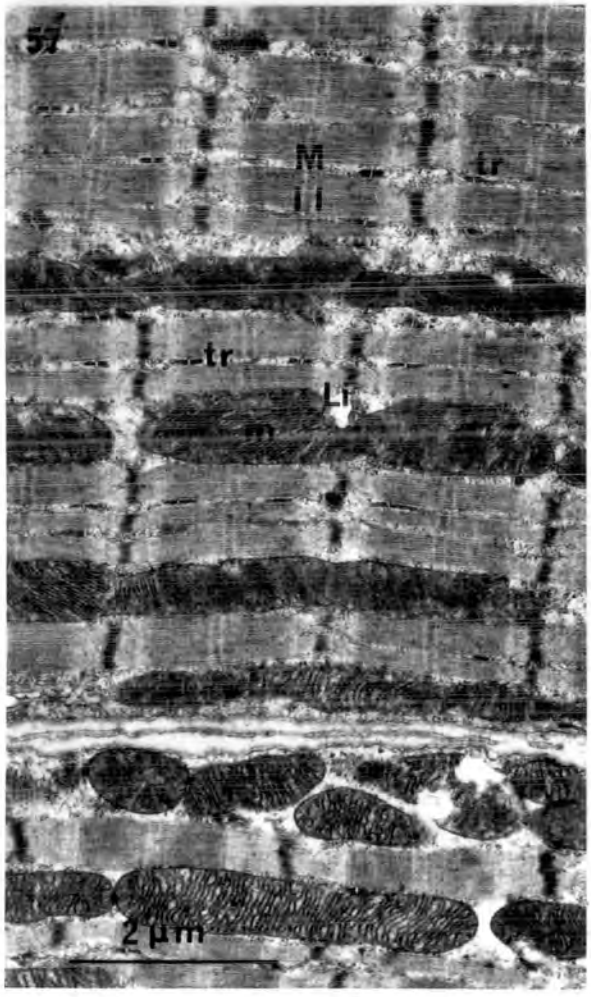
57
M
I I
tr
tr
Li
m
2 µm

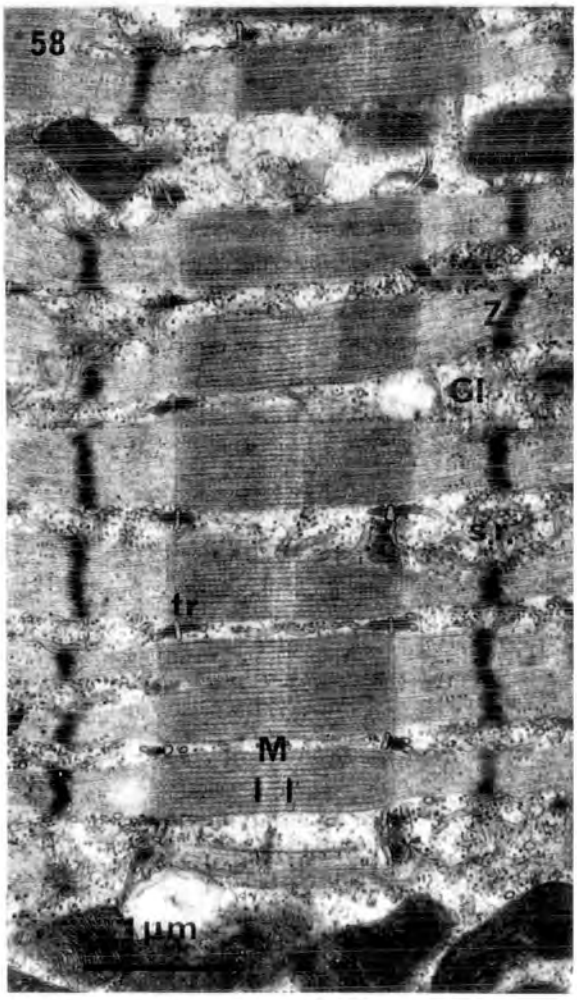
58
Z
CI
sr
tr
M
I I
1µm

Figures 59 to 61. Electron micrographs of transverse sections of the orbital rim layer in the belly region of SR.

Fig. 59. A low-power transverse section showing intermediate C (C), small C (c) and small-diameter G (g) fibre types. The C fibre types show small, well-delineated myofibrils and numerous large mitochondria. The intermediate C (C) fibre is slightly larger in diameter than the small C fibre and has characteristic subsarcolemmal accumulations of mitochondria. The small G fibres (g) in the belly of the muscle are extremely small in diameter, contain smaller mitochondria than the type C fibres and appear more homogeneous in transverse section. cap., blood capillary.

x 3,200

Fig. 60. Part of the above fig. 59 at higher magnification comparing the ultrastructure of a small G fibre (g) with that of an intermediate C (C) and a small C (c) fibre. Note that the mitochondria of the small G fibre are much smaller, although still relatively numerous, and that the myofibrils are less well-delineated, thus giving a more homogeneous appearance.

x 5,000

Fig. 61. Part of fig. 59 above at higher magnification showing the fine structure of a second small G fibre. The myofibrils are only poorly-delineated in the I band (I) by infrequent tubules of sarcoplasmic reticulum (s.r.), while in the A band (A) there is no delineation. The small mitochondria (m) are distributed evenly throughout the muscle fibre.

x 20,000

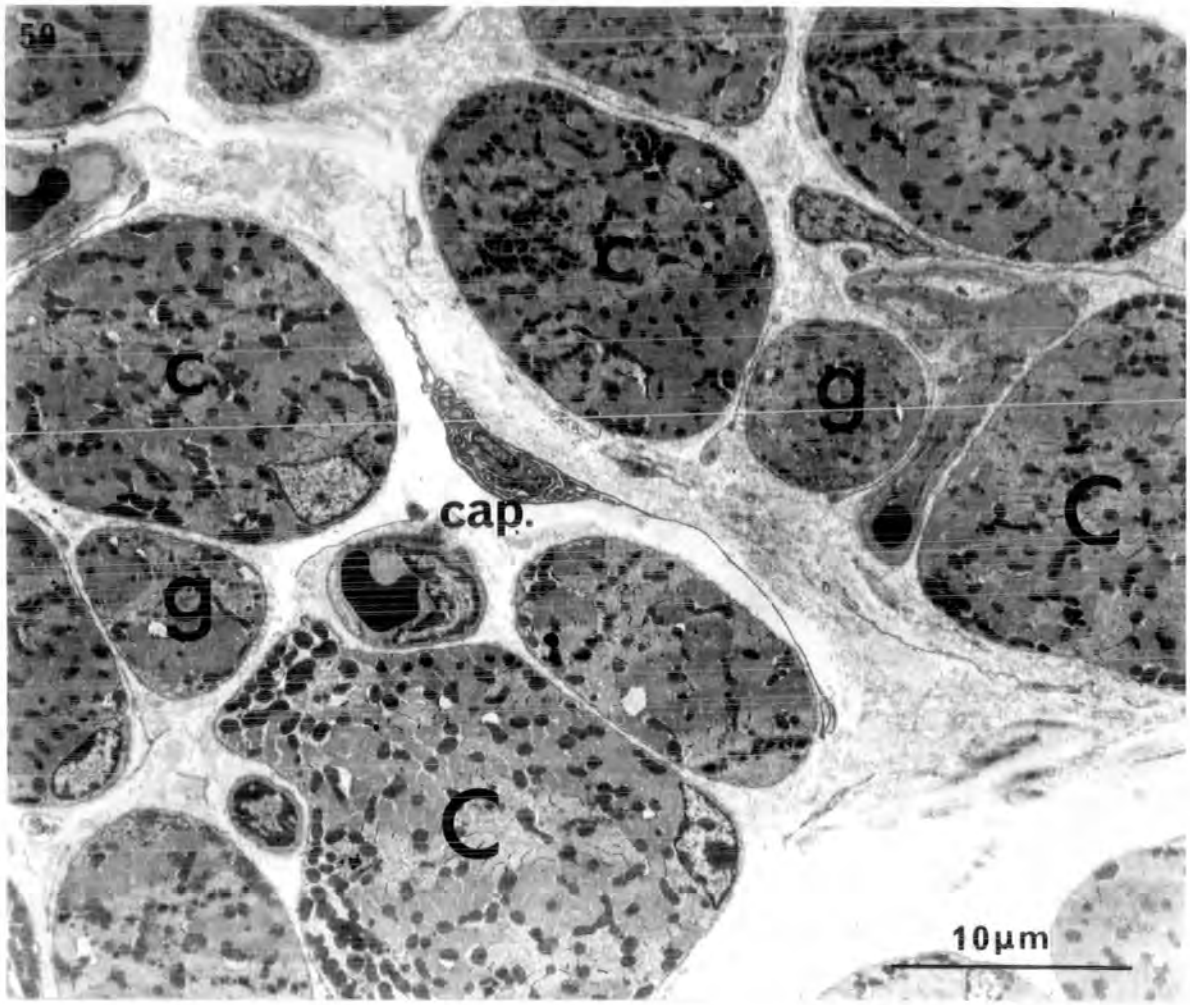
59
c
c
g
cap.
g
C
C
10µm

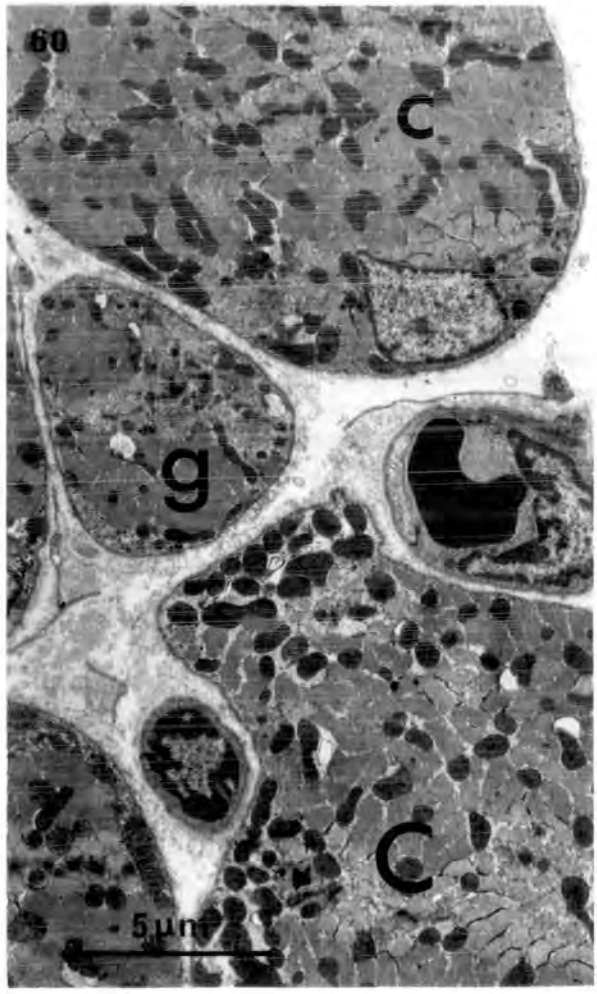
60
c
g
C
5µm

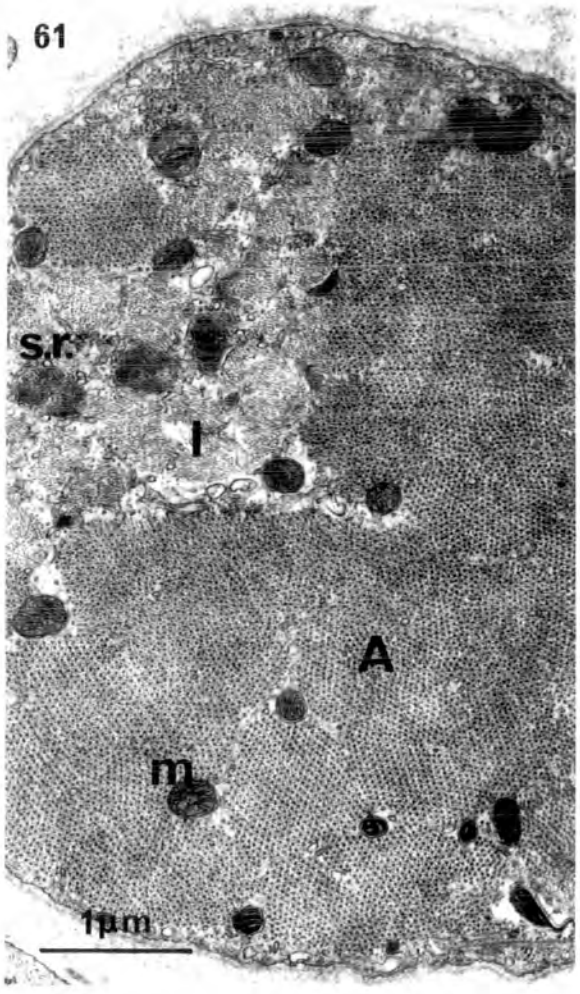
61
s.r.
I
A
m
1µm

Figures 62 to 65. Electron micrographs comparing the fine structure in transverse section of the small C and intermediate C fibre types from the orbital rim layer in the belly of SR.

Fig. 62. Intermediate C fibre.
Note the small myofibrils (mf); the numerous, large mitochondria (m); and the Z line (Z).
x 8,000

Fig. 63. Intermediate C fibre.
The myofibrils are delineated at the A/I band junction by transverse tubules (t.t.) and by a single layer of tubules of sarcoplasmic reticulum (s.r.) in the I band (I). Note the tightly-packed cristae of the mitochondria (m) and the lipid droplets (Li).
x 20,000

Fig. 64. Small C fibre.
Note the small myofibrils (mf) delineated at the A/I band junction by transverse tubules (t.t.) and within the I band (I) by tubules of sarcoplasmic reticulum; the numerous large mitochondria (m) scattered throughout the section; and the dense Z line (Z).
x 8,000

Fig. 65. Small C fibre.
Part of above fig. 64 at higher magnification. The myofibrils in the A band (A) are irregularly delineated by sarcoplasm with only infrequent tubules of sarcoplasmic reticulum (s.r.). The mitochondria show characteristic tightly-packed cristae.
x 20,000

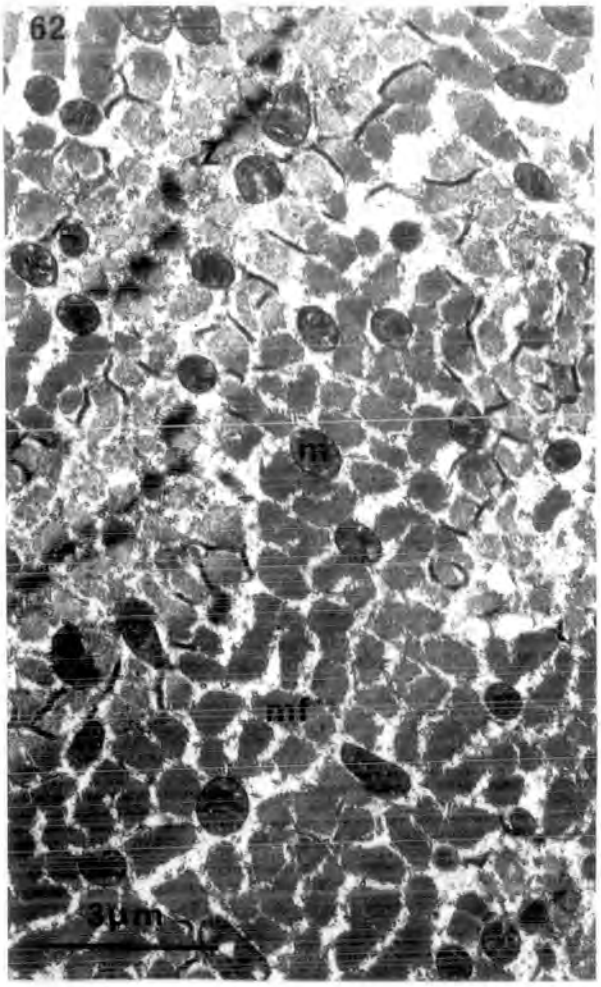
62
m
mf
3µm

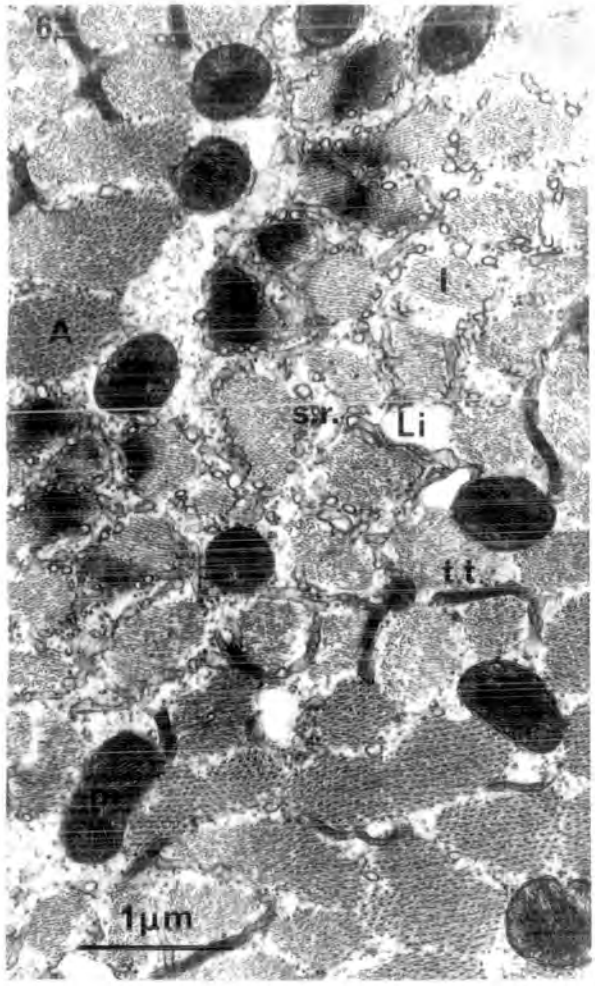
63
I
A
sr.
Li
t t
1µm

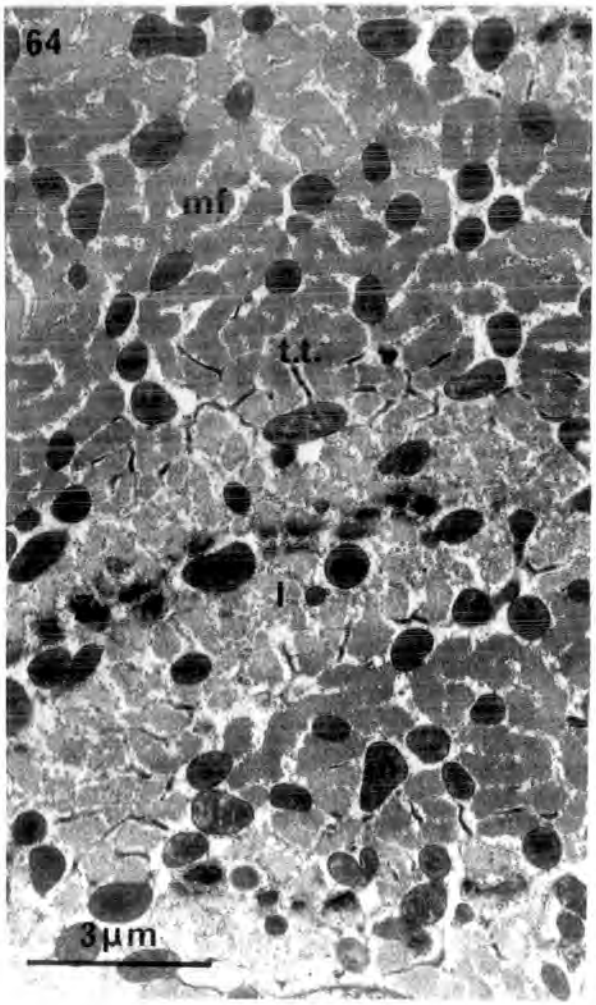
64
mf
t.t.
I
3µm

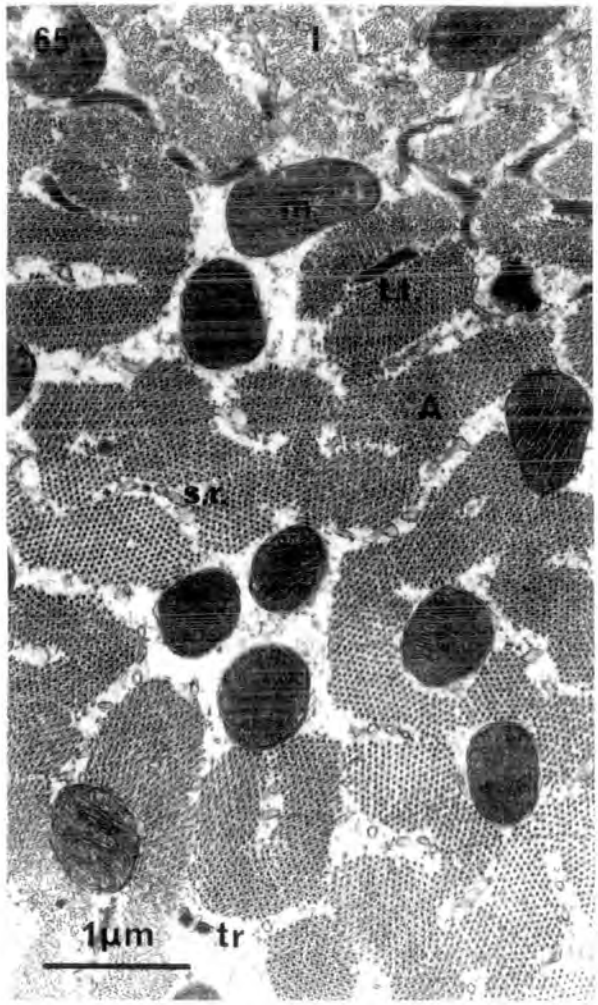
65
I
m
t.t.
A
sr.
1µm
tr

Figures 66 to 67. Electron micrographs of longitudinal sections of type C fibres from the orbital rim layer of SR.

Fig. 66. A low-power L.S. of a small C fibre showing the numerous large mitochondria (m) that form intermyofibrillary chains; the regular triads (tr) at the A/I band junction; the thick Z line (Z); and the faint M line (M) in the middle of the A band.

x 8,000

Fig. 67. Intermediate C fibre.
Note the tightly-packed cristae within the mitochondria (m); the lipid droplet (Li); the thick Z line (Z) with Z filaments; the moderate amounts of sarcoplasmic reticulum (s.r.) in the I band; the M line (M) within a pseudo-H zone (marked by lines); and the regular triads (tr).

x 20,000

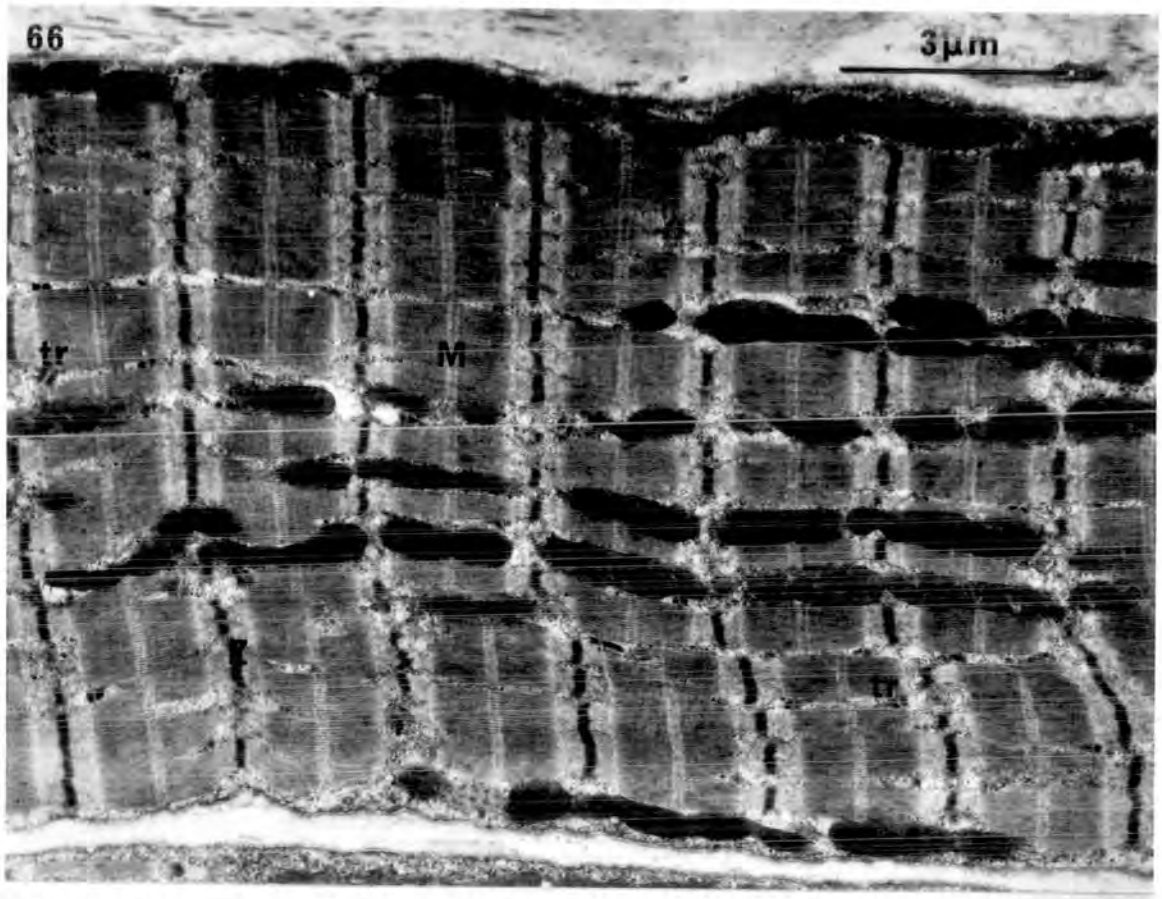
66
3µm
tr
M

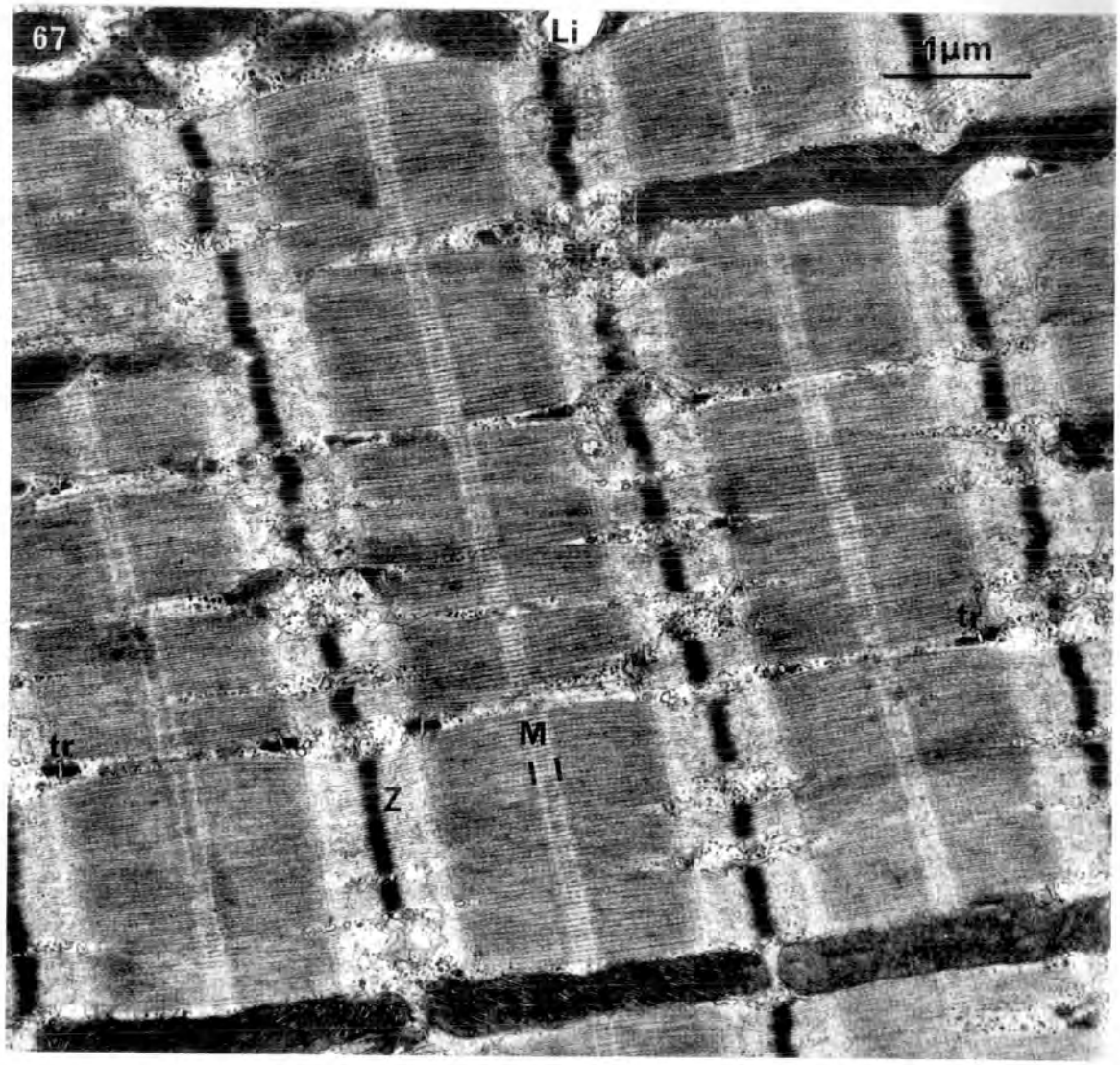
67
Li
1µm
tr
tr
M
Z

Figures 68 to 69. Electron micrographs of longitudinal sections of small G fibres from the orbital rim layer of SR.

Fig. 68. A low-power L.S. of a small G fibre showing the relatively numerous, small mitochondria (m); the irregular and infrequent triads (tr); the straight, thick Z line (Z); the lipid droplets (Li); and the absence of an M line from the middle of the A band.

x 8,000

Fig. 69. Higher magnification of small G fibre shown in fig. 68. Note the thick Z line (Z) with Z filaments; the infrequent triads (tr); the absence of an M line from the pseudo-H zone (marked by lines); and the poorly-developed sarcoplasmic reticulum (s.r.) that is restricted to the I band.

x 30,000

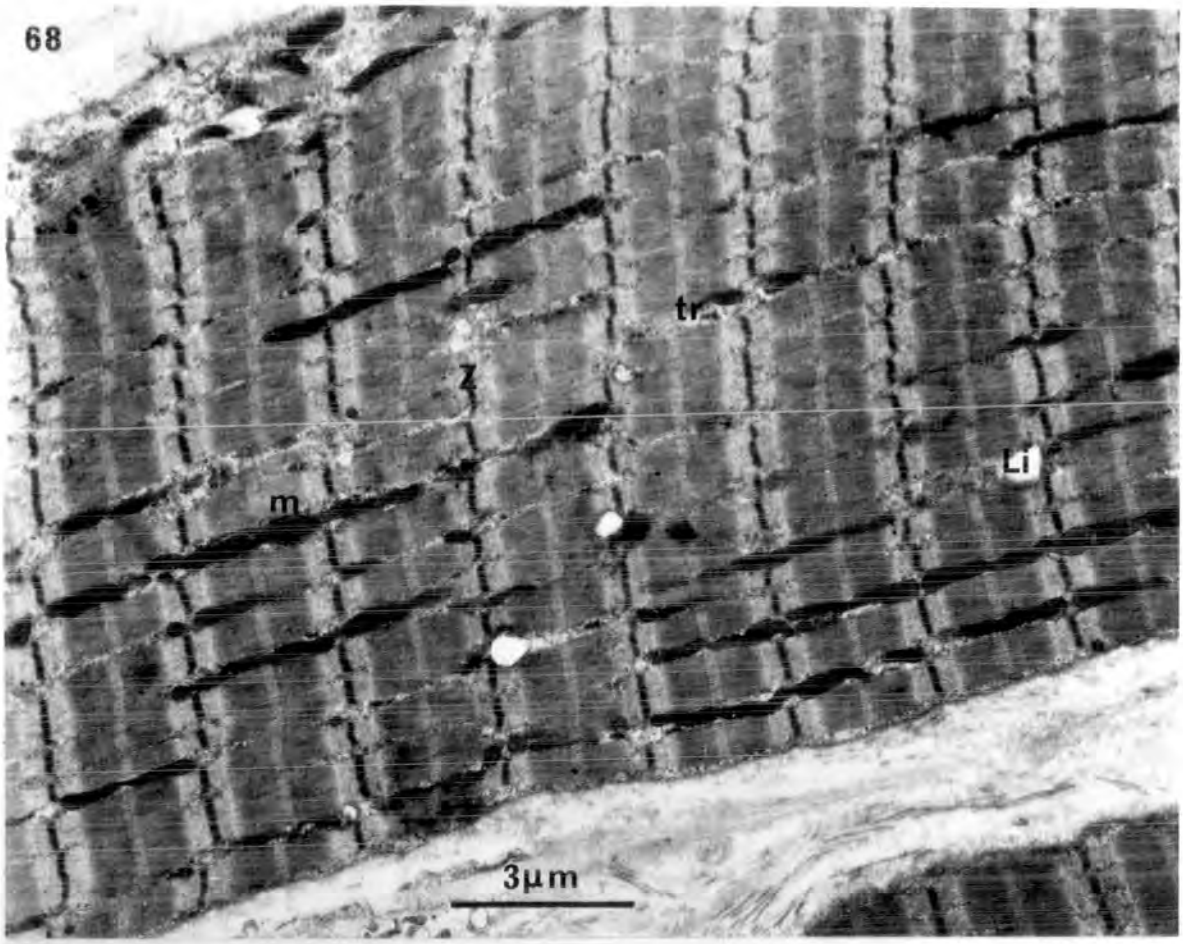
68
tr
z
m
Li
3µm

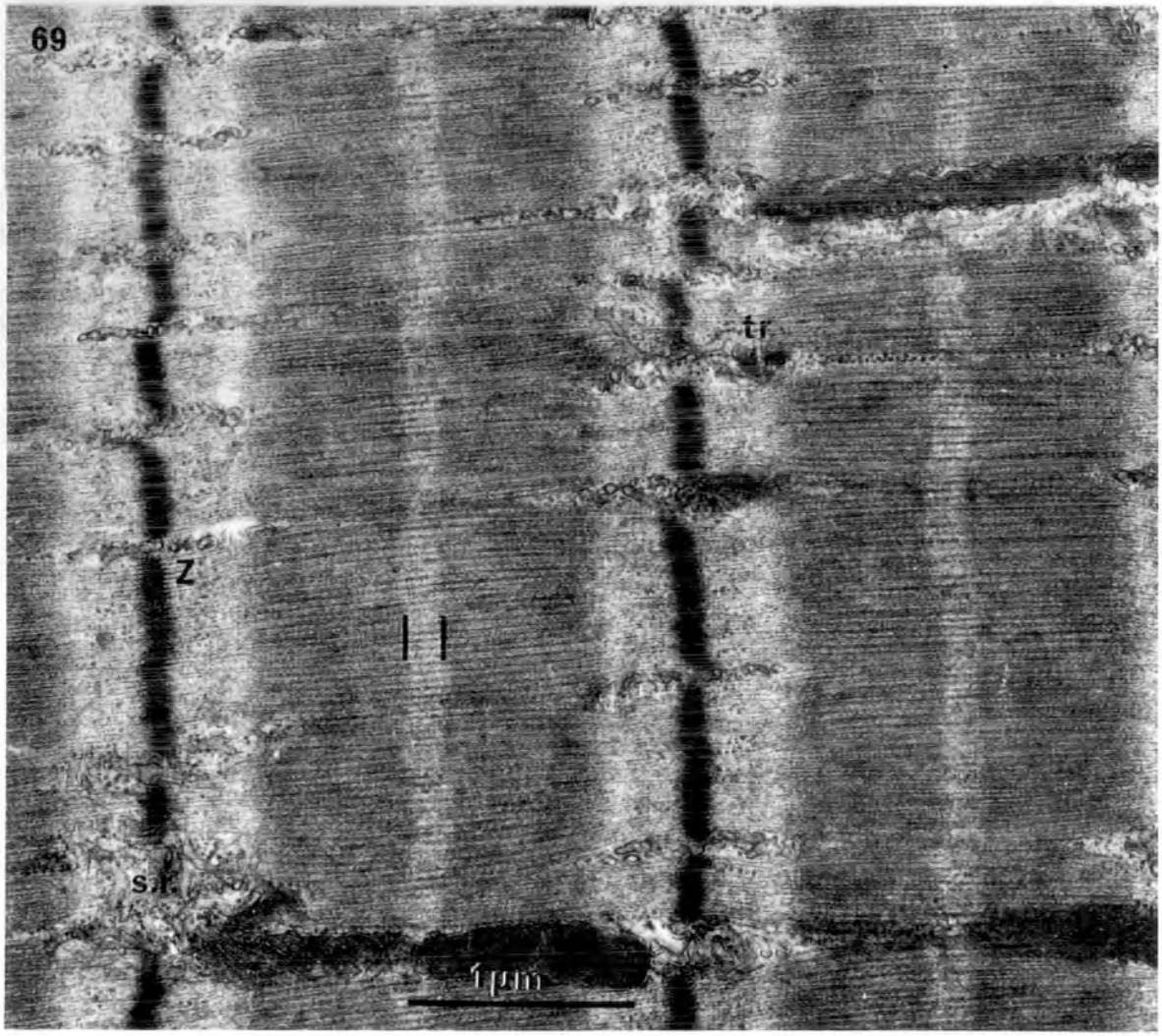
69
tr
z
s.r.
1µm

Figures 70 - 72. Electron micrographs of transverse sections of the orbital rim layer at a level between the belly and insertion of SR.

Fig. 70. A low-power T.S. showing a small G fibre (g) surrounded by a spectrum of C type fibres.
The small-diameter G fibre contains small mitochondria that are evenly distributed throughout a transverse section and which are relatively numerous. Note the blood capillary (cap.).

x 3,200

Fig. 71. Part of small G fibre in fig. 70 at higher magnification. Note the homogeneous appearance of the A band (A); the poorly-delineated myofibrils in the I band (I); and the Z line (Z) in transverse section.

x 5,000

Fig. 72. Small G fibre.
Note the appearance of triads (tr); the infrequent tubules of sarcoplasmic reticulum (s.r.) surrounding the myofibrils in the I band (I); and the small mitochondria (m) containing few cristae.

x 20,000

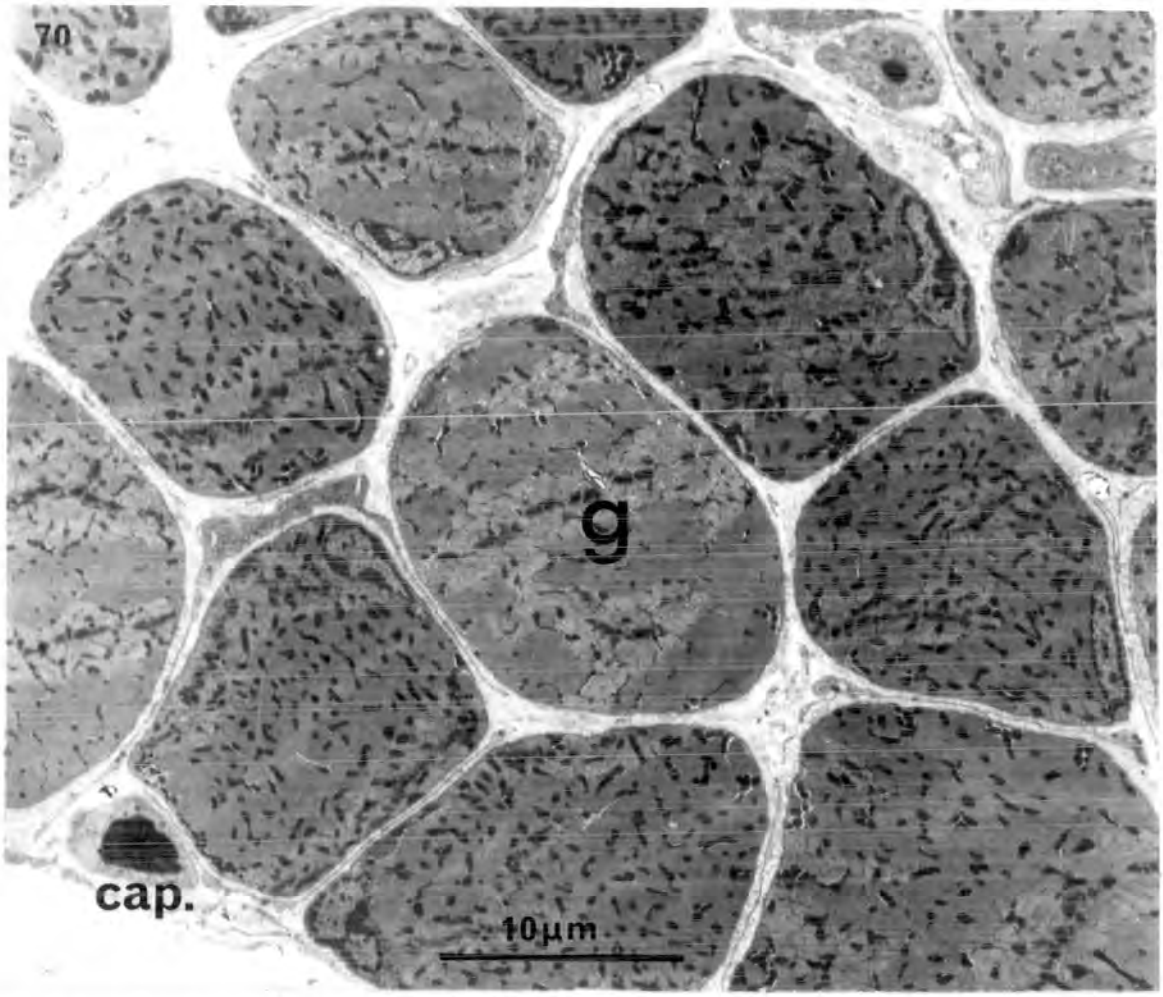
70
g
cap.
10µm

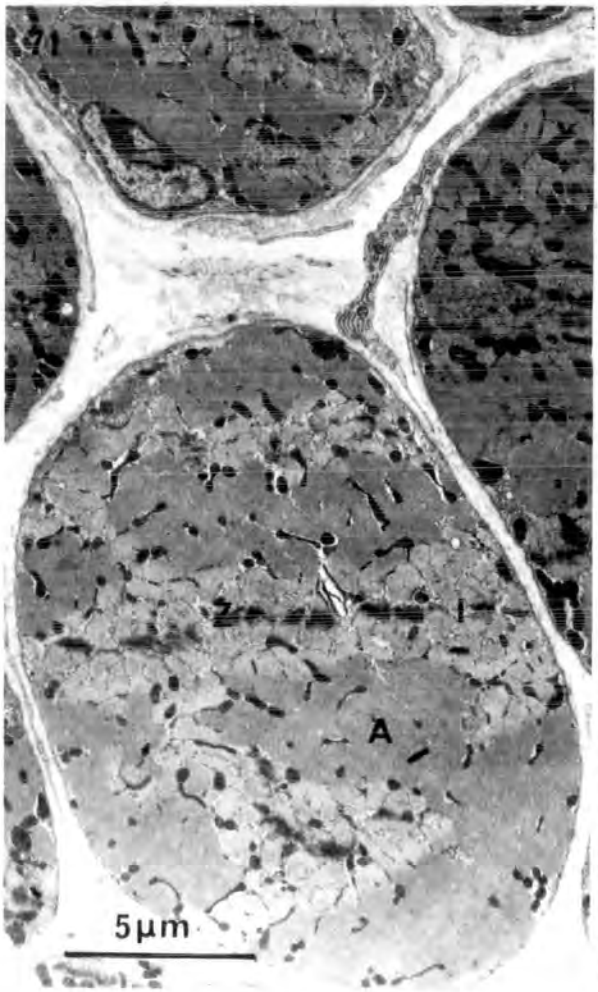
71
Z
I
A
5µm

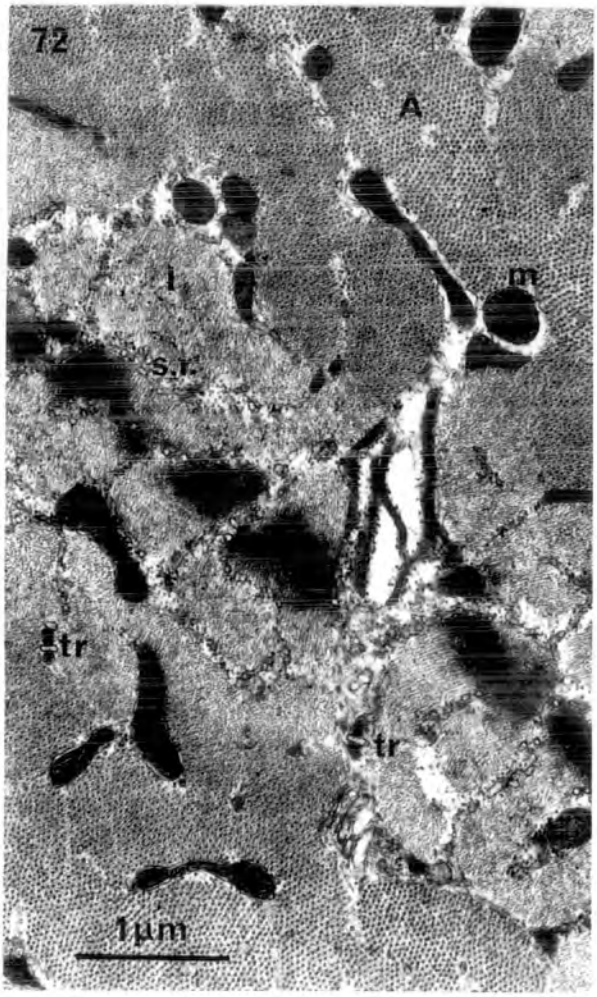
72
A
I
m
S.r.
tr
tr
1µm

Figures 73 to 75. Electron micrographs of transverse sections of 'tubular aggregates' in the orbital rim of SR.

Fig. 73. Low-power T.S. showing an extremely small-diameter G fibre (g) with 'tubule aggregates' (tub.); large C fibres (C) with subsarcolemmal aggregates of large mitochondria; small C fibres (c); and a blood capillary (cap.).

x 5,000

Fig. 74. Part of small G fibre in fig. 73 at higher magnification. Note the aggregation of regular, tubule-like structures (tub.) underneath the sarcolemma; and the triads (tr) cut in transverse section.

x 20,000

Fig. 75. 'Tubule aggregates' at high magnification.

x 80,000

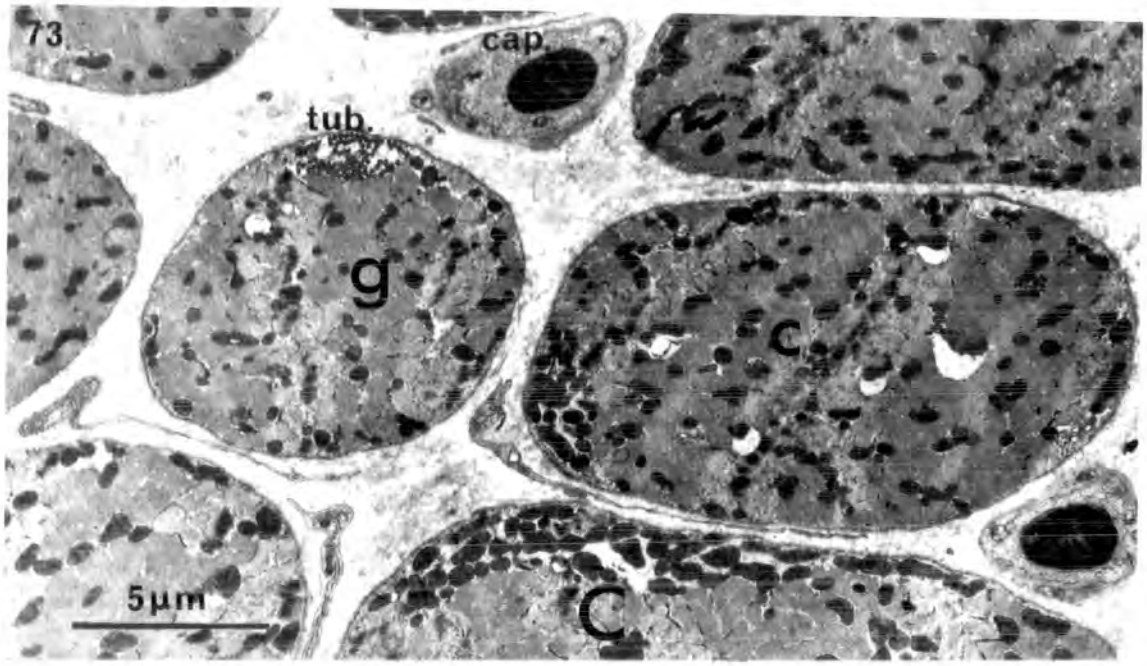
73
cap
tub.
g
c
C
5µm

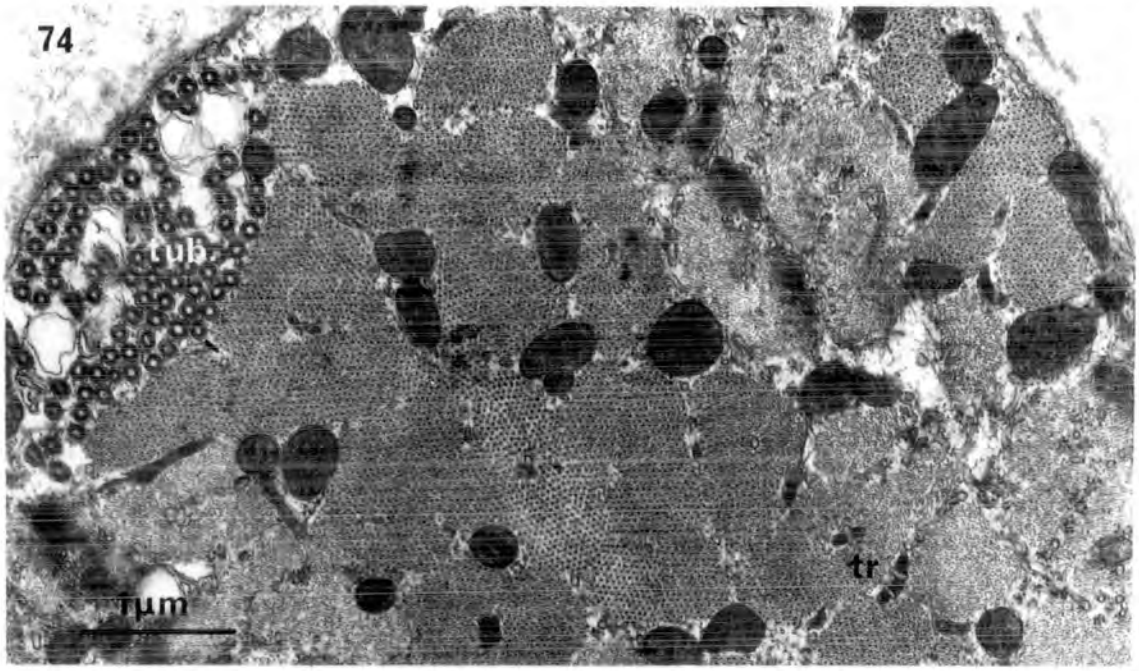
74
tub.
tr
1µm

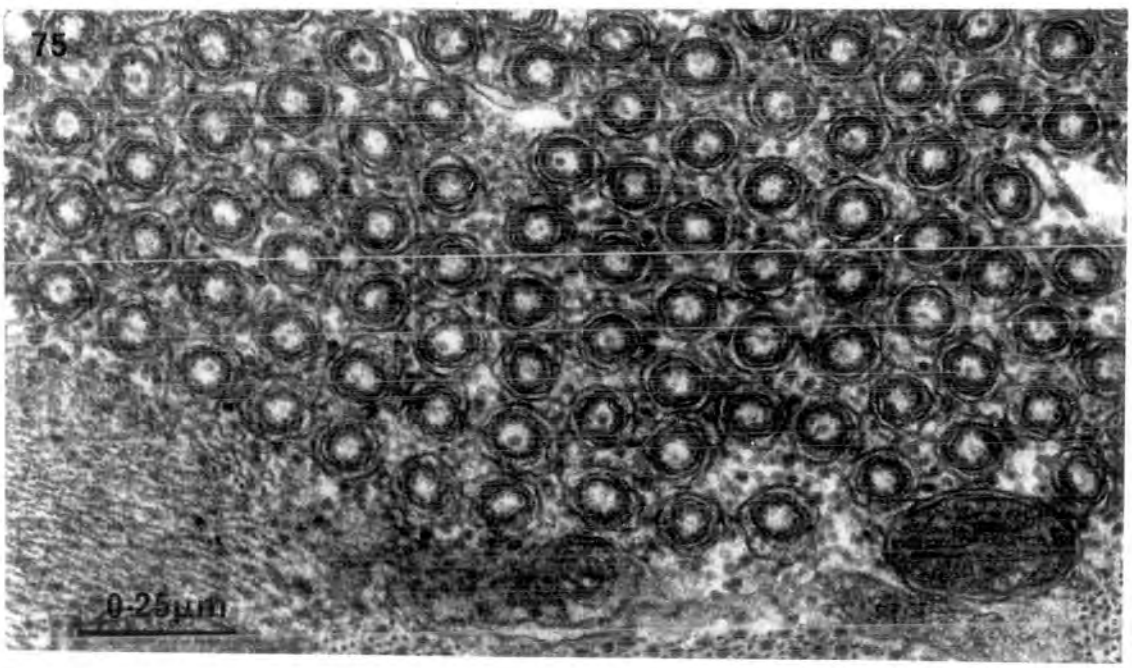
75
0·25µm

Figures 76 to 78. Electron micrographs of transverse sections of the peripheral patch layer at the insertion end of SR.

Fig. 76. A low-power T.S. of the peripheral patch layer showing the medium- to large-diameter G fibres (g) that are separated by connective tissue (conn. tissue). Note the unmyelinated nerve fibres (arrows) close to the surface of one of the G fibres; and the blood capillaries (caps.).

x 2,000

Fig. 77. Intermediate G fibre of peripheral patch layer. Note the small, numerous mitochondria (m) scattered evenly throughout the transverse section; the generally homogeneous appearance of the fibre; and the Z line (Z).

x 5,000

Fig. 78. Part of above fig. 77. at higher power showing the poor delineation of myofibrils in the I band (I) by tubules of sarcoplasmic reticulum; the lack of any delineation of myofibrils in the A band (A); the small mitochondria (m) with only few cristae.

x 20,000

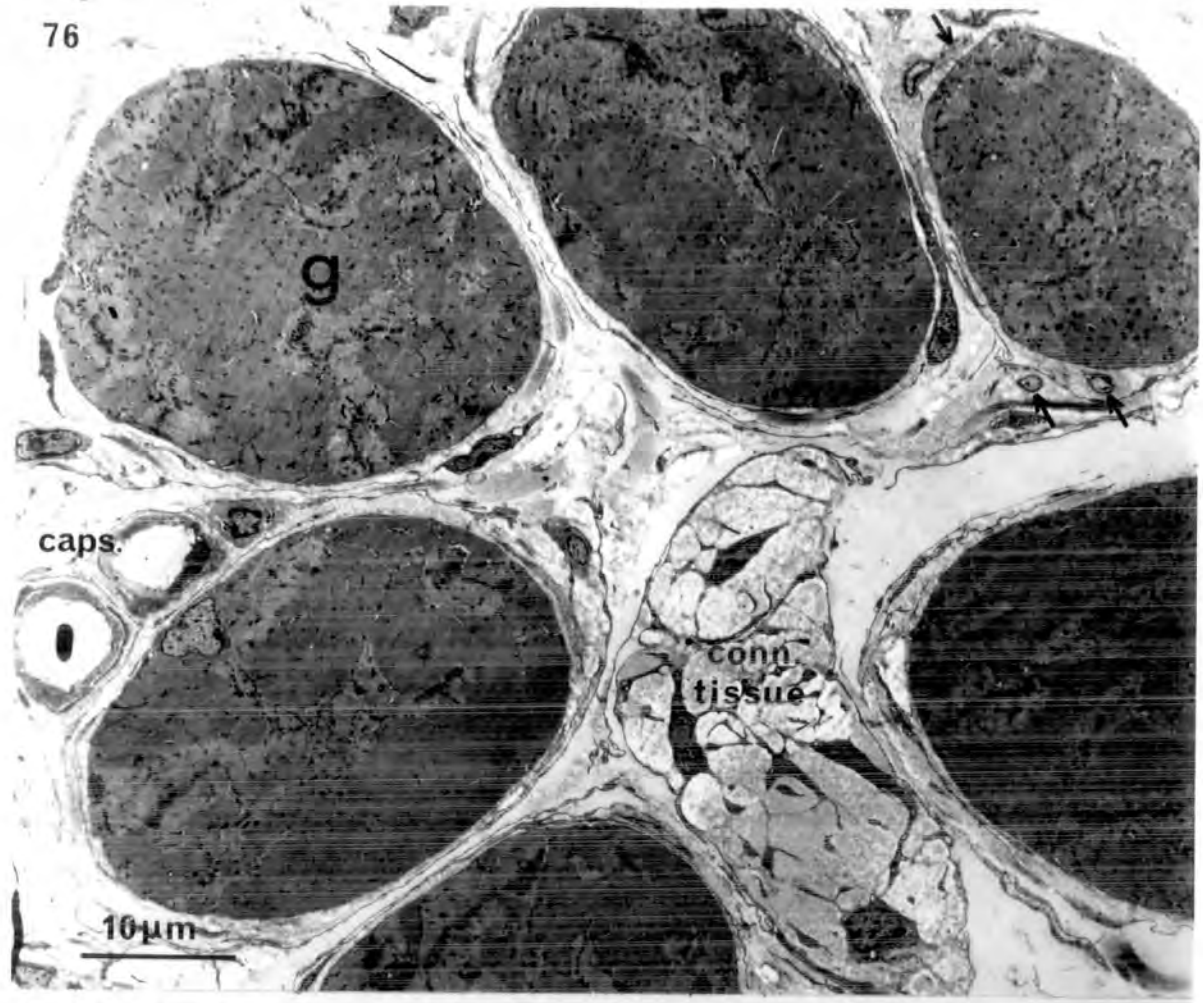
76
g
caps.
conn.
tissue
10µm

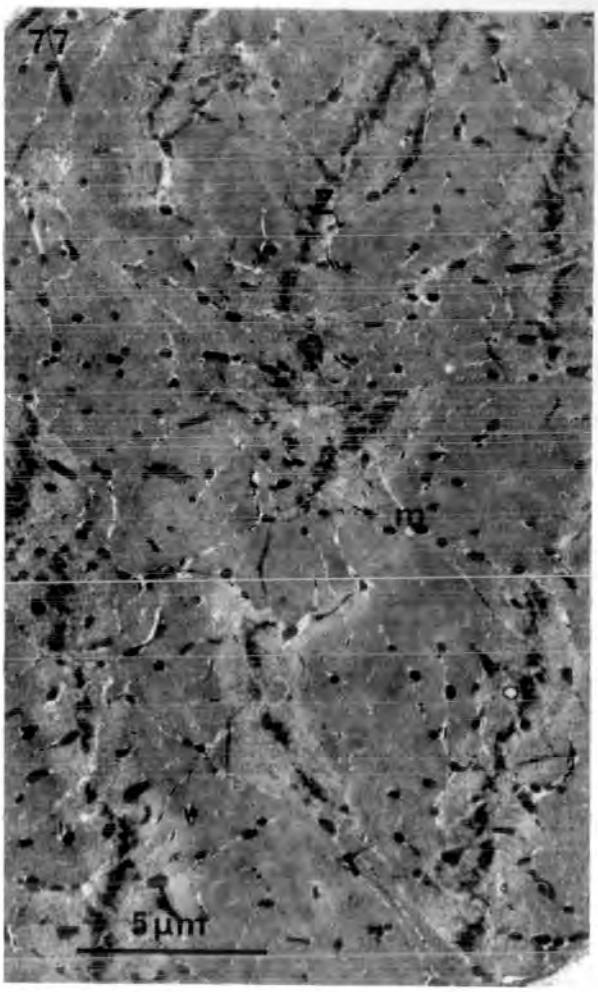
77
m
5µm

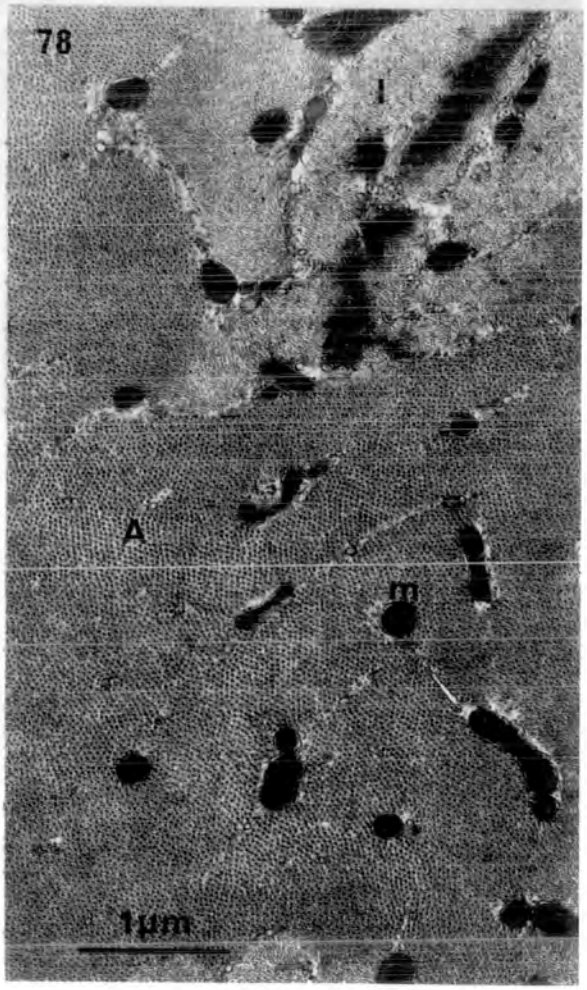
78
I
A
m
1µm

Figures 79 to 80. Electron micrographs of longitudinal sections of intermediate G fibres from the peripheral patch layer at the insertion end of SR.

Fig. 79. At low magnification note the small mitochondria (m); the irregular and infrequent triads (tr); the thick, wavy Z line (Z); the poorly-developed sarcoplasmic reticulum (s.r.); and the absence of an M line from the middle of the A band.

x 20,000

Fig. 80. One sarcomere of an intermediate G fibre. There is a clear pseudo-H zone (marked by lines); a thick Z line (Z) with Z filaments; and moderate amounts of glycogen granules (G1) associated with the sparse sarcoplasmic reticulum.

x 50,000

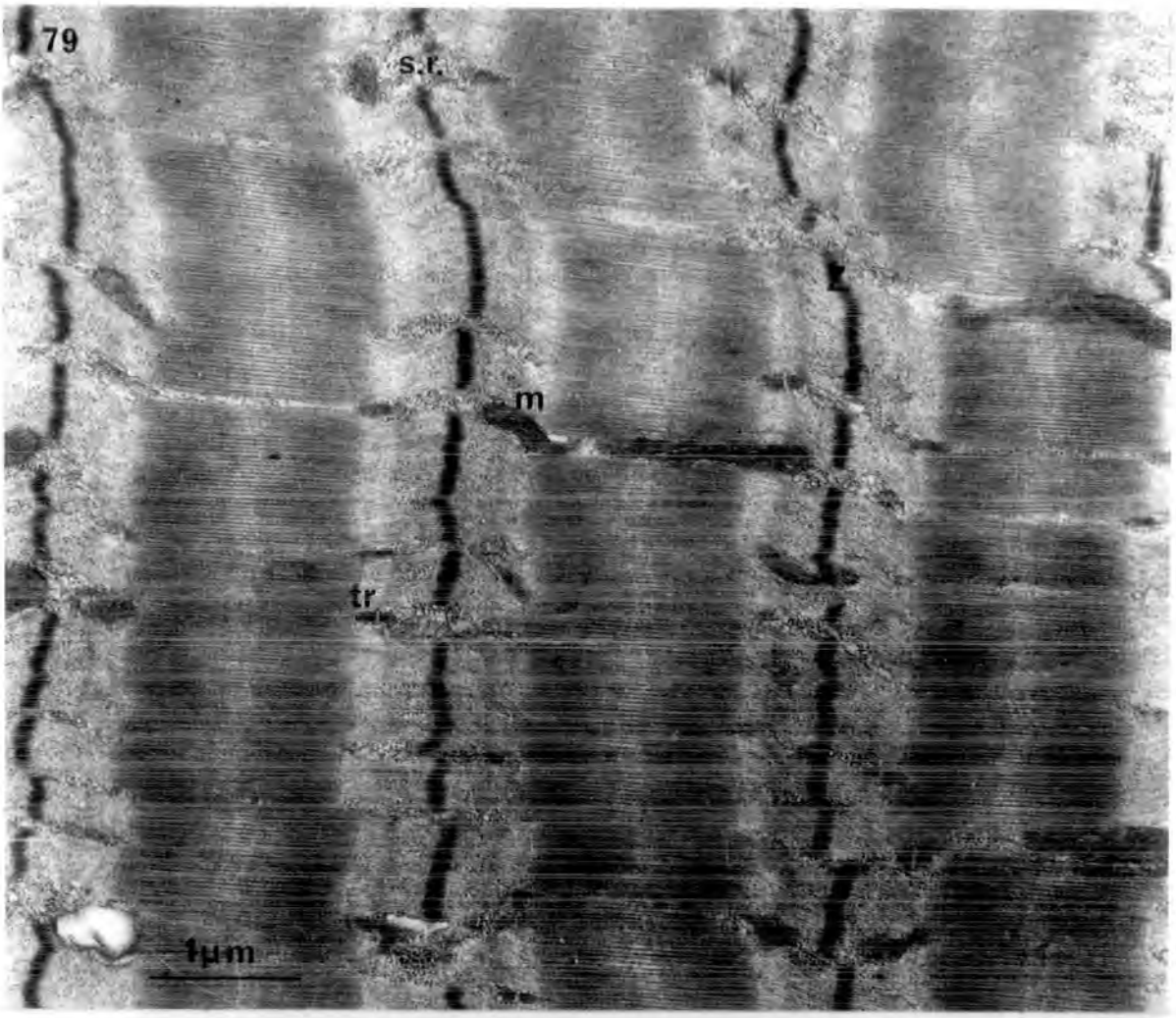
79
s.r.
m
tr
1µm

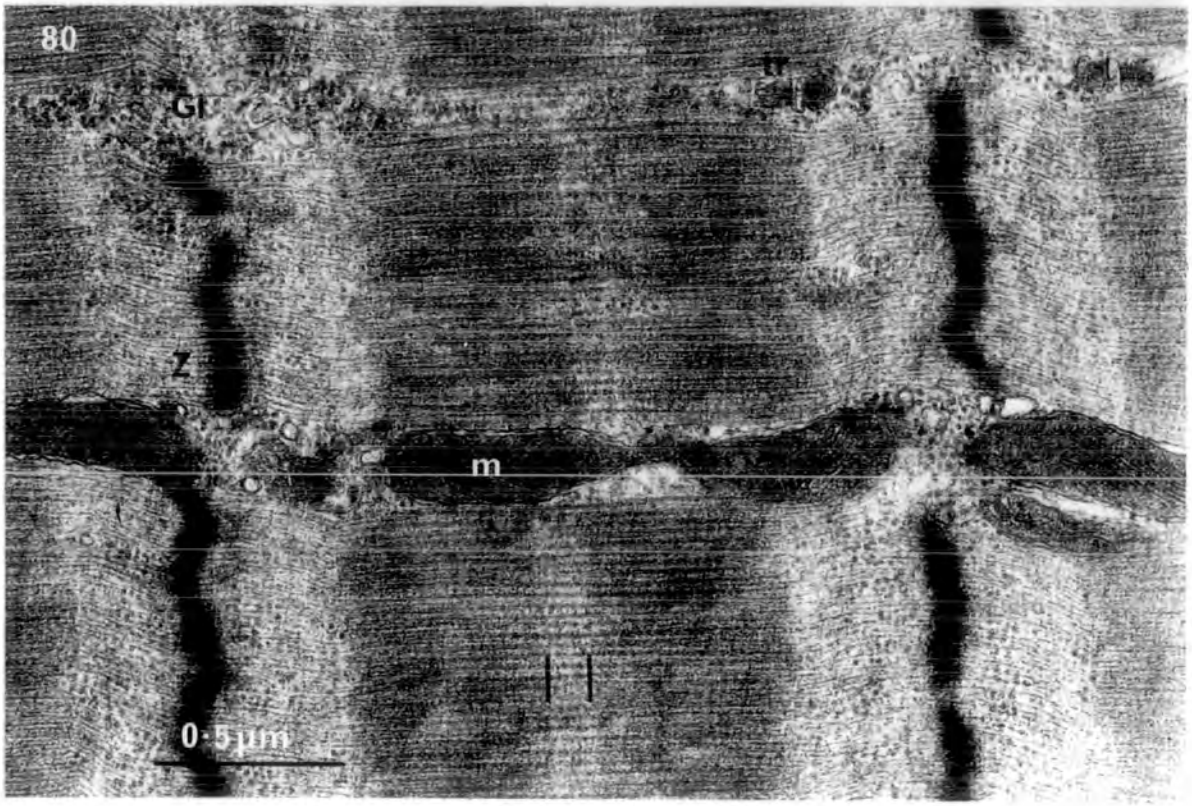
80
tr
GI
Z
m
0·5µm

Figures 81 to 82. Teased, cholinesterase preparations comparing fascicle bundles from SR and LP.

Fig. 81. Superior rectus.
Two clusters of intensely-staining end-plates (e-p's.) are shown with more diffuse grape endings scattered between (starred). The grape endings appear as small specks, of lower intensity than the larger, ovoid end-plates.

Fig. 82. Levator palpebrae.
Clusters of end-plates (e-p's.) are scattered throughout the muscle, as in SR, but diffuse grape endings are not shown.

Figs. 81 and 82 are the same magnification.


81
e-p's
e-p's
0·3mm


82
e-p's
e-p's

Figures 83 to 84. Teased, cholinesterase preparations comparing the pattern of multiterminal grape innervation in a peripheral patch G fibre and a central core G fibre from SR.

Fig. 83. Peripheral patch G fibre.
The extensive chains of cholinesterase-positive droplets form relatively long innervation zones that are irregularly spaced. The fibre divides as it passes toward the belly of SR (top of photomicrograph) and forms two daughter fibres, each smaller in diameter than the parent muscle fibre. That one of the daughter fibres is not an attachment may be seen by the continuity of the muscle fibre banding pattern through the region of division, and also by the absence of any cholinesterase-positive material that is normally present at the end of a muscle fibre.

Fig. 84. Central core G fibre.
The cholinesterase-positive droplets form relatively compact innervation zones (arrows) that are regularly spaced. Division of central core G fibres has not been observed.

Figs. 83 and 84 are the same magnification.

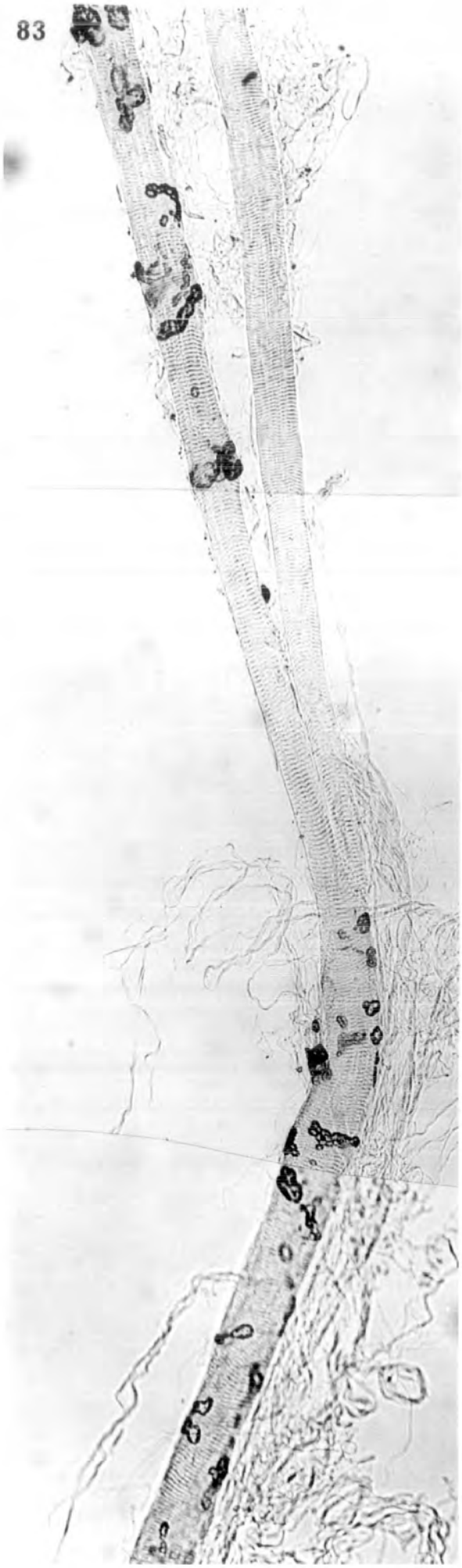
83

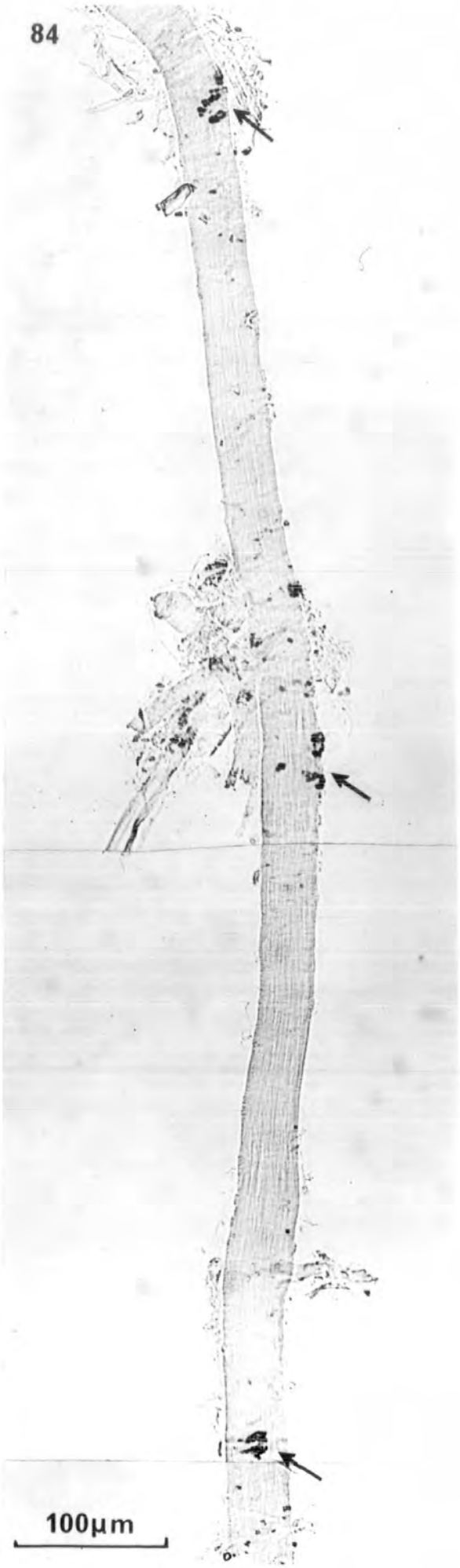
84
100µm

Figures 85 to 89. Teased, cholinesterase preparations from SR.

Fig. 85. Peripheral patch G fibre. Portion of innervation zone. The cholinesterase-positive droplets are of variable size and form. They spiral extensively around the muscle fibre.

Figs. 86 & 88 show central core G fibres with a complete innervation zone. The round or ovoid cholinesterase-positive droplets are relatively small and discrete, and form compact innervation zones.

Figs. 87 & 89. End-plates from muscle fascicles incubated for a short period. The size is comparable to the compact innervation zones of the central core G fibres, but the end-plates are always single and have complex post-synaptic guttering that is clearly visible if the end-plates are not overstained.

Figs. 86 - 89 are all the same magnification.

85

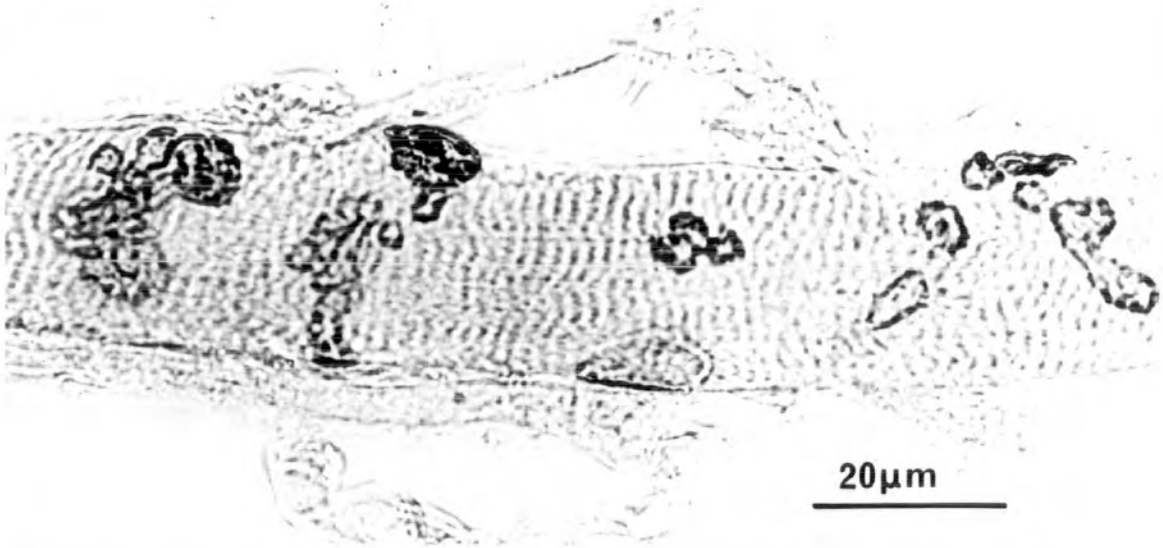

86

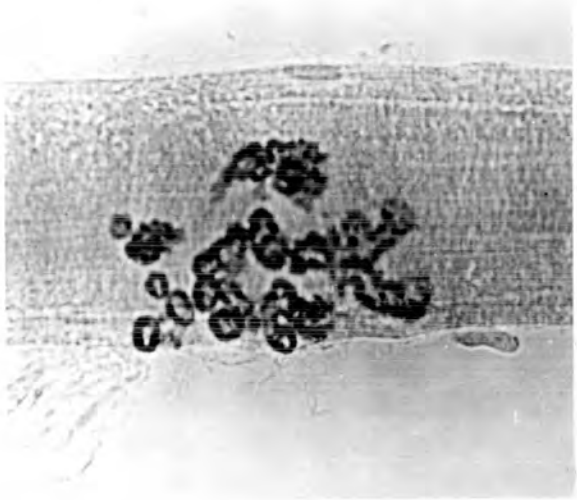

87

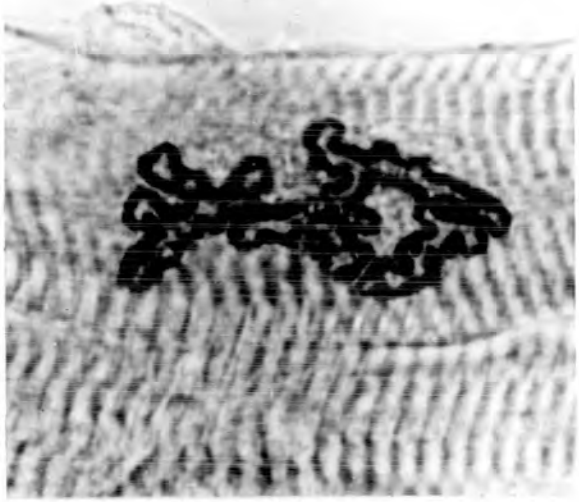

88

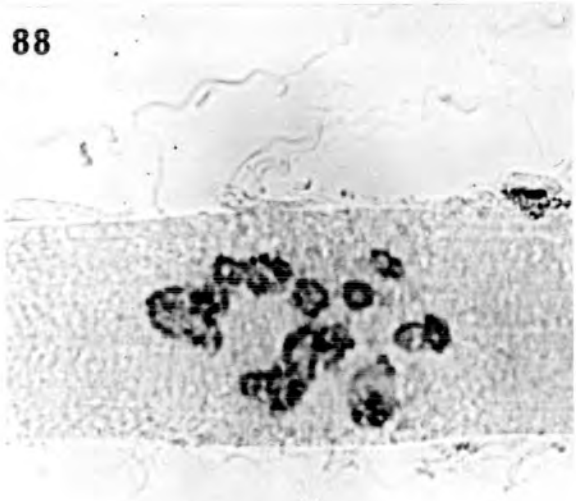

89

Figures 90 to 93. Additional cholinesterase-positive structures found in SR.

Fig. 90. A cholinesterase cuff (Couteaux, 1953).

A palisade of cholinesterase-positive material is located around the end of a muscle fibre at a musculo-tendinous junction. Teased, cholinesterase preparation of a single muscle fibre.

Figs. 91 & 92. Cholinesterase-positive muscle fibre interconnections among the fibres of the peripheral patch and orbital rim layers.

Fig. 91. An attachment with little interposition of tendinous material.

The peripheral G fibre (G) has divided to give a short branch and a continuing fibre that is smaller in diameter. A palisade of cholinesterase-positive material is located around the end of the attached C type muscle fibre (C) and also around the end of the short branch of the peripheral G fibre. The attachment is almost end-to-end with little interposed tendinous material.

Fig. 92. An attachment with the interposition of tendinous material.

The peripheral G fibre (G) forms a buttress-like attachment point and continues as a smaller-diameter fibre. Palisade material is located around the end of the attached muscle fibre and also on the attachment point. The two muscle fibres are separated by an appreciable amount of tendinous material (tend. mat.).

Fig. 93. A fibre divided into two daughter fibres. Cholinesterase preparation.

After cholinesterase staining the banding pattern is not as prominent as with silver staining (fig. 97), but may be traced by using phase microscopy. The palisade of cholinesterase-positive material, normally located at the end of muscle fibres is not present where there is an actual division of the parent muscle fibre.

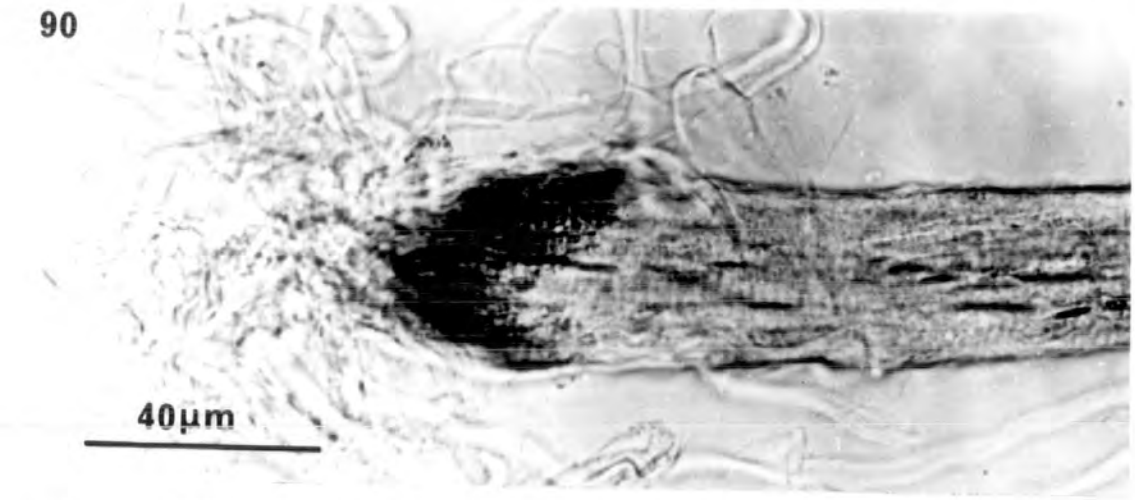
90
40µm

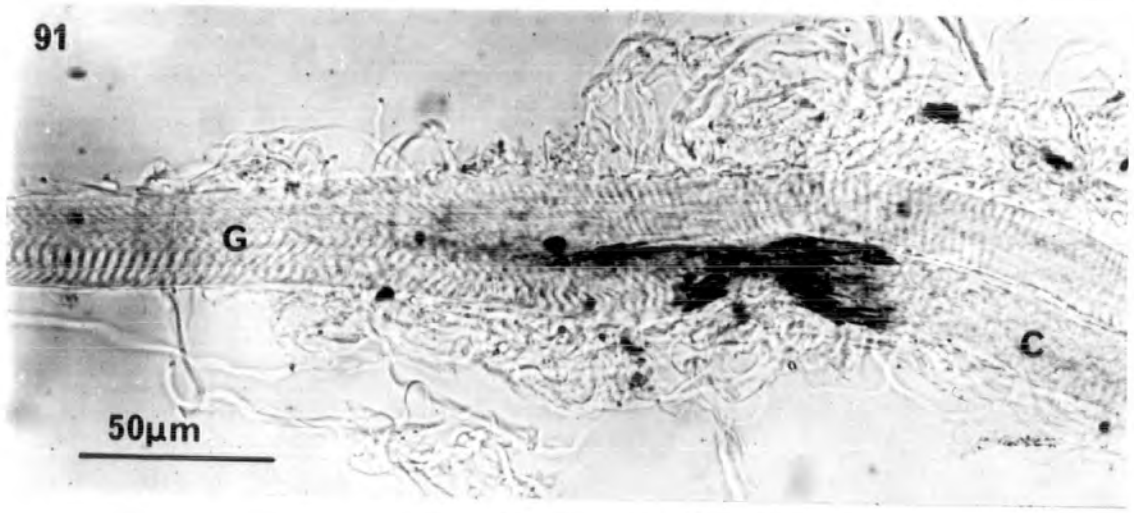
91
G
C
50µm

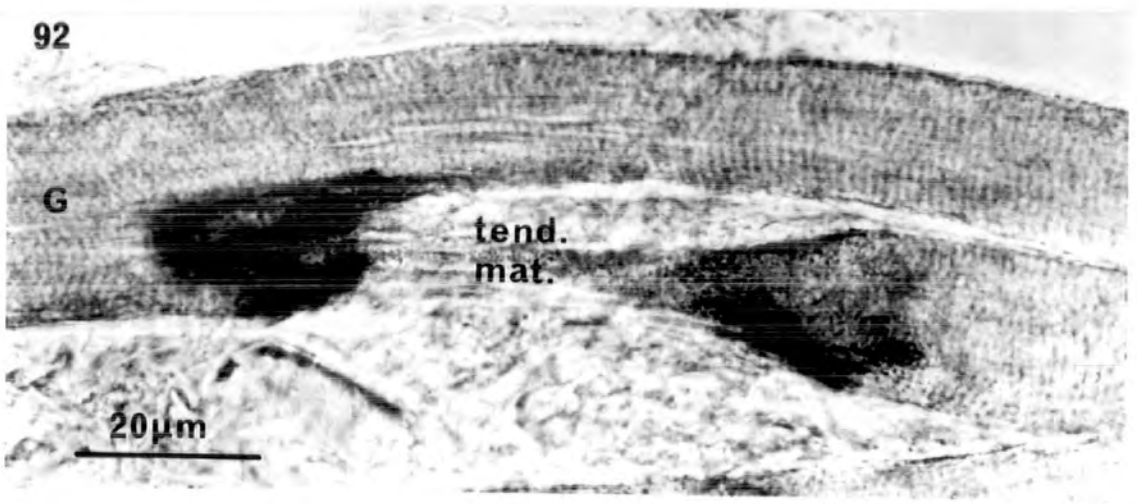
92
G
tend.
mat.
20µm

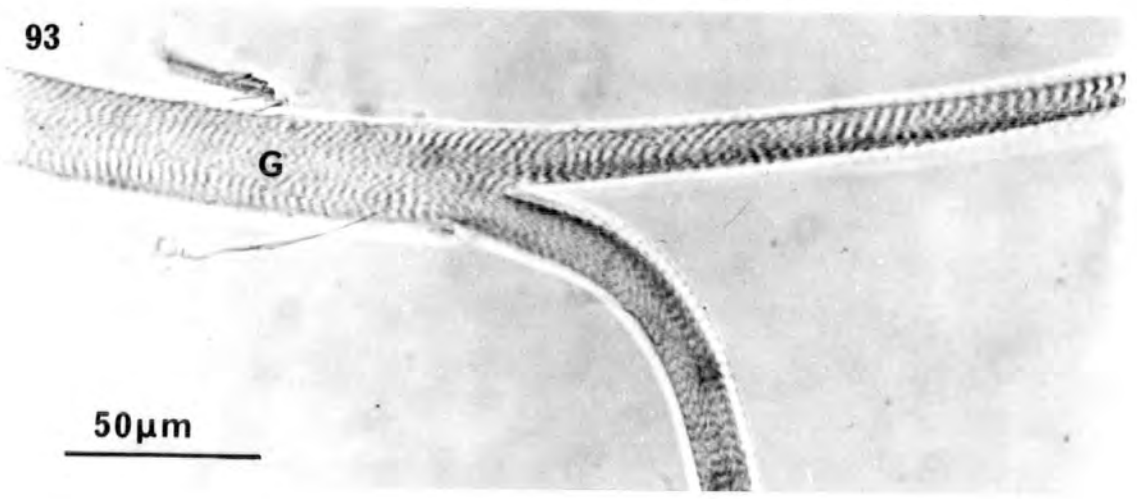
93
G
50µm

Figures 94 to 97. Teased, silver preparations showing the attachments of muscle fibres in the peripheral fascicles of SR.

Fig. 94. An attachment without any buttressing or splitting of the 'parent' muscle fibre. A small C fibre (c) ends in tendinous material (tend. mat.) and is attached to the 'parent' muscle fibre by extensive connective tissue (c.t.).
Barker & Ip silver method.

Fig. 95. An attachment in which the two muscle fibres are closely apposed with only little interposition of tendinous material.
A peripheral G muscle fibre (G) splits to give a buttress attachment point for a type C (C) fibre. Compare with the cholinesterase preparation shown in fig. 91.
Barker & Ip silver method.

Fig. 96. A peripheral G muscle fibre (G) forms a buttress for the attachment of a small C (c) fibre. There is appreciable separation of the fibres by tendinous material and connective tissue (c.t.). Compare with the cholinesterase preparation shown in fig. 92.
Barker & Ip silver method.
Figs. 94 - 96 are the same magnification.

Fig. 97. A peripheral G fibre divided into two smaller-diameter daughter fibres. Overstaining has made the cross striations clearly visible. Note the continuity of the banding pattern from the left of the photomicrograph up to a point immediately prior to the division. Compare with fig. 93.
Barker & Ip silver method.

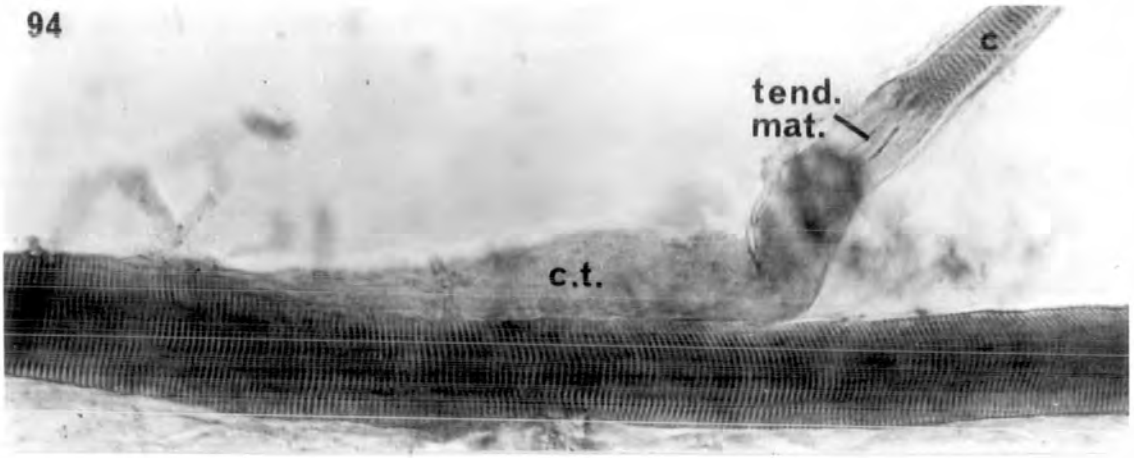
94
c
tend.
mat.
c.t.

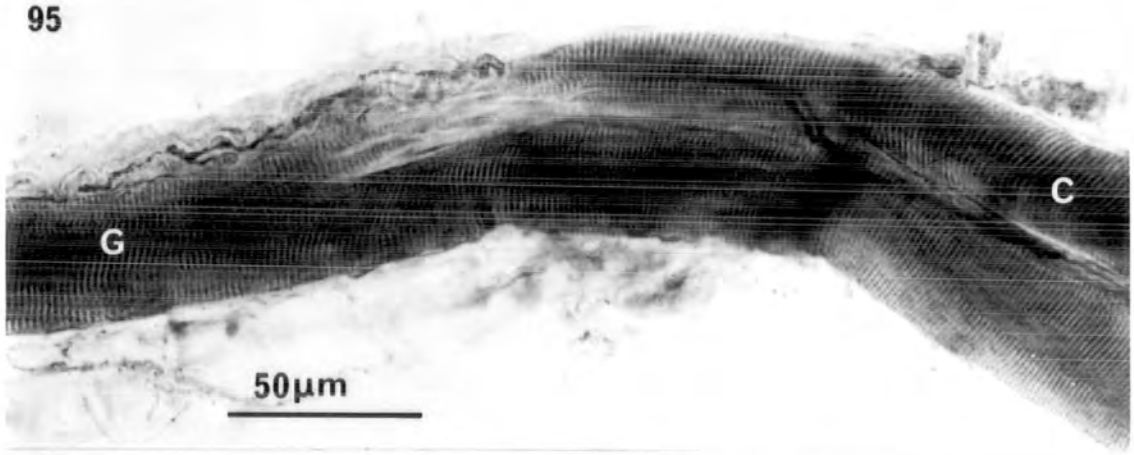
95
C
G
50µm

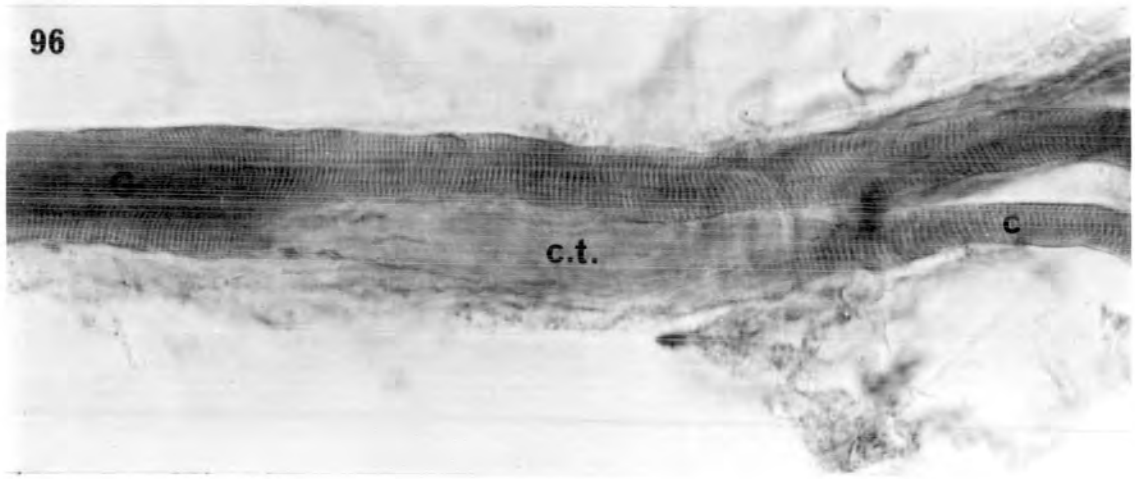
96
c.t.
c

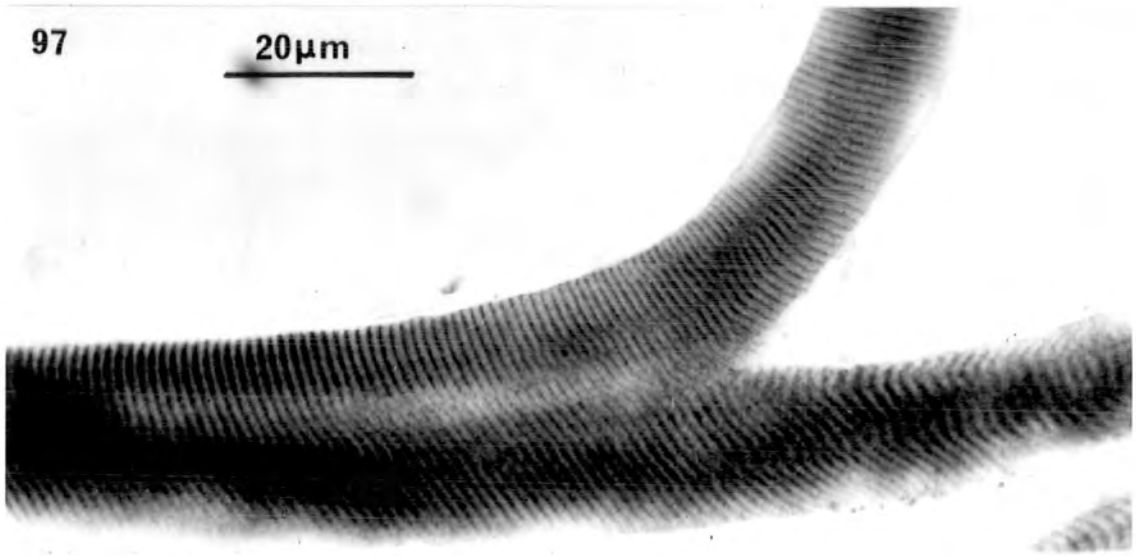
97
20µm

Figures 98 to 100. <u>Teased, silver preparations of extrafusal motor end-plates from SR.</u>

Fig. 98. Groups of motor end-plates (e-p) are derived from small nerve bundles (n.b.) of medium- to large-diameter nerve fibres that pass at 90^{o} over the muscle fibres (m.f.). The 3 end-plates in this particular focal plane are of the T_1 type and are derived from a single, unbranched terminal axon.
Barker & Ip silver method.

Fig. 99. A more complex end-plate configuration in SR shows a T_1 termination with 2 non-myelinated contributions (con) to the end-plate from the first and second pre-terminal nodes of Ranvier. Subsequent myelination of these contributions would provide a T_3 end-plate configuration.
Barker & Ip silver method.

Fig. 100. A T_1 configuration in SR with the terminal axon myelinated within the end-plate region (my.a.). The internode distances are very small and unmyelinated terminal branches leave the nerve at the nodes to give contributions (con) to the end-plate region.
Barker & Ip silver method.

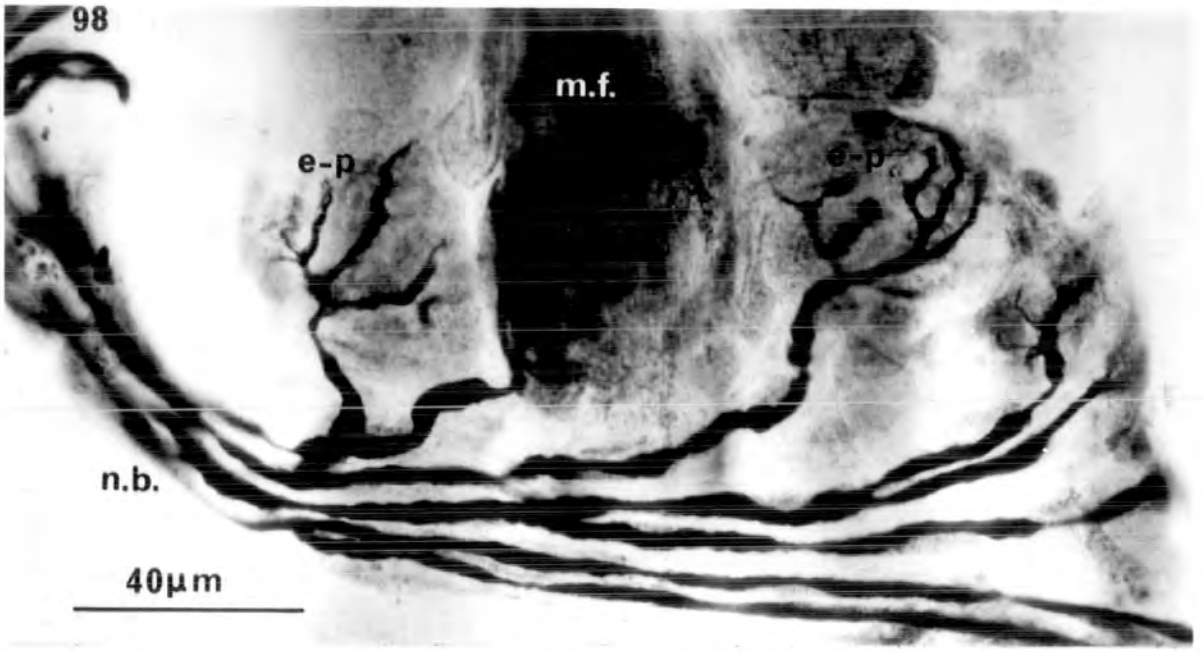
98
m.f.
e-p
e-p
n.b.
40µm

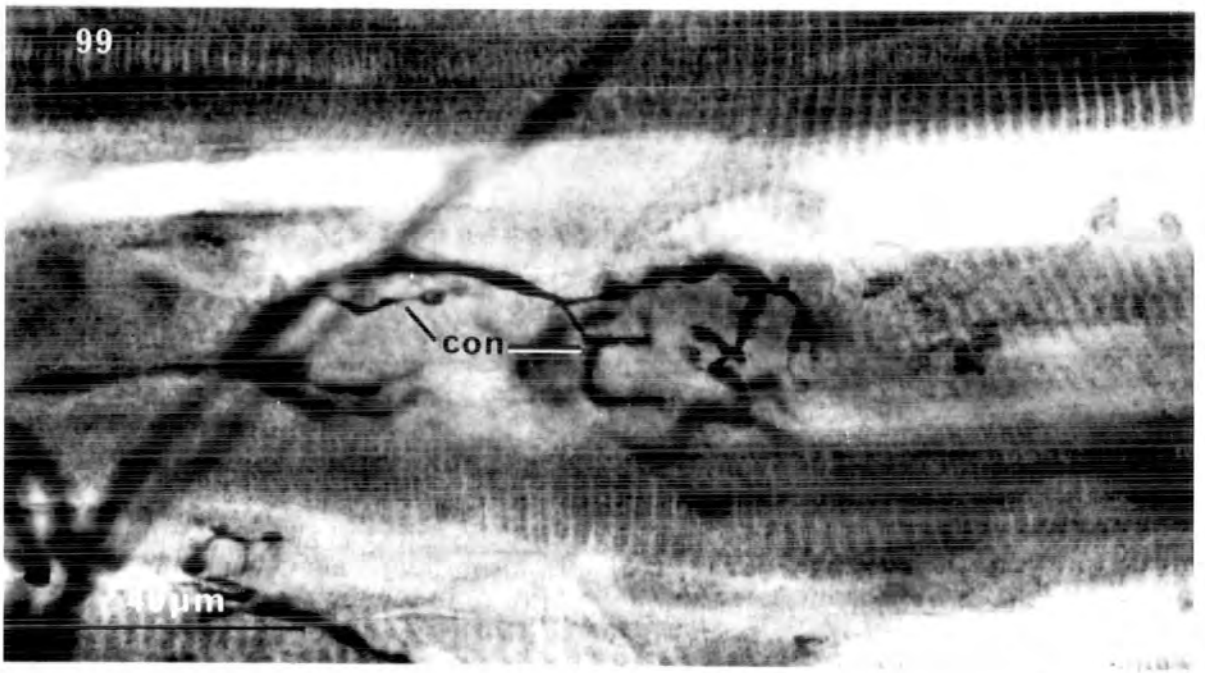
99
con

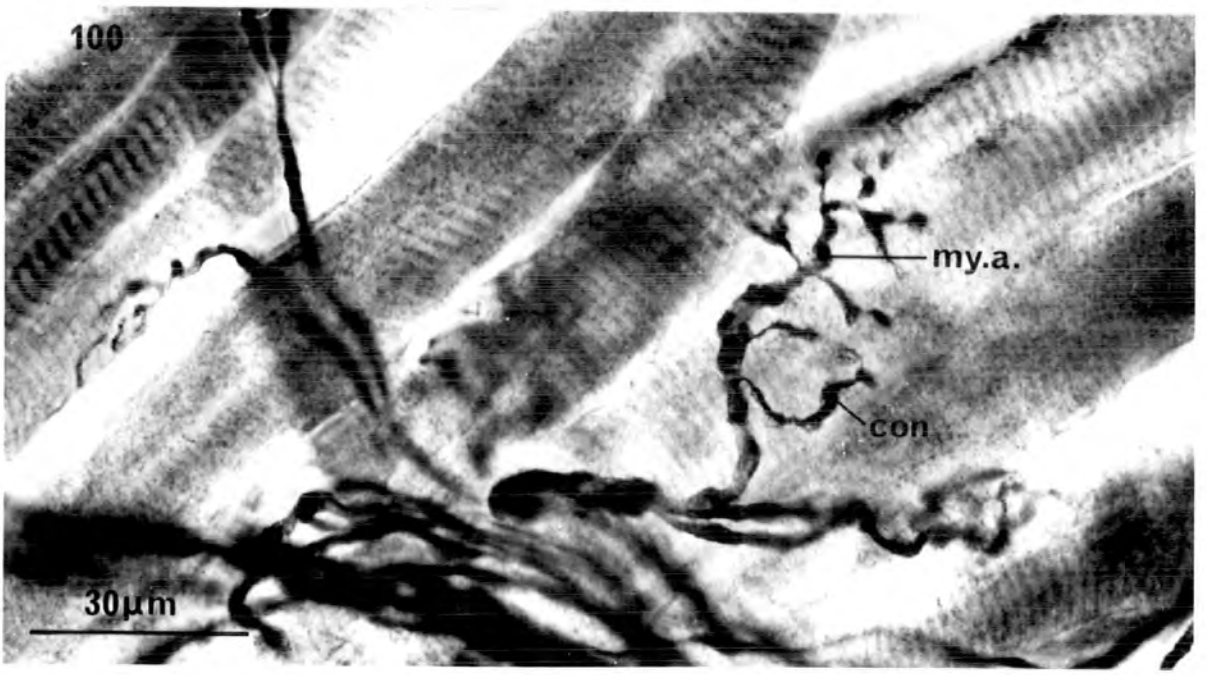
100
my.a.
con
30µm

Figures 101 to 104. Teased, silver preparations of extrafusal motor end-plates from SR illustrating complex configurations.

Fig. 101. A T_2 configuration.
The thickly-myelinated branch (arrow) of a terminal axon (t.a.) supplies the majority of the terminals of the end-plate. The thinly-myelinated branch (star) of the same terminal axon supplies a simple loop ending.

Fig. 102. A T_3 configuration.
Three myelinated branches supply the terminals of the end-plate (the terminals of one branch, marked with a star, are out of the plane of focus).

Fig. 103. A T_2 configuration.
Two myelinated branches from a terminal axon (t.a.) form two end-plate-like regions on the same muscle fibre (m.f.).

Fig. 104. A T_4 configuration.
The end-plate is supplied by four myelinated branches from a single terminal axon. The muscle fibre supplied by the end-plate is from the orbital rim layer and is of relatively small diameter.

Figs. 101 - 104 are all the same magnification.

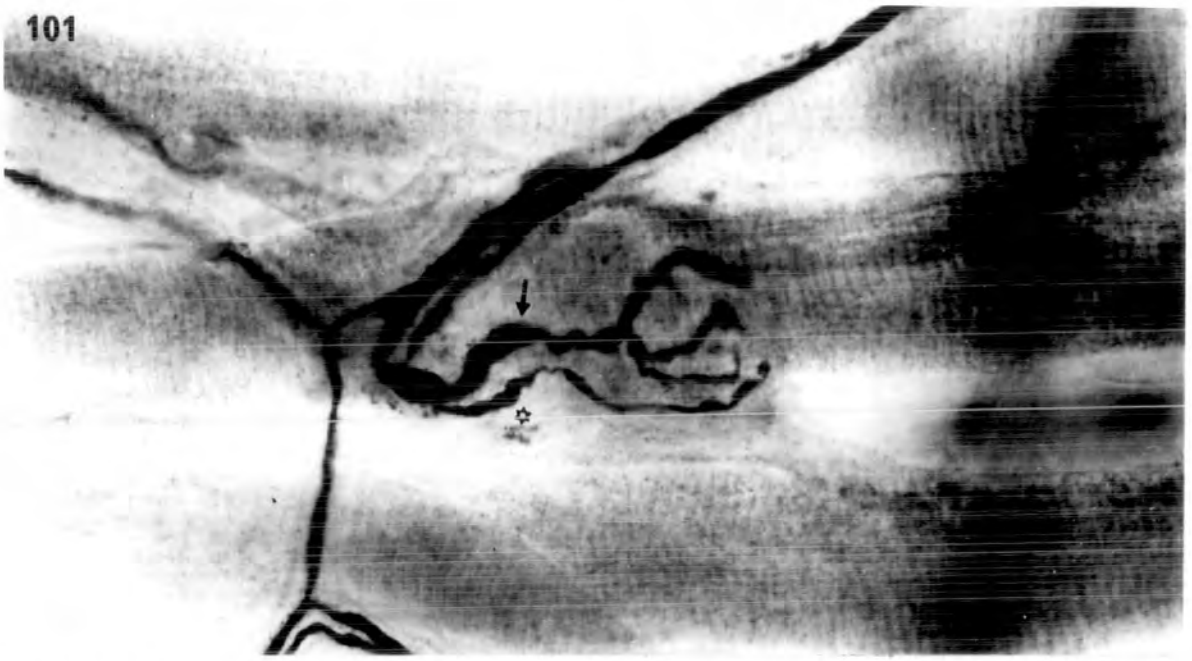
101

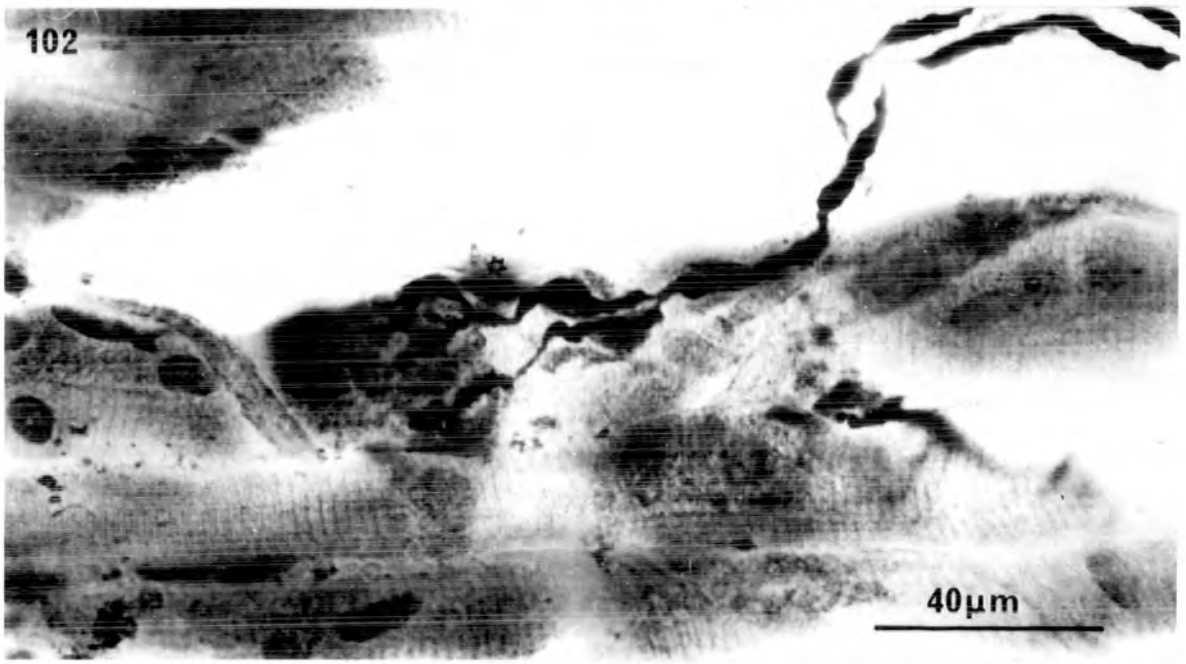
102
40µm

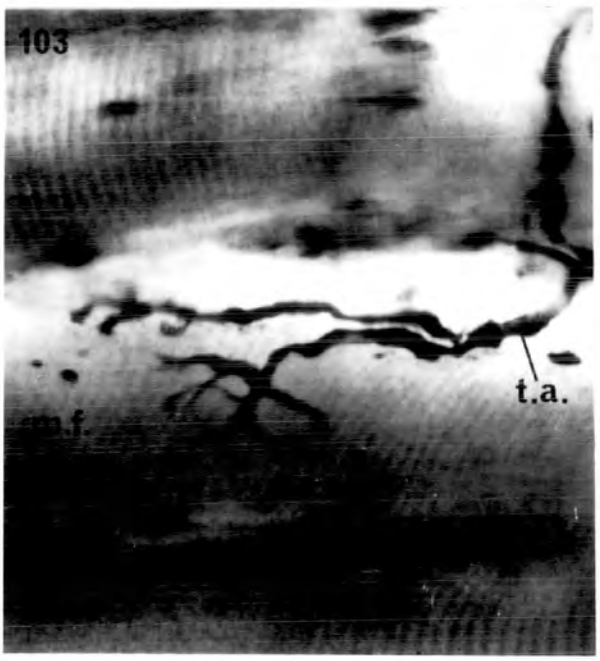
103
t.a.
m.f.

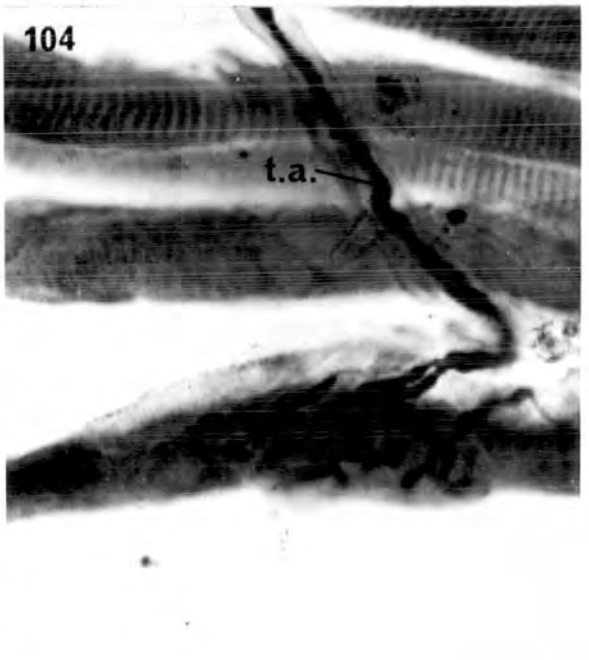
104
t.a.

Figures 105 to 107. Teased, silver preparations of extrafusal grape endings from the peripheral patch layer at the insertion end of SR.

Fig. 105. Compact grape terminations in the peripheral patch layer. A thinly-myelinated axon supplies non-myelinated terminal fibrils that branch repeatedly to form axoplasmic swellings and loop endings.

Fig. 106. Linear grape terminations in the peripheral patch layer. The thinly-myelinated axon passes along the muscle fibre for a considerable distance before finally terminating on it. At regular intervals non-myelinated branches are given off which form small knob-like endings. The terminal portion of the axon progressively loses its myelin and forms axoplasmic swellings at regular intervals.

Fig. 107. Compact grape configuration (on the right) and linear grape configuration (on the left) that are both derived from a common stem axon. A classic 'bunch of grapes' termination is shown (arrow) among the linear endings.

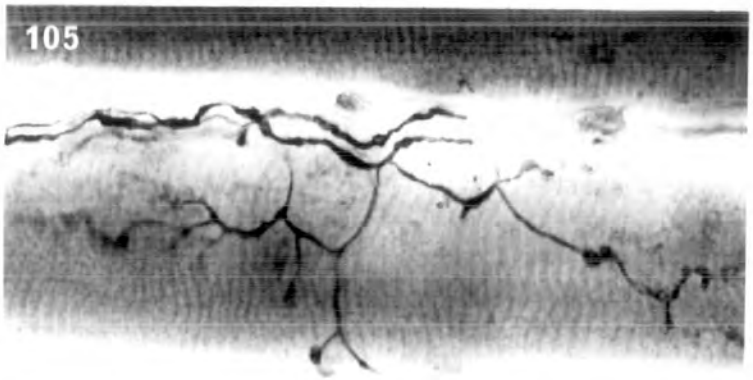

40µm

40µm

Figures 108 to 111. Teased, silver preparations of extrafusal grape endings from the peripheral fascicles of SR.

Fig. 108. Compact grape terminations on a large-diameter fibre from the peripheral patch layer at insertion end of SR.

Fig. 109. Linear grape terminations on a peripheral patch G fibre that has branched to give a short attachment point (att. p.) and a continuing, smaller-diameter G fibre. The thinly-myelinated axon supplies four non-myelinated terminal fibrils to the muscle fibre.

Figs. 110 & 111. Linear grape terminations on small-diameter muscle fibres from the orbital rim layer of SR.

Figs. 108 - 111 are all the same magnification.

108

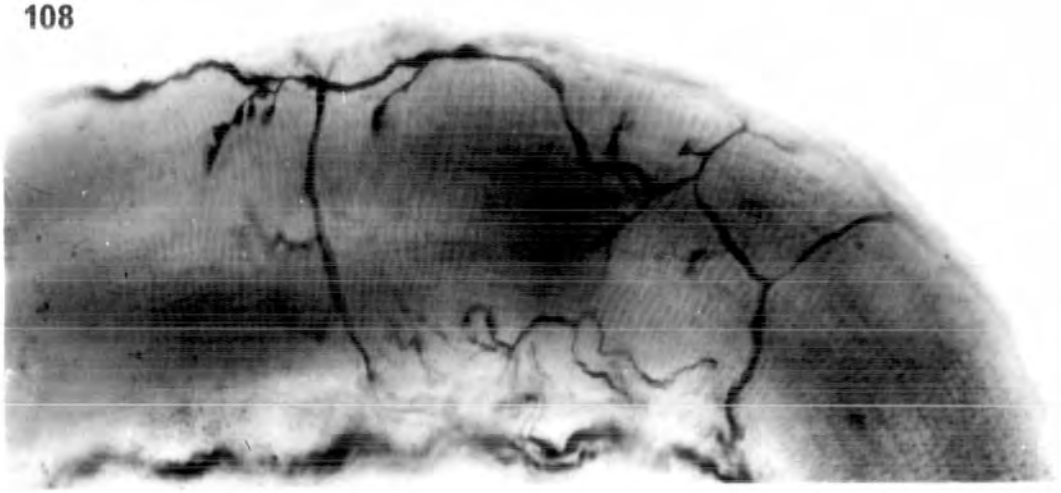

109

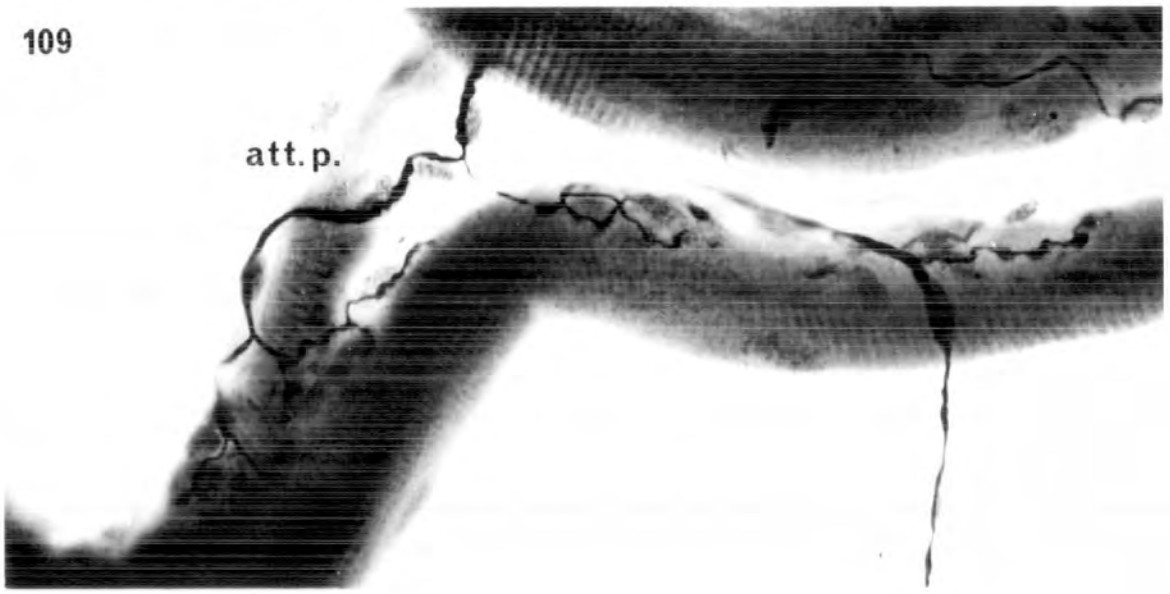

110

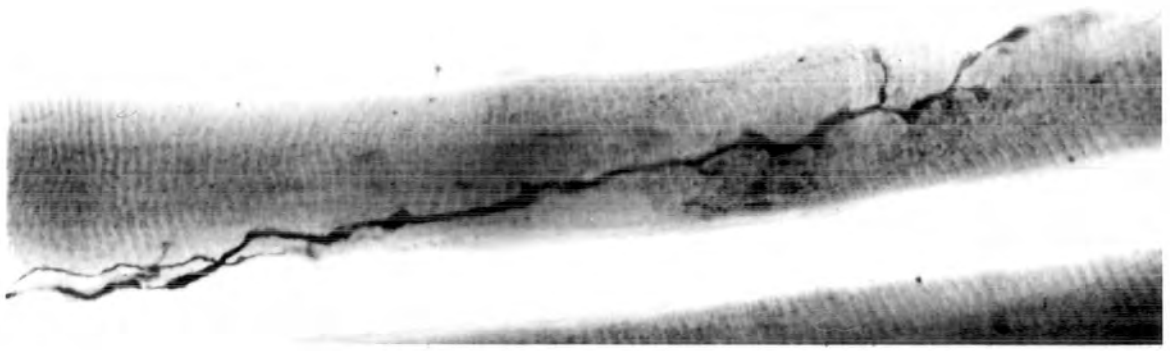

111

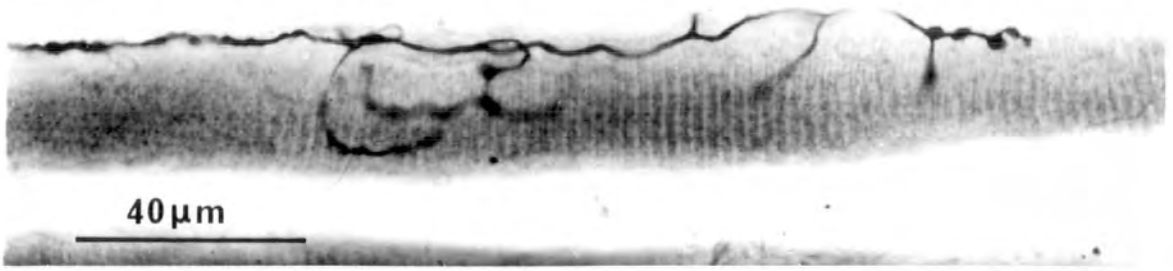

Figures 112 to 116. <u>Teased, silver preparations of extrafusal grape endings from the central core layer of SR.</u>

Figs. 112 - 114 show the same central core grape ending in three different planes of focus. A thinly-myelinated stem axon (s.a.) spirals around the muscle fibre and branches to give fine terminals that end in axoplasmic knobs and swellings (arrows). There are several nuclei (n) within the compact innervation zone. The stem axon leaves (star) to innervate other central core G fibres.

Figs. 115 - 116. Grape endings in the central core layer that show extremely fine terminals some of which end in loops (arrow). The underlying muscle fibres are among the largest in diameter in the central core layer.

Both figs. are the same magnification.

112

113

114

115

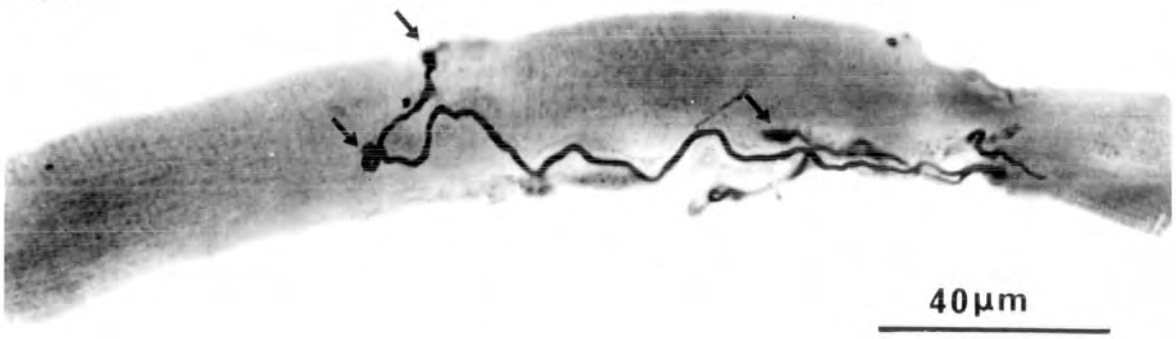

116

Figures 117 to 120. Teased, silver preparations of extrafusal grape endings from the central core layer of SR.

Fig. 117. Compact, 'plate-like' grape endings in the central core layer.
The terminals of the ending on the right resemble those of a classic motor end-plate and similarly lie among nuclei (n). However, the diameter of the stem axon is small and the muscle fibre is multiterminally innervated. The endings on the left (arrowed) are, in fact, derived from the same parent axon as the ending on the right.

Figs. 118 - 120 show a central core grape ending at three different planes of focus.
The thinly-myelinated stem axon spirals around the muscle fibre before terminating in coarse knobs (arrows). Compare with figs. 112 - 114.

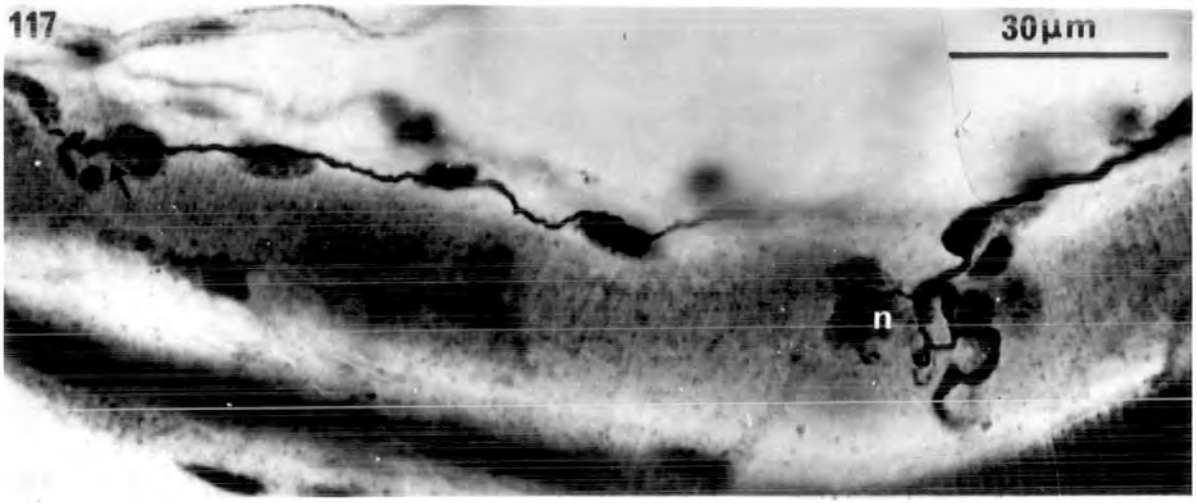

40µm

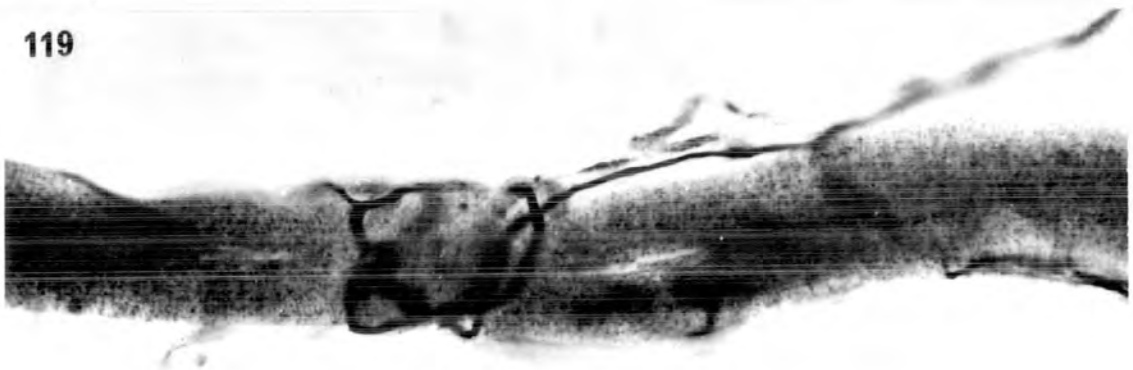

Figures 121 - 123. Electron micrographs of the myoneural junctions of large A fibres in the central core layer of SR.

Fig. 121. Longitudinal section of a myoneural junction on a large A fibre. (Note the M line, straight Z line, abundant sarcoplasmic reticulum, and regular triads.) The axon terminals (a.t.) are elongated and overlie numerous regular junctional folds (j.f.).

x 8,000

Fig. 122. Part of the section above at higher magnification.
The axon terminals (a.t.) contain accumulations of mitochondria (m), synaptic vesicles (s.v.) and neurofilaments (nf). Occasional dense-core vesicles (solid arrowhead) are present. The synaptic cleft is filled with amorphous basement membrane (b.m.) and the post-synaptic membrane (p.s.m.) is electron dense. Junctional folds (j.f.) are long, narrow and usually single, with only occasional expansions at their base (star).

x 20,000

Fig. 123. Compactly-arranged axon terminals (a.t.) located on the raised Doyère's emminence portion of the end-plate region, comprising the sole plate (s.p.) with sole plate nuclei (s.p.n.).

x 5,000

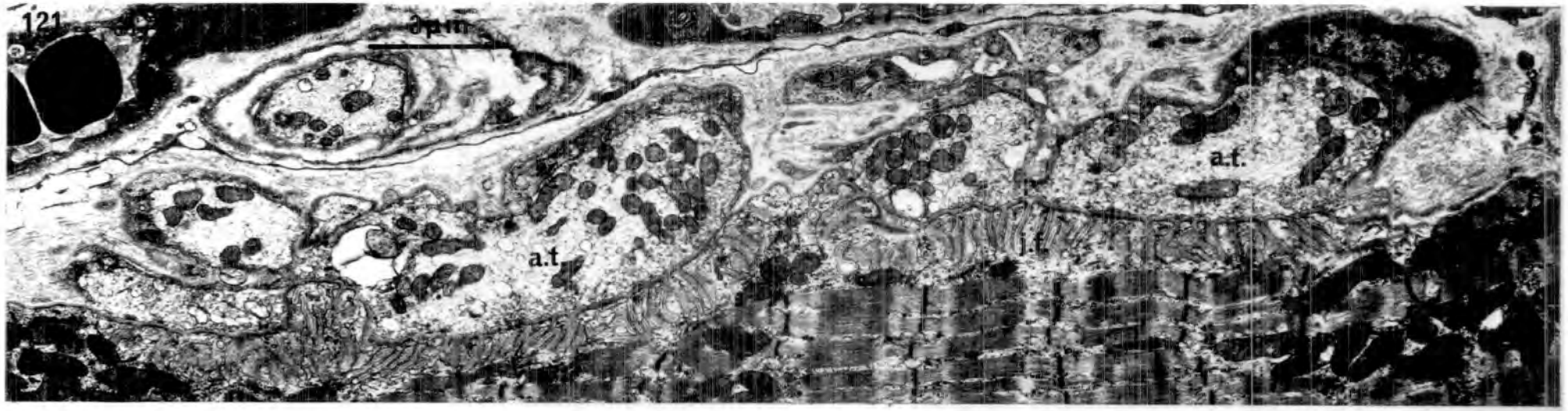
121
3µm
a.t.
a.t.
j.t.

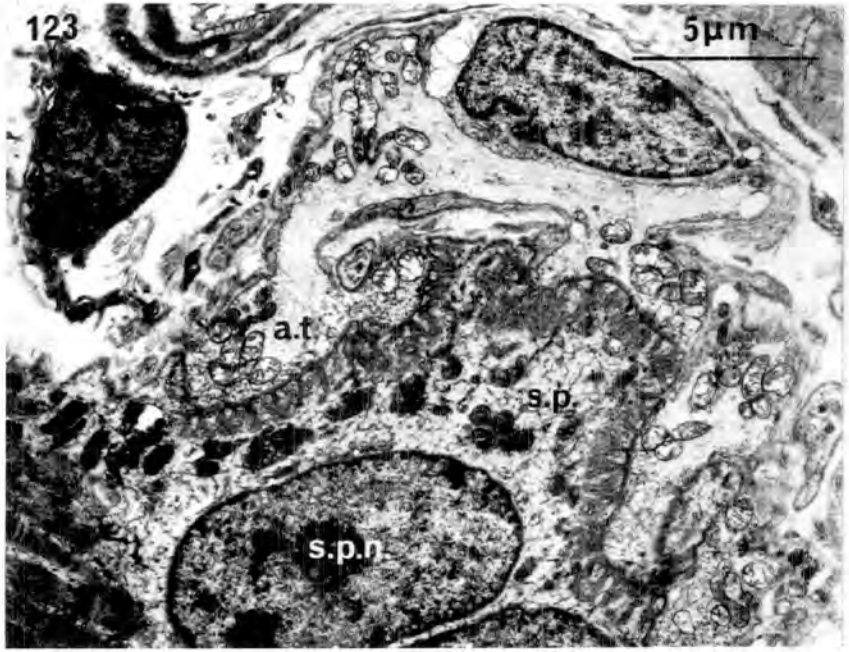
123
5µm
a.t
s.p.
s.p.n

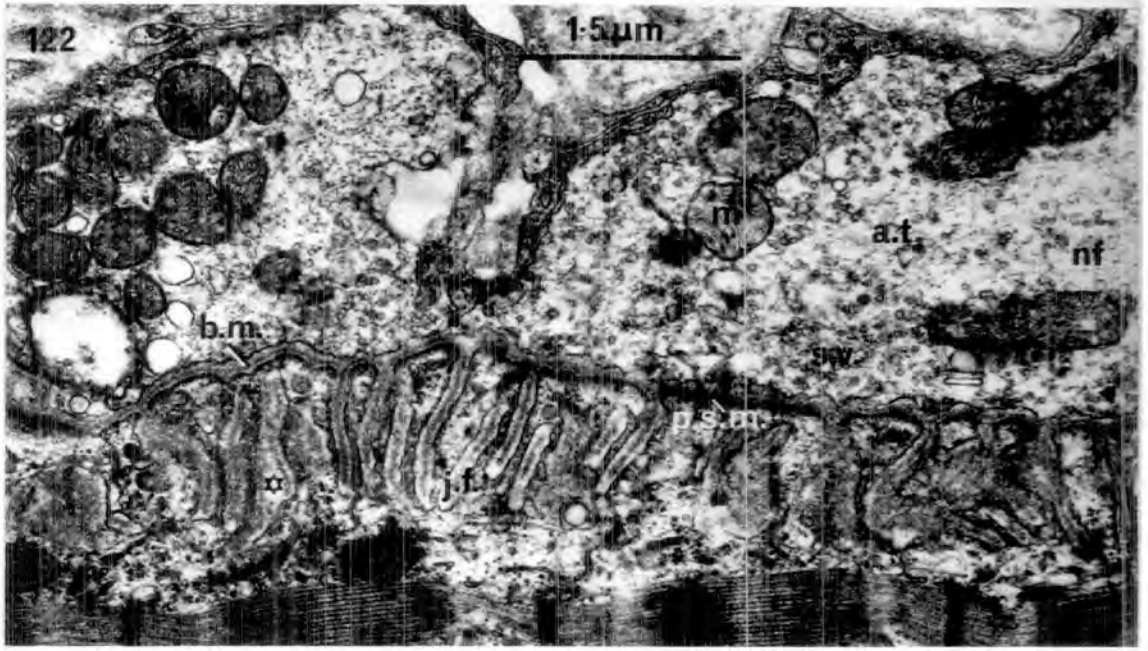
122
1·5µm
m
a.t.
nf
b.m.
s.v.
s.p.
j.t.

Figures 124 to 125. Electron micrographs of a myoneural junction on an intermediate C fibre from the central core layer of SR.

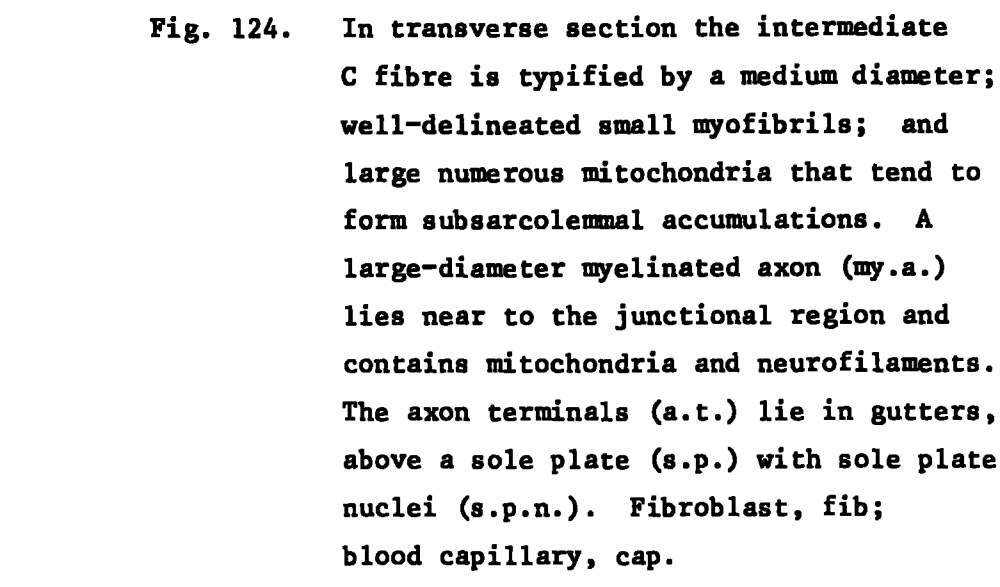

Fig. 124. In transverse section the intermediate C fibre is typified by a medium diameter; well-delineated small myofibrils; and large numerous mitochondria that tend to form subsarcolemmal accumulations. A large-diameter myelinated axon (my.a.) lies near to the junctional region and contains mitochondria and neurofilaments. The axon terminals (a.t.) lie in gutters, above a sole plate (s.p.) with sole plate nuclei (s.p.n.). Fibroblast, fib; blood capillary, cap.

x 5,000

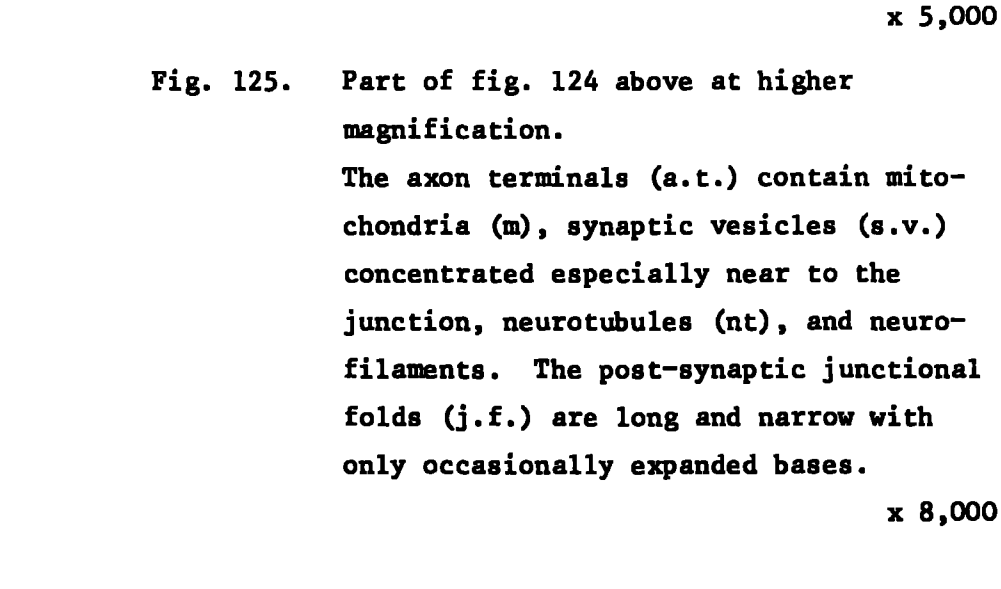

Fig. 125. Part of fig. 124 above at higher magnification.
The axon terminals (a.t.) contain mitochondria (m), synaptic vesicles (s.v.) concentrated especially near to the junction, neurotubules (nt), and neurofilaments. The post-synaptic junctional folds (j.f.) are long and narrow with only occasionally expanded bases.

x 8,000

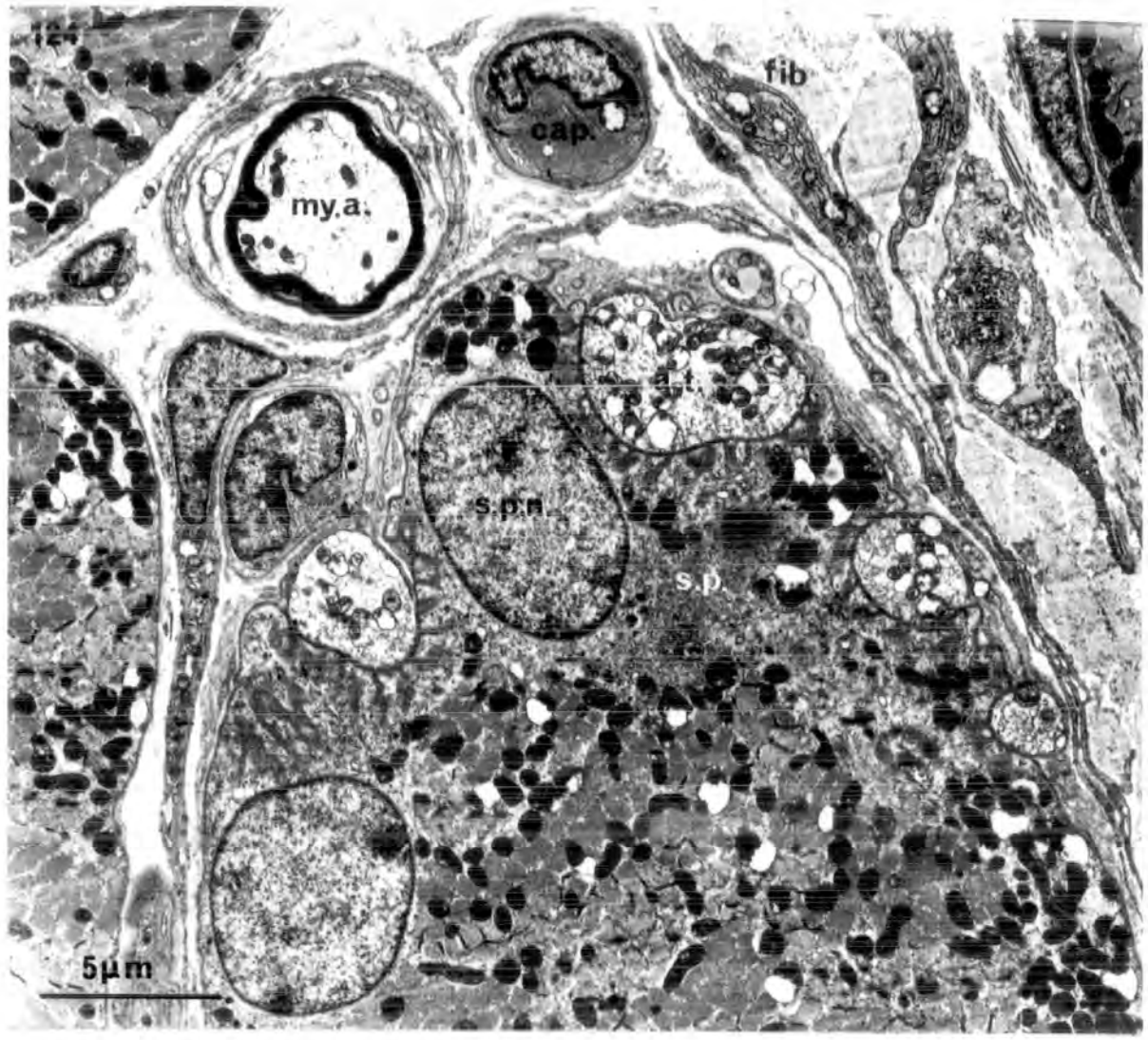
124
fib
cap.
my.a.
a.t.
s.p.n.
s.p.
5µm

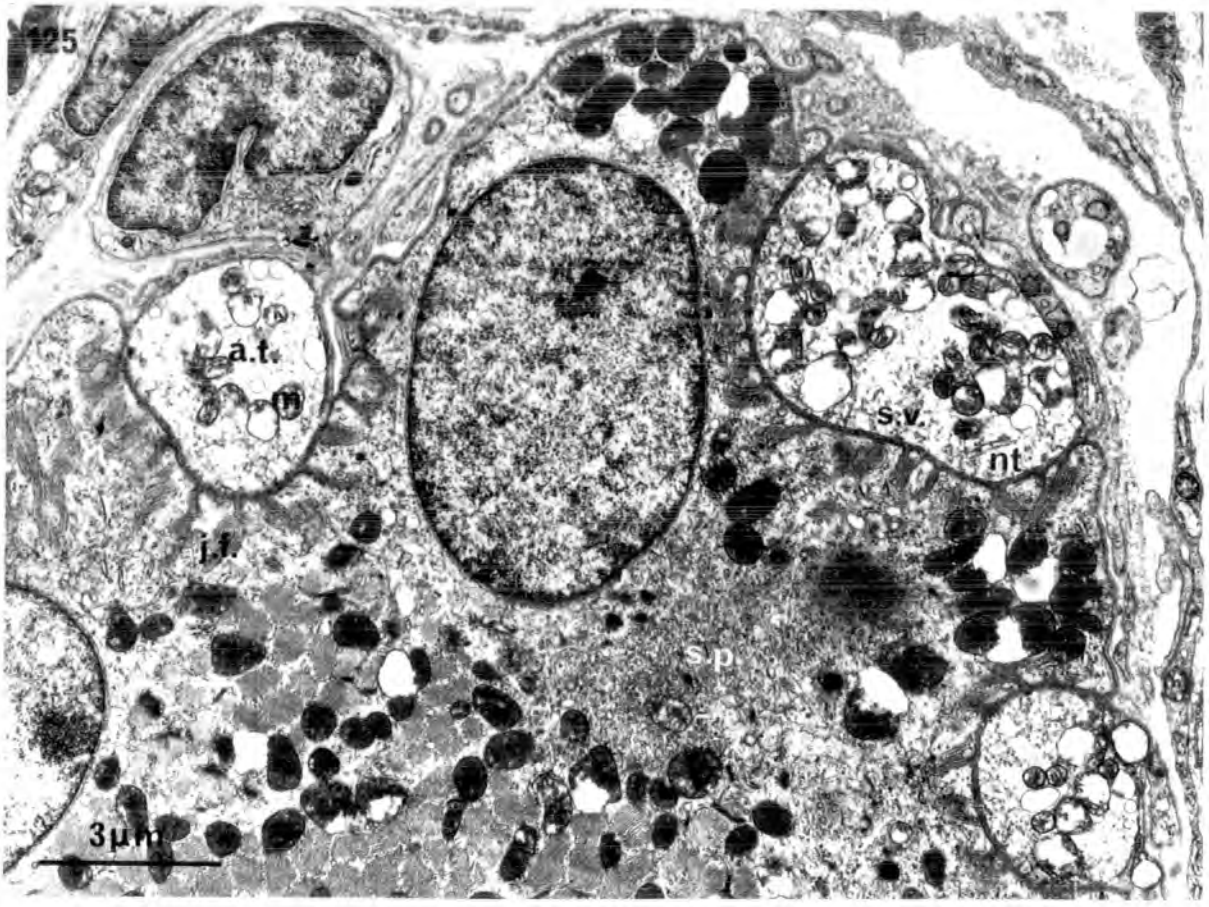
125
a.t.
m
s.v.
nt
i.f.
s.p.
3µm

Figures 126 to 127. Electron micrographs of myoneural junctions on intermediate C fibres from the orbital rim layer of SR.

Fig. 126. Transverse section of a myoneural junction on an intermediate C fibre (medium diameter; small, well-delineated myofibrils; numerous, large mitochondria). The axon terminals (a.t.) lie in gutters, above a sole plate (s.p.) with sole plate nuclei (s.p.n.). Compare with fig. 124.

x 5,000

Fig. 127. Transverse section of an axon terminal applied to an intermediate C fibre. The post-synaptic junctional folds (j.f.) have occasional expanded bases (arrows). The folds appear to be less frequent and regular than those of the large A fibre. Compare with fig. 122. Note the dense-core vesicle (arrowhead).

x 12,600

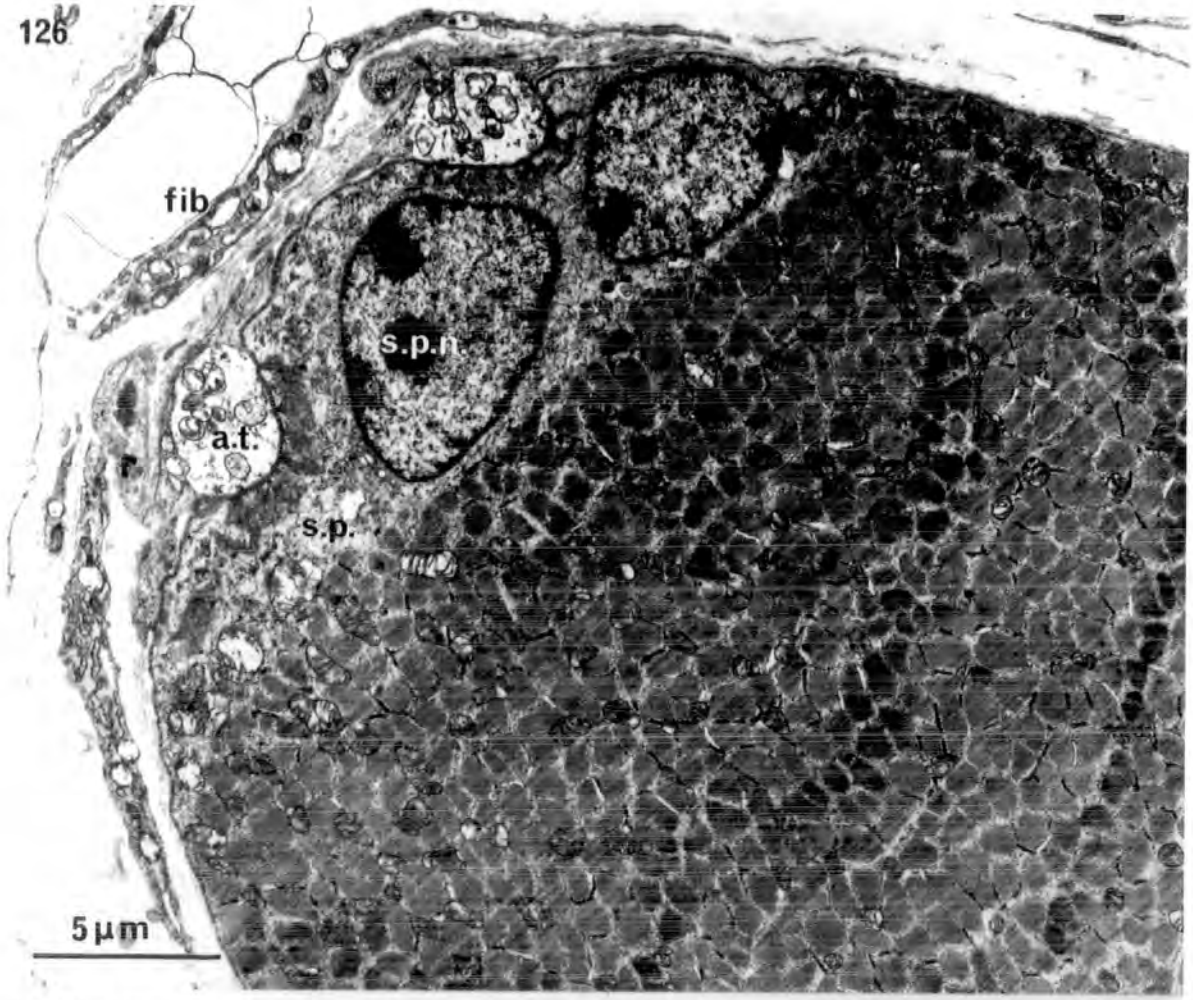
126
fib
s.p.n
a.t.
s.p.
5 µm

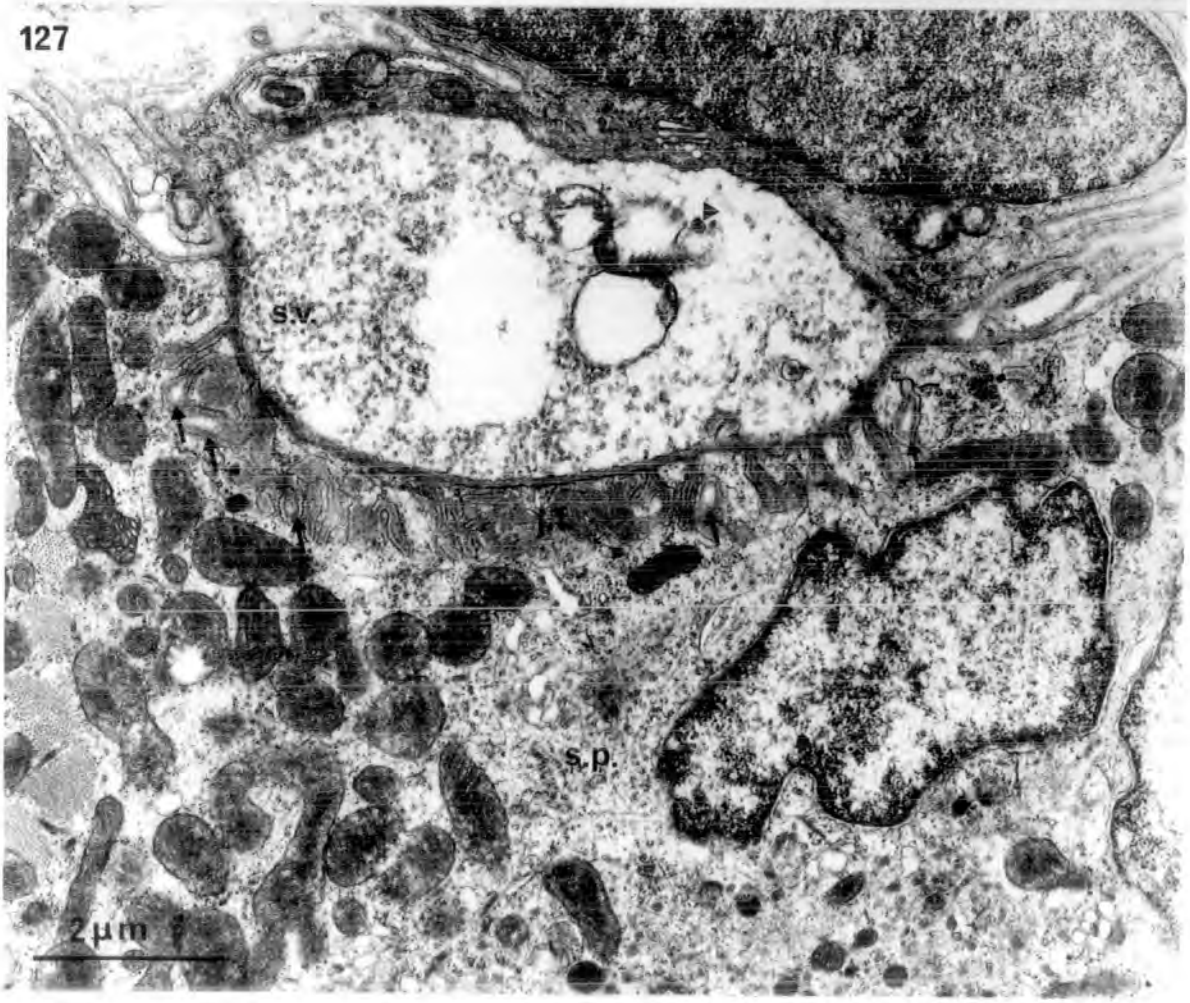
127
s.v.
s.p.
2 µm

Figures 128 to 130. Electron micrographs of the myoneural junctions of small C fibres from the orbital rim layer of SR.

Fig. 128. In transverse section the small C fibre is characterised by its small diameter; small, well-delineated myofibrils; and numerous large mitochondria that are scattered evenly throughout the fibre. The axon terminals (a.t.) are compactly arranged and cover a large proportion of the fibre perimeter. They overlie a thin sole plate (s.p.) and the post-synaptic membrane is folded (j.f.).

x 5,000

Fig. 129. Part of fig. 128 above at higher magnification. The axon terminals contain numerous mitochondria (m) and synaptic vesicles (s.v.), with occasional dense-core vesicles (solid arrowheads). Several junctional folds (j.f.) are expanded at their bases (arrows).

x 12,600

Fig. 130. Longitudinal section of a myoneural junction on a small C fibre.
The muscle fibre is typified by regular triads (tr) and numerous large mitochondria (m) with packed cristae that are associated with lipid droplets (Li). There is no visible M line in the region illustrated, but one is detectable elsewhere in the section. The axon terminals (a.t.) overlie a thin sole plate (s.p.) with an associated nucleus (s.p.n.). The junctional folds of the post-synaptic membrane appear irregular : many are either curved or expanded at their base (arrows). Such folds appear as 'vacuoles' beneath the post-synaptic membrane.

x 8,000

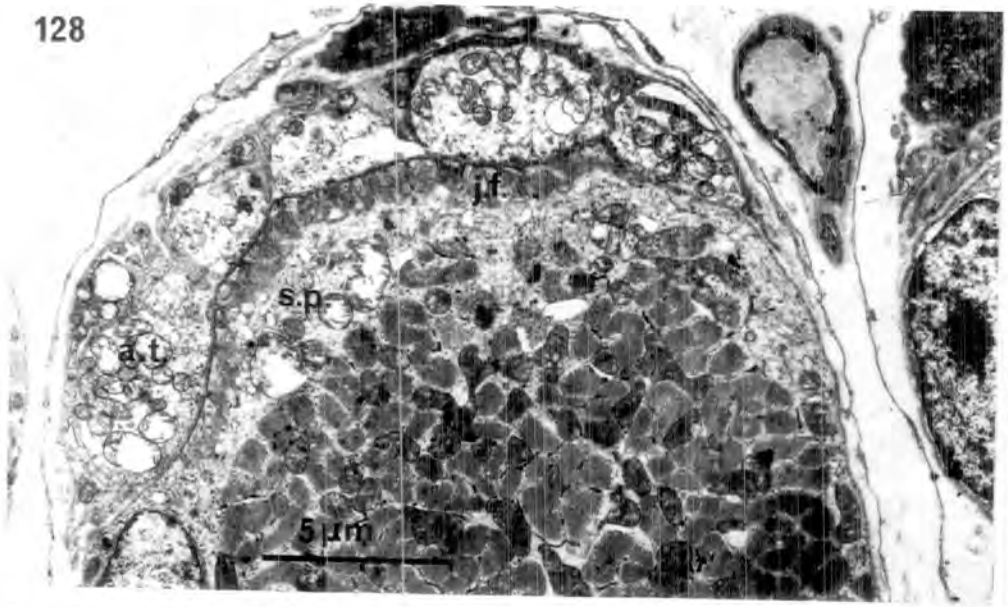
128
j.f.
s.p.
a.t.
5 µm

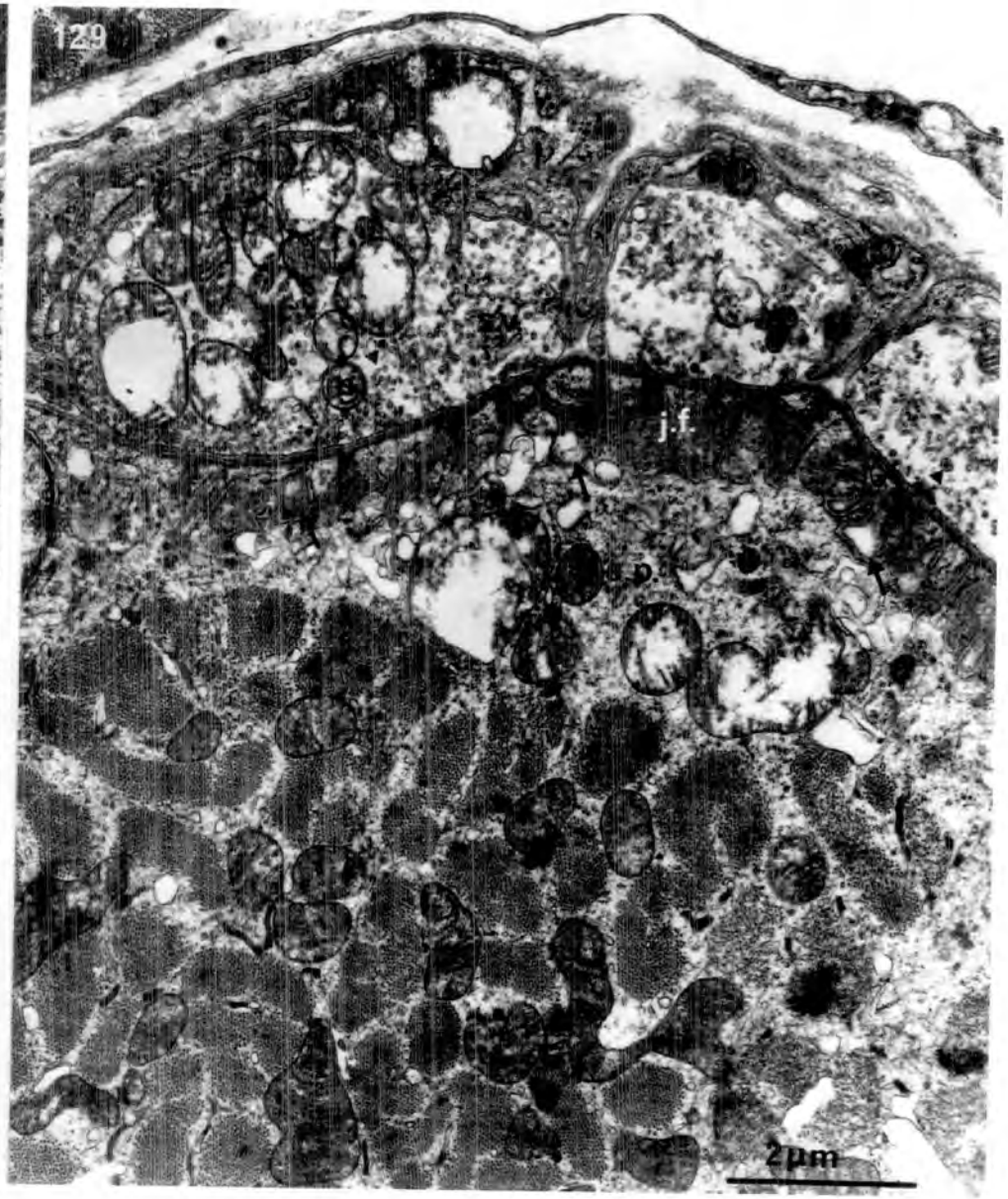
129
j.f.
2µm

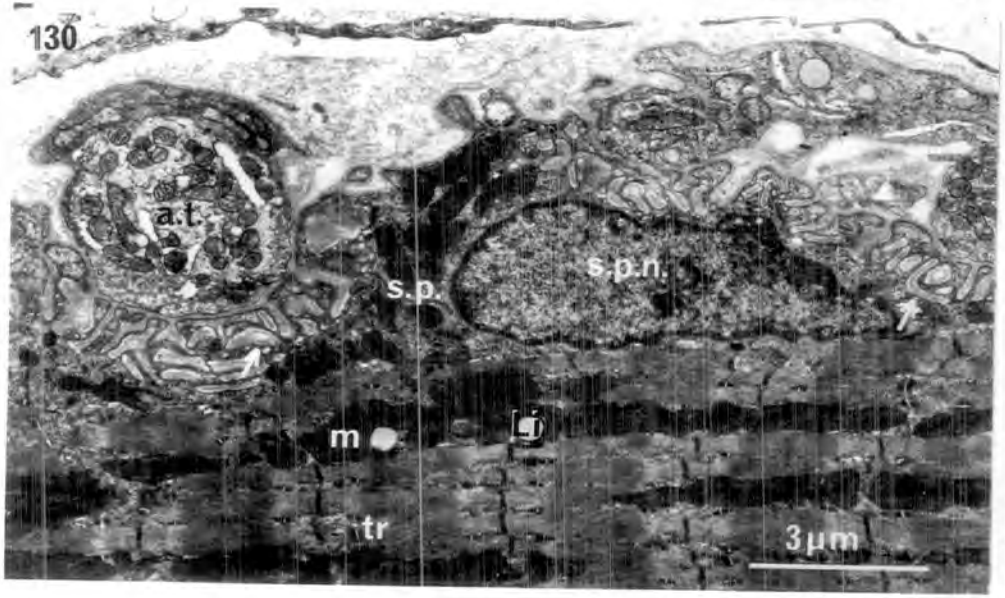
130
a.t.
s.p.
s.p.n.
m
tr
3µm

Figures 131 to 133. Electron micrographs of the myoneural junctions of small/intermediate G fibres from the peripheral layers of SR.

Fig. 131. Transverse section of four axon terminals (a.t.) on a peripheral patch G fibre. Note the poor delineation of the myofibrils, even in the I band, and the numerous small mitochondria. The terminal axons are small in comparison with those of the compact plate endings (e.g. fig. 129). The four axon terminals in this particular transverse section thus cover only a minor proportion of the periphery of the fibre. They are applied to the surface of the muscle fibre. There is very little underlying sole plate material.

x 12,600

Fig. 132. Transverse section of a single axon terminal (a.t.) on an orbital rim G fibre. Occasional, irregular folding appears as vacuoles (arrows) that lie beneath the post-synaptic membrane, lined with basement membrane. fib. , fibroblast.

x 12,600

Fig. 133. Transverse section of a single axon terminal applied to a peripheral patch G fibre. The axon terminal (a.t.) contains mitochondria (m), synaptic vesicles (s.v.) and occasional dense-core vesicles (arrowheads). It is associated with a Schwann cell (S.c.). The synaptic gutter is smooth with basement membrane (b.m.) interposed between pre- and post-synaptic membranes. Junctional folds are irregular and appear as vacuoles (arrows). coll. , collagen fibres.

x 20,000

131

132

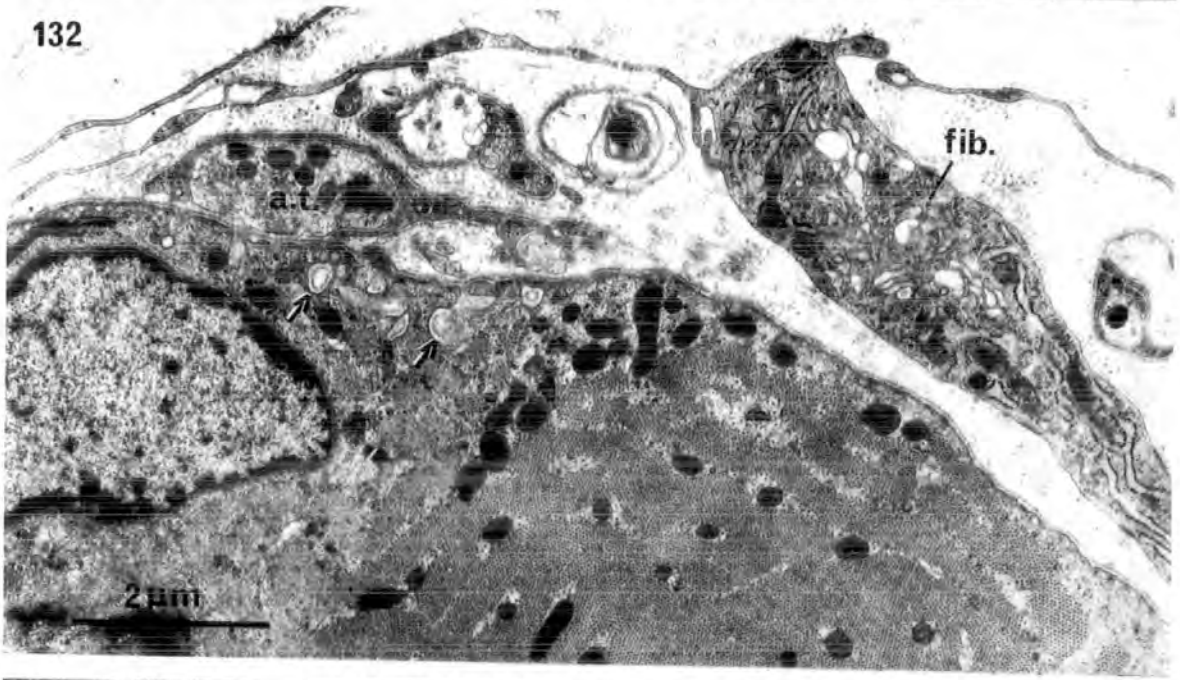

133

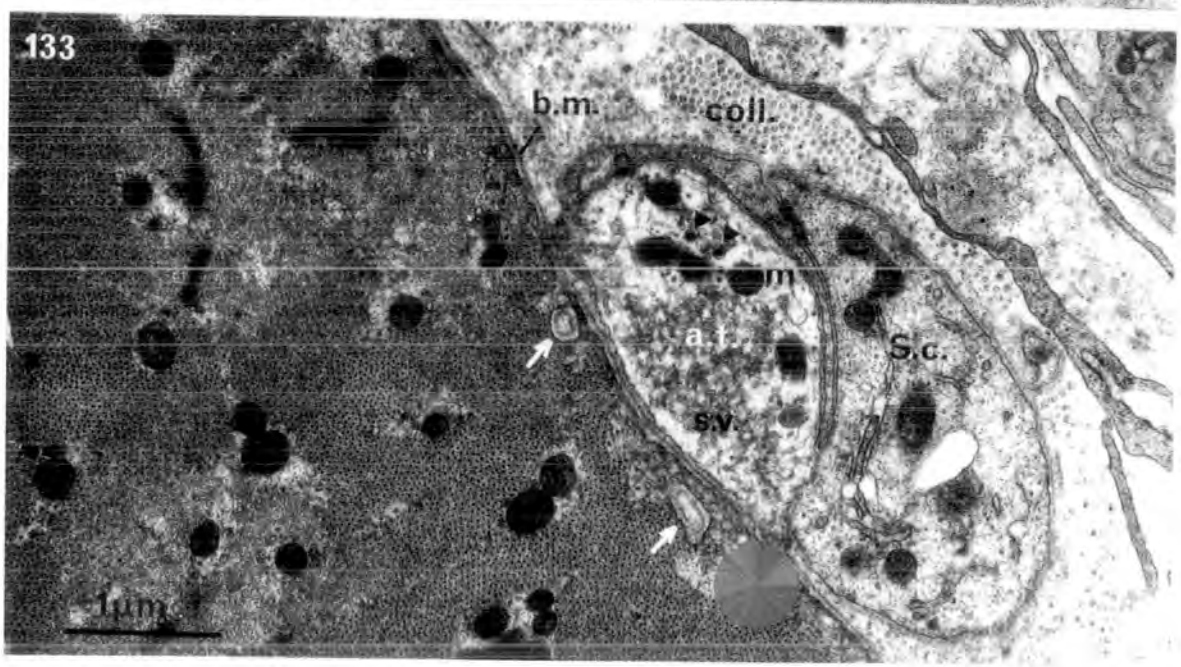

Figure 134. Electron micrograph showing the longitudinal section of a myoneural junction applied to a large G fibre from the central core layer of SR.

The central core large G fibre is typified by a prominent M line (M); a straight Z line (Z); and infrequent and tiny mitochondria (m). The axon terminals (a.t.) overlain by Schwann cell (S.c.), are compactly grouped and are applied to the surface of the muscle fibre. The synaptic gutter is mainly smooth with only infrequent, irregular junctional folds (arrows). The sole plate (s.p.) beneath the ending is very thin. coll. , collagen.

x 10,000

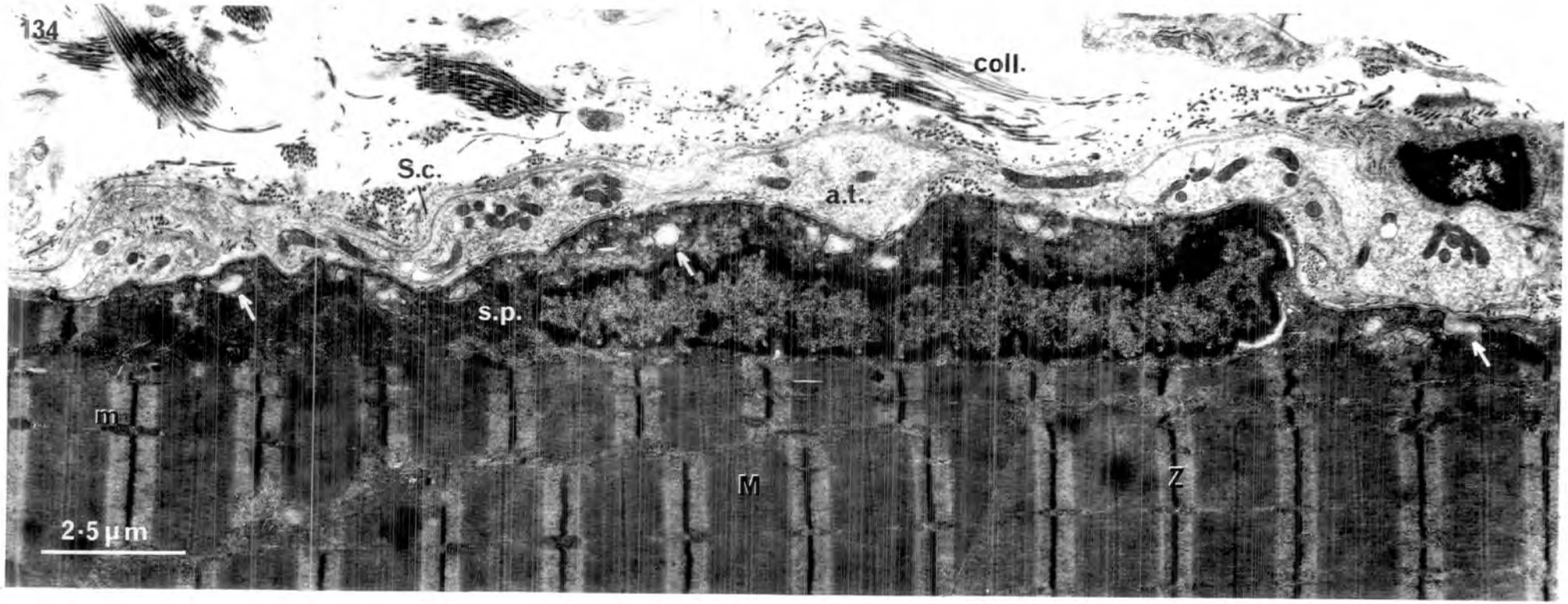
134
coll.
S.c.
a.t.
s.p.
m
M
Z
2·5 µm

Figures 135 to 137. **Electron micrographs of longitudinal sections of axon terminals applied to large G fibres from the central core layer of SR.**

Figs. 135 & 136. Axon terminals from the previous ending series (Fig. 134) at higher magnification. Note that the axon terminals (a.t.) contain numerous synaptic vesicles (s.v.) and occasional dense-core vesicles (arrowheads), and that they overlie a mainly-smooth post-synaptic membrane (p.s.m.). Basement membrane (b.m.) lies in the synaptic gutter.

x 20,000

Fig. 137 illustrates the maximum development of junctional folds beneath the axon terminals of large G fibres. Wide, irregular folds, lined with basement membrane (b.m.) may form loops or be branched (i.j.f.).

x 32,000

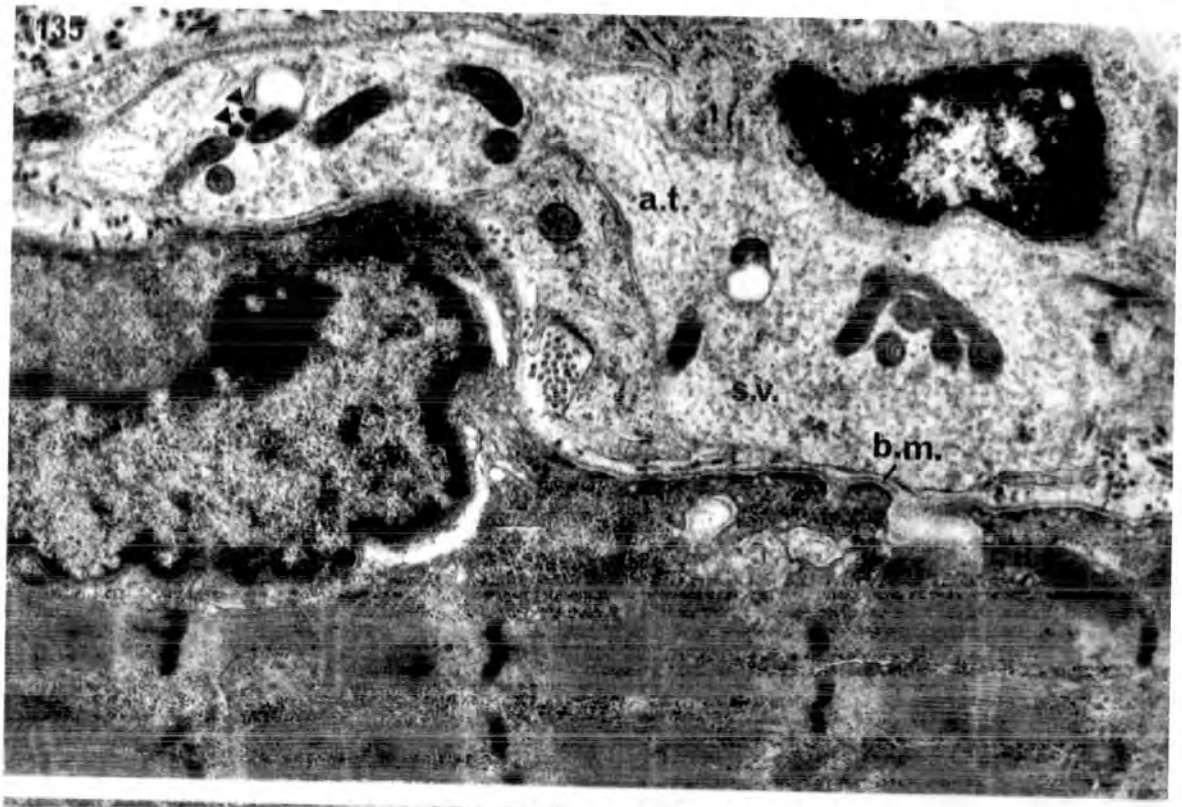
135
a.t.
s.v.
b.m.

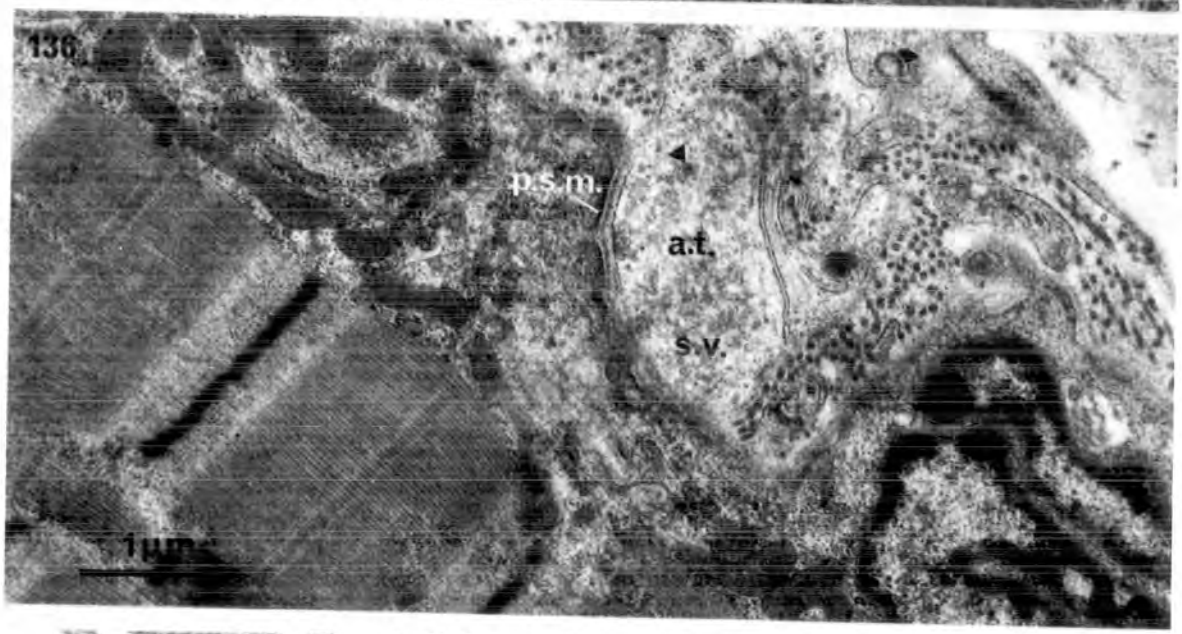
136
p.s.m.
a.t.
s.v.
1µm

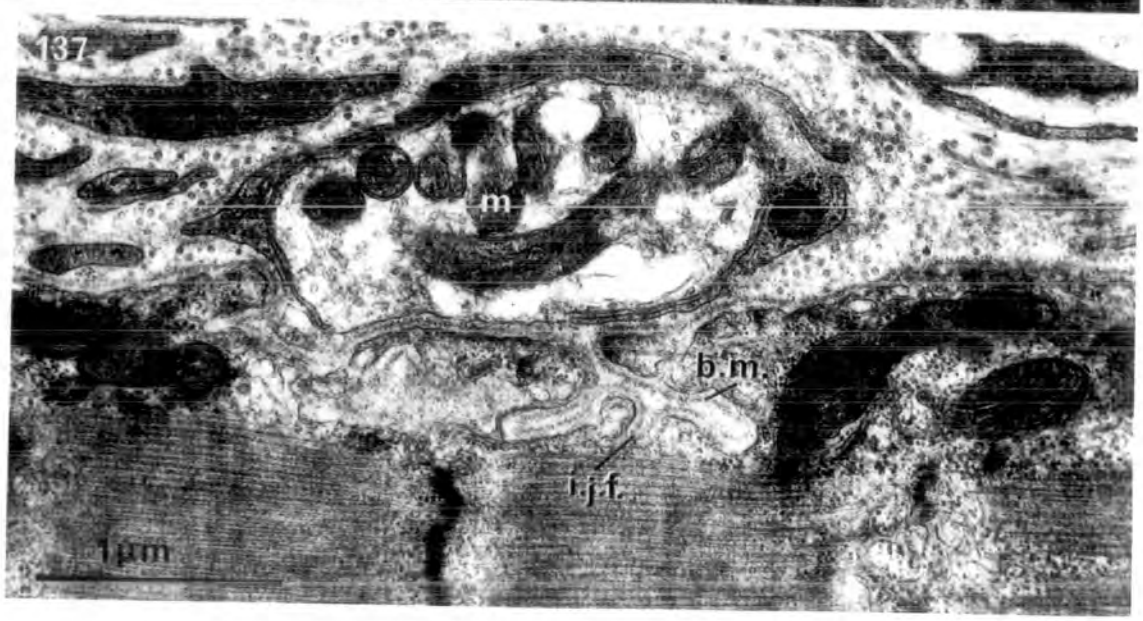
137
m
b.m.
i.j.f.
1µm

Figures 138 to 141. Division of peripheral patch G fibres.

Figs. 138 - 140 are light micrographs of thick (1.5 μm) Epon sections stained with toluidine blue. They show in transverse section the progressive splitting and separation of daughter fibres g_1 and g_2. A neighbouring fibre (g_3) is of large diameter.

x 1,800

Fig. 141 shows the fine structure of the grape axon terminal (a.t.) present in the constricted region of g_1 and g_2 (see fig. 142). The small axon terminal is overlain by Schwann cell (S.c.) and contains mitochondria (m), clear synaptic vesicles (s.v.), and occasional dense-core vesicles (arrowhead). The terminal is not applied to the flat surface of the muscle fibre as is normally the case, but is located in a shallow synaptic gutter (s.g.).

x 20,000

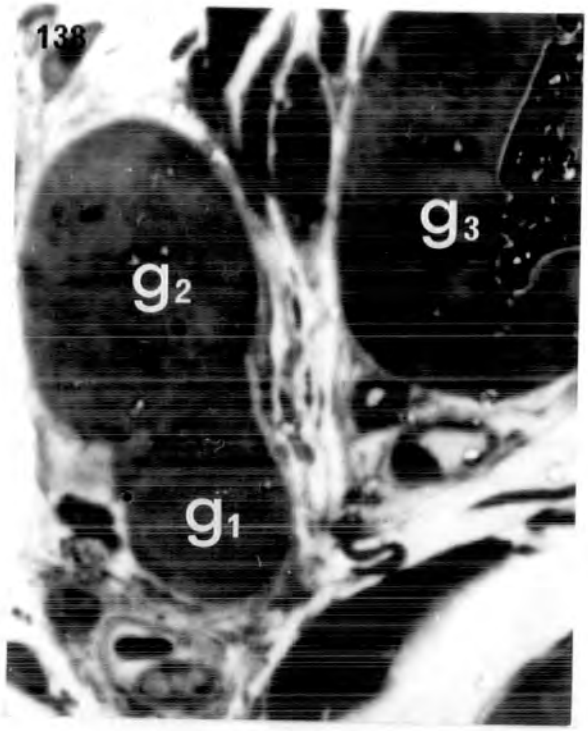
138
g2
g3
g1

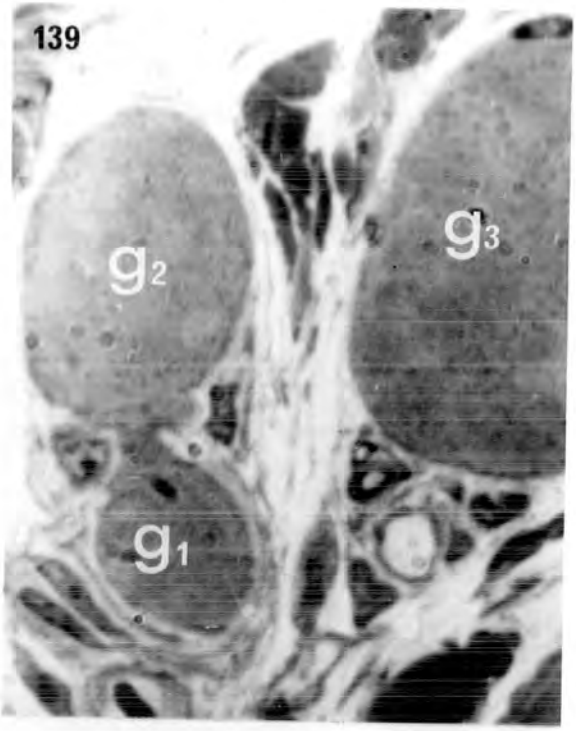
139
g2
g3
g1

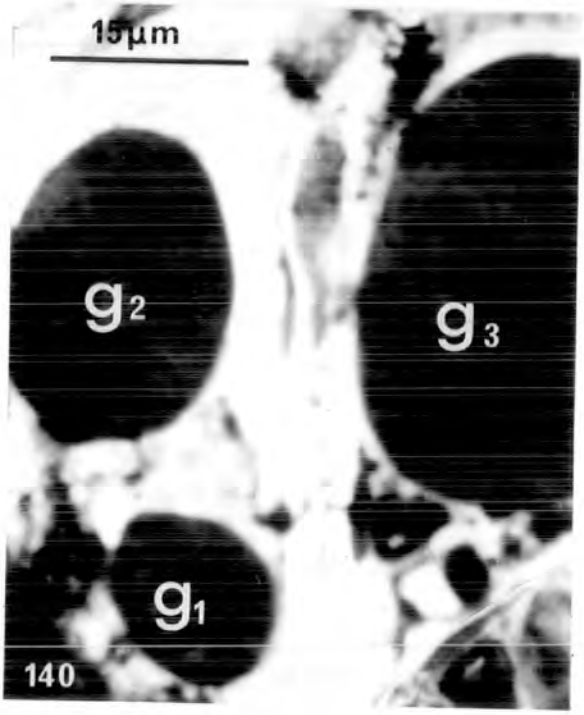
15µm
g2
g3
g1
140

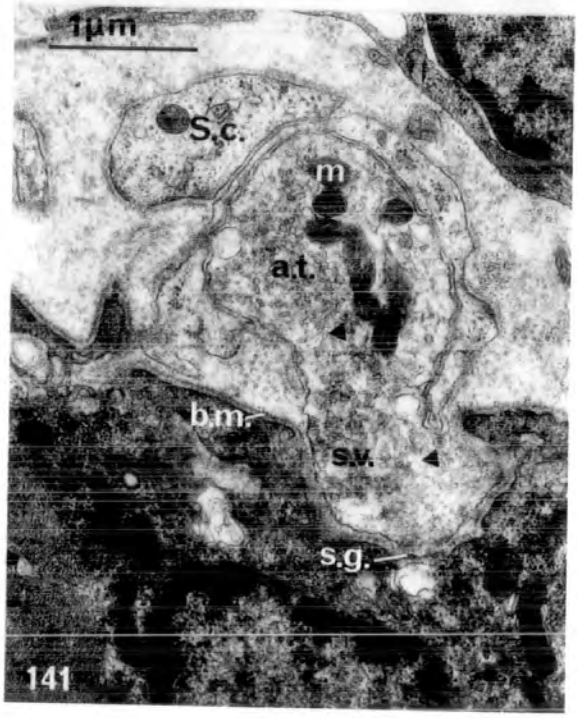
1µm
S.c.
m
a.t.
b.m.
s.v.
s.g.
141

Figures 142 to 143. <u>Electron micrographs illustrating the division of peripheral patch G fibres shown in figs. 138 - 140.</u>

Fig. 142. Transverse section of the peripheral patch layer at the insertion end of SR. The intermediate G fibres (g) are characteristically separated from each other and are typified by their homogeneous appearance, with little delineation of the myofibrils and numerous small mitochondria. Note the myelinated axon (my.a.) near to fibre g_3 and the non-myelinated axon (non-my.a.) near to the muscle fibre surface. An axon terminal (a.t.) is located in a shallow groove on the surface of fibre g_1/g_2, which is beginning to constrict into two portions.

x 3,200

Fig. 143. A transverse section taken nearer the belly. Note the axon terminals (a.t.) applied to the surface of fibre g_3. Fibre g_1/g_2 has constricted into a 'dumb-bell' shape and is about to divide into two separate daughter fibres. (See also figs. 138 - 141.)

x 3,200

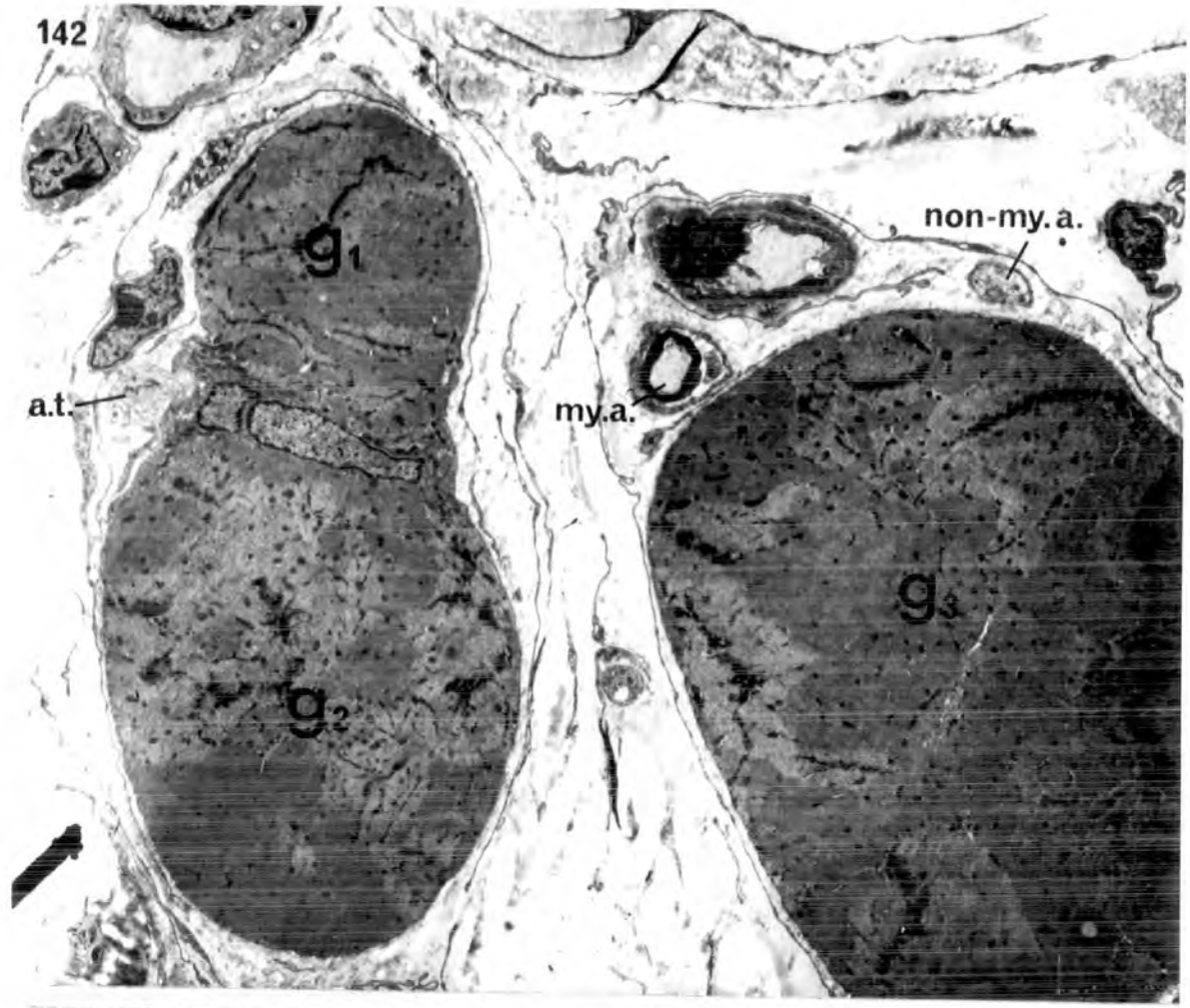
142
g1
non-my.a.
a.t.
my.a.
g2
g3

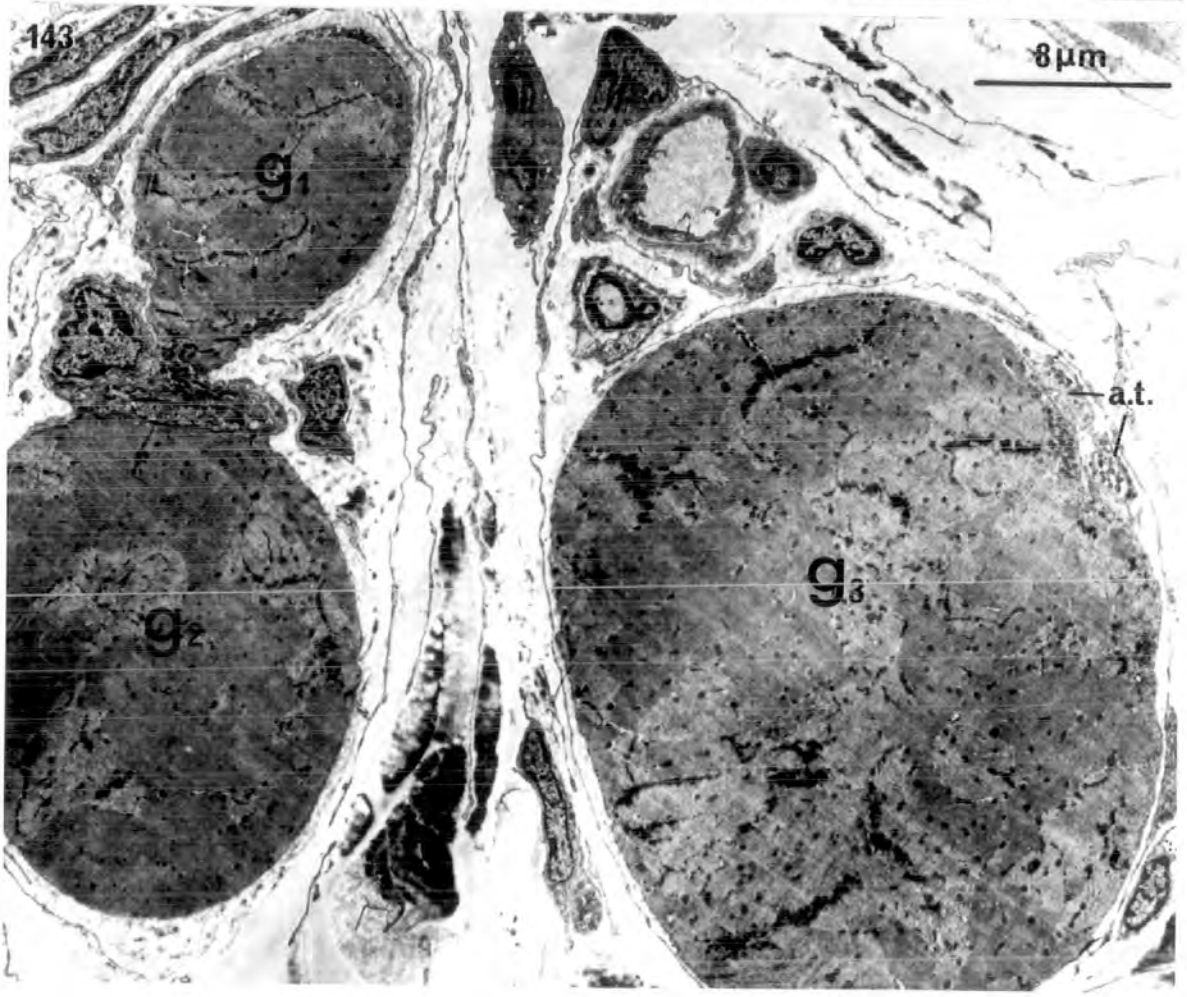
143
8µm
g1
a.t.
g2
g3

Figures 144 to 145. Gross organisation of LP in transverse section.

Fig. 144. Phosphorylase.
The organisation remains unchanged throughout the length of the muscle. There are no distinct layers comparable to those of SR. Muscle fibre types are distributed throughout the transverse section although large-diameter fibres of high activity appear more common in the central fascicles, and small-diameter fibres of low activity are more common around the periphery. The capsule regions of a number of muscle spindles are marked with circles.

Fig. 145. Acid-preincubated actomyosin ATPase.
This transverse section from a different LP muscle shows the relative concentration around the periphery of LP of small-diameter muscle fibres that are acid-stabile. They are picked out clearly in black with Acid ATPase. Encapsulated spindles are marked with circles.

Figures 146 to 149. Histochemical fibre types in the central fascicles of LP.

Serial transverse sections stained to demonstrate the following enzymes:

Fig. 146. Phosphorylase.

Fig. 147. Succinic dehydrogenase.

Fig. 148. Alkali-preincubated actomyosin ATPase.

Fig. 149. Acid-preincubated actomyosin ATPase.

The central fascicles are composed of about 55% of large A fibres (A); 25% of intermediate C (C) fibres; and about 20% of small B (B) fibres. In addition, some extremely small-diameter muscle fibres are present (arrows) that are the extracapsular portions of nuclear-bag fibres.

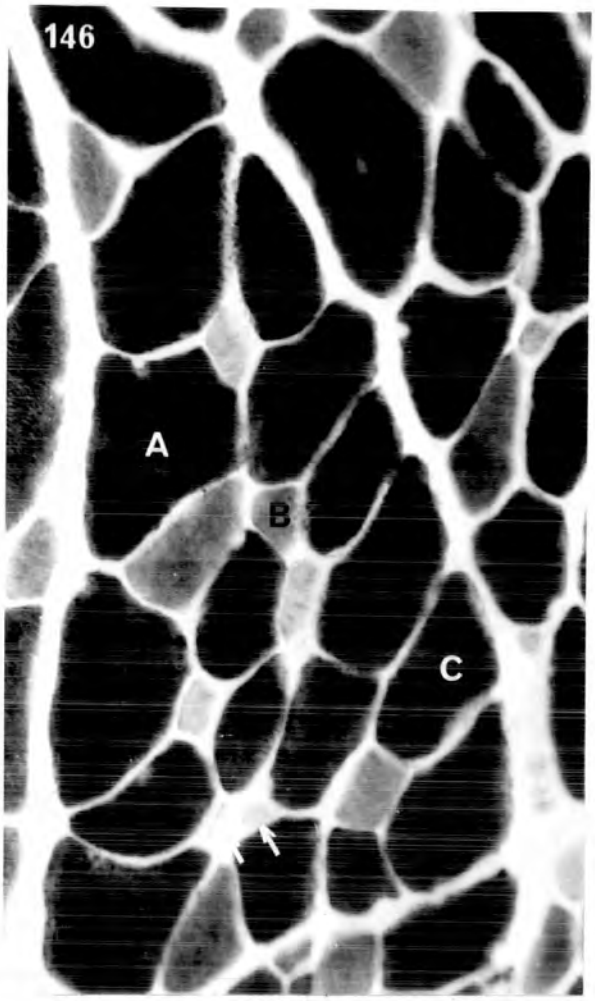
146
A
B
C

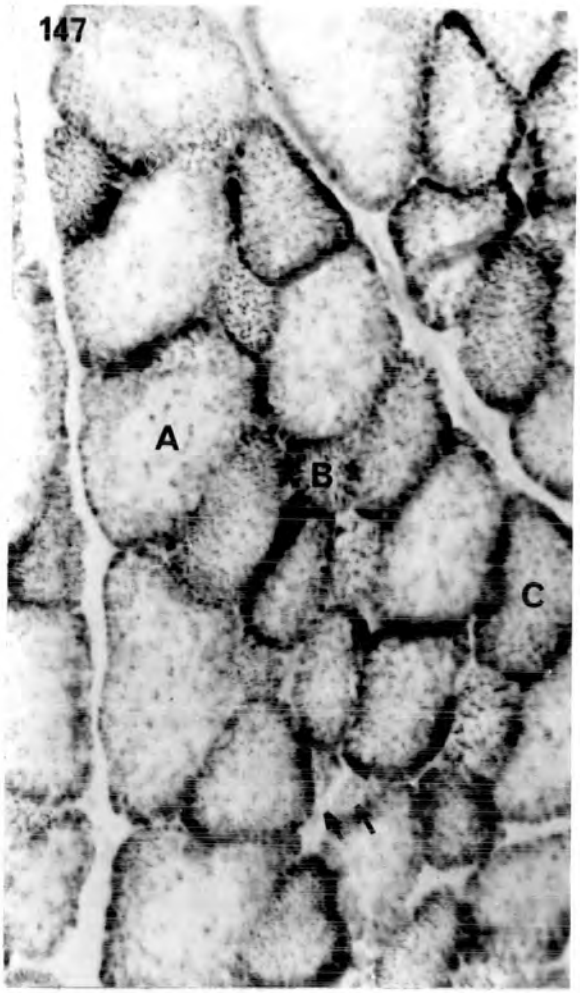
147
A
B
C

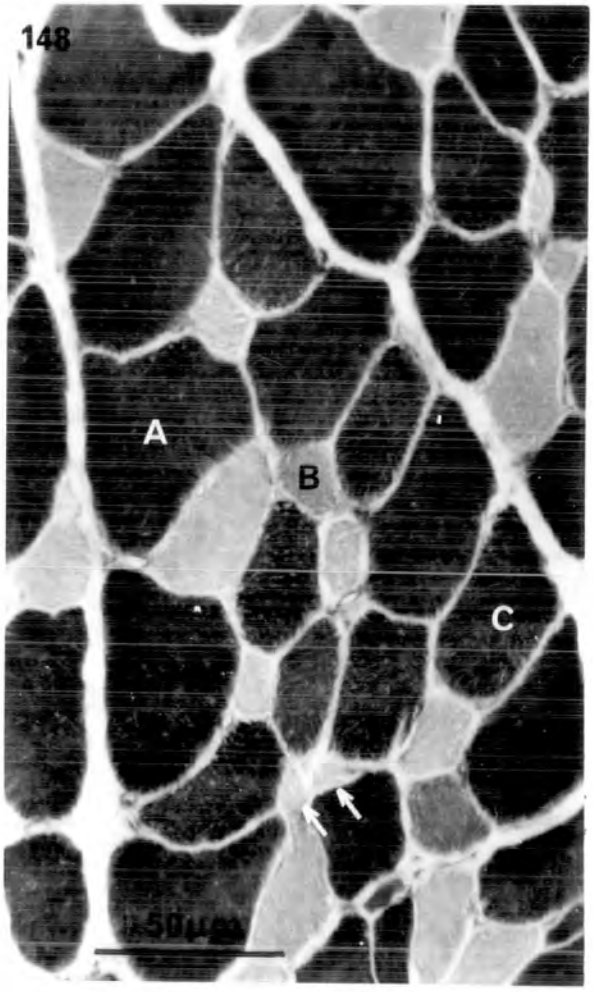
148
A
B
C
50µm

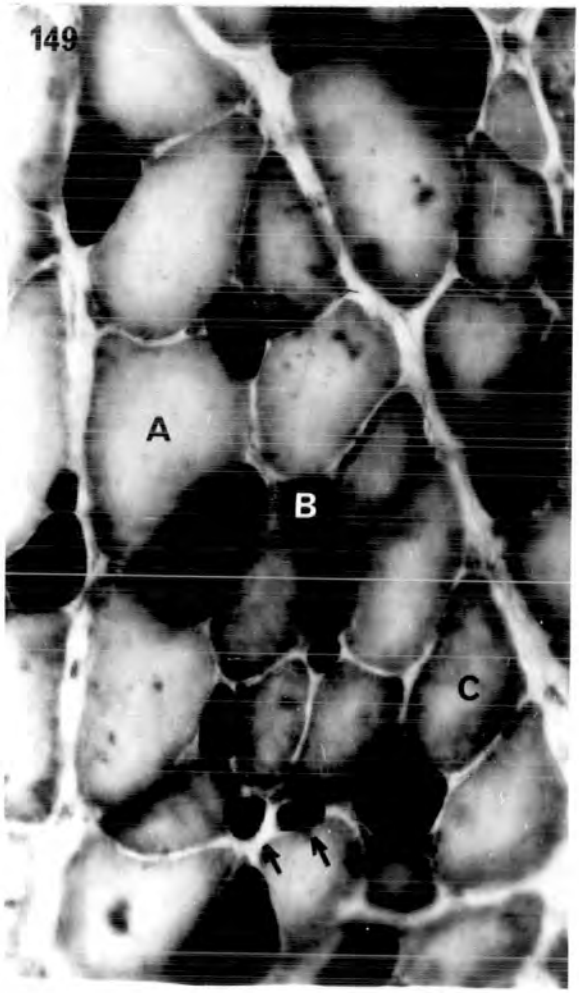
149
A
B
C

Figures 150 to 152. Semi-thin (1.5 μm) transverse Epon sections stained with toluidine blue comparing portions of SR, LP and PB muscles.

Fig. 150. Superior rectus, central core layer. Note the large A (A), large G (G), intermediate C (C), and small C (c) fibre types.

Fig. 151. Levator palepbrae, central fascicle. Note the large A (A), intermediate C (C), and small B (B) fibre types. Compare with fig. 150 above.

Fig. 152. Peroneus brevis, distal portion. Note, in comparison to the two figs. above, the larger diameter of the muscle fibres; the small size and general sparsity of mitochondria; and the clearly fibrillar appearance of the muscle fibres in transverse section.

All photomicrographs are at the same magnification.

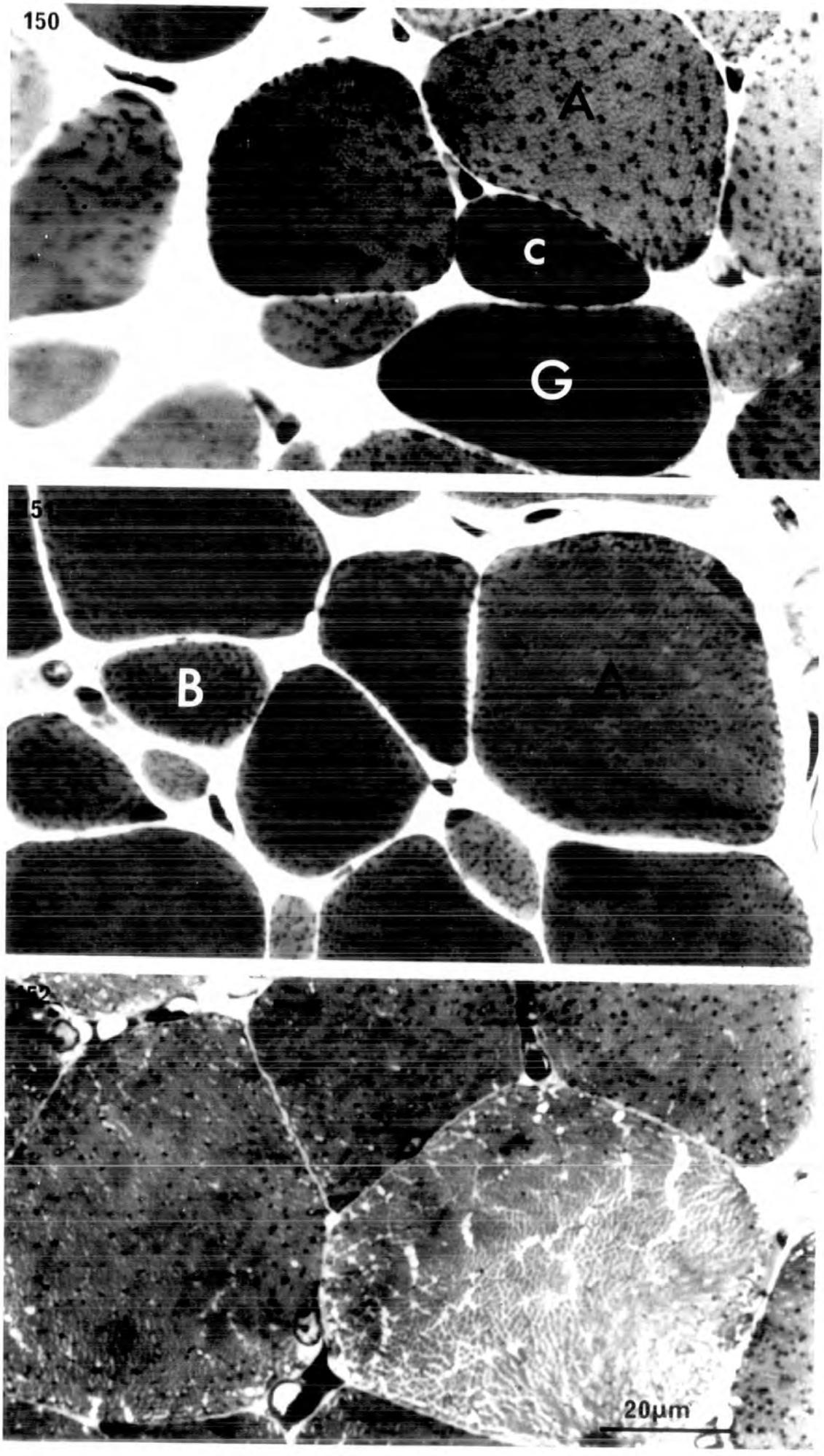
150
A
C
G
5
B
A
20µm

Figures 153 to 154. Electron micrographs of transverse sections of LP.

Fig. 153. Large A (A), intermediate C (C), and small B (B) fibres are shown at low magnification. Note the differences in diameter of the muscle fibres and also the differences in size, abundance and distribution of mitochondria.

x 2,000

Fig. 154. Large A fibre.
The small myofibrils (mf) are well-delineated in the I band (I) by tubules of sarcoplasmic reticulum (s.r.), and in the A/I band junction by extensive transverse tubules (t.t.). Numerous glycogen granules (Gl) are associated with the sarcoplasmic reticulum in the I band and also located within the myofibrils of this region. The A band (A) shows only isolated tubules of sarcoplasmic reticulum and the myofibrils remain poorly delineated at this level. The mitochondria (m) are sparse, small, and contain few cristae. Note the Z band (Z) in transverse section.

x 20,000

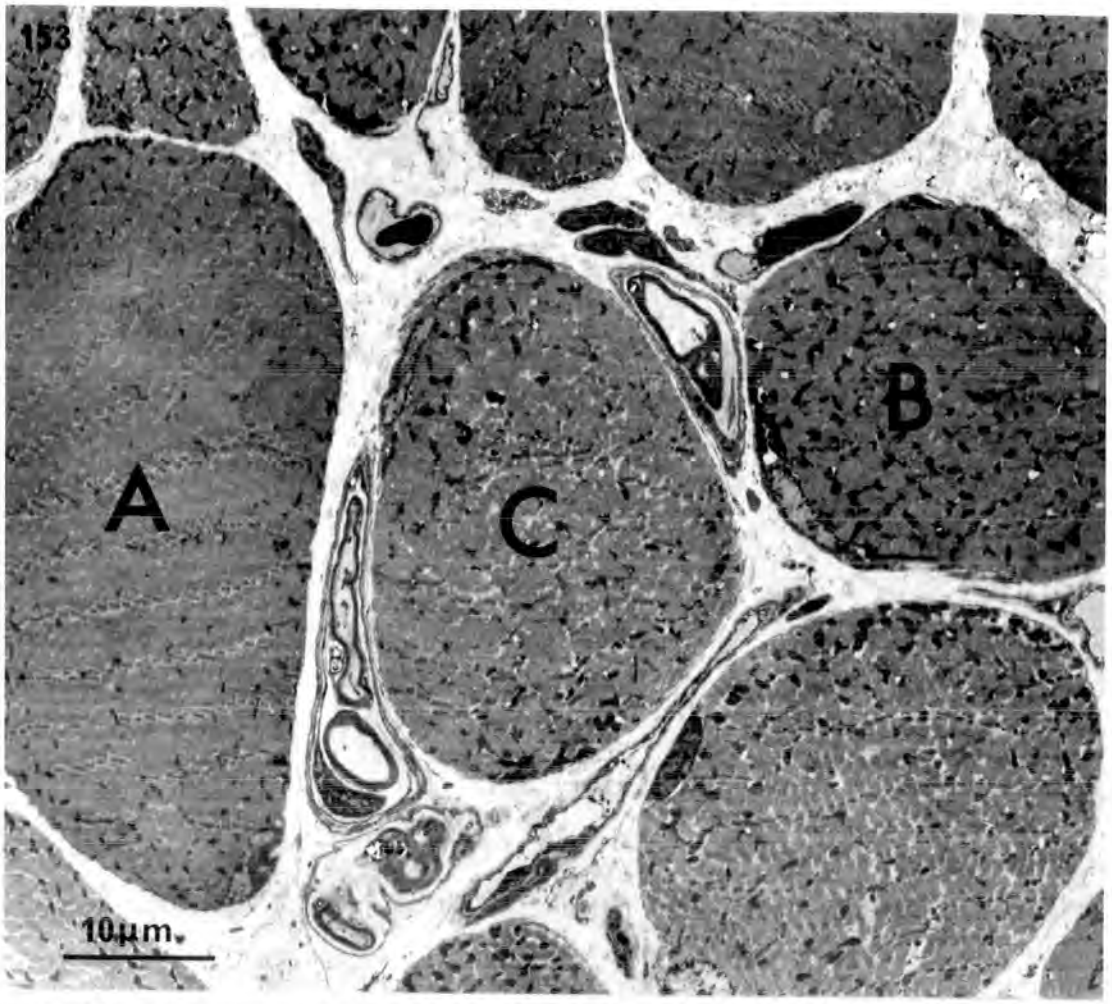
153
A
C
B
10µm.

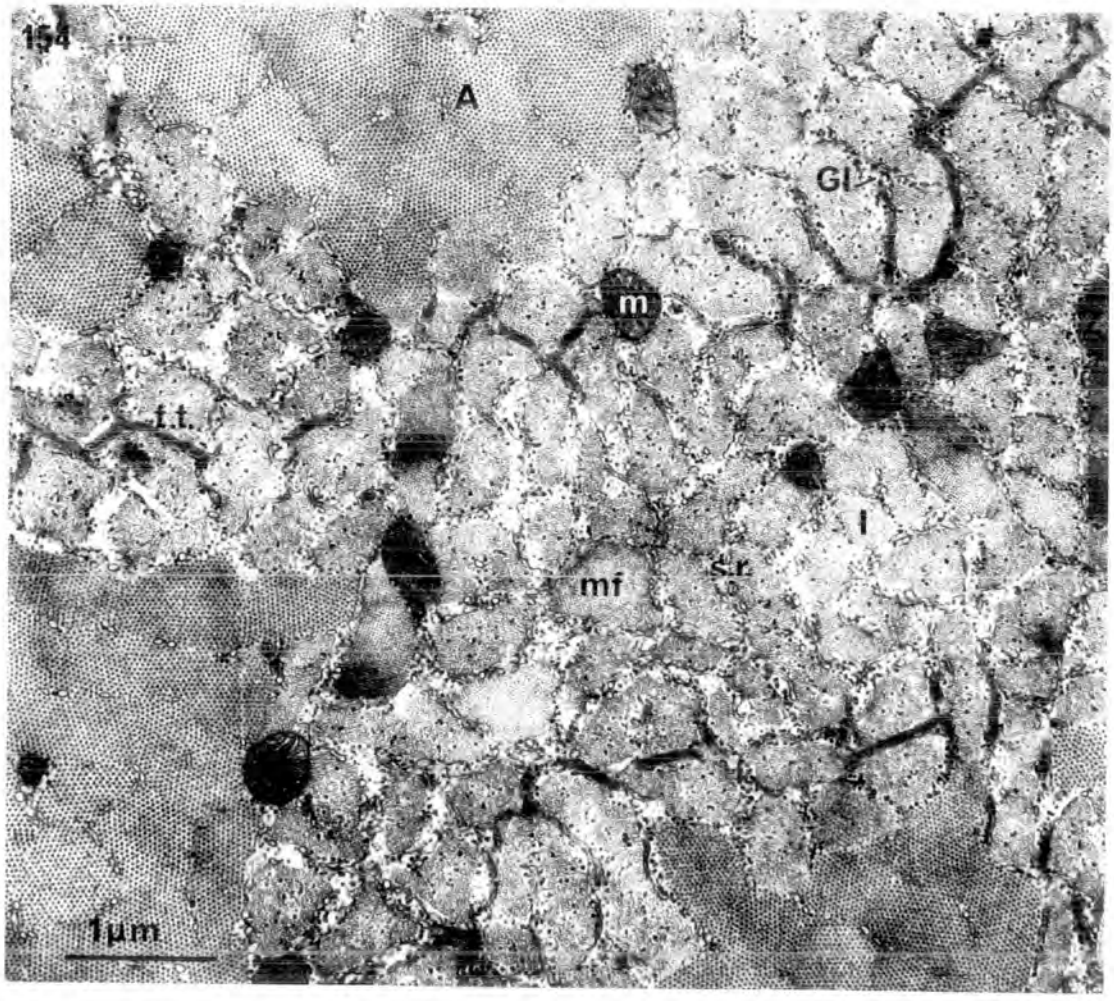
154
A
Gl
m
t.t.
l
mf
s.r.
1µm

Figures 155 to 156. Electron micrographs of transverse sections of LP.

Fig. 155. Intermediate C fibre.
The general appearance of this fibre is similar to the large A fibre of LP. In the I band (I) the small myofibrils are delineated by transverse tubules (t.t.) and sarcoplasmic reticulum (s.r.), while in the A band (A) delineation is poor. Glycogen granules (Gl) are abundant. The mitochondria (m) are more numerous than in the large A fibre and they are also slightly larger.

x 20,000

Fig. 156. Small B fibre.
The manner of delineation of the myofibrils by transverse tubules and sarcoplasmic reticulum resembles that of the large A and intermediate C fibre types. Glycogen granules (Gl) are abundant. The mitochondria (m) appear more numerous and generally larger in diameter than those of the intermediate C fibre. An area of cross-linked myosin filaments is arrowed.

x 20,000

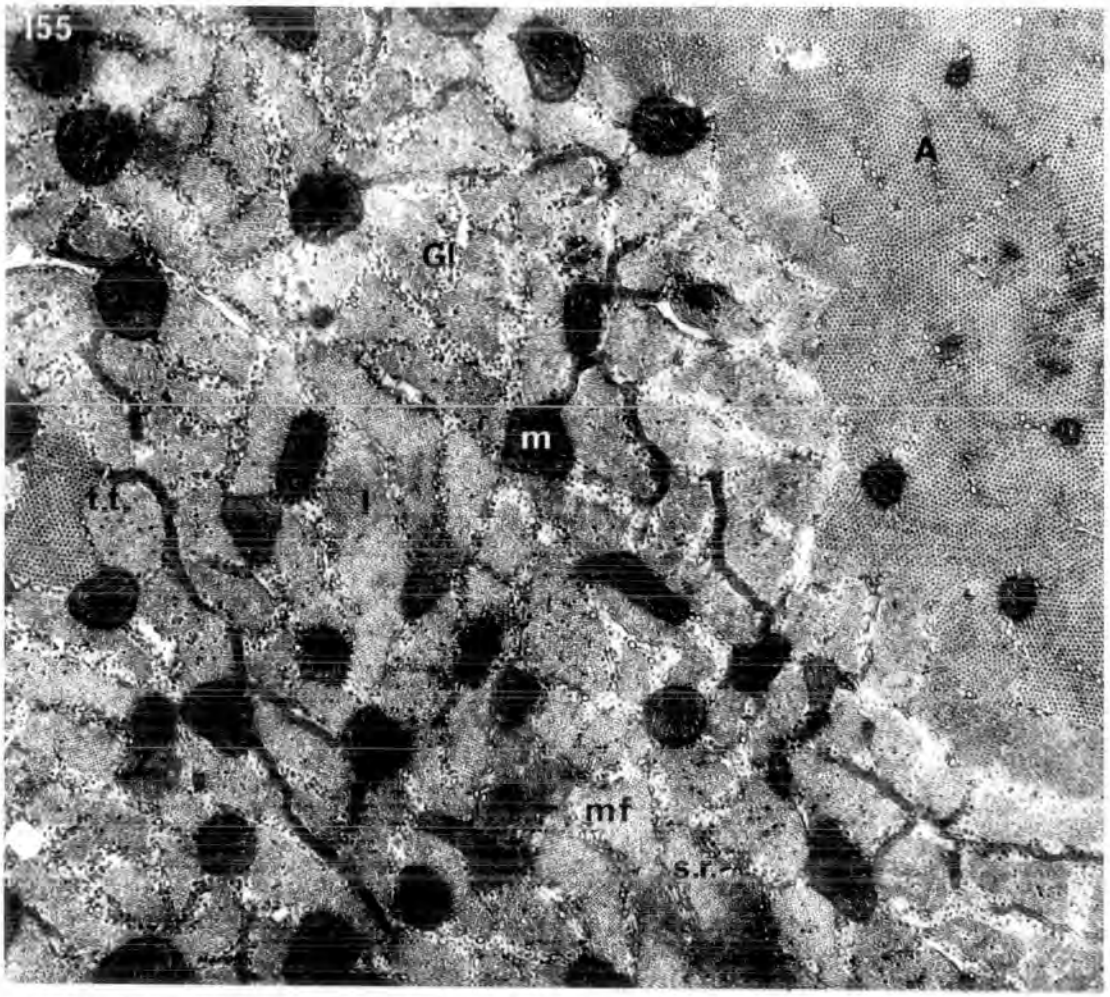
155
A
Gl
m
t.t.
l
mf
s.r.

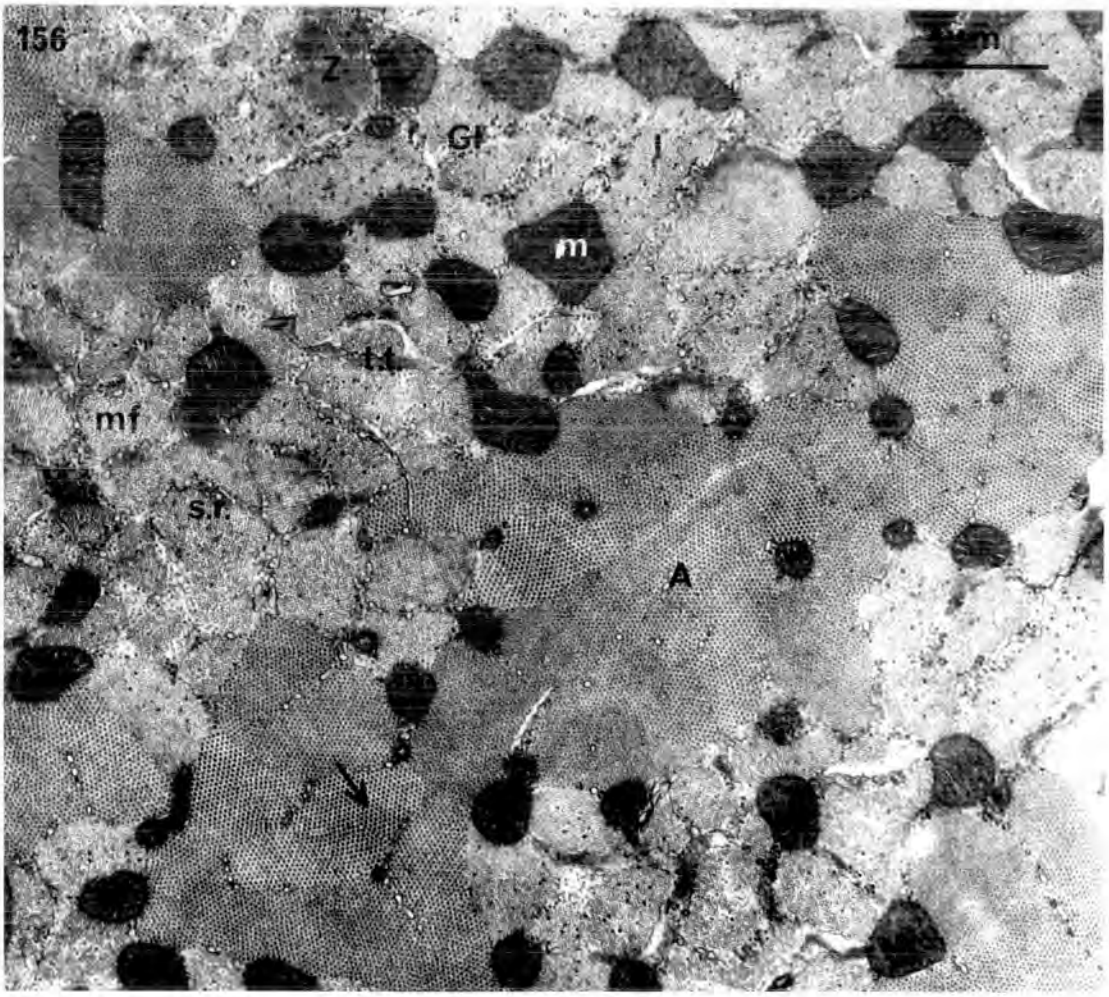
156
Z
Gl
l
m
t.t.
mf
s.r.
A

Figures 157 to 159. <u>Electron micrographs comparing the fine structure in longitudinal section of the large A, intermediate C and small B fibre types of LP</u>.

All fibre types possess prominent M lines (M), regular triads (tr), and abundant sarcoplasmic reticulum (s.r.) and glycogen granules (Gl.) in the I band.

Fig. 157. Large A fibre.
The mitochondria (m) are small and relatively infrequent; the Z lines (Z) are fairly straight and are the thinnest of all three fibre types.

x 15,000

Fig. 158. Intermediate C fibre.
Mitochondria are slightly larger and more abundant than in the large A fibre; Z lines are slightly wider and more wavy.

x 15,000

Fig. 159. Small B fibre.
Mitochondria are the most numerous and largest of all three fibre types; Z lines are the thickest and most wavy.

x 15,000

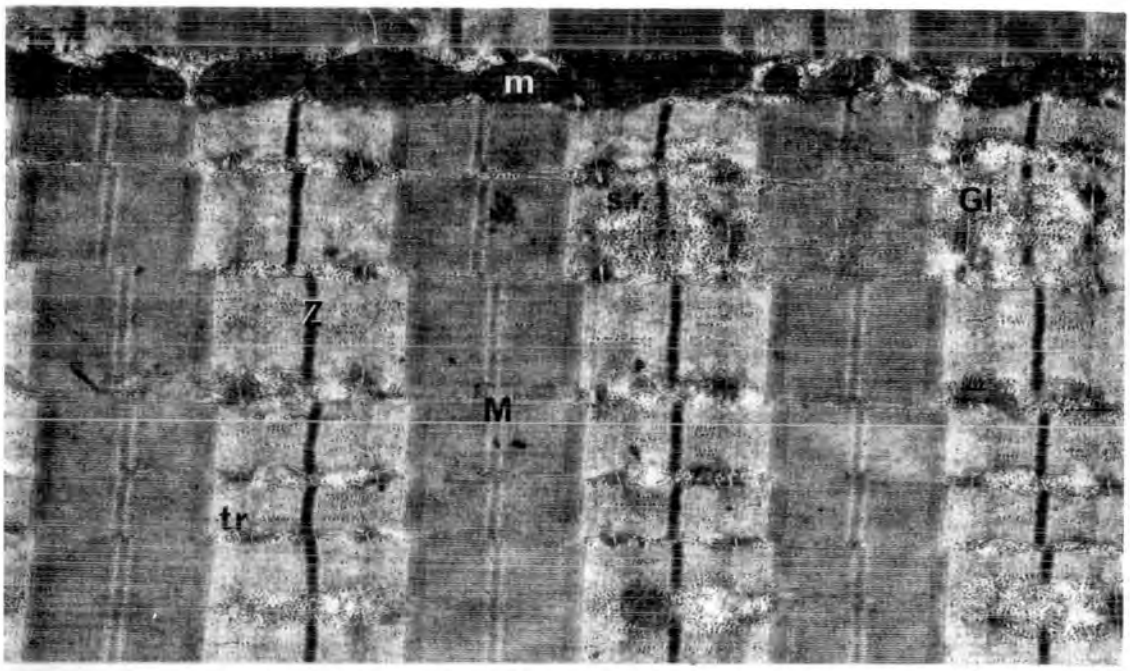
m
S.r.
Gl
Z
M
tr

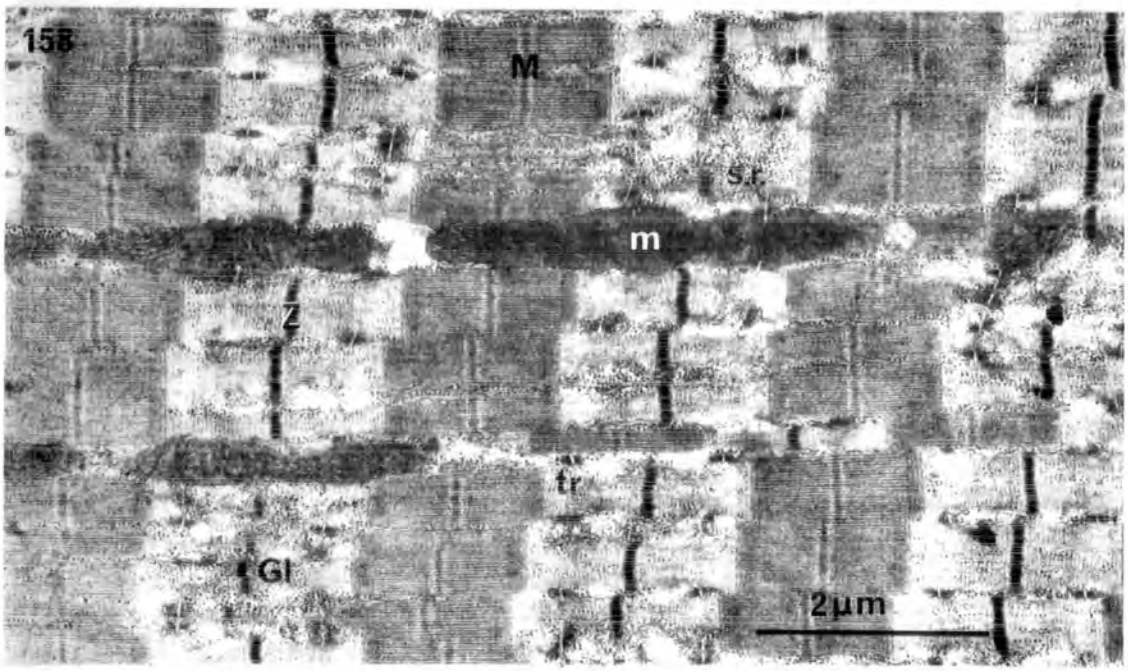
158
M
S.r.
m
Z
tr
Gl
2µm

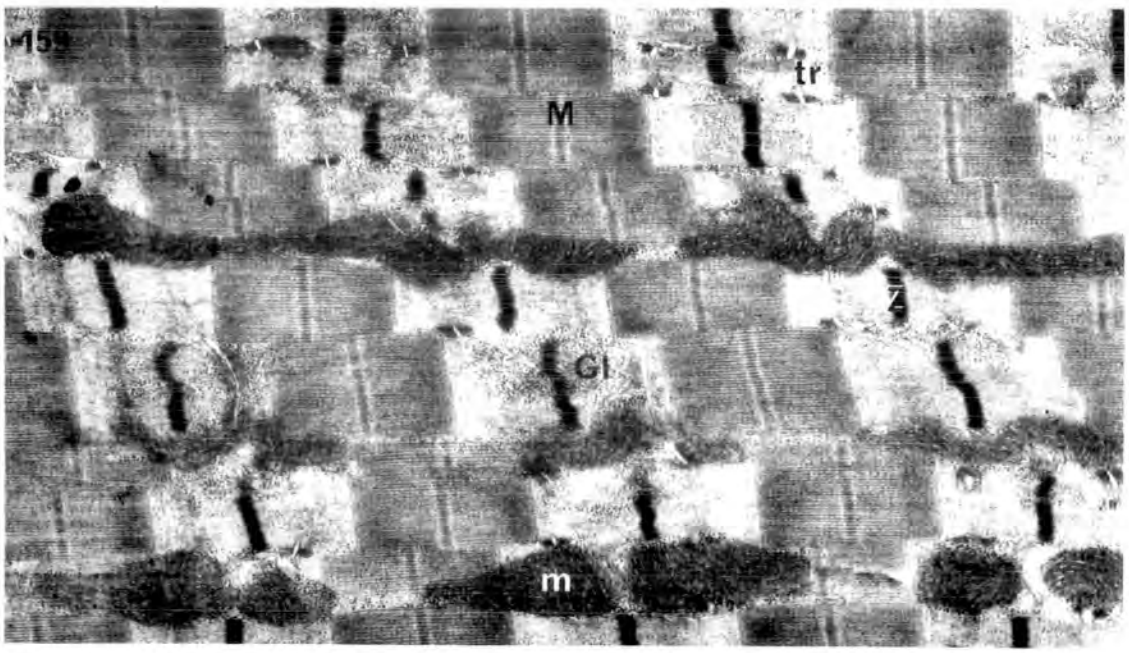
159
tr
M
Z
Gl
m

Figures 160 to 161. Electron micrographs of the myoneural junctions of the large A fibres in LP.

Fig. 160. Transverse section of a myoneural junction on a large A fibre. Four axon terminals (a.t.) lie in gutters, above a substantial sole plate (s.p.) with sole plate nuclei (s.p.n.).

x 8,000

Fig. 161. An axon terminal (a.t.) supplying a large A fibre shown at higher magnification. The axon terminal contains mitochondria (m), numerous synaptic vesicles (s.v.), and occasional dense-core vesicles (arrowheads). The junctional folds (j.f.) are long, narrow, mainly unbranched and closely-packed.

x 20,000

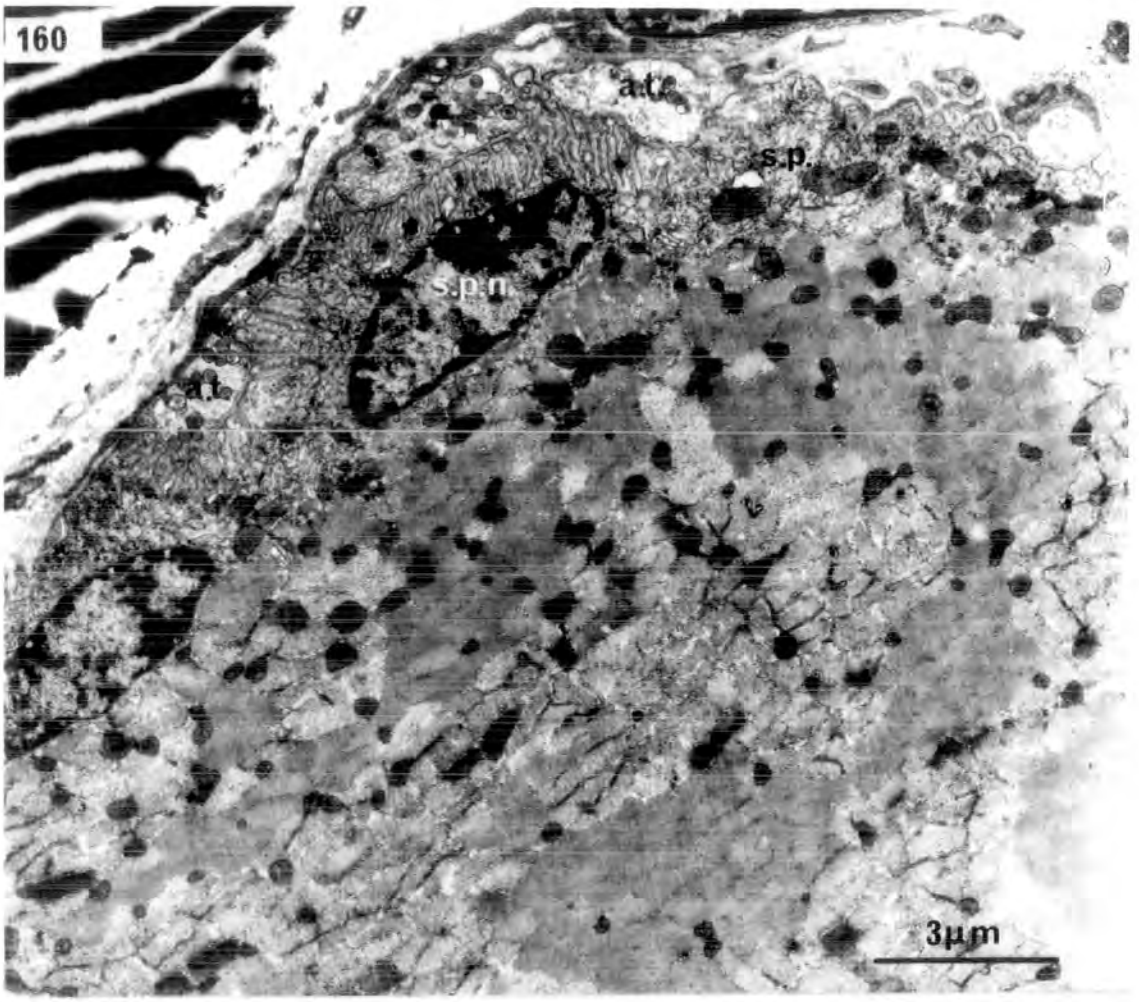
160
a.t.
s.p.
s.p.n.
a.t.
3µm

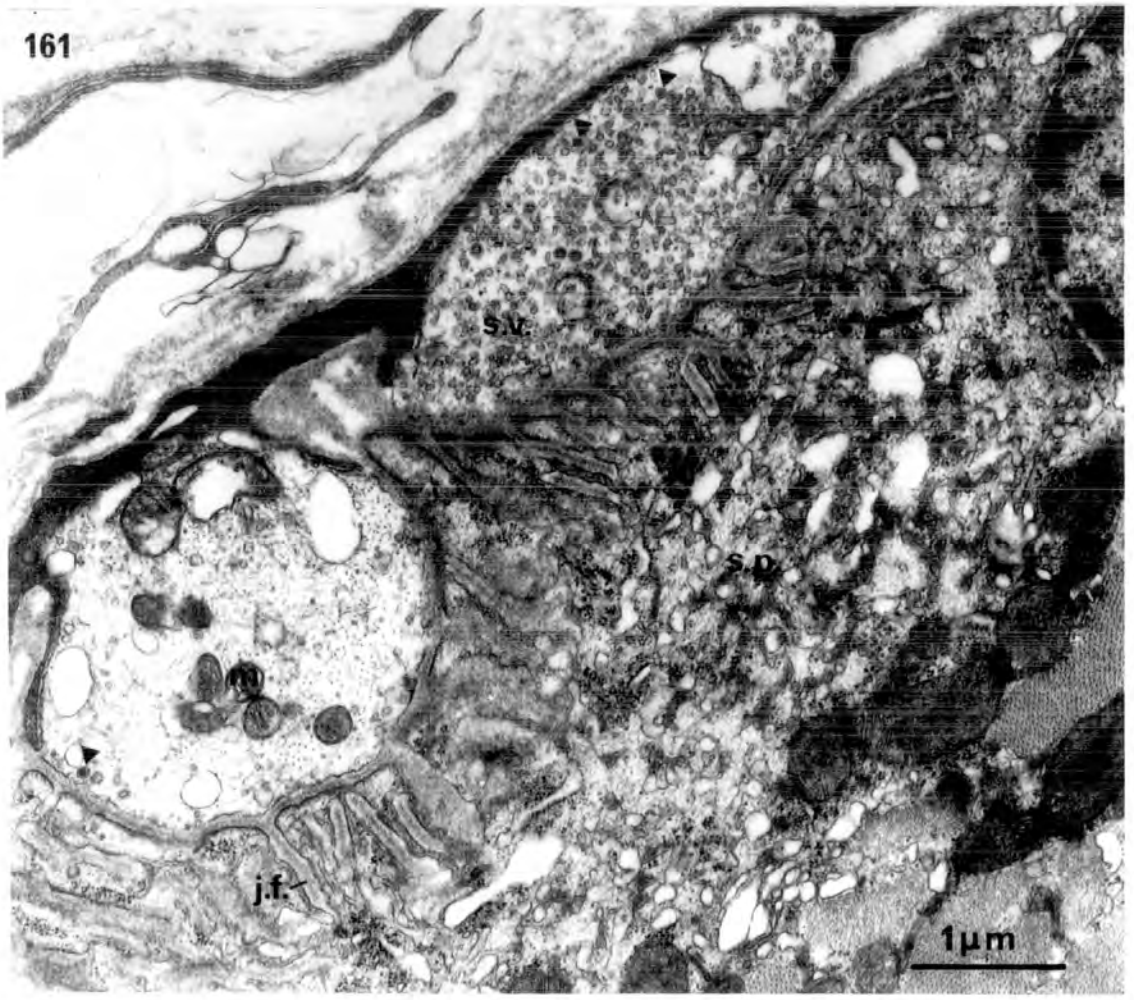
161
s.v.
s.p.
m
j.f.
1µm

Figures 162 to 163. Electron micrographs showing the fine structure of the myoneural junctions applied to the intermediate C fibres of LP.

Fig. 162. Low-power transverse section of two axon terminals (a.t.), packed with synaptic vesicles, overlying a relatively thin sole plate (s.p.).

x 12,600

Fig. 163. The axon terminals contain numerous mitochondria (m) and synaptic vesicles (s.v.). Junctional folds are frequently bulbous (star) and occasionally branched.

x 20,000

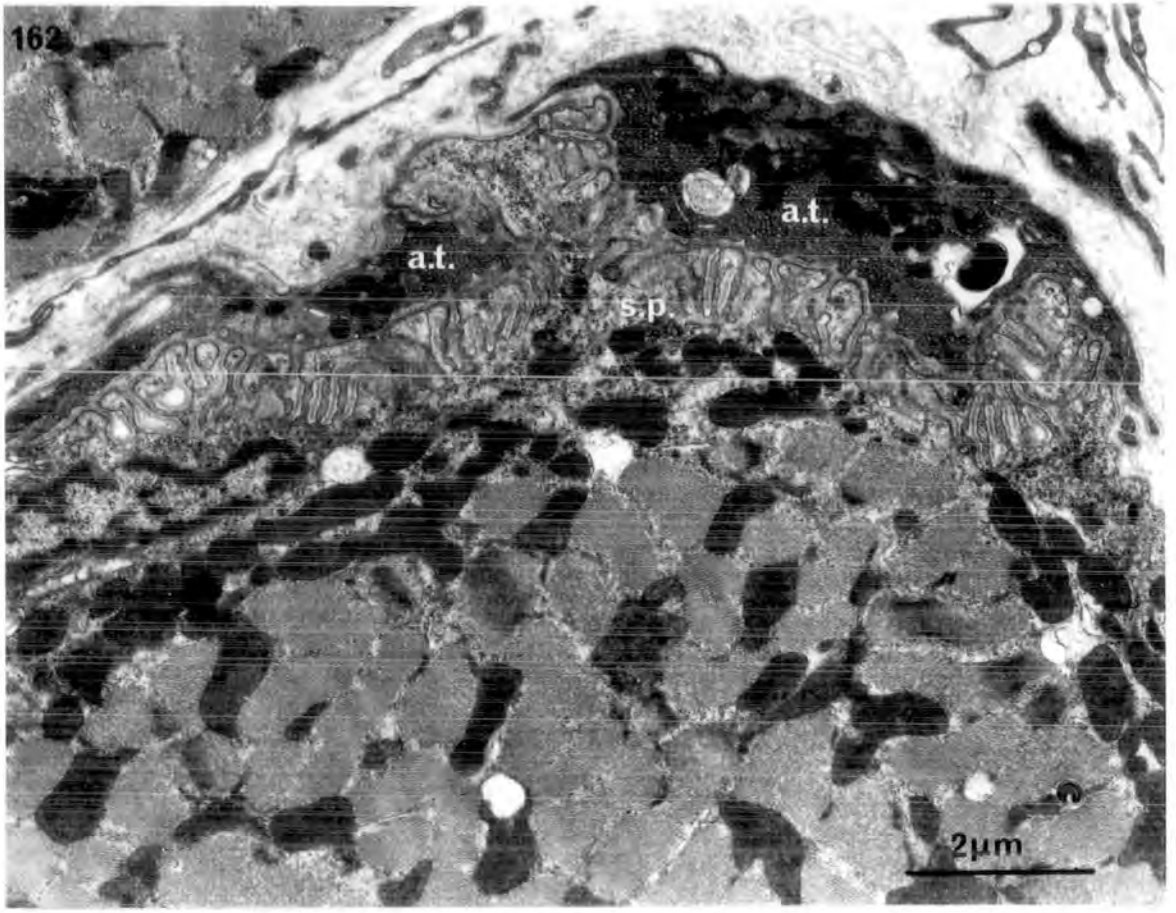
162
a.t.
a.t.
s.p.
2µm

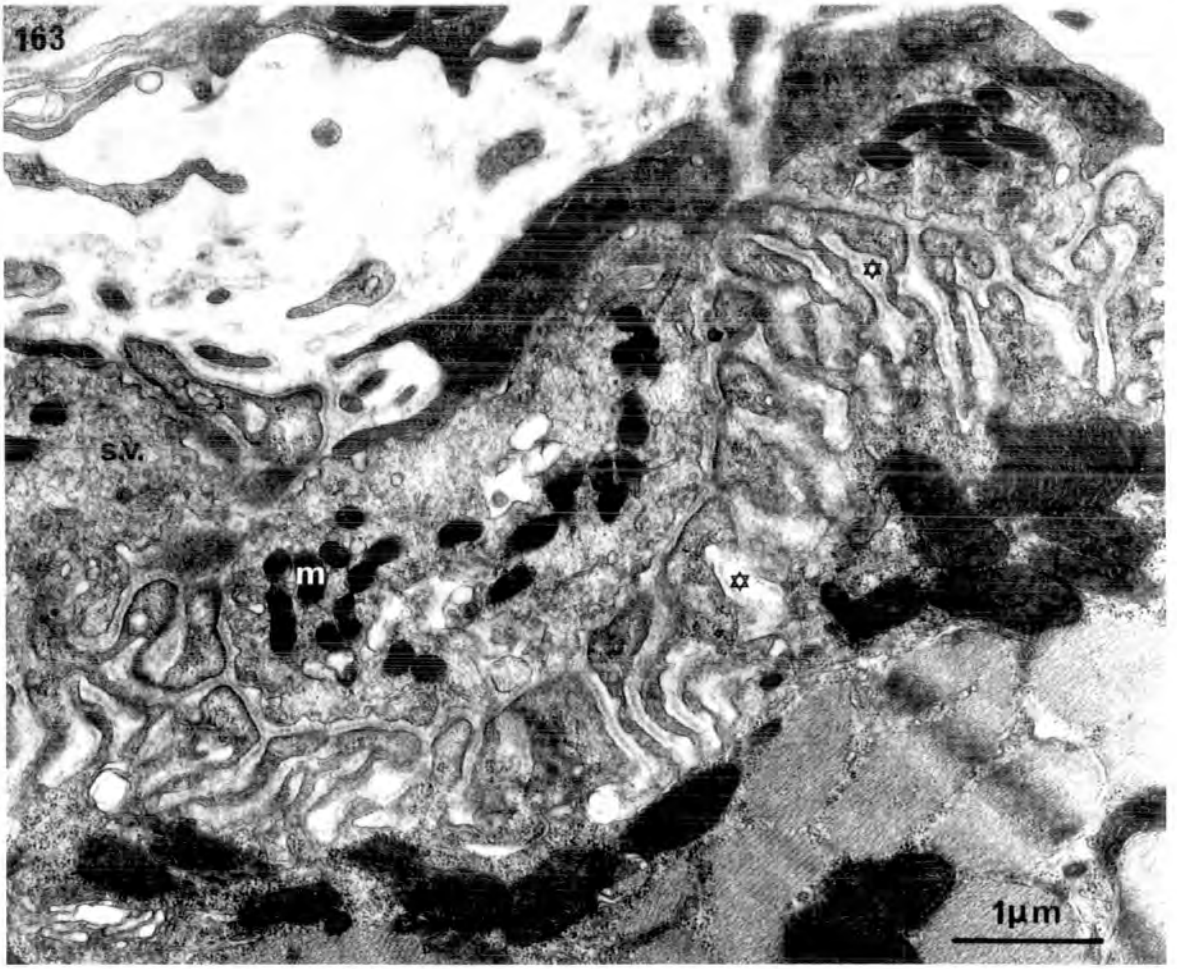
163
s.v.
m
1µm

Figures 164 to 165. Electron micrographs showing the fine structure of axon terminals applied to the small B fibres of LP.

Fig. 164. The axon terminals (a.t.) are small and overlie thin sole plates (s.p.). The junctional folds are widely spaced and frequently bulbous in form (star). Note the two dense-core vesicles (arrowheads). x 20,000

Fig. 165. An axon terminal at higher magnification. Note the mitochondria (m), synaptic vesicles (s.v.) and the bulbous junctional folds, one of which is branched (arrow). x 40,000

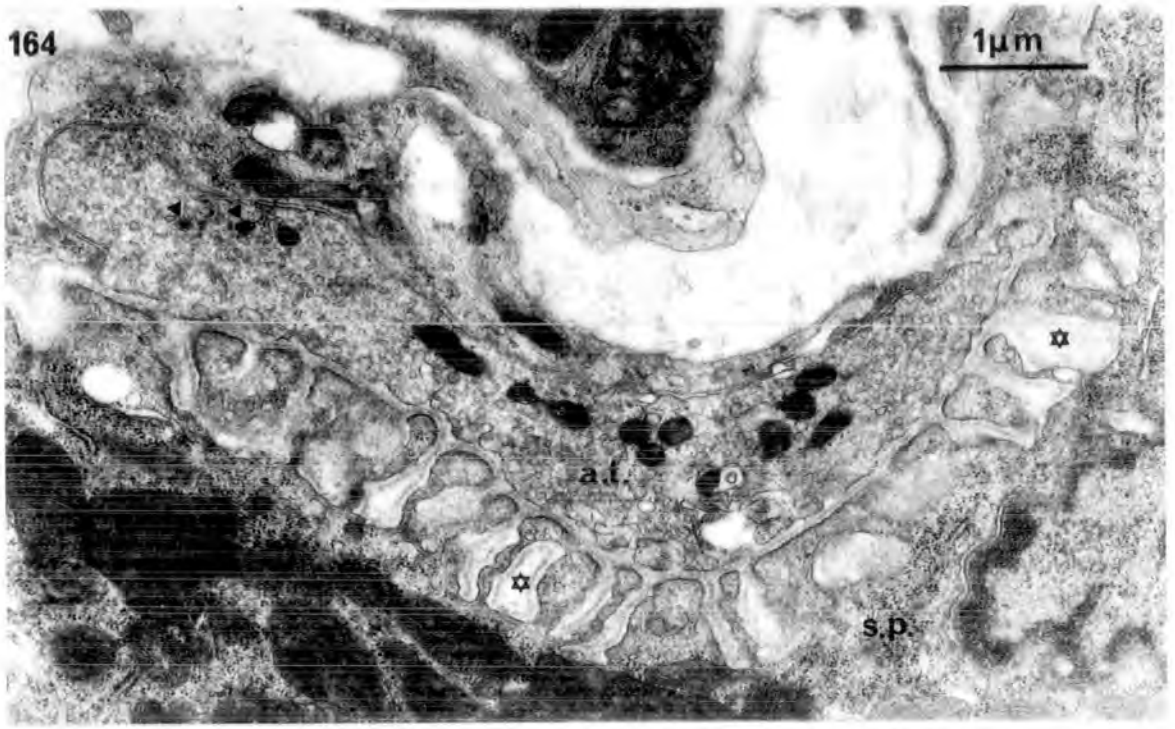
164
1µm
a.f.
s.p.

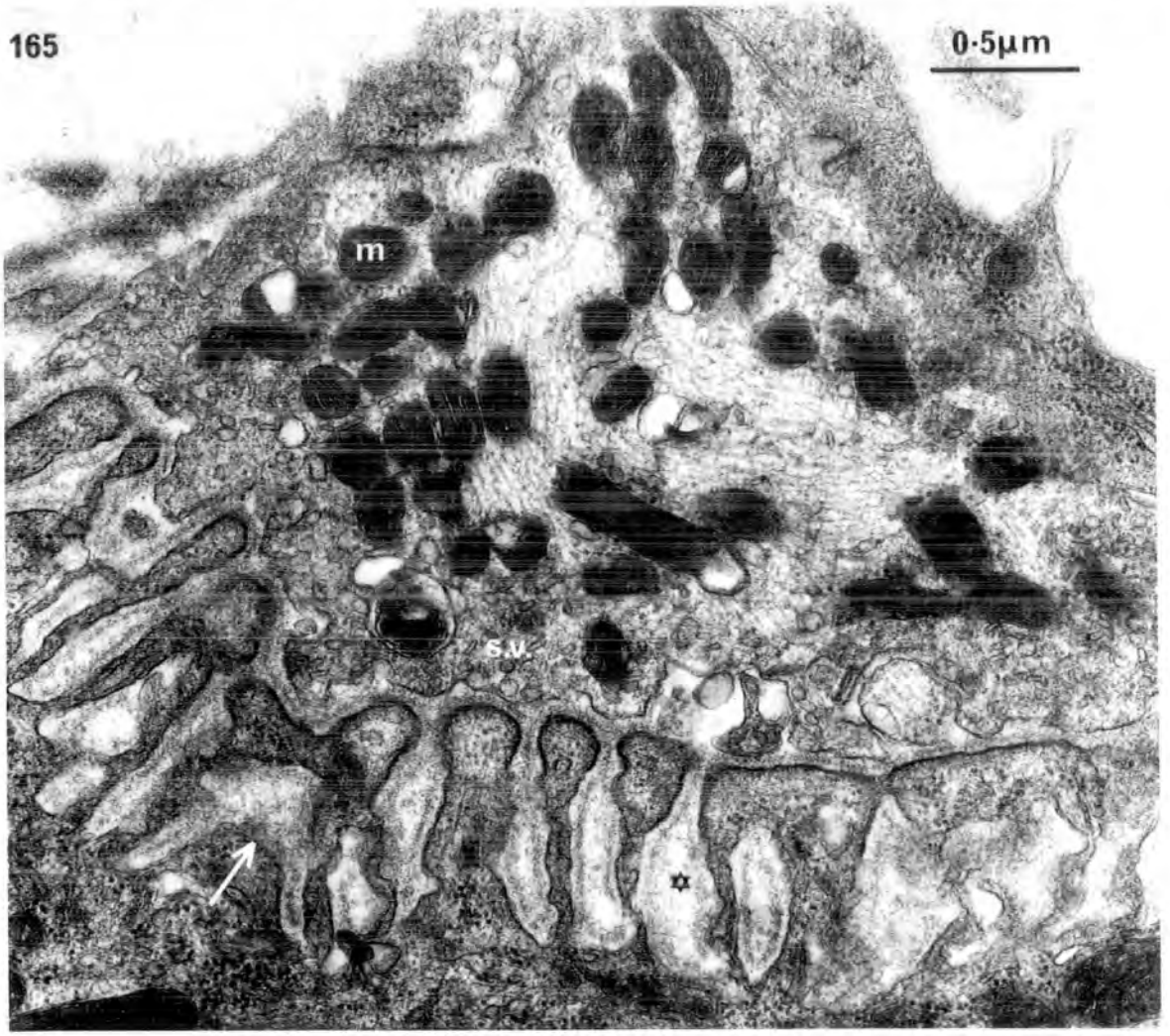
165
0·5µm
m
s.v.

Figures 166 to 169. Histochemical fibre types in an unidentified flexor muscle of the sheep hind foot.

Successive serial transverse sections stained to demonstrate:

Fig. 166. Toluidine blue (histological stain).

Fig. 167. Alkali-preincubated actomyosin ATPase.

Fig. 168. Phosphorylase.

Fig. 169. Succinic dehydrogenase.

Large A, intermediate C, and small B fibres are present. Large A fibres (A) are high for Alk ATPase and P'ase, and low for SDH; intermediate C fibres (C) are high for Alk ATPase, P'ase and SDH; small B fibres (B) are low for Alk ATPase and P'ase, and high for SDH.

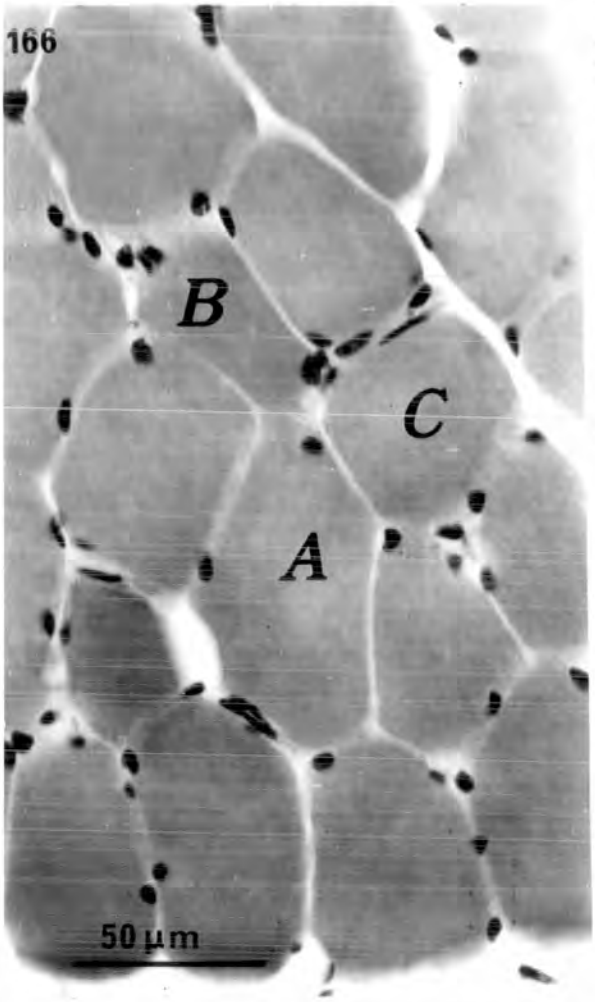
166
B
C
A
50 µm

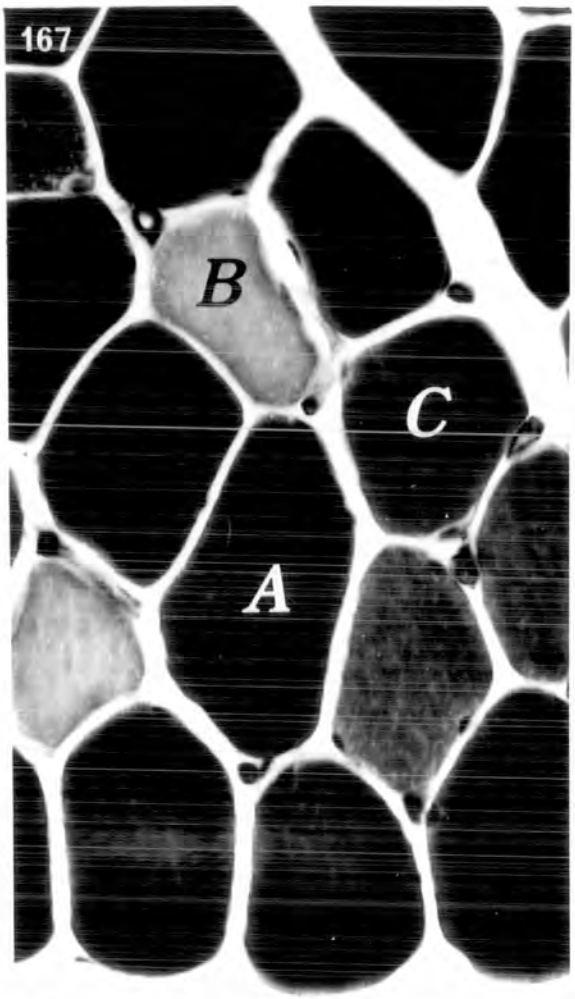
167
B
C
A

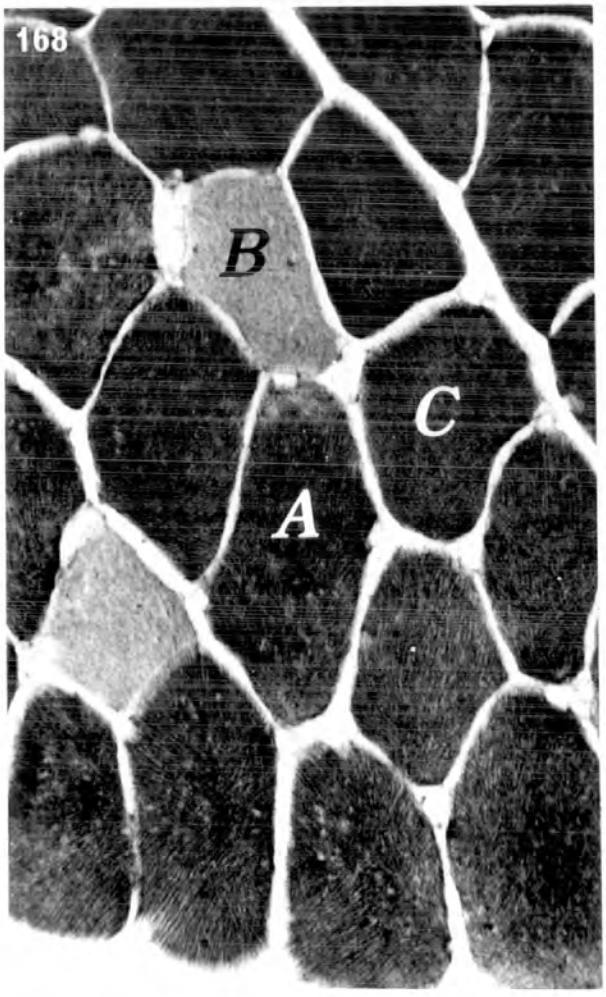
168
B
C
A

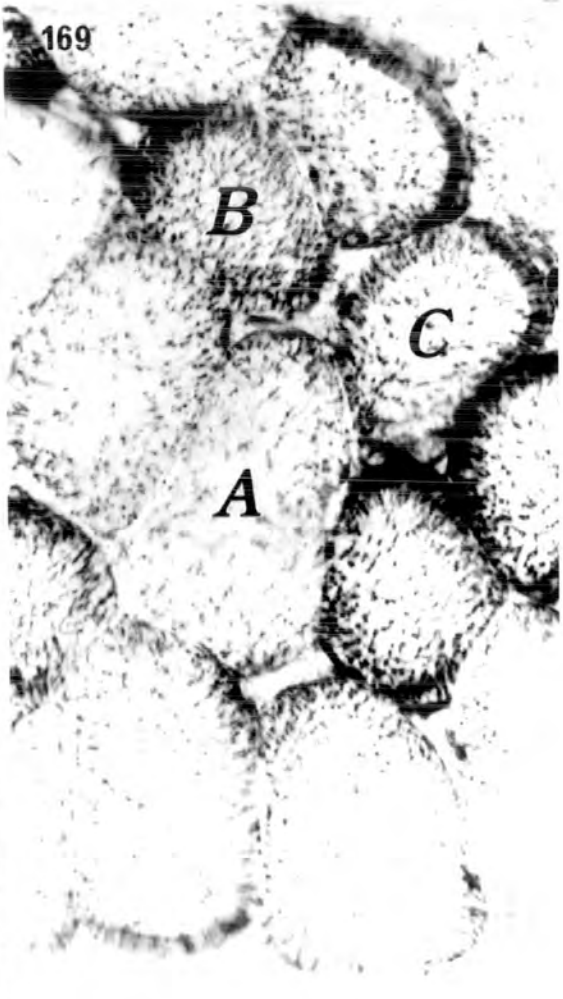
169
B
C
A

Figures 170 to 172. Histochemical fibre types in the distal portion of peroneus brevis from the hind limb of the sheep.

Serial transverse sections stained to demonstrate the following:

Fig. 170. Phosphorylase. Only a few fibres (B types) are low in activity.

Fig. 171. Succinic dehydrogenase. All fibres have a similar, relatively high activity. Note the highly-reactive intrafusal muscle fibres (int.m.f.).

Fig. 172. Alkali-preincubated actomyosin ATPase. Note the high proportion of fibres with low activity.

The muscle is composed of about 1% B type fibres (B); 39% of 'conventional type C' fibres (C); and 60% of 'modified type C' fibres (C^1) that are low with Alk ATPase.

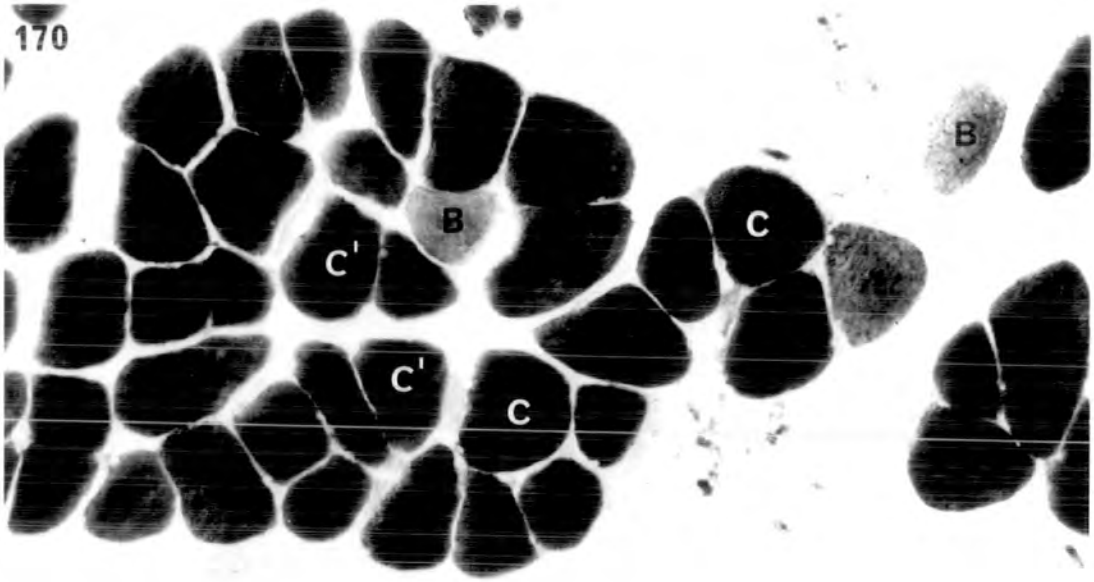
170
B
C
C'
C'
C
B

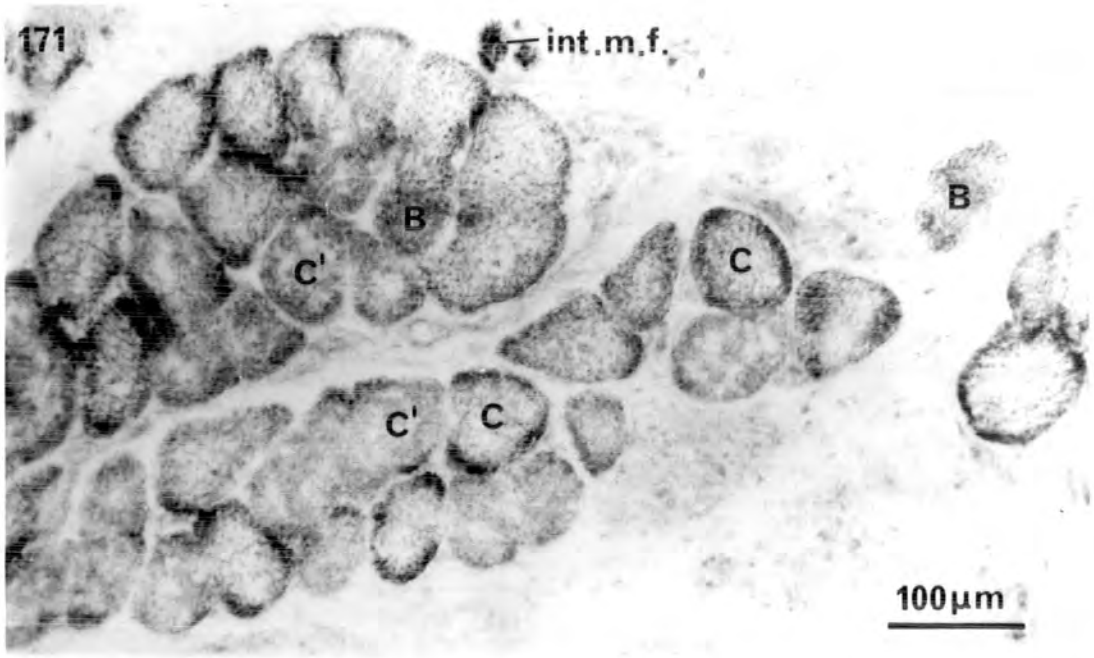
171
int.m.f.
B
C'
C
B
C'
C
100µm

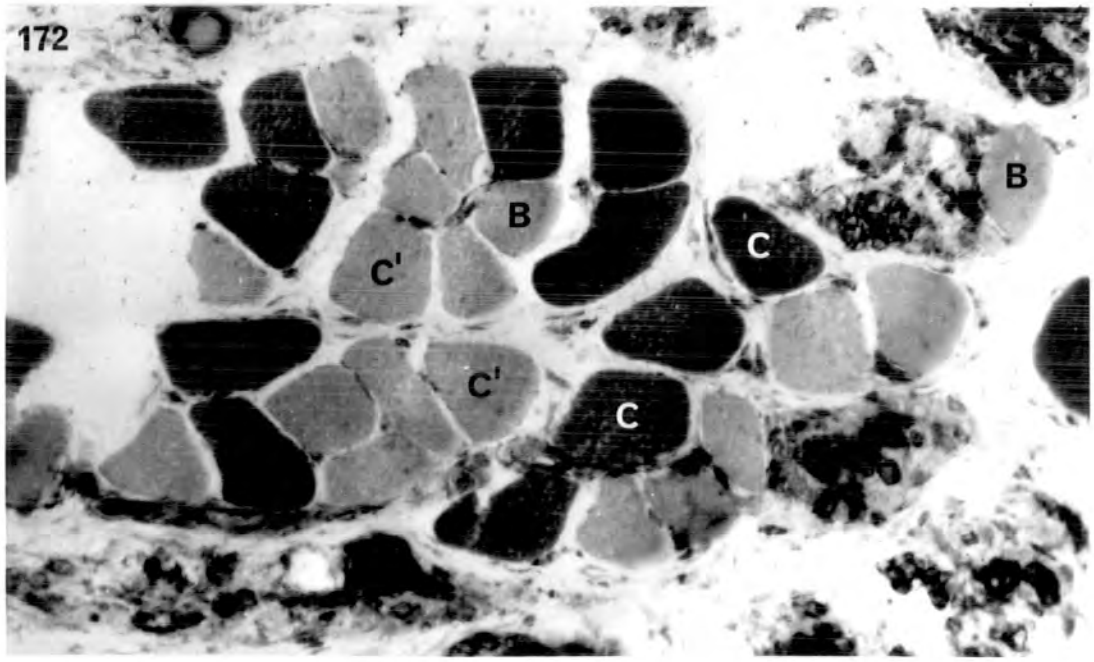
172
B
C'
C
B
C'
C

Figure 173. Electron micrograph of a longitudinal section through a representative PB muscle fibre.

Note the triads (tr) that occur regularly at the A/I band junction; the sarcoplasmic reticulum (s.r.); the Z line (Z) with Z filaments; and the prominent M line (M) within a pseudo-H zone (marked by lines).

x 26,600

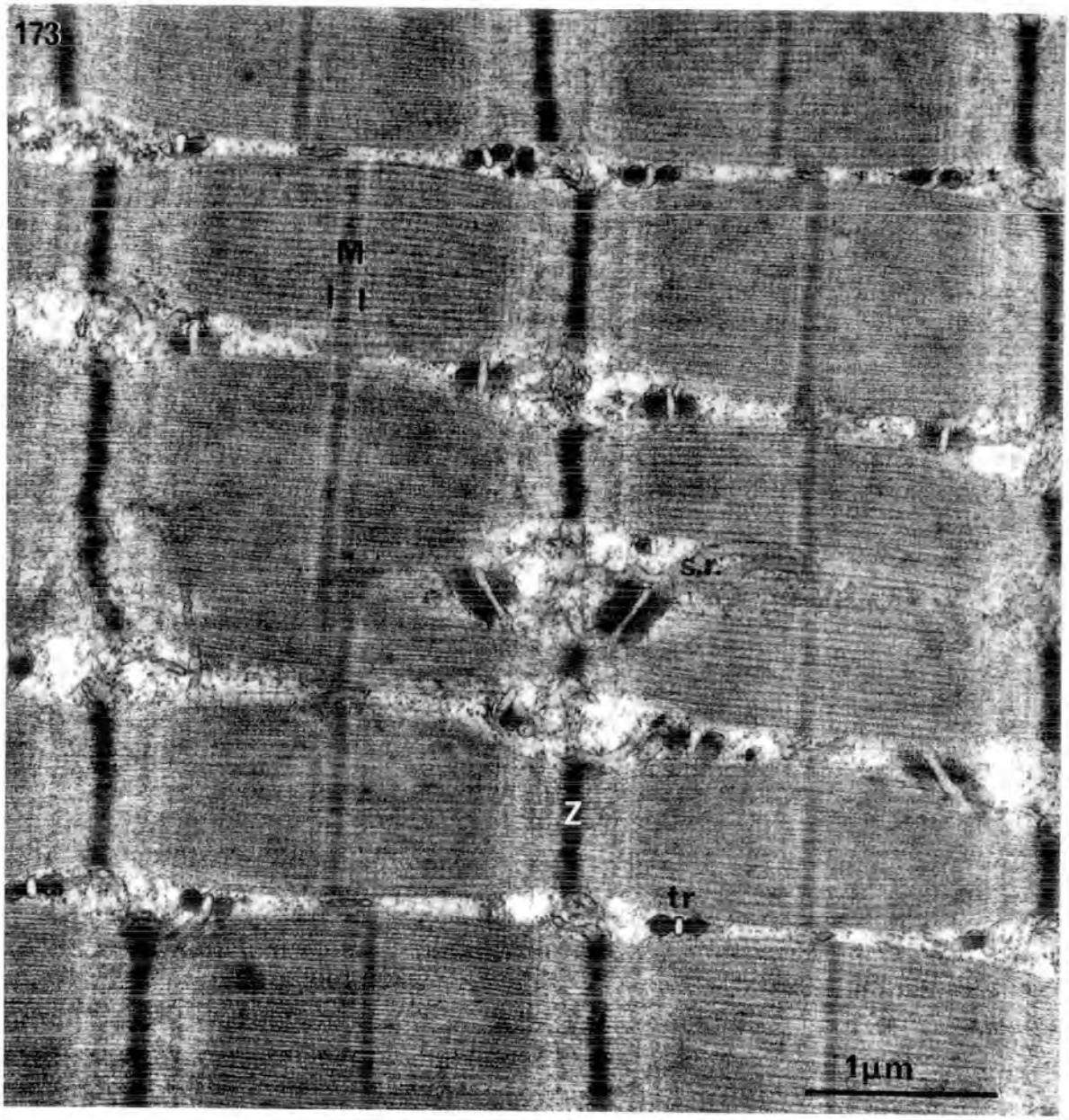
173
M
S.R.
Z
tr
1µm

Figures 174 to 175. Electron micrographs of the myoneural junctions in sheep peroneus brevis muscle.

Fig. 174. Transverse section of a typical myoneural junction. Three axon terminals (a.t.) lie in gutters above a substantial sole plate (s.p.) with sole plate nuclei (s.p.n.). The myofibrils (mf) are small and well-delineated. Mitochondria (m) are small and scattered throughout a transverse section.

x 8,000

Fig. 175. Transverse section of a myoneural junction at slightly higher magnification. The axon terminals contain mitochondria (m) and synaptic vesicles (s.v.). The junctional folds (j.f.) are long and narrow and project well into the extensive sole plate.

x 12,600

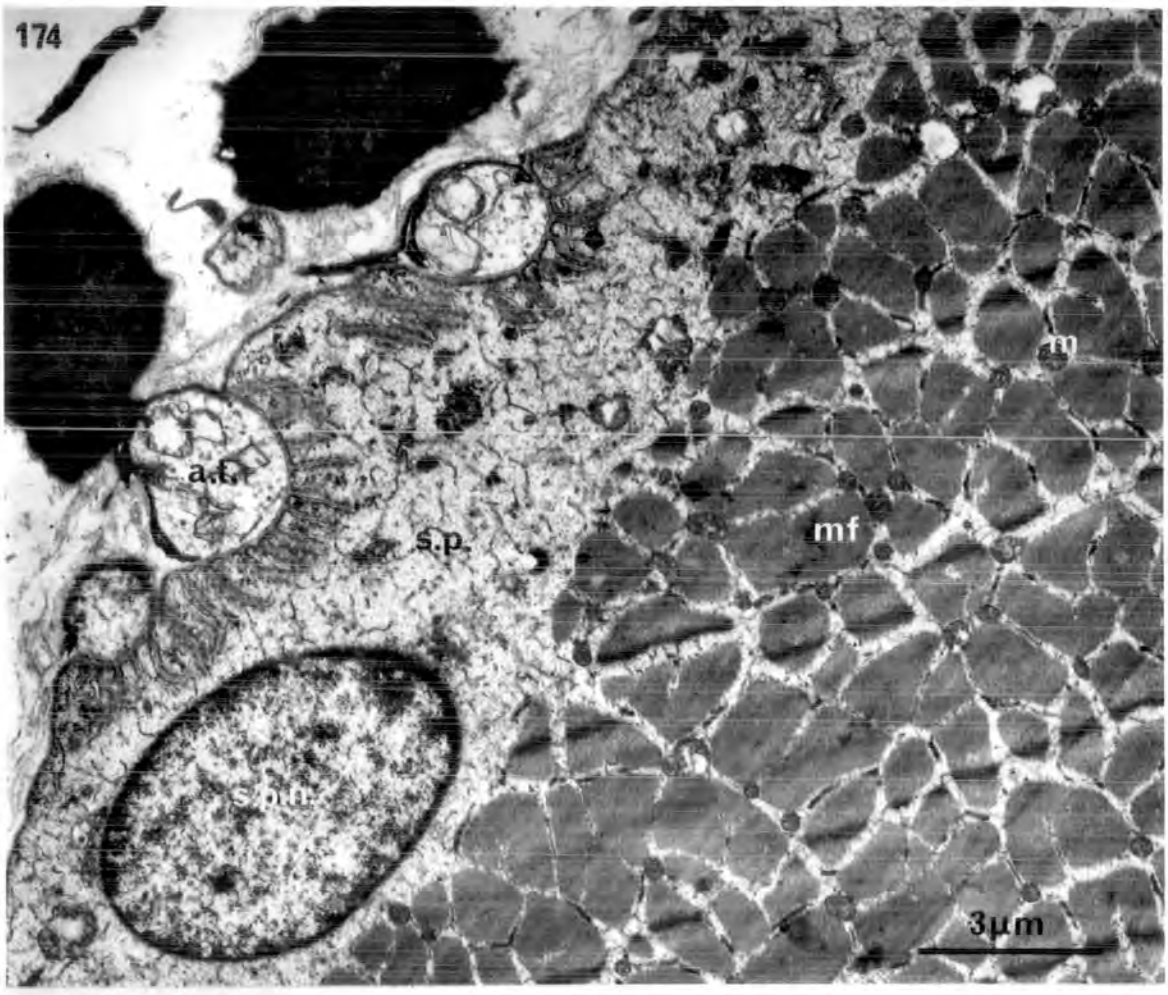
174
a.t.
s.p.
s.n.
m
mf
3µm


175
m
s.v.
j.f.
s.p.
s.p.
2µm

Figures 176 to 179. Longitudinal division of muscle fibres in PB.

A series of low-power electron micrographs show the division of an extrafusal muscle fibre in transverse section. All x 2,000

Fig. 176. The outer membrane is slightly constricted (arrows) while the myofibrils retain their normal pattern.

Fig. 177. A line of separation has formed that follows a curve between the constrictions (arrows).

Fig. 178. The sarcolemma invaginates to form a thin fold at one end of the separation line.

Fig. 179. The daughter fibre (DF) eventually separates from the parent muscle fibre (PF).

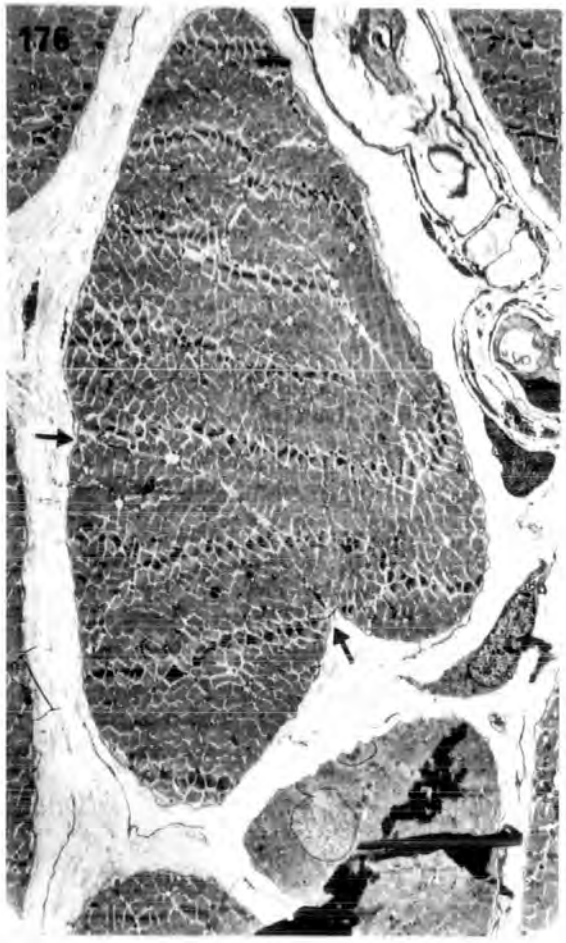
176


177


178
100µm

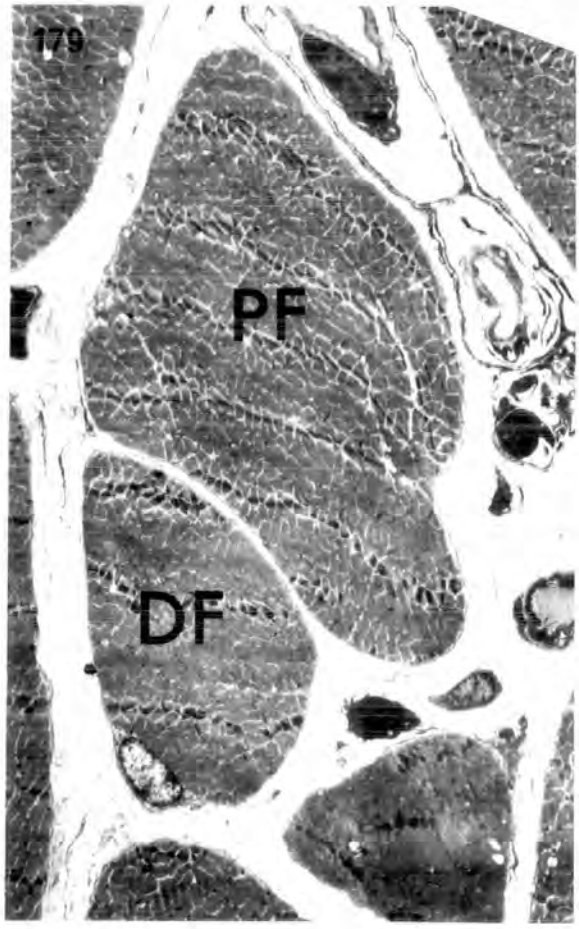
179
PF
DF

Figures 180 to 181. Longitudinal division of muscle fibres in PB.

A parent muscle fibre is shown at the stage of incipient division into two equal daughter fibres.

Fig. 180. The invaginating fold has spread just over half of the way along the line of separation (star).

x 2,000

Fig. 181. Part of fig. 180 at higher magnification to show the pinocytotic vesicles (p.v.) lining the tip of the invaginating fold and the zone immediately beyond it, which is incompletely divided.

x 12,600

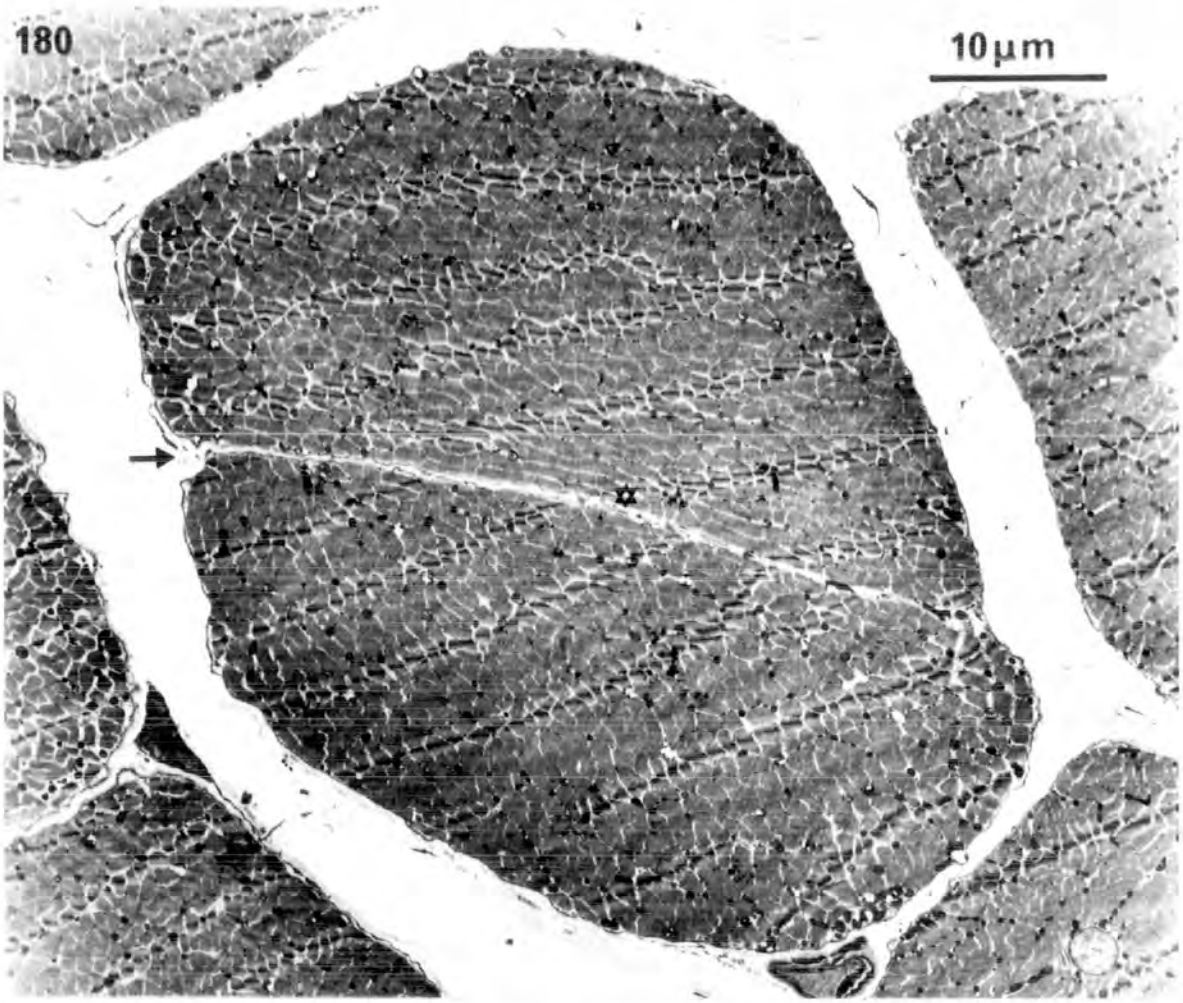
180
10µm

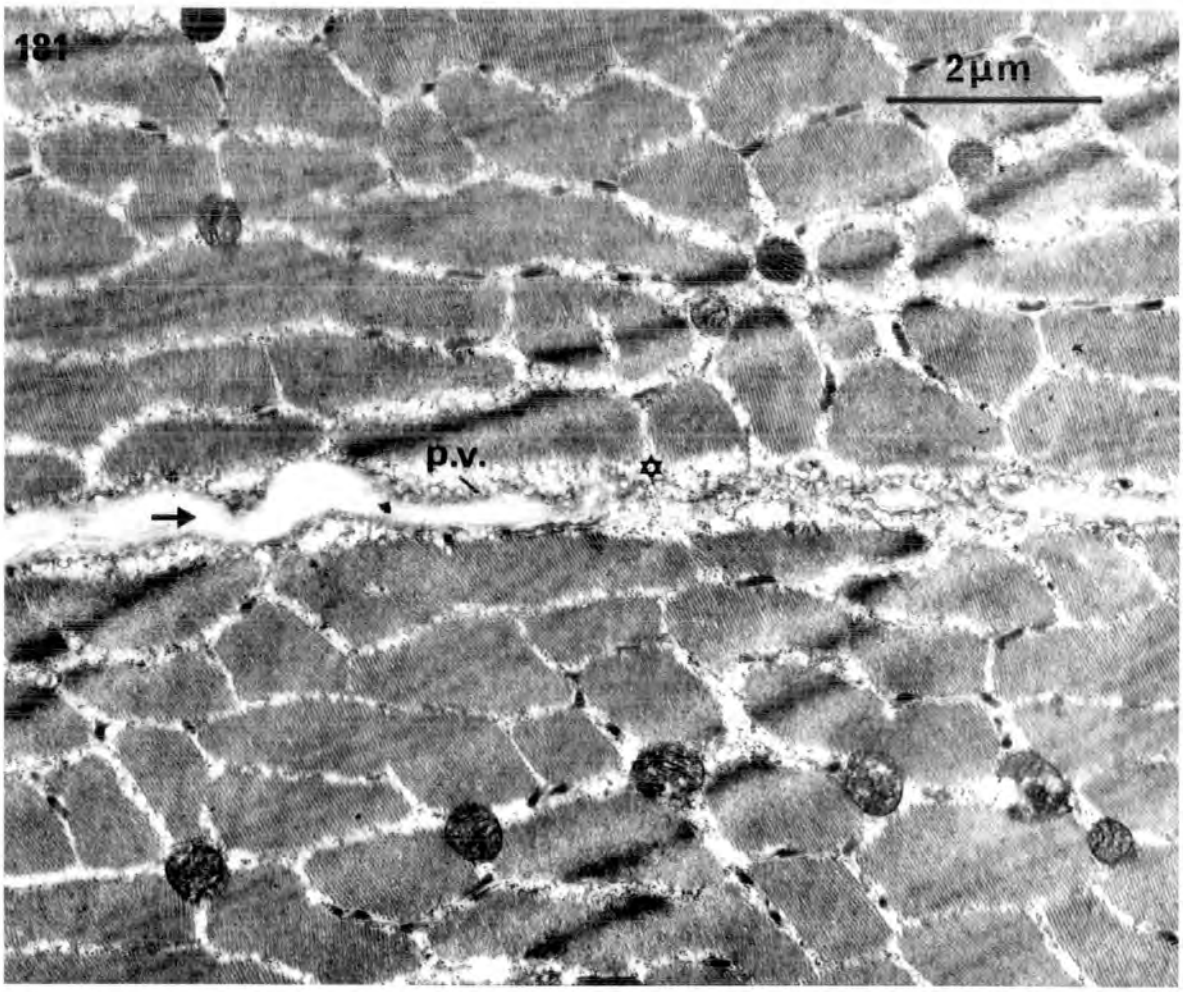
181
2µm
p.v.

Figures 182 to 183. Electron micrographs of the occasional 'fragmented' muscle fibres in the distal portion of PB.

Fig. 182. Low-power transverse section showing a single muscle fibre (MF), the majority of which appears normal, and a portion of which is extensively fragmented (FP).

x 2,000

Fig. 183. Part of fig. 182 above at higher magnification showing the fragmented portion of the muscle fibre. The whole portion is well-separated from the parent muscle fibre, while within the portion the myofibrils are divided into irregular pieces, some of which are smaller than a single myofibril.

x 5,000

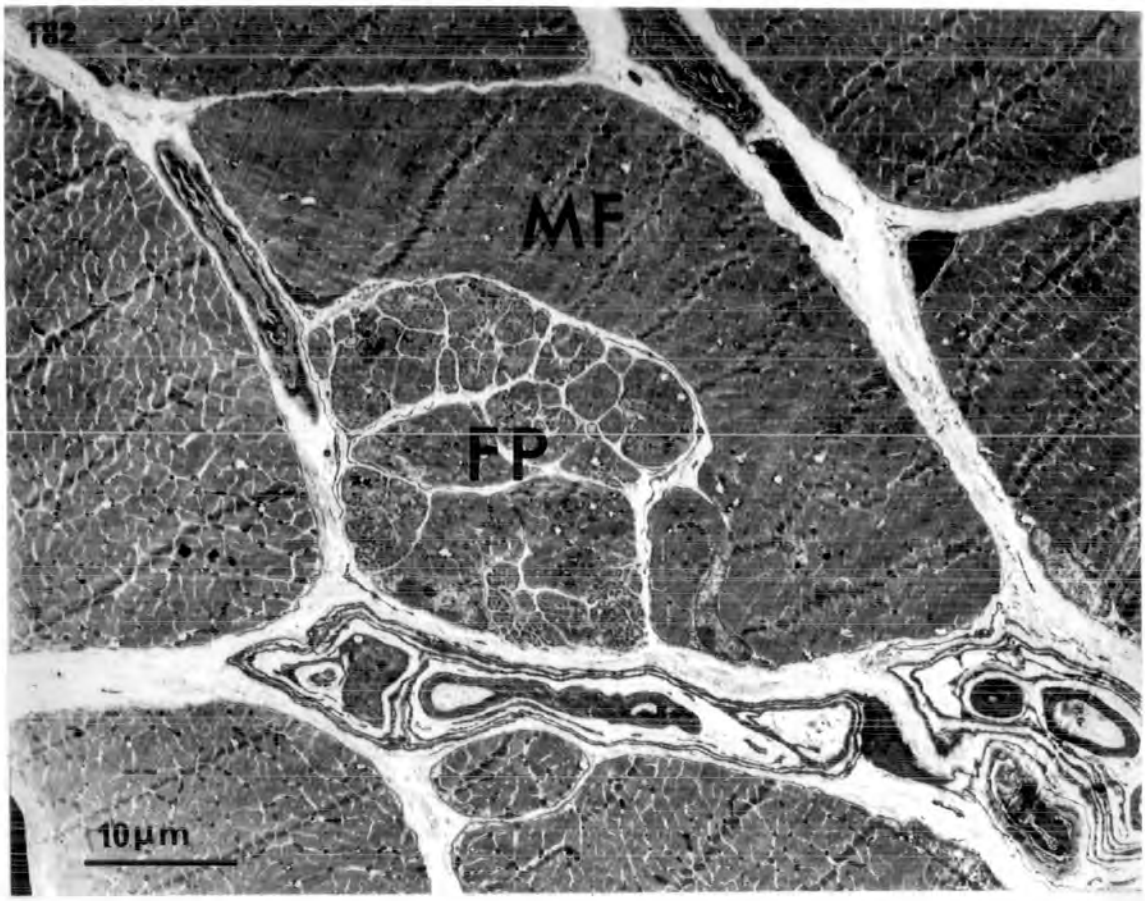
182
MF
FP
10µm

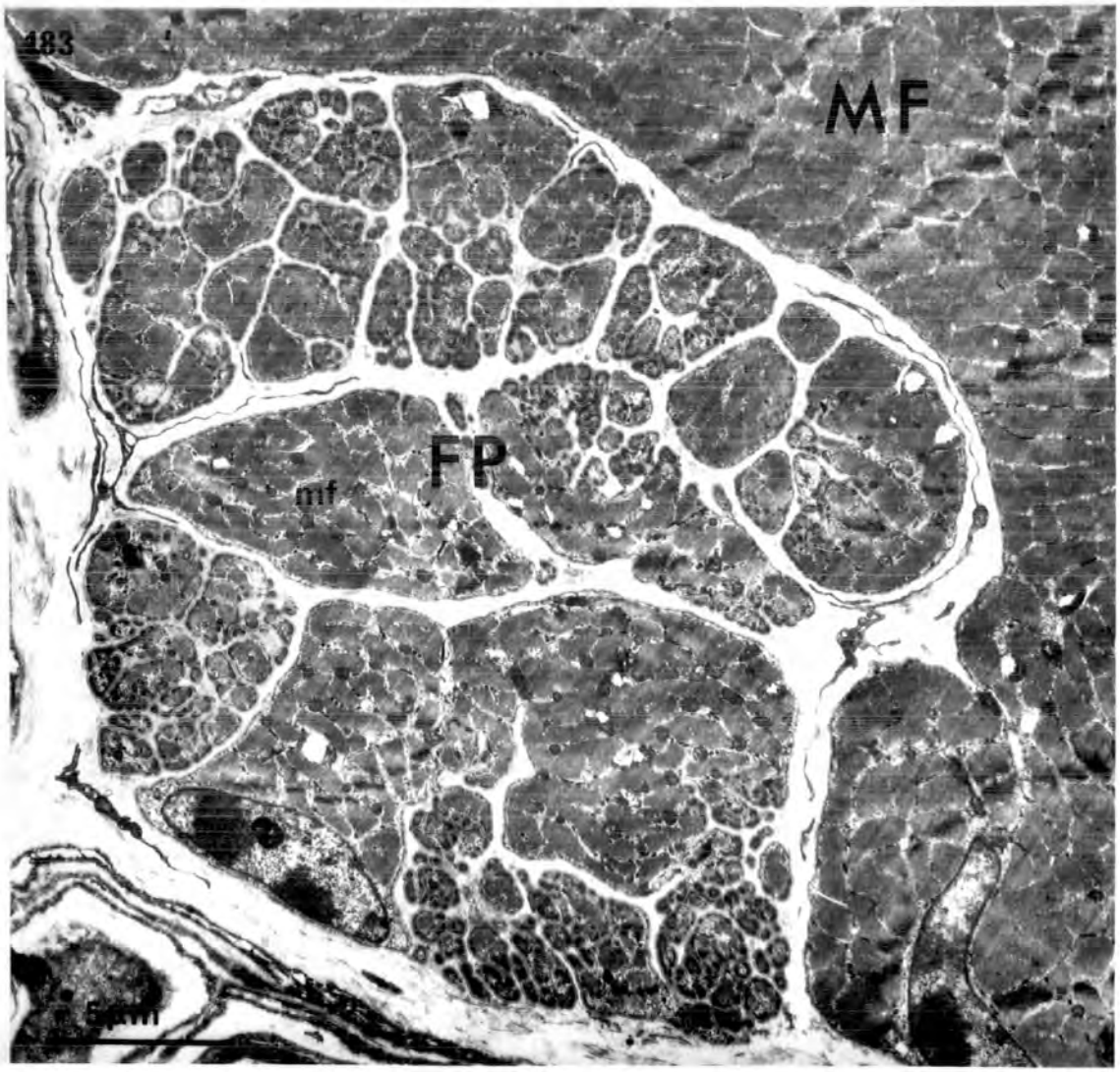
183
MF
FP
mf
10µm

Figures 184 to 186. Parasitic infection of extraocular muscle by Sarcocystis.

Fig. 184. Light micrograph of teased, silver preparation of a single muscle fibre that contains a central cyst.

Figs. 185 & 186. Electron micrographs of a transverse section through a sarcocyst in levator palpebrae. The complex cyst wall (c.w.) separates the central spores (sp.) from the peripheral rim of myofibrils (mf.). Fine trabeculae (trab.) run between each group of spores.

Fig. 185 x 2,000
Fig. 186 x 8,000

184

185

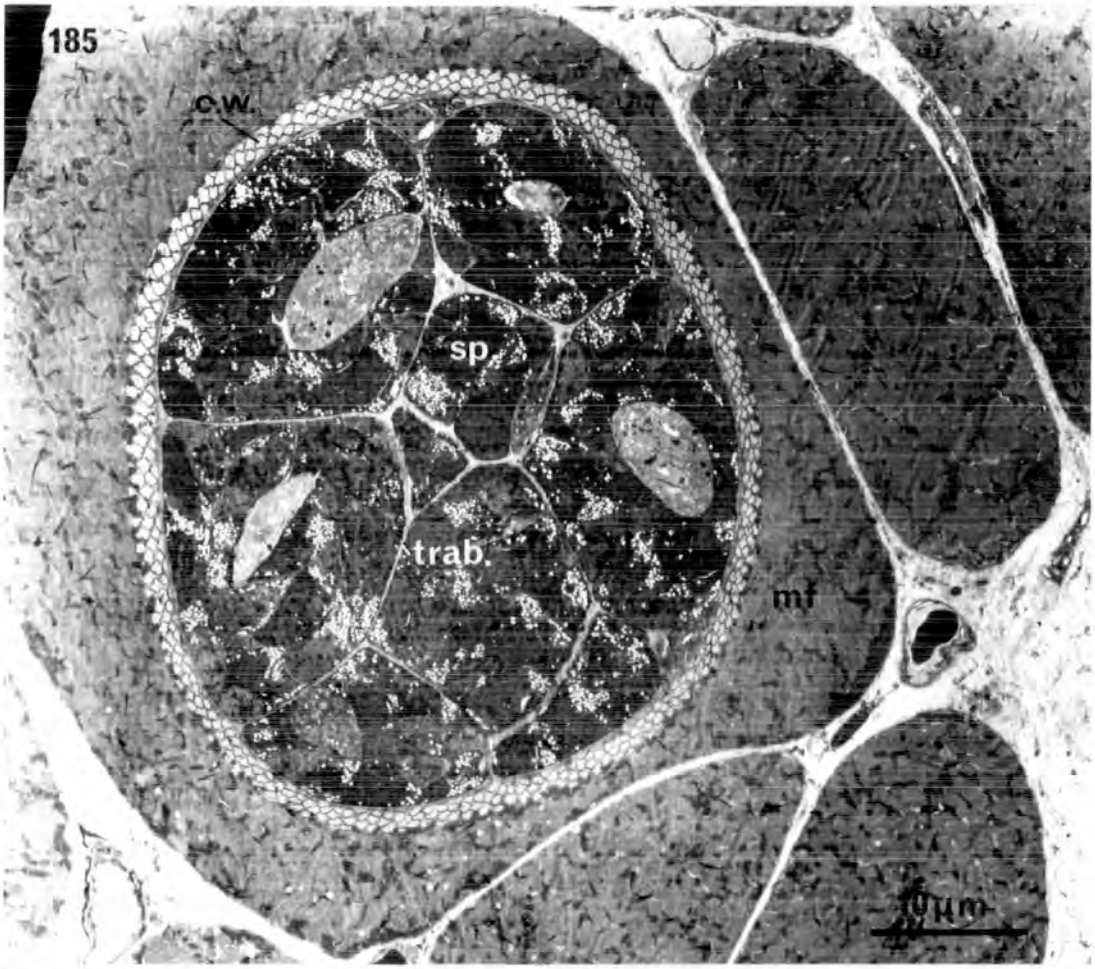

186

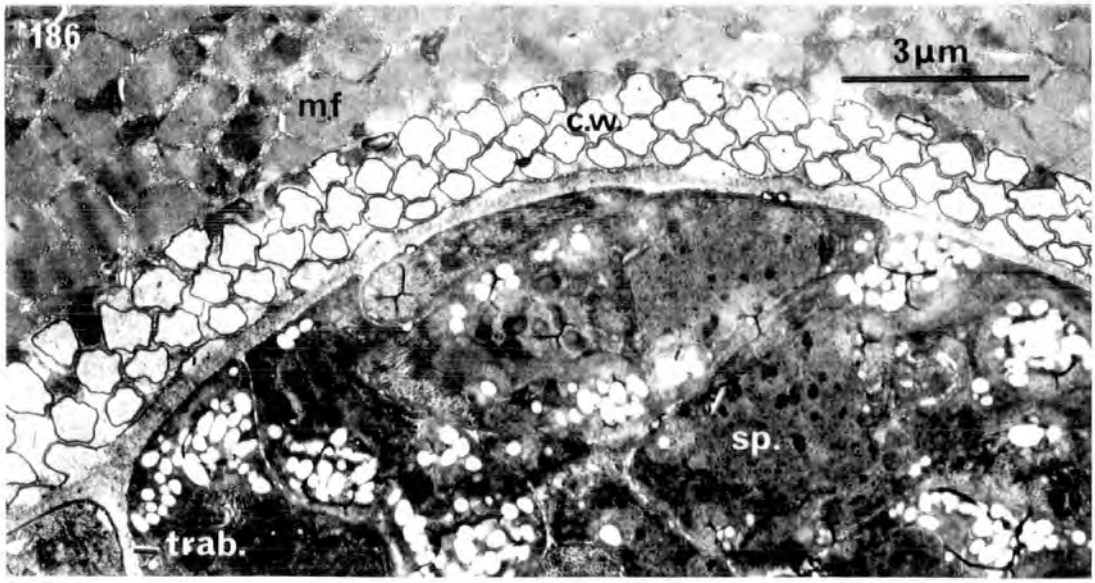

Figures 187 to 188. A complex parallel spindle system in SR.

Successive serial transverse sections processed for:

Fig. 187. Weigert & van Gieson histological stain.

Fig. 188. Succinic dehydrogenase.

The axial bundle is composed of two sets of intrafusal muscle fibres (separated by dotted lines) enclosed within a common capsule (cps.). The set of fibres on the left contains two bag fibres (arrows) and eleven chain fibres, whereas the set on the right contains one bag fibre and six chain fibres.

In fig. 188 the bag fibres exhibit low activity with SDH (compare with fig. 187) and most of the chain fibres show high activity. However, the six chain fibres on the right are close to the equatorial region and are consequently greatly reduced in diameter, have central nuclei (n), and show reduced histochemical activity. pa.s., periaxial space; ext.m.f., extrafusal muscle fibre.

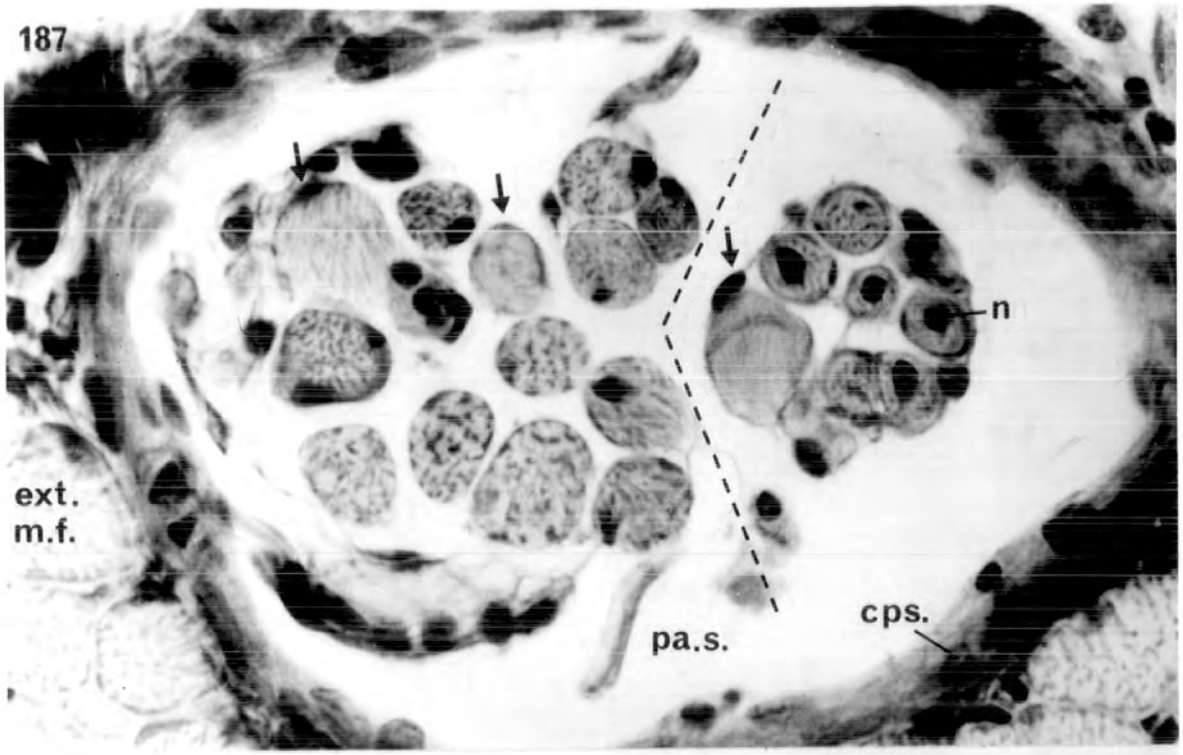
187
n
ext.
m.f.
pa.s.
cps.

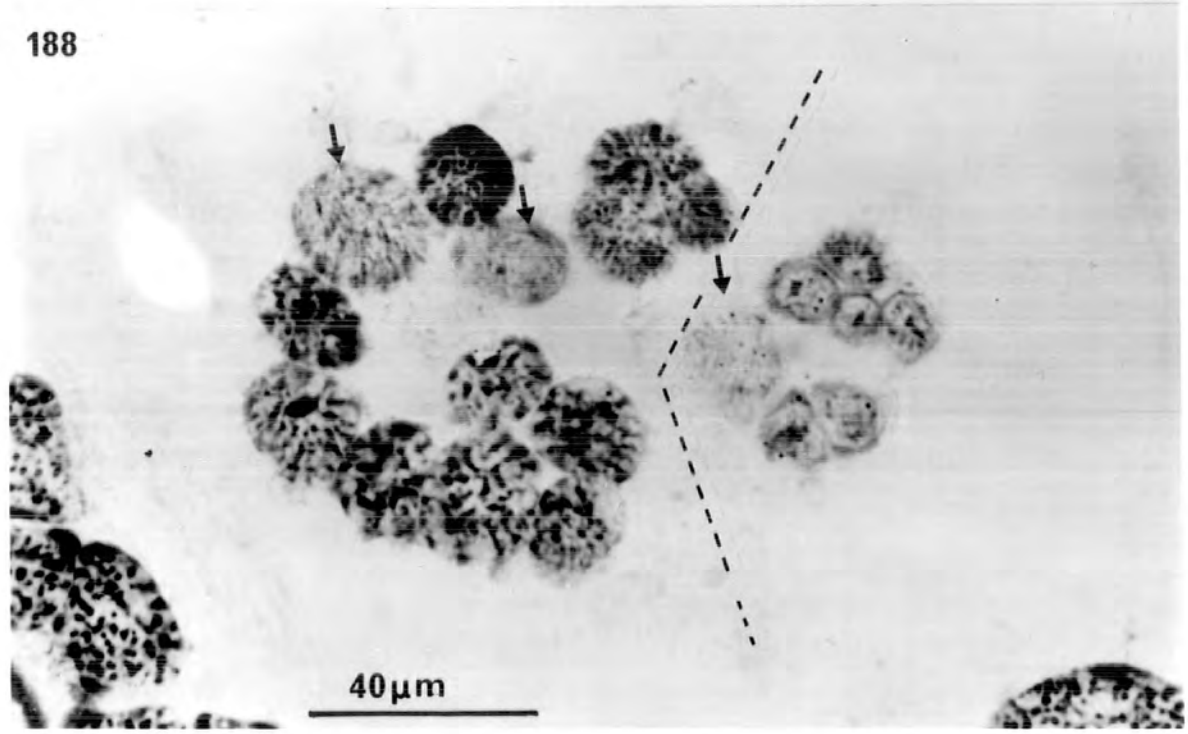
188
40µm

Figure 189. Projection plan of SR and LP muscles showing the distribution of muscle spindle capsules.

The position and lengths of the capsules are plotted as lines within the limits of a single representative longitudinal section. The 181 capsules in SR and the 61 capsules in LP are distributed evenly throughout the lengths of the muscles.

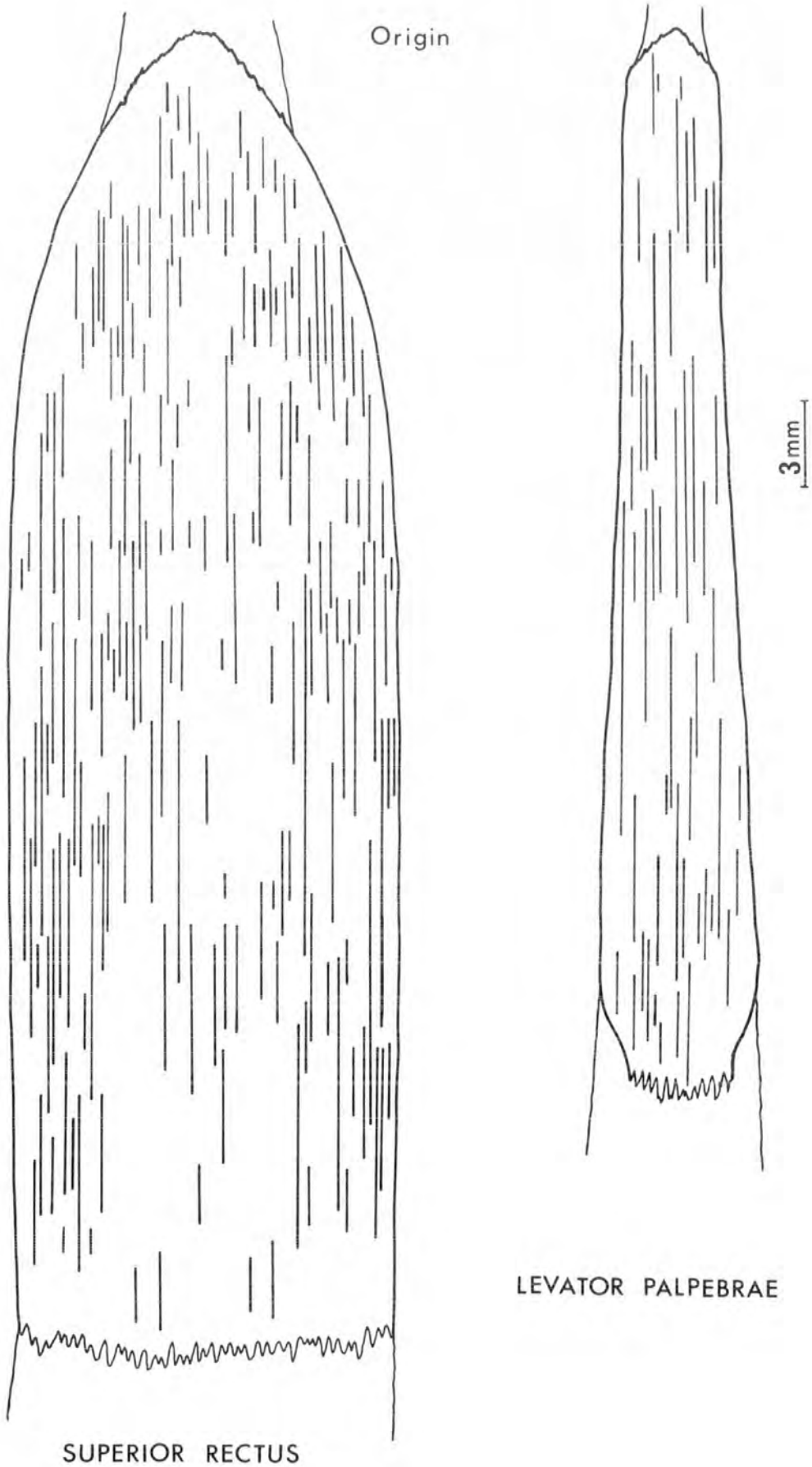
Origin
3mm
SUPERIOR RECTUS
LEVATOR PALPEBRAE

Figure 190. Schematic representation of the location of spindles in SR.

The diagrams are based on sections stained to demonstrate phosphorylase activity (see figs. 10 & 7). The section representing the insertion end is taken from the middle of the distal third of the muscle, and that representing the belly from the centre of the muscle. At the insertion end most spindles (ringed) are located in the junctional region between the peripheral patch and orbital rim layers. In the belly the spindles are still peripheral, but lie in the orbital rim layer.

INSERTION

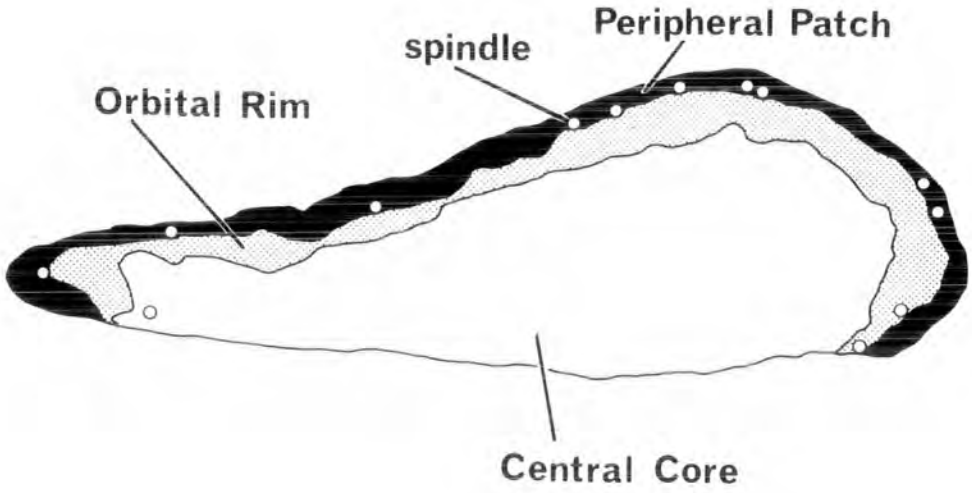

BELLY

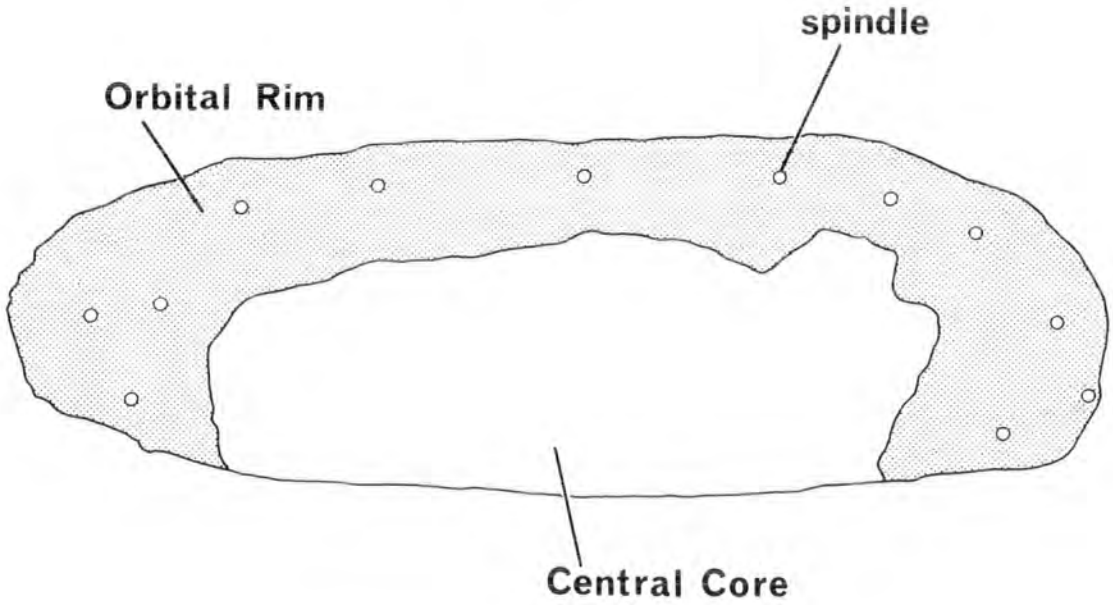

Figures 191 to 196. The histochemistry of intrafusal muscle fibres in SR.

Figs. 191 to 194. Successive serial transverse sections through the mid-polar region of a spindle, stained to demonstrate:

Fig. 191. Phosphorylase.

Fig. 192. Succinic dehydrogenase.

Fig. 193. Alkali-preincubated actomyosin ATPase.

Fig. 194. Acid-preincubated actomyosin ATPase. Note the G-type histochemical profile of the single bag fibre (arrow) and the C-type profile of the three chain fibres. cps., capsule.

Figs. 195 to 196. Serial transverse sections through the juxta-equatorial region of a spindle, stained to demonstrate:

Fig. 195. Alkali-preincubated actomyosin ATPase.

Fig. 196. Acid-preincubated actomyosin ATPase.

Note that one of the bag fibres (star) has a slightly higher activity with Alk ATPase, but that both bag fibres stain intensely with Acid ATPase. (n-b.)

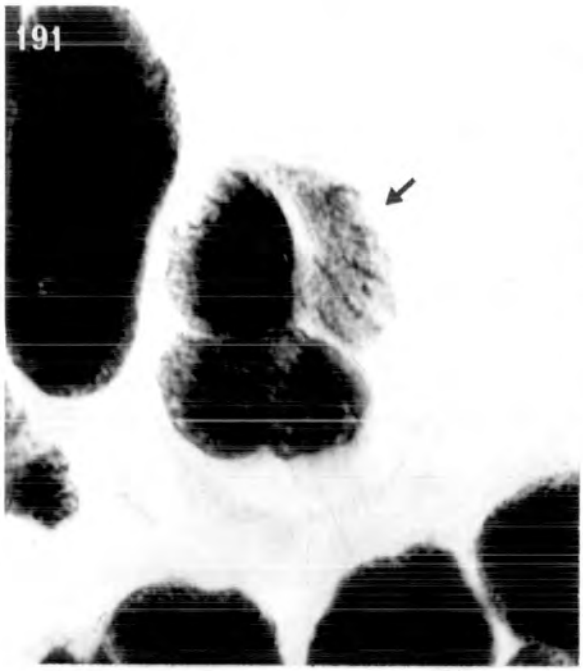
191

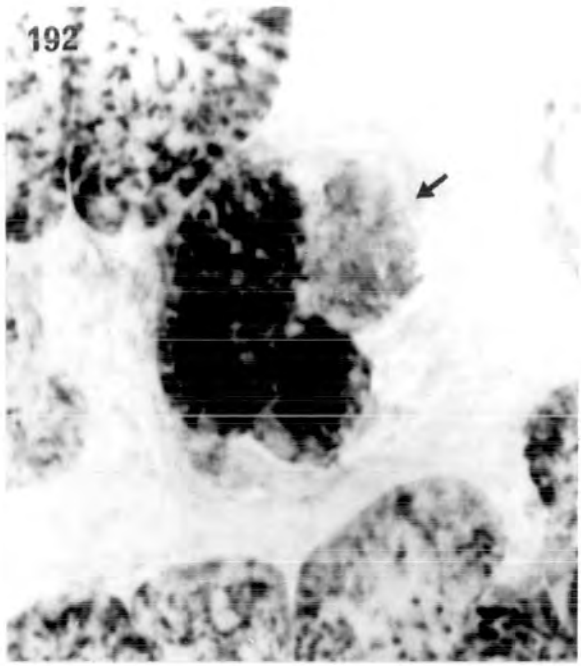
192

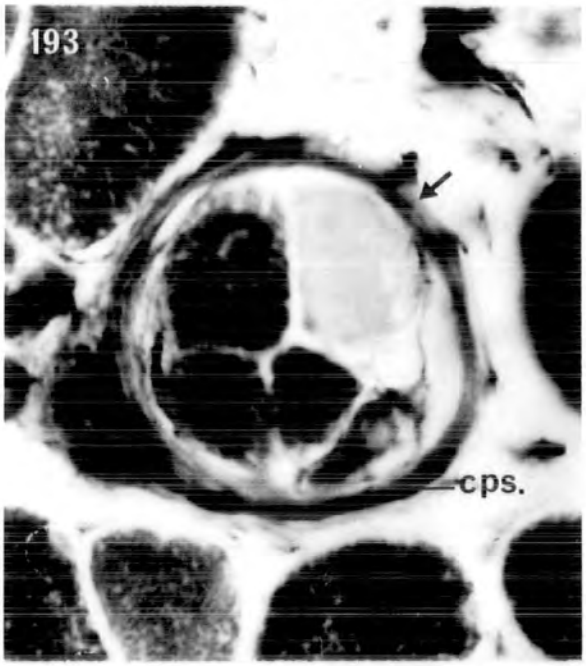
193
cps.

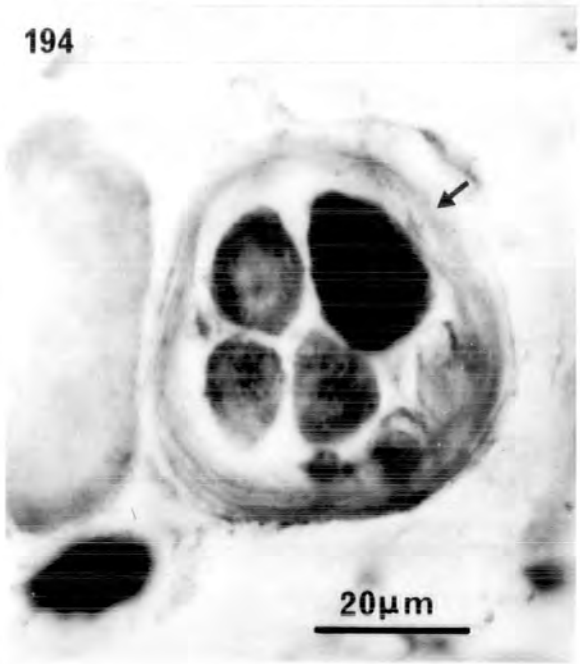
194
20µm

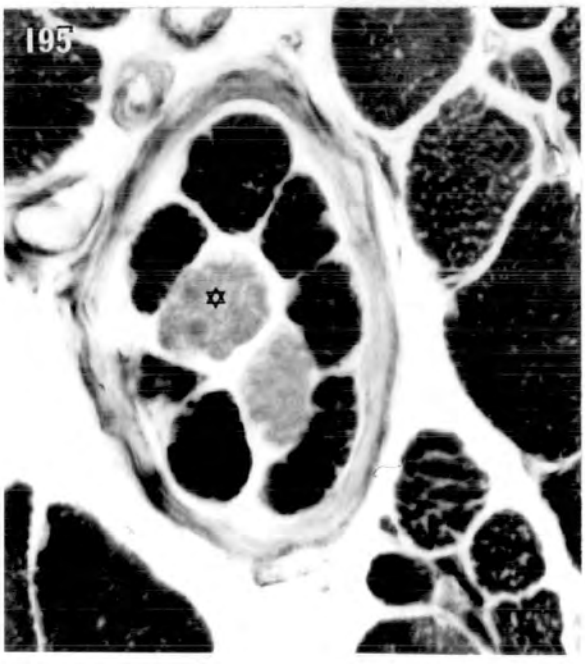
195

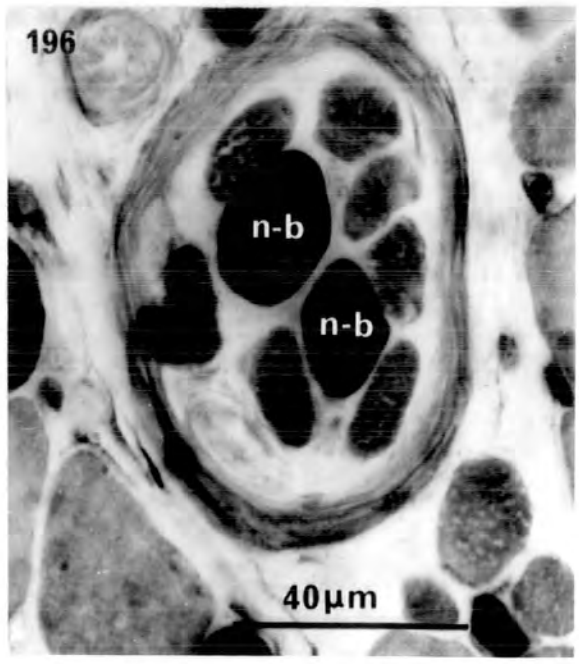
196
n-b
n-b
40µm

Figures 197 to 206. <u>The histochemistry of intrafusal muscle fibres in SR</u>.

Successive serial transverse sections through the juxta-equatorial region of one spindle (on the left), and through the extreme polar region of a second spindle (on the right), stained to demonstrate:

Figs. 197 & 198. Weigert & van Gieson.

Figs. 199 & 200. Phosphorylase.

Figs. 201 & 202. Succinic dehydrogenase.

Figs. 203 & 204. Alkali-preincubated actomyosin ATPase.

Figs. 205 & 206. Acid-preincubated actomyosin ATPase.

The first spindle, located in the peripheral patch layer, is composed of one bag fibre (n-b) and one chain fibre (n-c) only.

The second spindle, at the given level of section, shows two bag fibres (n-b) and one chain fibre (n-c). Note that both bag fibres give the acid-reversal with Acid ATPase (Fig. 206). cps., capsule.

All figures are the same magnification.

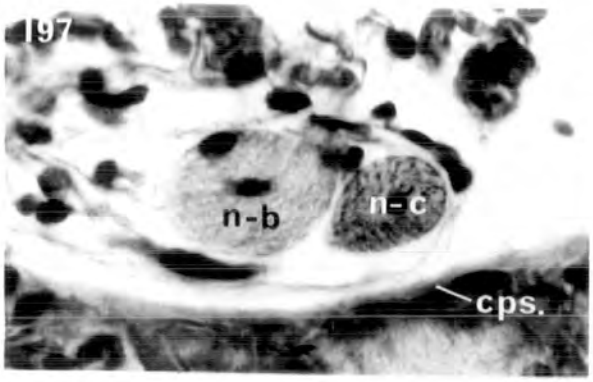
197
n-b
n-c
cps.

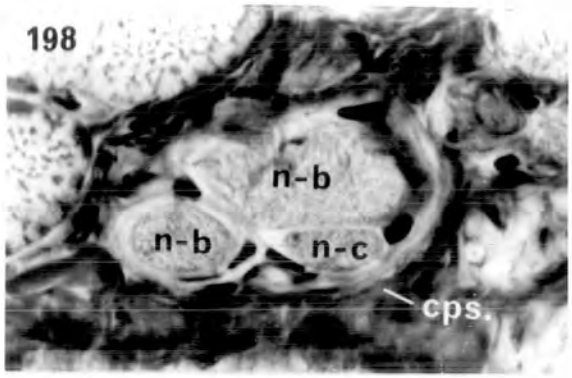
198
n-b
n-b
n-c
cps.

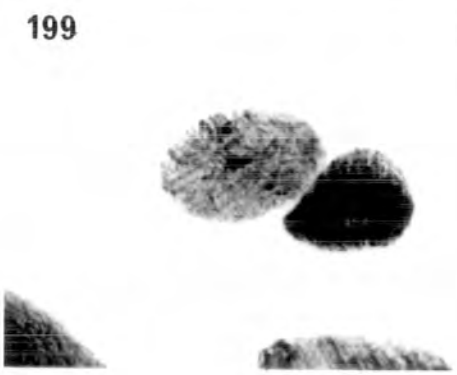
199

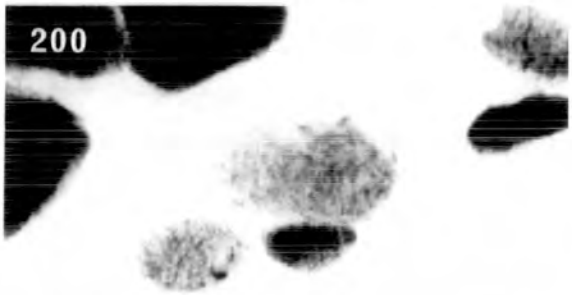
200


201

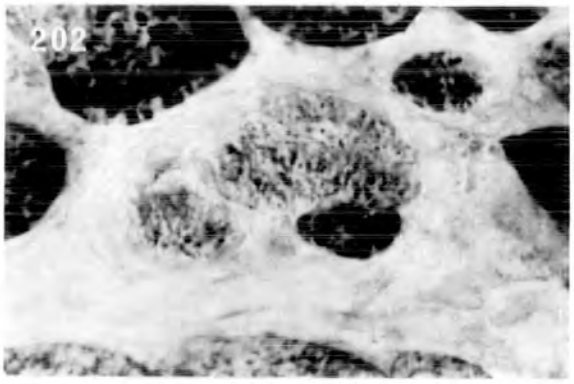
202

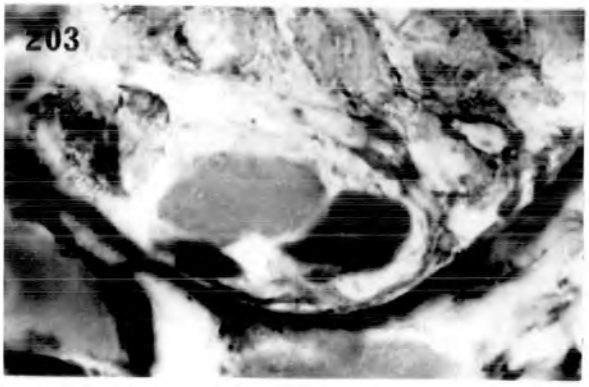
203


204

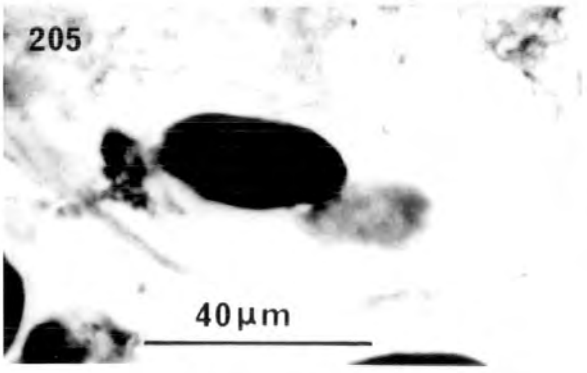
205
40µm

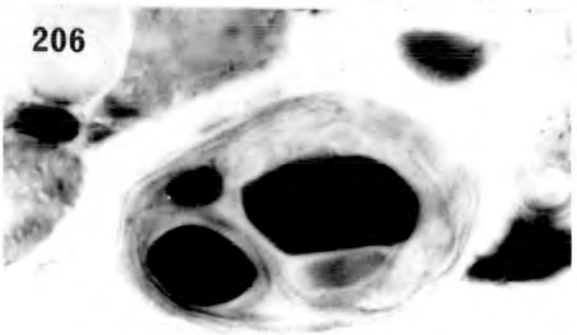
206

Figures 207 to 211. The histochemistry of intrafusal muscle fibres in LP.

Serial transverse sections through the juxta-equatorial region of one spindle (figs. 207 - 209), and through the mid-polar region of a second spindle (figs. 210 - 211), stained to demonstrate:

Figs. 207 & 210. Alkali-preincubated actomyosin ATPase.

Fig. 208. Phosphorylase.

Figs. 209 & 211. Succinic dehydrogenase.

The bag fibres (arrows) show low activity with all three histochemical reactions, whereas the chain fibres show high activity. cps., capsule.

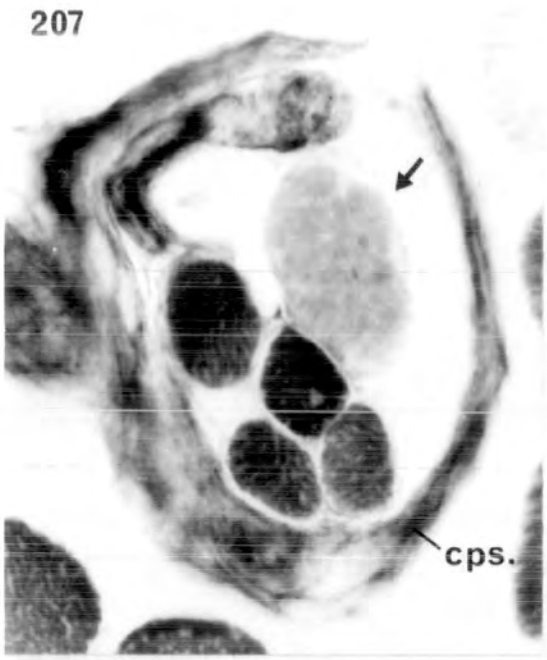
207
cps.

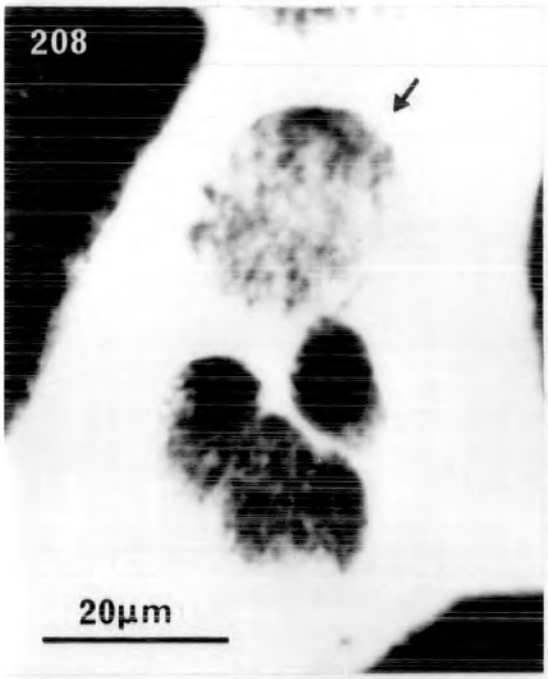
208
20µm


209


210
cps.


211
20µm

Figures 212 to 217. <u>The histochemistry of intrafusal muscle fibres in peroneus brevis</u>.

Serial transverse sections of the same spindle through polar (figs. 212 - 214) and extreme polar (figs. 215 - 217) regions, stained to demonstrate:

Figs. 212 & 215. Alkali-preincubated actomyosin ATPase.

Figs. 213 & 216. Succinic dehydrogenase.

Figs. 214 & 217. Phosphorylase.

In figs. 212 - 214 the small-diameter chain fibres show high activity with all three histochemical stains. One of the bag fibres (n-b2) has a similar staining profile to the chain fibres; the other bag fibre (n-b1) exhibits low activity with Alk ATPase and moderate activity with P'ase.

In figs. 215 - 217 only the nuclear-bag fibres are present, of which the fibre with low Alk ATPase activity (arrow) is the longest.

All figures are the same magnification.

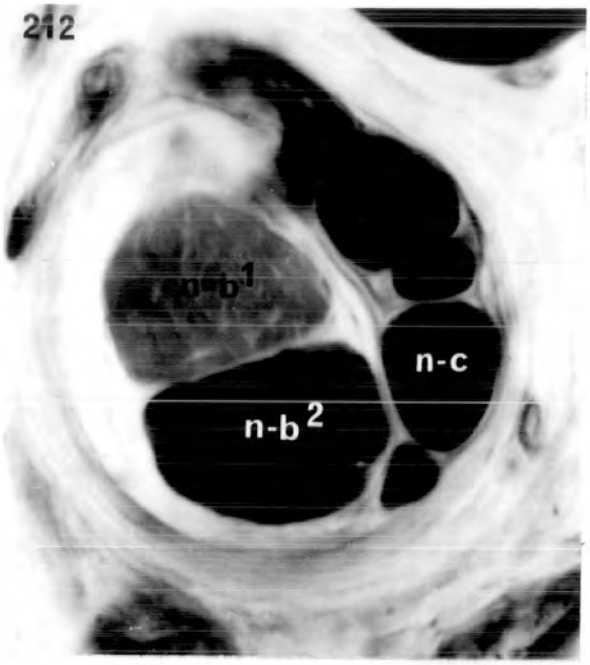
212
n-b1
n-c
n-b2

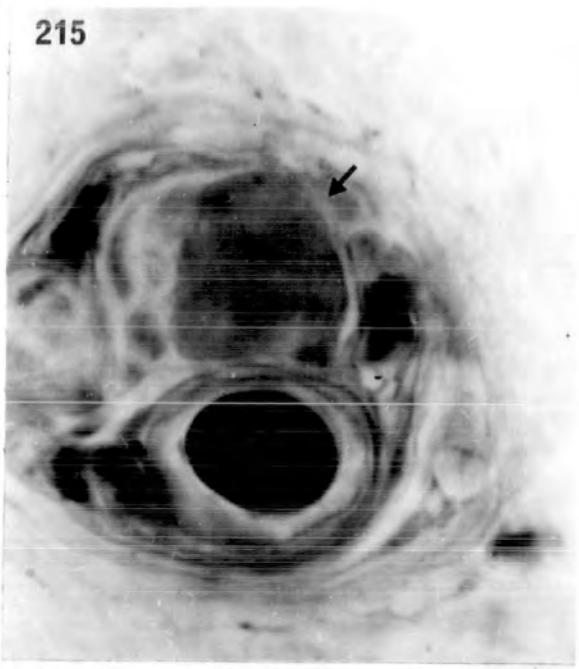
215

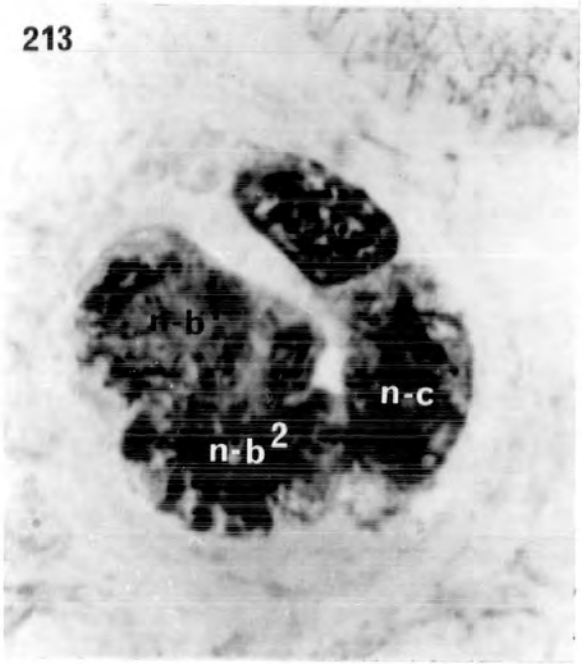
213
n-b1
n-c
n-b2

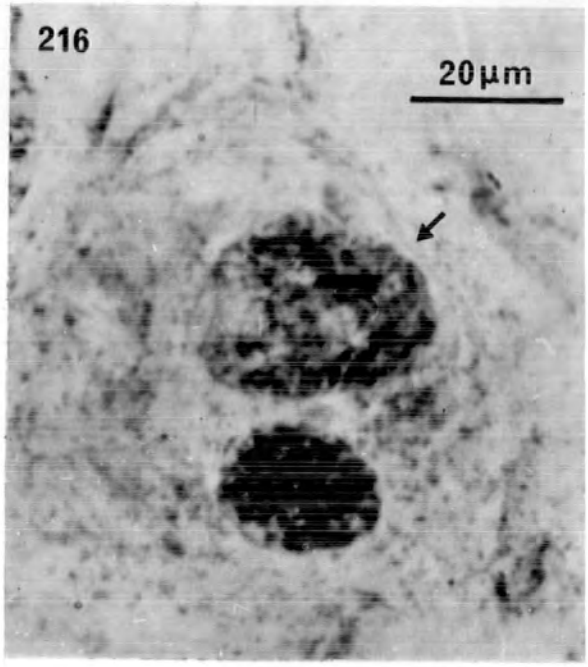
216
20µm

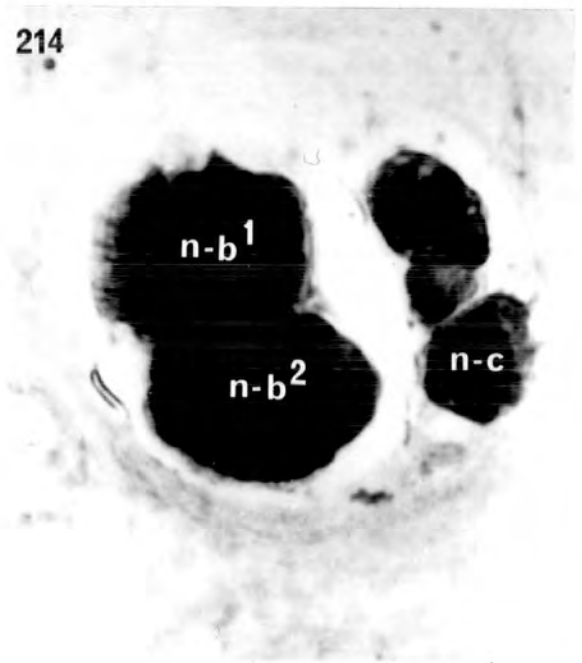
214
n-b1
n-b2
n-c


217

Figure 218. The ultrastructure of the capsule in sheep extraocular muscle spindles.

Transverse section of a type C muscle fibre (C) with an associated blood capillary (cap.) penetrating a spindle capsule in SR. The layers of overlapping capsular sheet cells (cap.sh.c.) alternate with layers of elastic (e) and collagen (coll.) fibrils. Fibrocyte cells (fibr.) form the innermost layer of the capsule. b.m., basement membrane; p.v., pinocytotic vesicles.

x 12,600

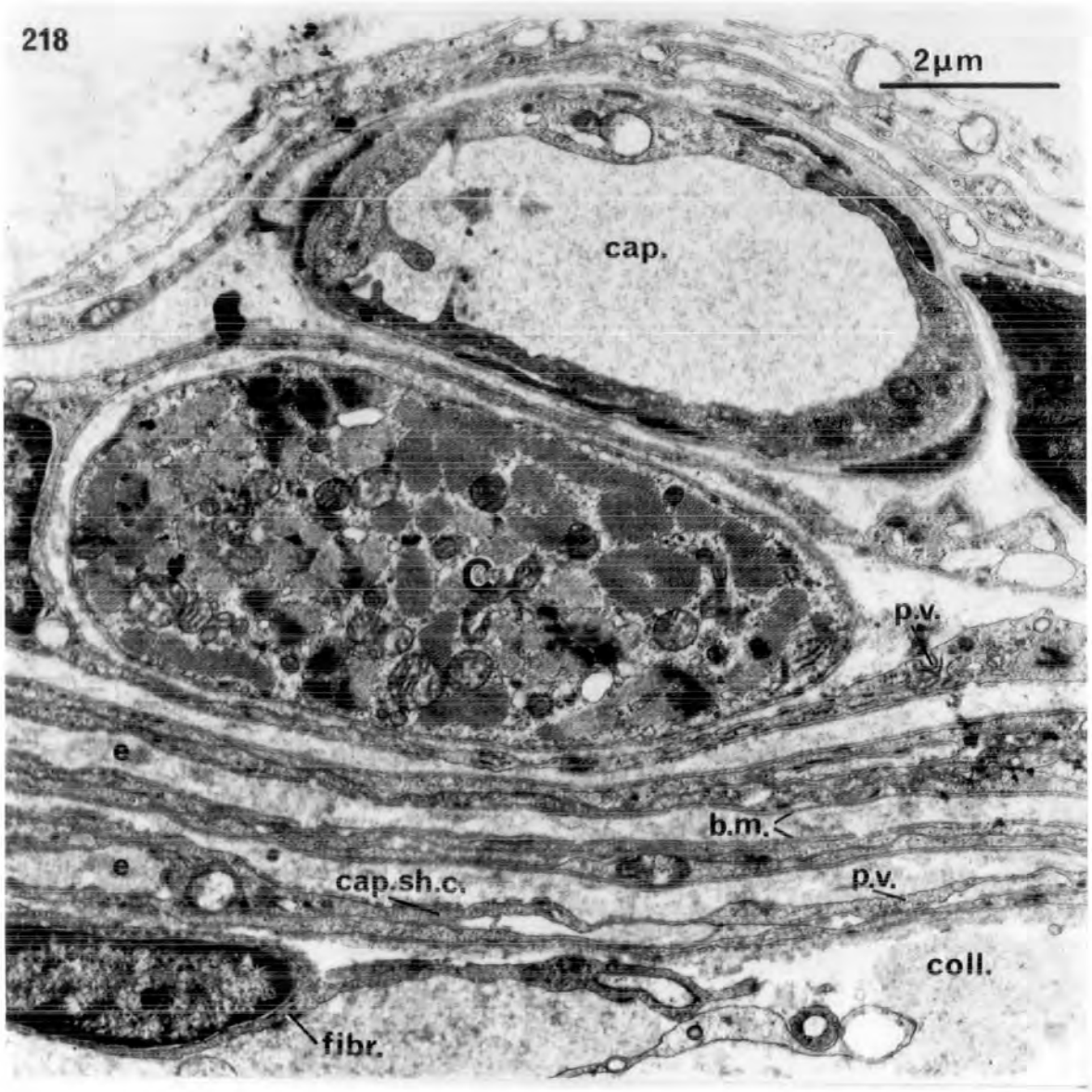
218
2µm
cap.
C.
p.v.
e
e
b.m.
cap.sh.c.
p.v.
coll.
fibr.

144

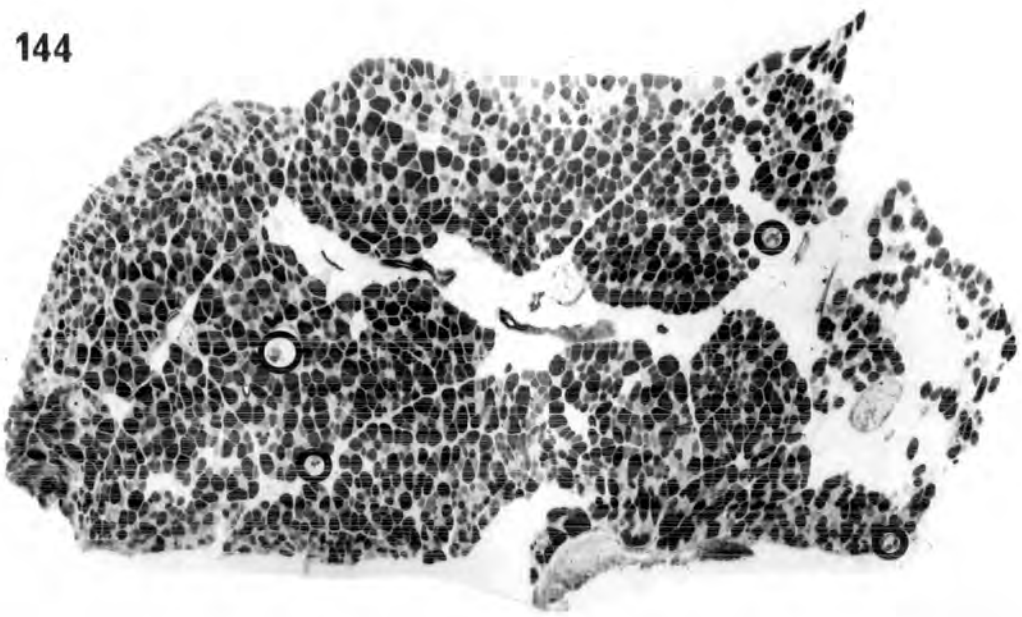

1mm

145

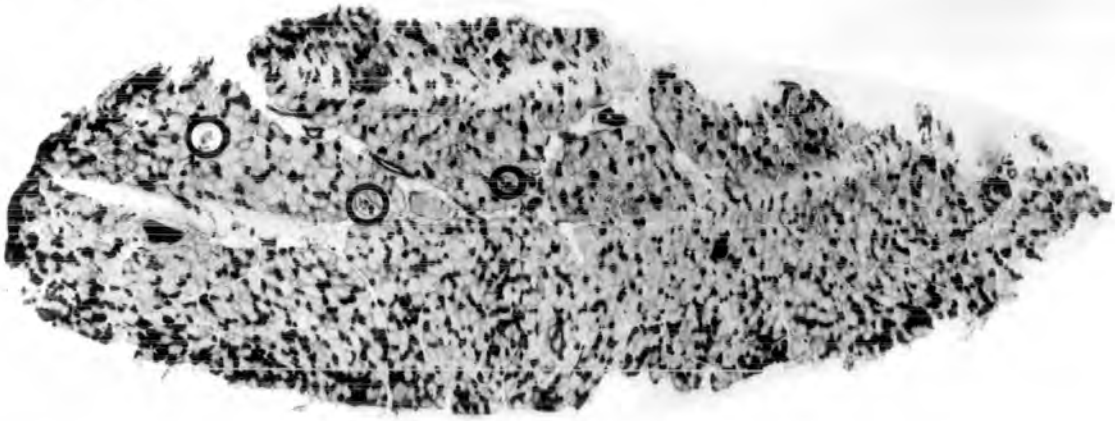

Figures 219 to 220. The ultrastructure of intrafusal muscle fibres in sheep SR.

Fig. 219. Transverse section through the polar region of a bag fibre. Note the small mitochondria (m) scattered throughout the fibre; the lack of delineation of myofibrils in the A band (A); the poorly-developed tubules of sarcoplasmic reticulum (s.r.) in the I band (I); the occasional triads (tr); and the Z line (Z).

x 20,000

Fig. 220. Transverse section through the polar region of a chain fibre. Note the numerous large mitochondria (m) with tightly-packed cristae; the tubules of sarcoplasmic reticulum (s.r.) encircling the myofibrils in the I band; the relatively frequent triads (tr); and the large amounts of glycogen granules (Gl). pv, pinocytotic vesicles.

x 20,000

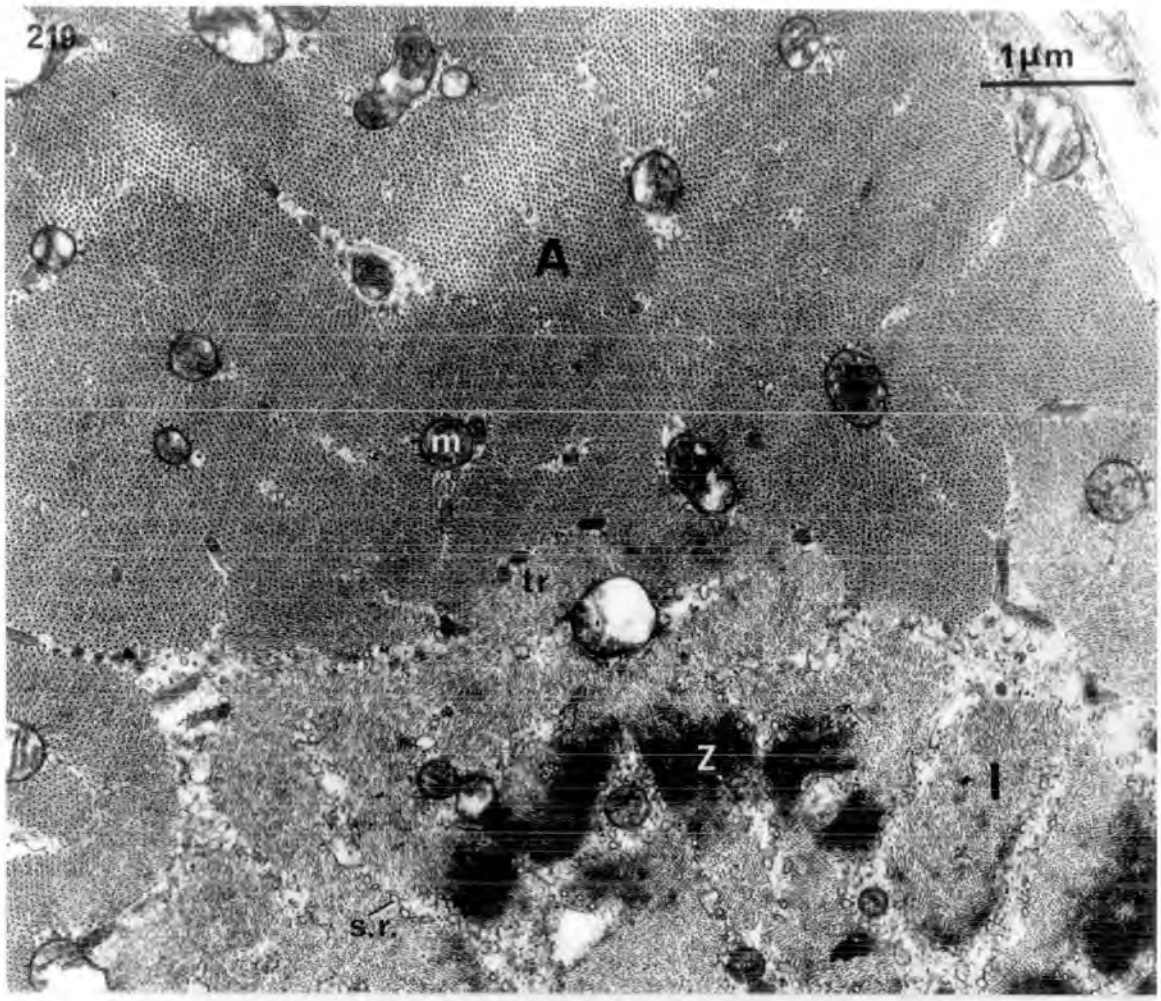
219
1µm
A
m
tr
Z
I
s.r.

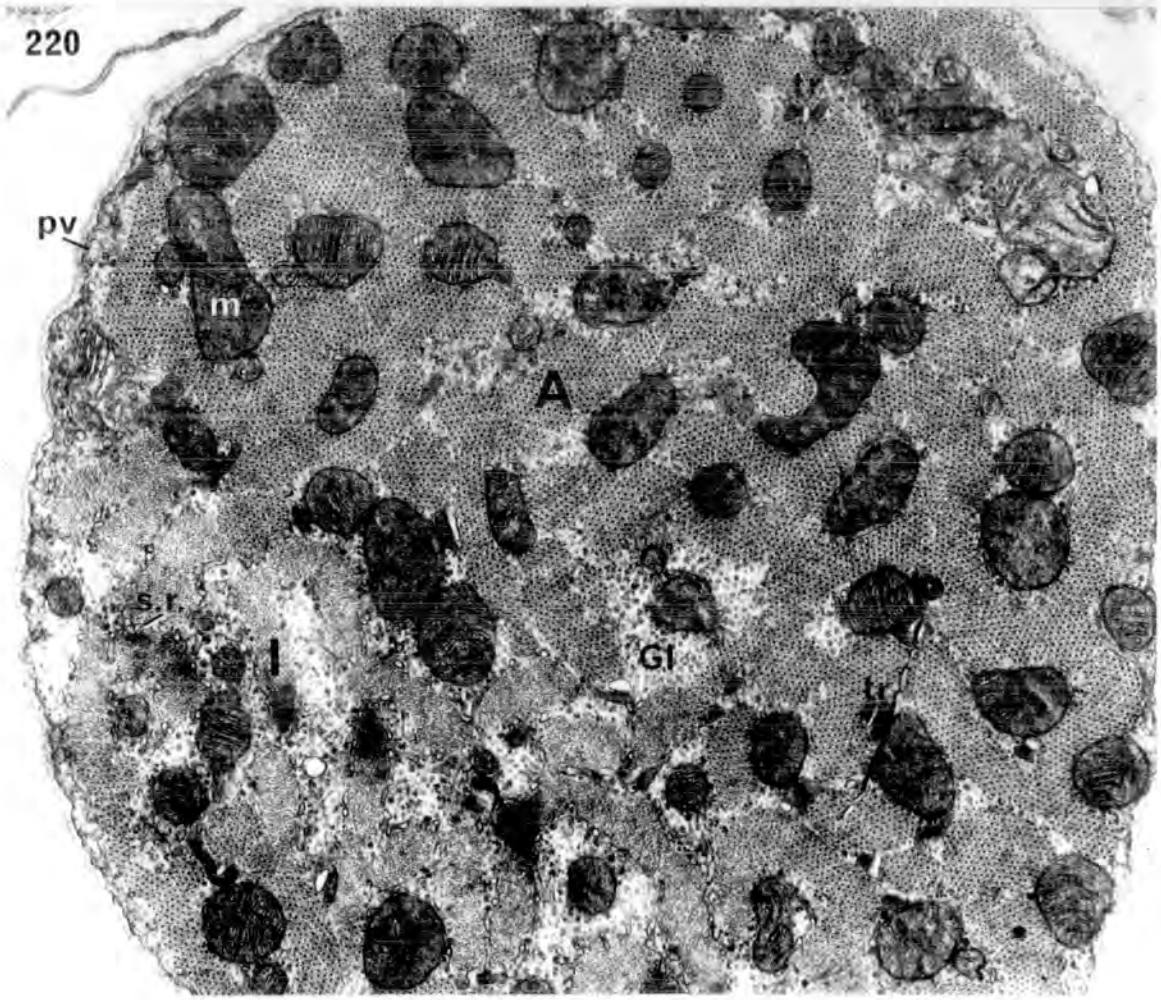
220
tr
pv
m
A
s.r.
I
GI
tr

Figures 221 to 222. The ultrastructure of chain fibres in sheep SR.

Fig. 221. Longitudinal section through the polar region of a chain fibre. Note the myofibrils that are well-delineated by abundant sarcoplasm and chains of mitochondria (m); the distinct M lines (M); and the thick, wavy Z lines (Z).

x 15,750

Fig. 222. At higher magnification note that the elongated mitochondria have tightly-packed cristae and are associated with lipid droplets (Li); the triads (tr) occur regularly; the Z line has Z filaments; and the M line lies in the middle of a pseudo-H zone (marked by lines).

x 25,000

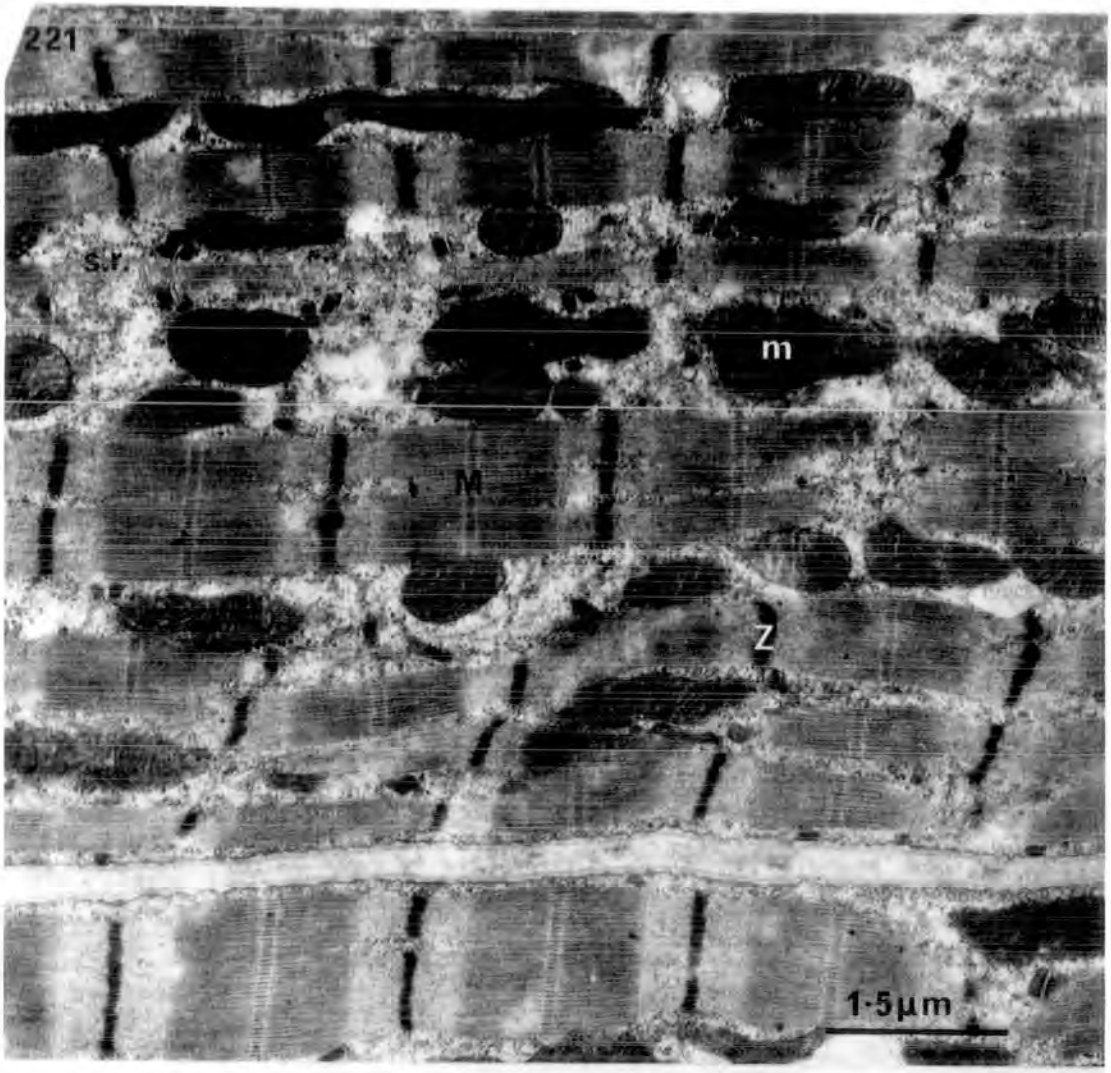
221
s.r.
m
M
Z
1·5µm

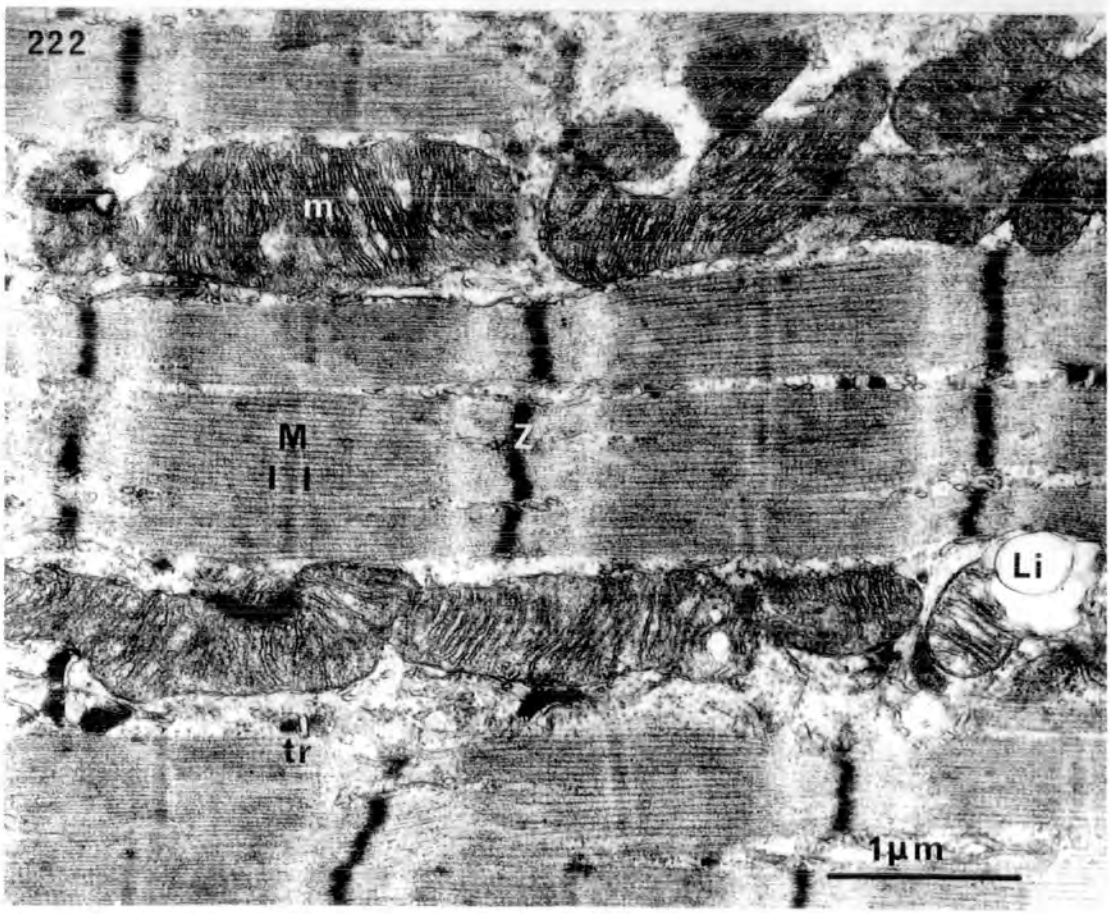
222
m
M
I I
Z
Li
tr
1µm

Figures 223 to 224. <u>The ultrastructure of bag fibres in sheep SR</u>.

Fig. 223. Longitudinal section through the polar region of a bag fibre. Note the poor delineation of myofibrils by sarcoplasm; the small, sparse mitochondria (m); the absence of an M line; the thick, wavy Z line (Z); and the microladder or leptofibrils (lept.) near the surface of the fibre.

x 20,000

Fig. 224. At higher magnification note the poor development of the sarcotubular system; the clear pseudo-H zone (marked by lines); and, at this particular level, patches of glycogen granules (Gl).

x 32,000


252
s.c-t.
3µm
c
s.t.
b


253
s.t.
m
s.t.
3µm

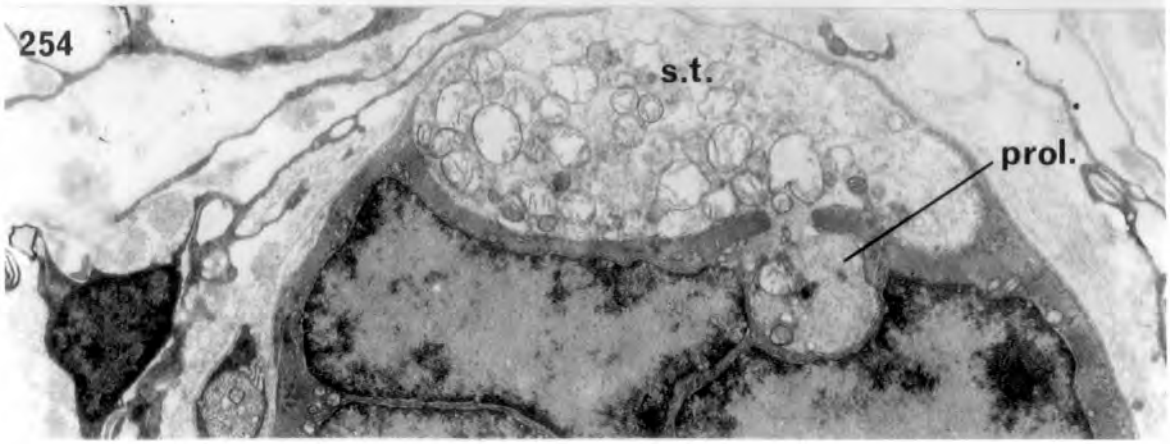
254
s.t.
prol.

Figures 252 to 254. Electron micrographs of the equatorial region of spindles from SR.

Fig. 252. Transverse section through a sensory cross-terminal (s.c-t.) linking a bag fibre (b) and a chain fibre (c). This type of cross linkage is comparatively rare.

x 6,720

Fig. 253. Longitudinal section through the myotube region of a chain fibre showing a structure resembling an enlarged sensory axon terminal ('s.t.') with densely-packed mitochondria (m). Compare with the conventional sensory terminal (s.t.) on the opposite side of the fibre.

x 8,000

Fig. 254. Transverse section through the equator of a bag fibre showing a prolongation (prol.) of the primary sensory terminal (s.t.) that interdigitates with the underlying muscle fibre.

x 8,000

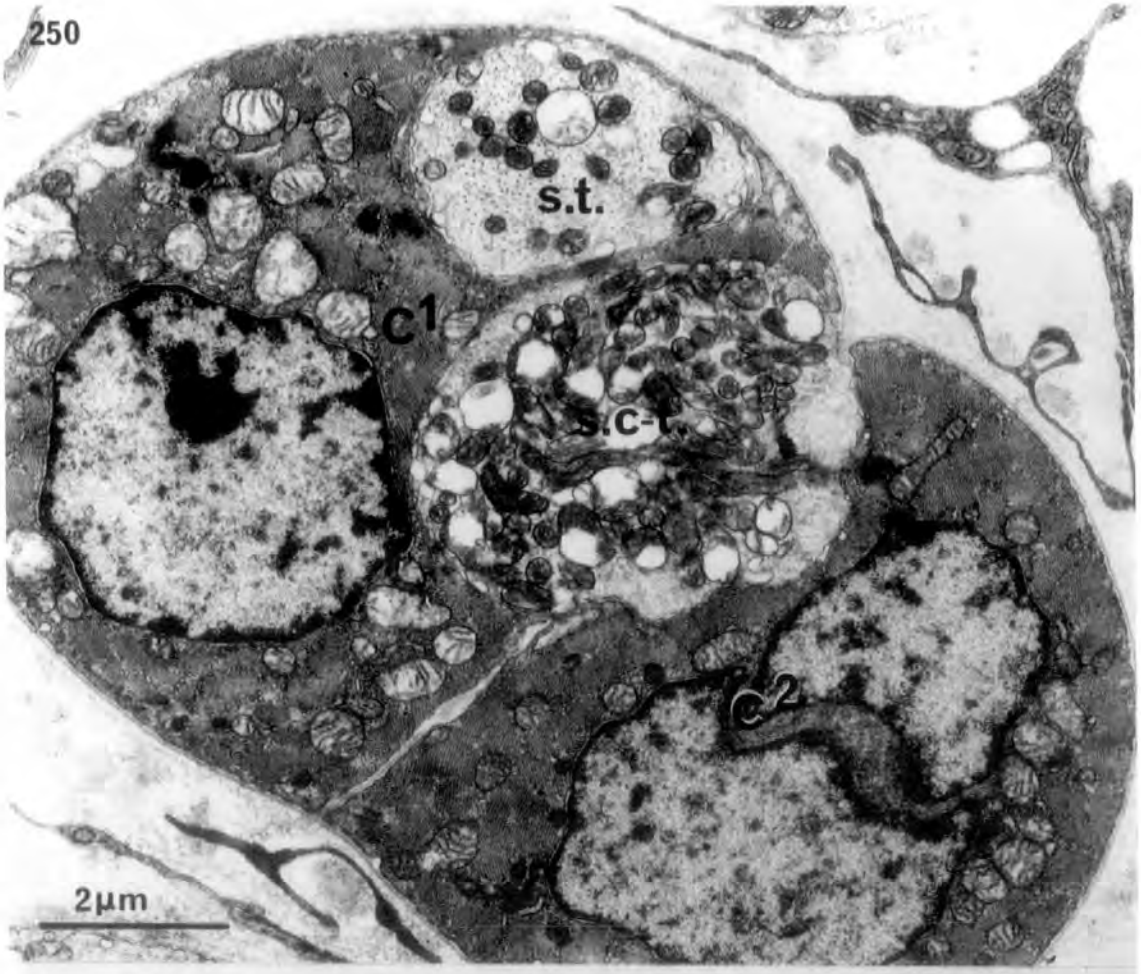
250
s.t.
c1
s.c-t.
c2
2µm


251
s.c-t.

Figures 250 to 251. Electron micrographs of transverse sections through the myotube region of a spindle from SR showing sensory cross-terminals.

Fig. 250. The sensory cross-terminal (s.c-t.) links two paired chain fibres (C1 & C2). Another sensory axon terminal (s.t.) is completely enclosed within the sarcoplasm of chain C1. Note the central nuclei in the chain fibres.

x 12,600

Fig. 251. The sensory cross-terminal (s.c-t.) linking chain fibres C1 & C2 almost encircles chain fibre C1 and is probably a primary (annulospiral) axon terminal. Note that the margin of chain fibre C2 is prolonged as a thin lip of sarcolemma (arrow).

x 12,600

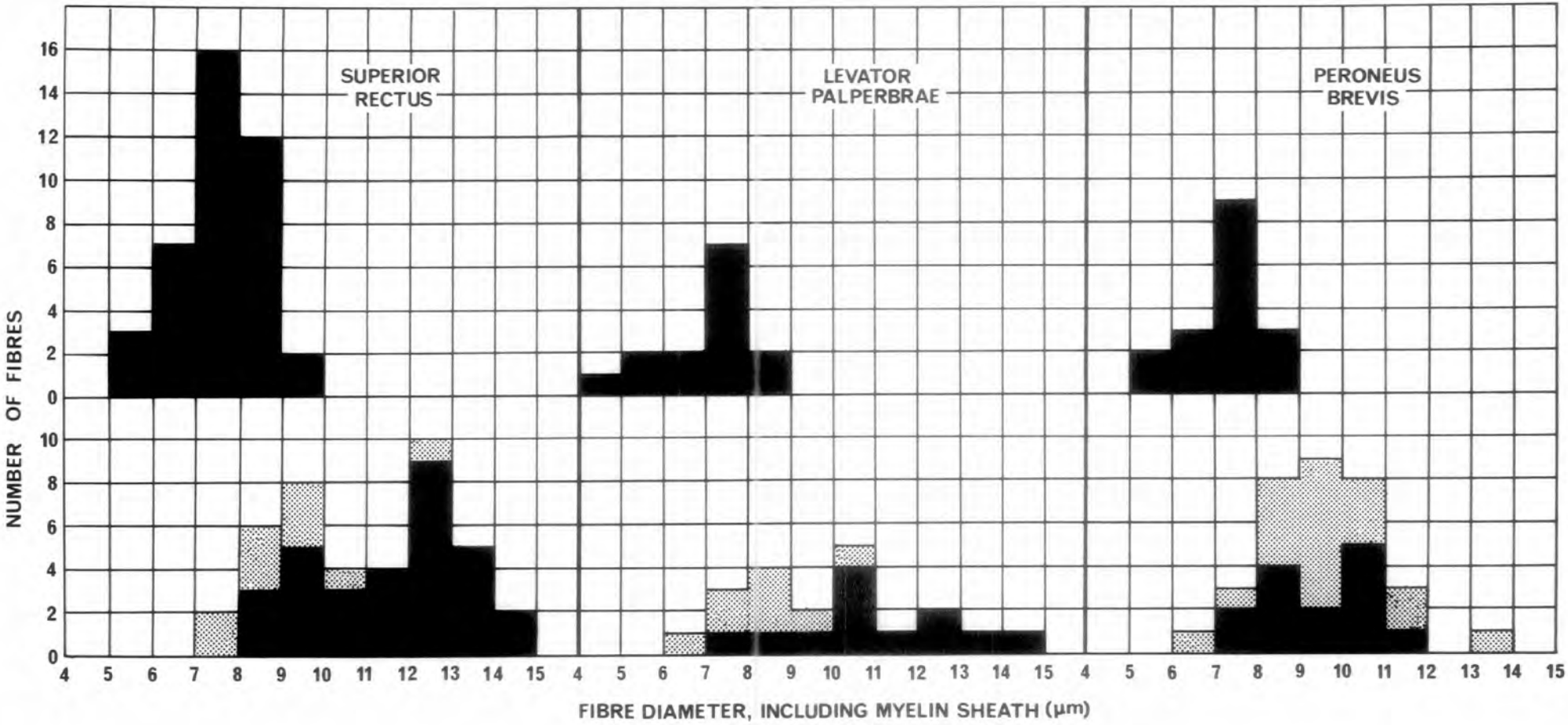
SUPERIOR RECTUS
LEVATOR PALPERBRAE
PERONEUS BREVIS
NUMBER OF FIBRES
FIBRE DIAMETER, INCLUDING MYELIN SHEATH (µm)

Figure 249. Distribution of primary and secondary sensory nerve-fibre diameters (including the myelin sheath) for SR, LP and PB muscle spindles.

The histograms of the total diameter of secondary afferent fibres are drawn above the histograms of the primary afferent fibres for each muscle.

The primary afferent fibres that supply simple spindles (primary only) are represented by stippled shading.

Fibre diameters measured in teased, silver preparations about 1 mm from spindle entry.

246

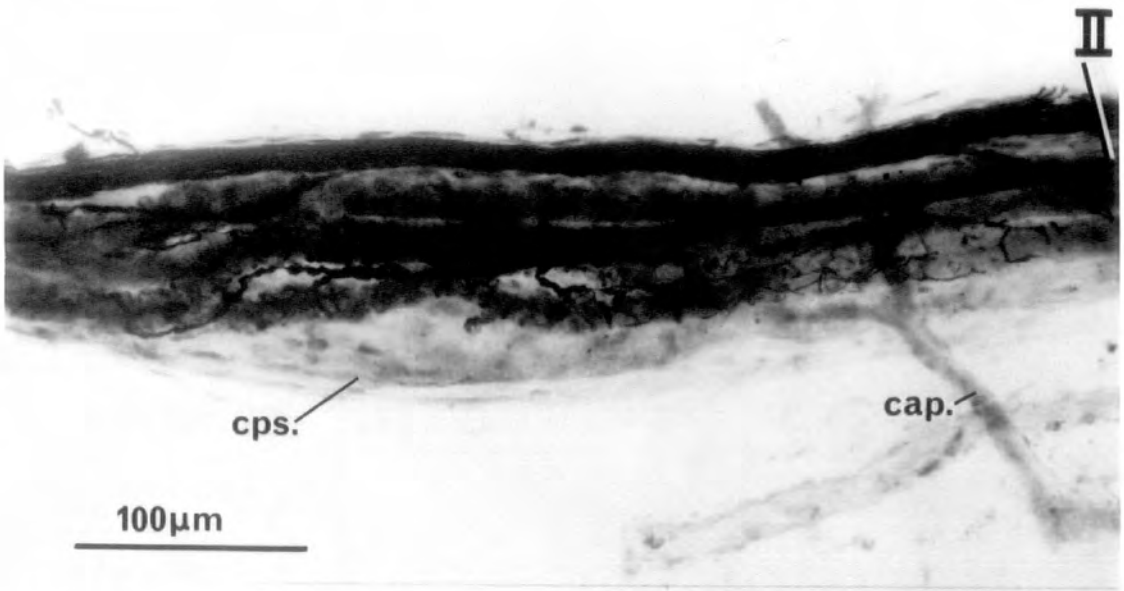

247

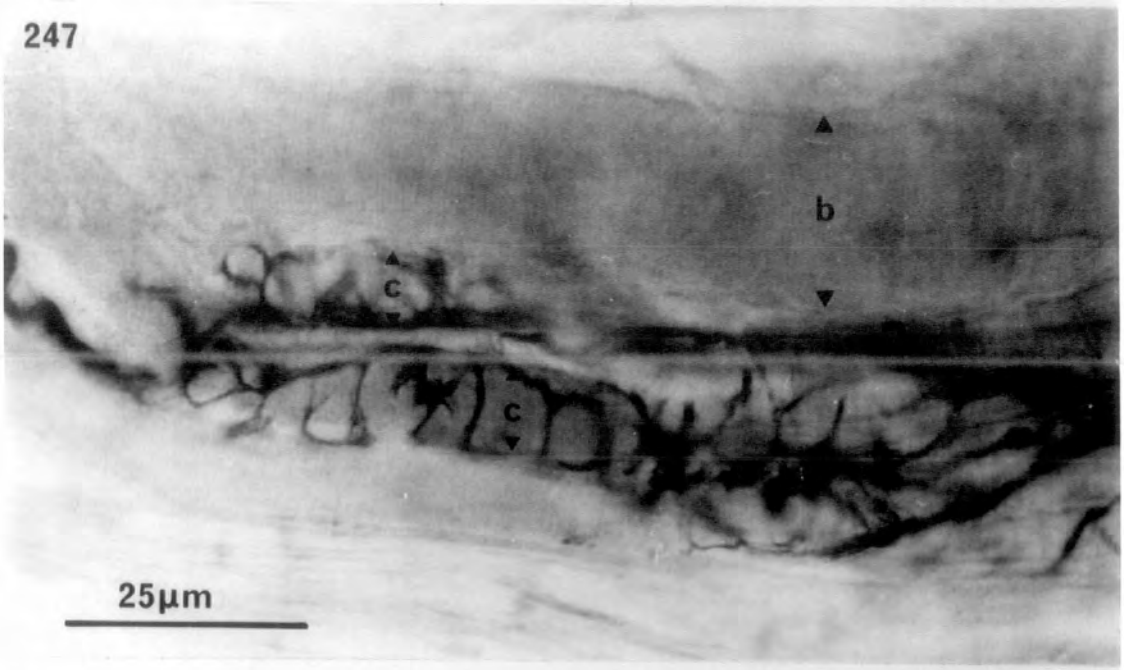

248

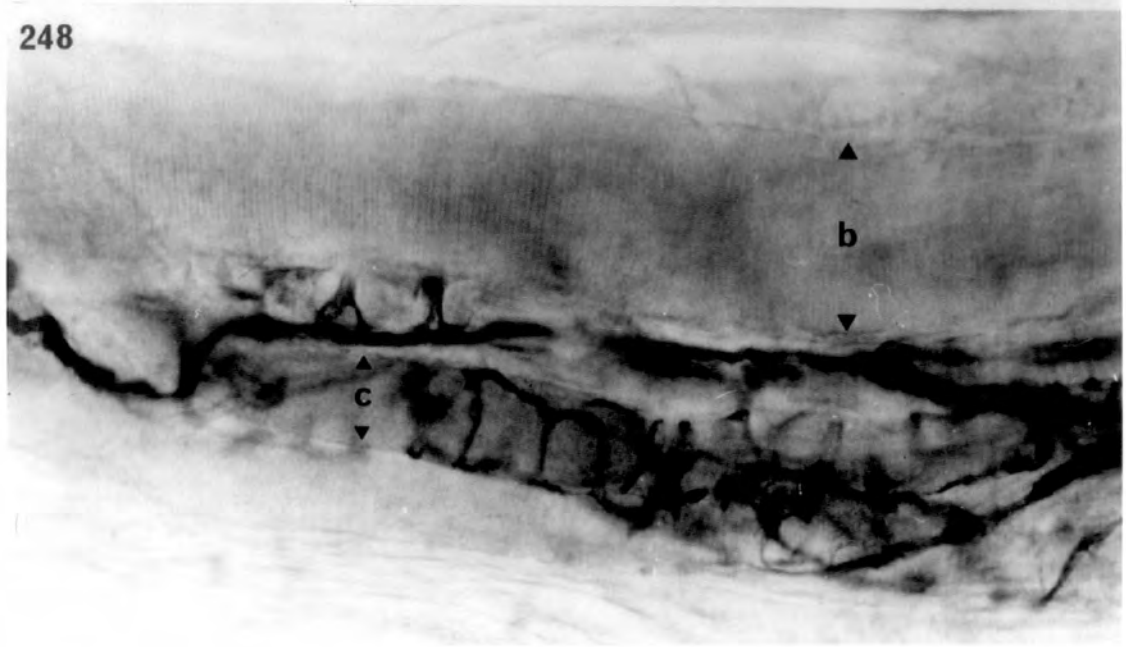

Figures 246 to 248. The juxta-equatorial region of a spindle teased from SR muscle after impregnation with silver.

Fig. 246. Low-power photomicrograph showing a secondary afferent (II) that branches to supply the intrafusal bundle with an irregular annulospiral secondary ending. cap., blood capillary; cps., capsule.

Figs. 247 - 248. The same region of a secondary ending at two different planes of focus. The irregular annulospiral terminations are wrapped around the small-diameter chain fibres (c), but not around the large-diameter bag fibre (b) lying above.

243

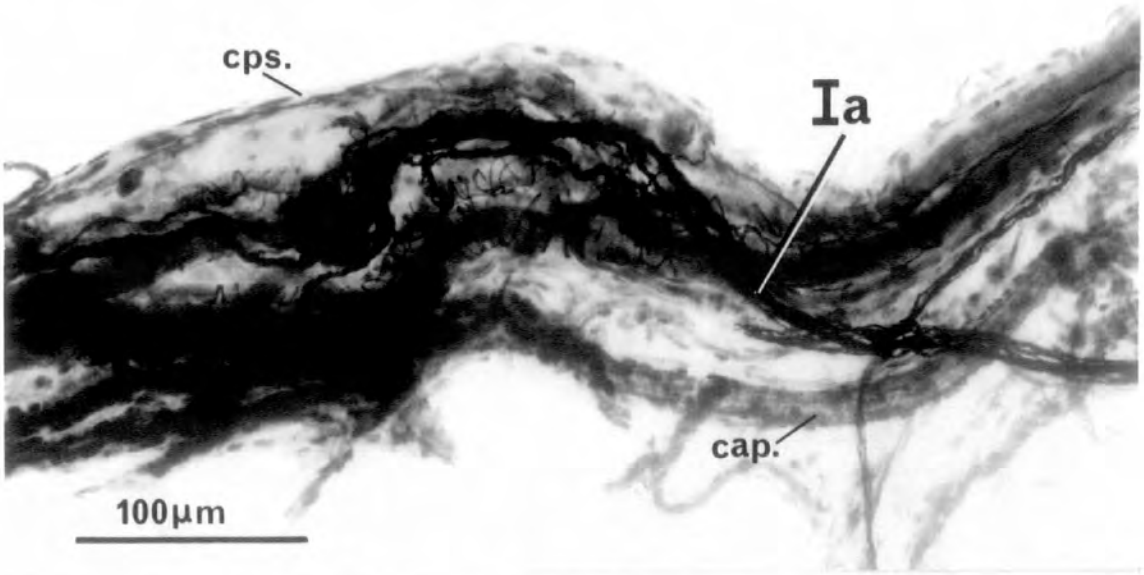

244

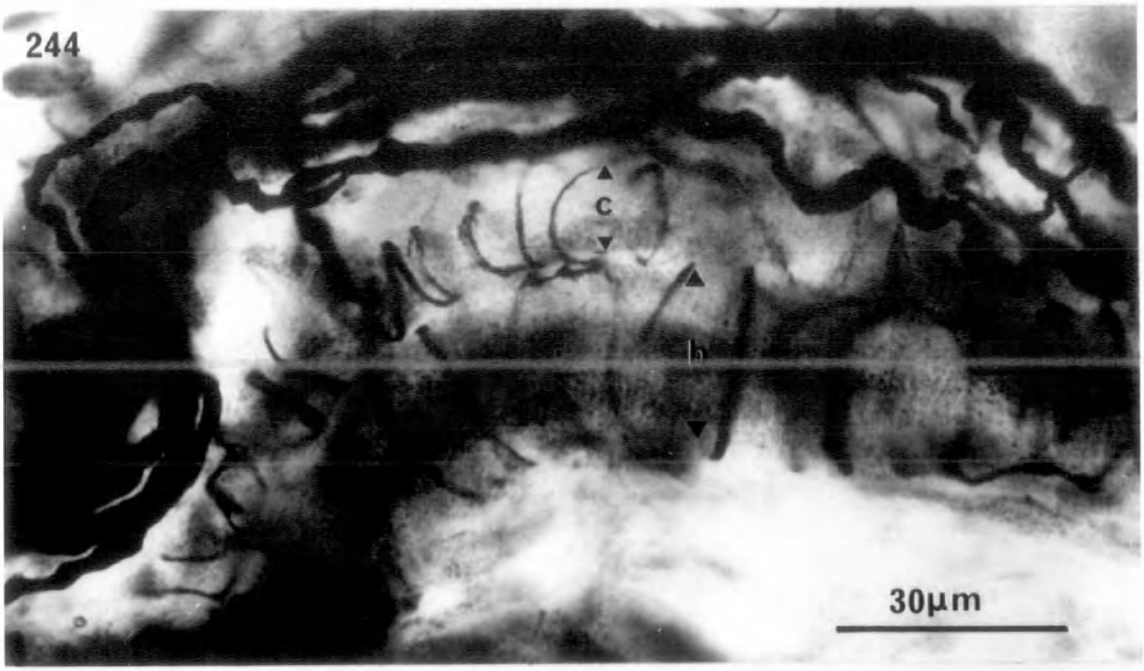

245

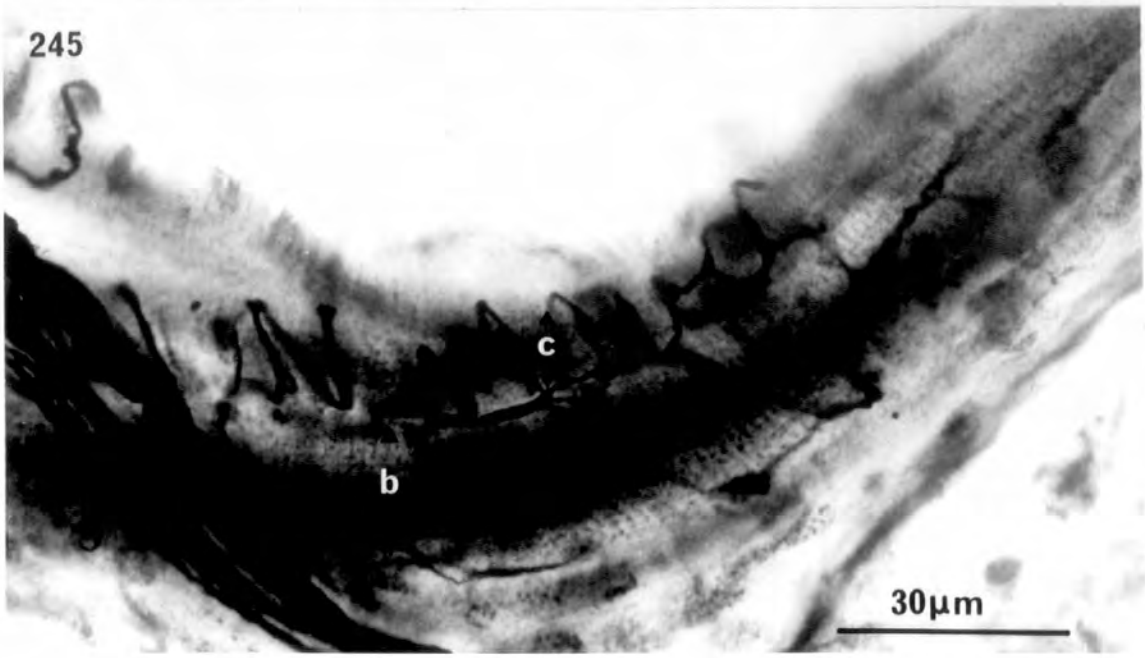

Figures 243 to 245. The equatorial region of a spindle teased from SR muscle after impregnation with silver.

Fig. 243. Low-power photomicrograph showing a thick primary afferent (Ia) that enters the spindle capsule (cps.) obliquely to supply the intrafusal bundle with an annulospiral primary ending. cap., blood capillary.

Figs. 244 - 245. Two different regions of the above primary ending at higher magnification showing the large-diameter annulospiral terminations around the bag fibres (b) and those of smaller diameter around the chain fibres (c).

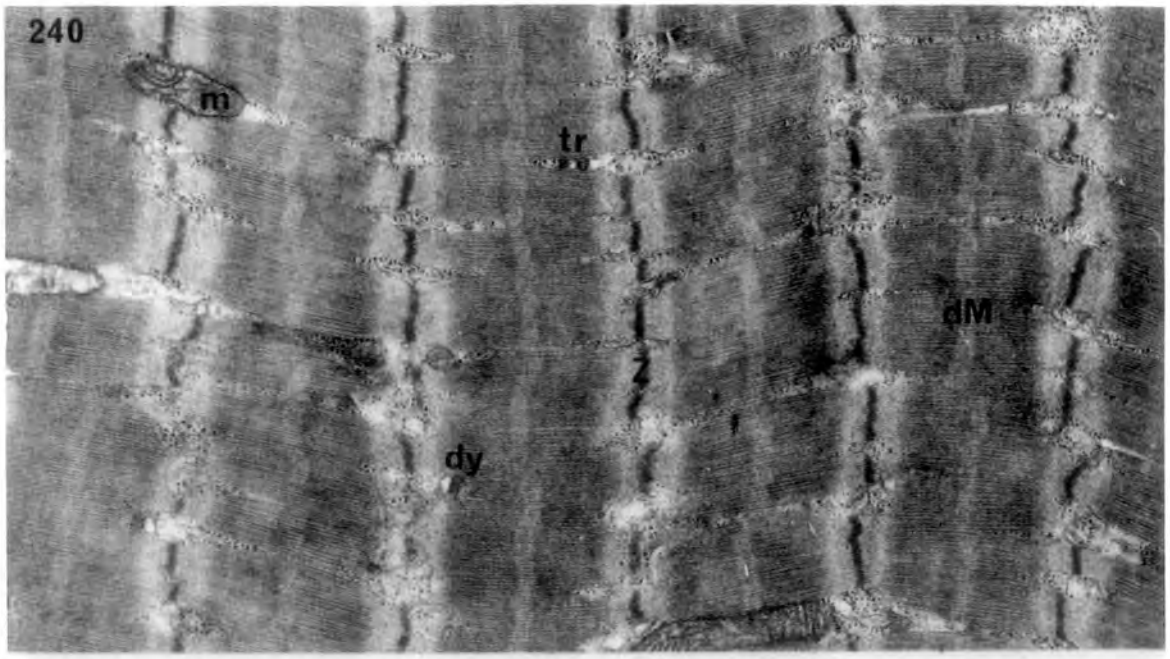
240
m
tr
dM
Z
dy

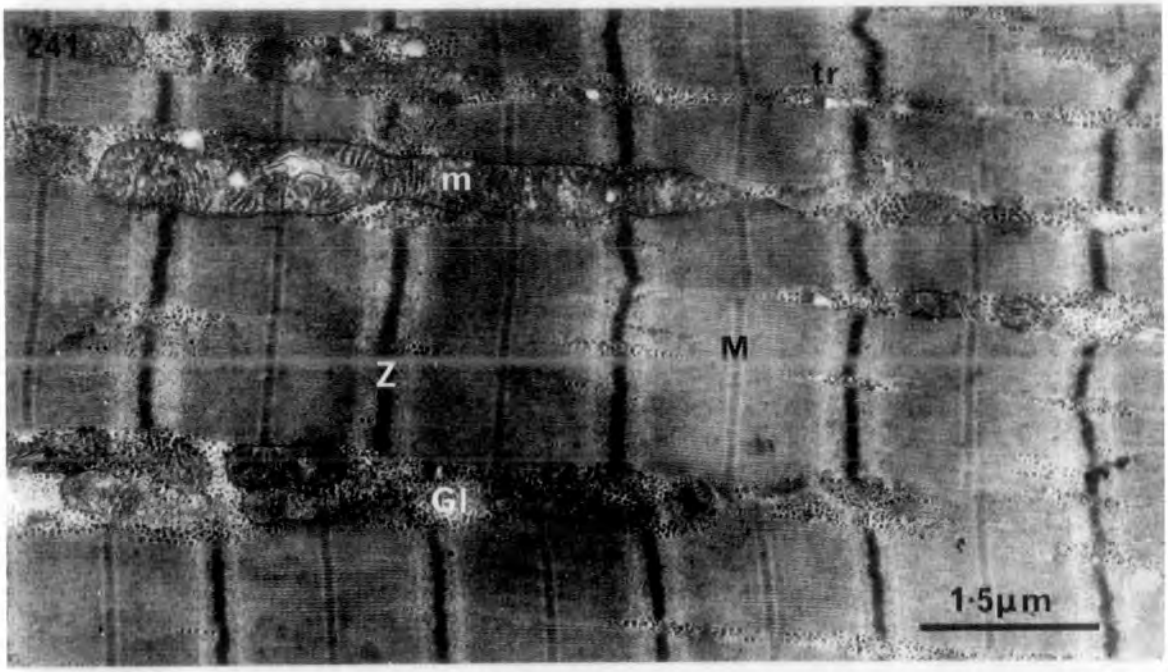
241
tr
m
M
Z
Gl
1·5µm

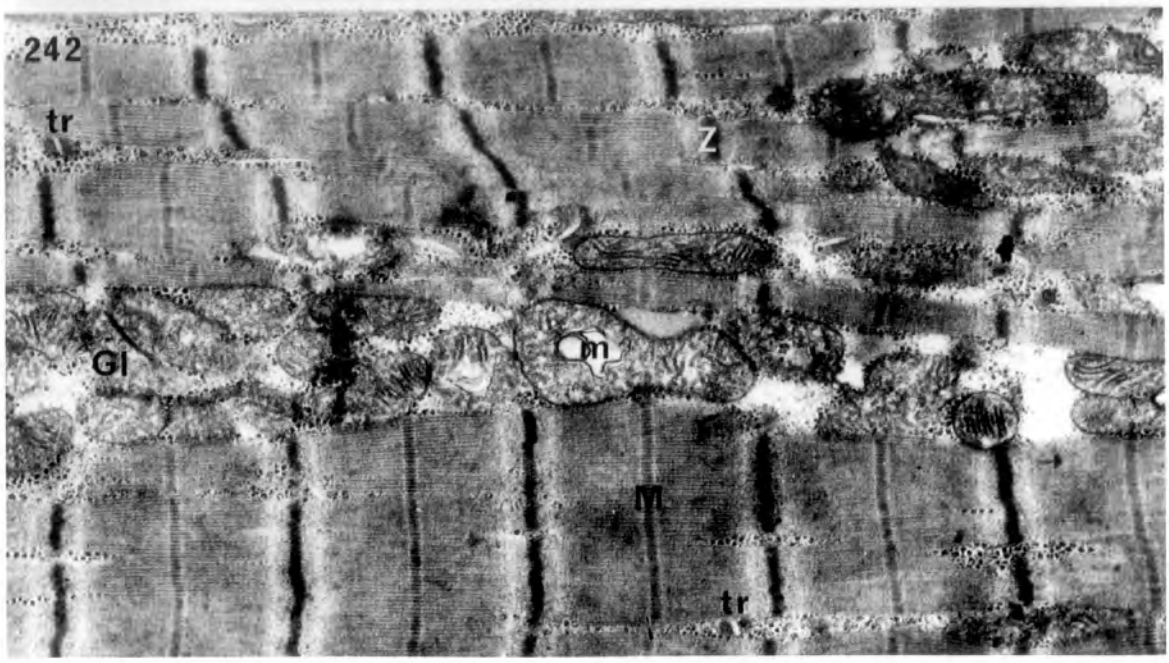
242
tr
Z
Gl
m
M
tr

Figures 240 to 242. The ultrastructure of intrafusal fibres in sheep PB hindfoot muscle.

Fig. 240. Longitudinal section at the mid-polar level of a typical bag fibre. The M line is either indistinct or in the form of two parallel lines (dM); the Z line (Z) is straight and thin; sarcoplasmic reticulum and glycogen granules are poorly developed; the mitochondria (m) are small and do not form chains; and the dyads (dy) or triads (tr) occur infrequently.

X 15,750

Fig. 241. Longitudinal section at the mid-polar level of an intermediate bag fibre. The M line (M) is distinct; the Z line is thick; sarcoplasmic reticulum and glycogen granules are fairly well developed; mitochondria are larger and more numerous than in the typical bag fibre; triads are fairly regular.

x 15,750

Fig. 242. Longitudinal section at the mid-polar level of a chain fibre. The M line is distinct; The Z line is thick and slightly wavy; sarcoplasmic reticulum and glycogen granules are abundant; mitochondria are large and numerous, and tend to form chains; and there is a regular system of triads.

x 15,750

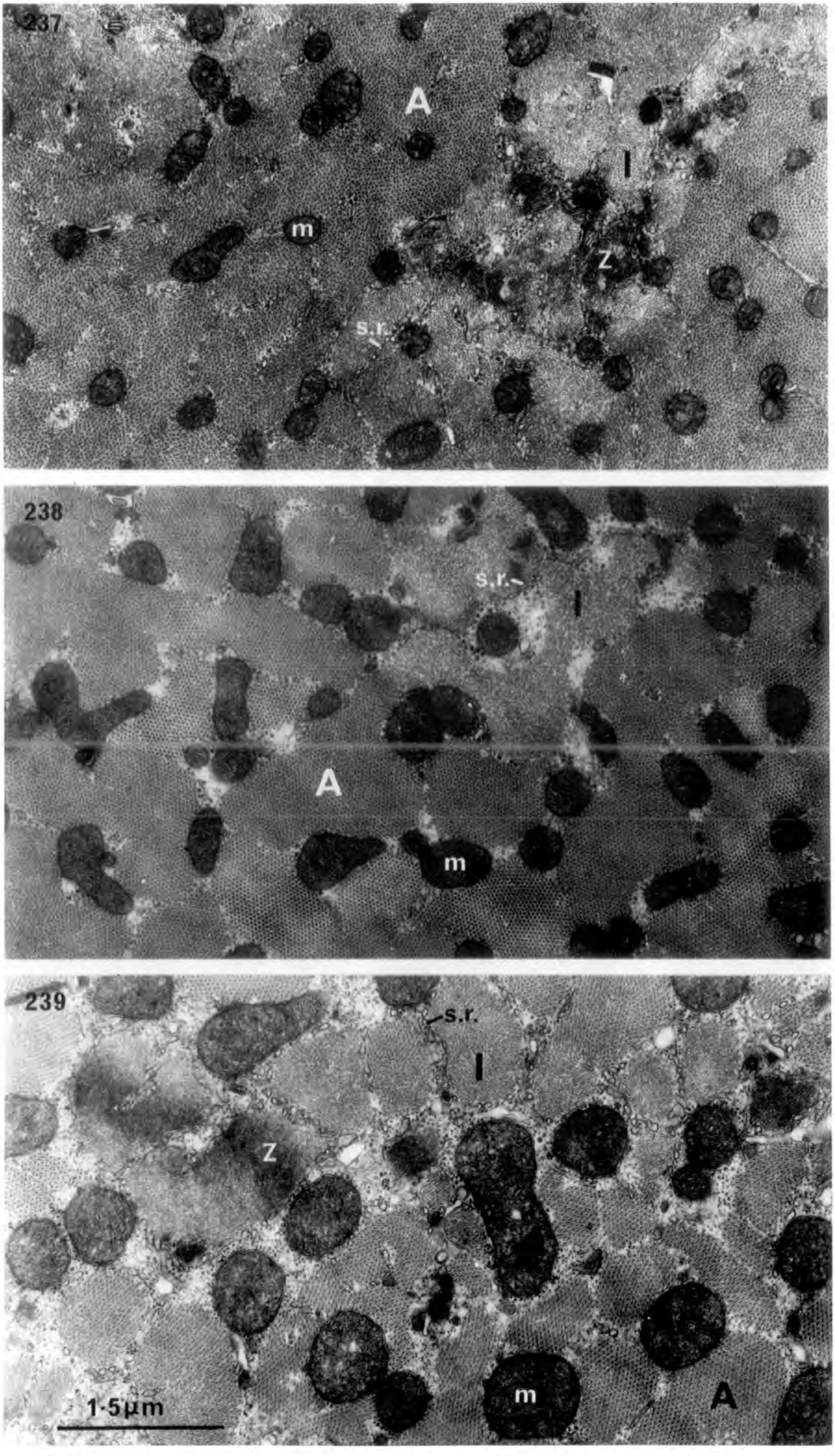
237
A
I
m
Z
s.r.
238
s.r.
I
A
m
239
s.r.
I
Z
m
A
1·5µm

Figures 237 to 239. The ultrastructure of intrafusal fibres in sheep PB hindfoot muscle.

Fig. 237. Transverse section through the juxta-equatorial region of a typical bag fibre. Note the small, numerous mitochondria (m) scattered throughout the fibre and the paucity of interfibrillar sarcoplasm and tubules of sarcoplasmic reticulum (s.r.) even in the I band (I).

x 20,000

Fig. 238. Transverse section through the juxta-equatorial region of an intermediate bag fibre. Note the increased size of mitochondria and increased abundance of sarcoplasm and greater delineation of myofibrils.

x 20,000

Fig. 239. Transverse section through the juxta-equatorial region of a chain fibre. Note the large mitochondria and the layer of tubules of sarcoplasmic reticulum (s.r.) encircling each myofibril in the I-band region.

x 20,000

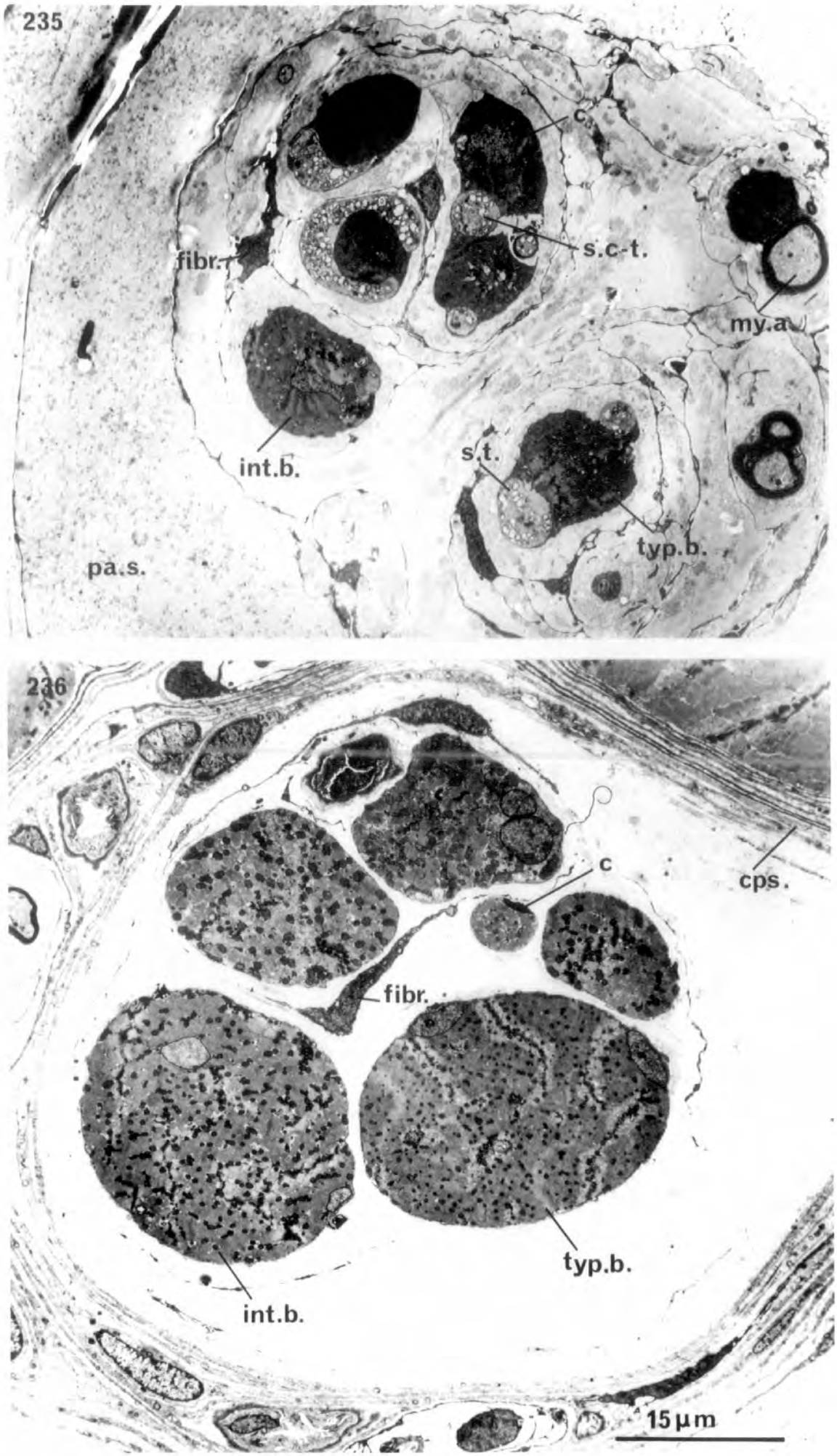
235
c
s.c-t.
fibr.
my.a
int.b.
s.t.
typ.b.
pa.s.
236
cps.
c
fibr.
typ.b.
int.b.
15 µm

Figures 235 to 236. The ultrastructure of intrafusal fibres in sheep PB hindfoot muscle.

Fig. 235. A low-power electron micrograph of a transverse section through the equatorial region of a spindle from PB. Note the drastic reduction in diameter of all intrafusal fibres types compared to fig. 236 (both figs. are the same magnification). The typical bag (typ.b.) and intermediate bag (int.b.) fibres pass through the equator separate from the chain fibres (c), which group together. Two of the chain fibres are linked by a sensory cross-terminal (s.c-t.). my.a., myelinated axon; fibr., fibrocyte; s.t., sensory terminal; pa.s., periaxial space.

x 2,000

Fig. 236. A low-power transverse section of the same spindle in the juxta-equatorial region. Note the differences in mitochondrial size between the typical bag, intermediate bag and chain fibre types. One of the four chain fibres (c) is very short in this pole. cps., capsule.

x 2,000

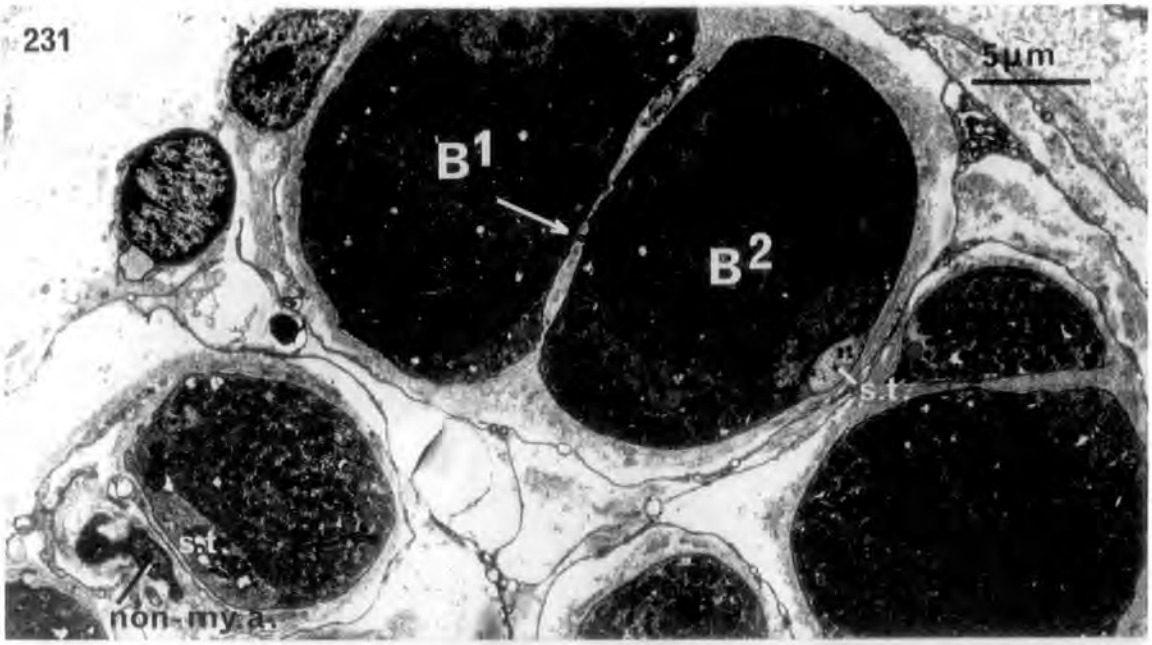
231
5µm
B1
B2
s.t.
s.t.
non-my.a.

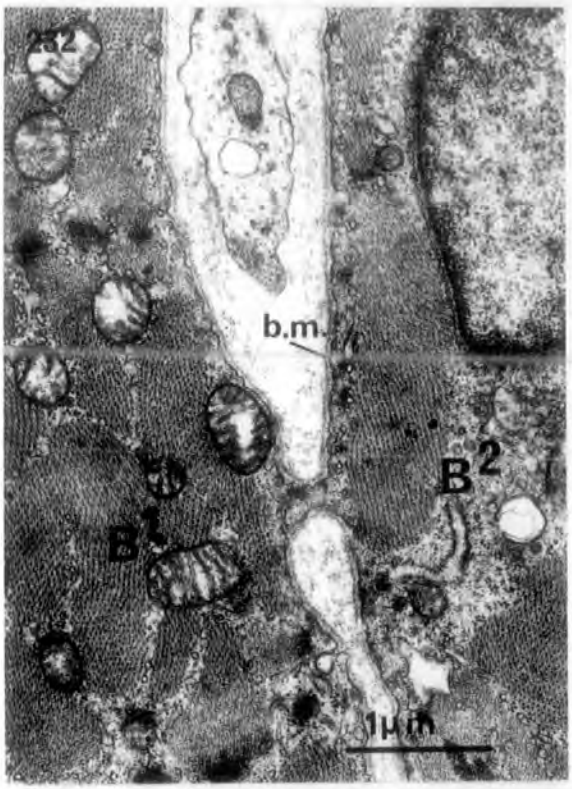
232
b.m.
B2
B1
1µm

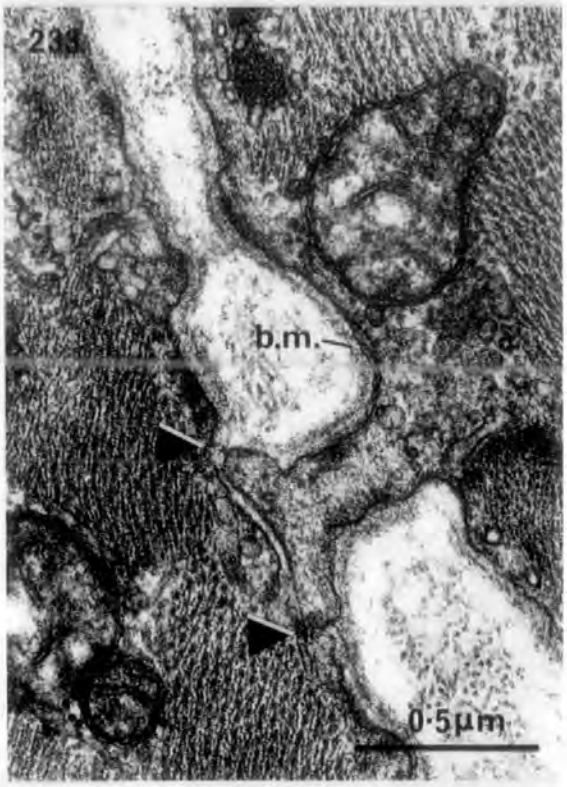
233
b.m.
0·5µm

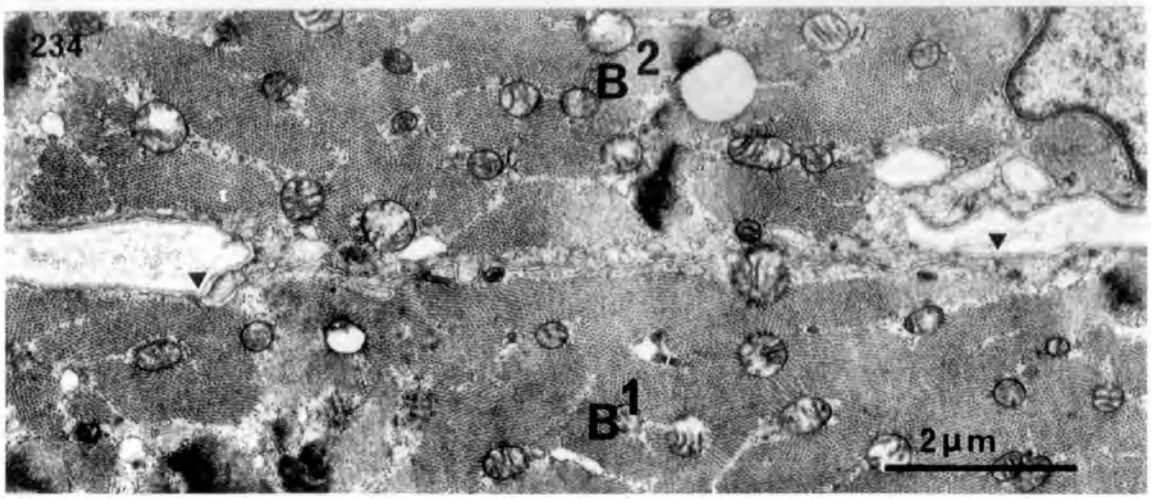
234
B2
B1
2µm

Figures 231 to 234. Close apposition of bag fibres in a spindle from SR.

Fig. 231. A low-power electron micrograph of a transverse section through the juxta-equatorial region of a compound spindle. Note the area of initial contact (arrow) between the two bag fibres (B1 & B2). s.t., sensory terminal; non-my.a., non-myelinated axon.

x 3,200

Fig. 232. Transverse section of the pseudopodial projection from B2 to B1. Note the reflection of basement membrane (b.m.) between the adjacent muscle fibres.

x 20,000

Fig. 233. A serial transverse section at higher magnification. At the base of the projection the plasma membranes are in close apposition over a short distance (marked by arrowheads).

x 50,000

Fig. 234. Serial transverse section showing the later, extended region of close apposition.

x 13,200

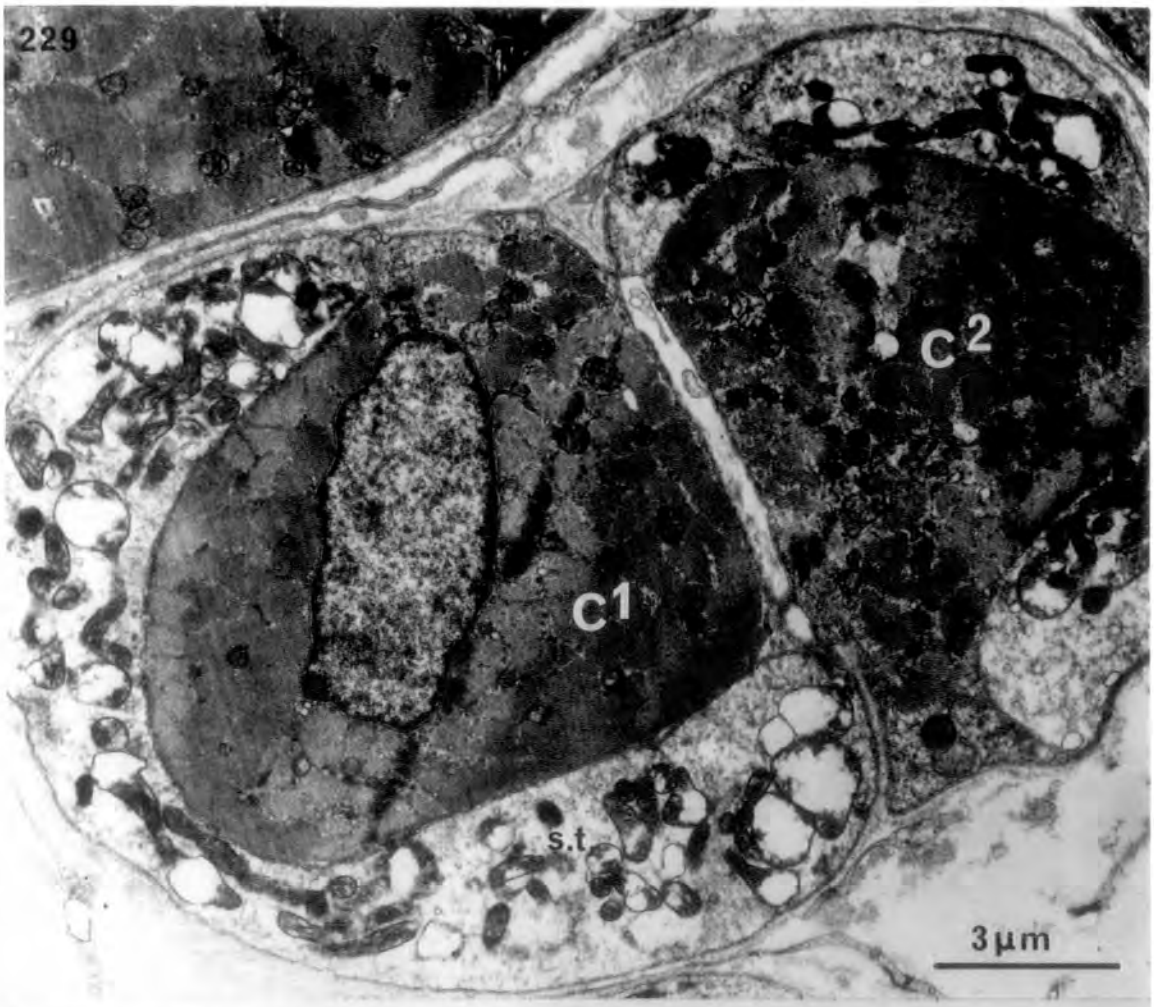
229
C2
C1
s.t.
3µm

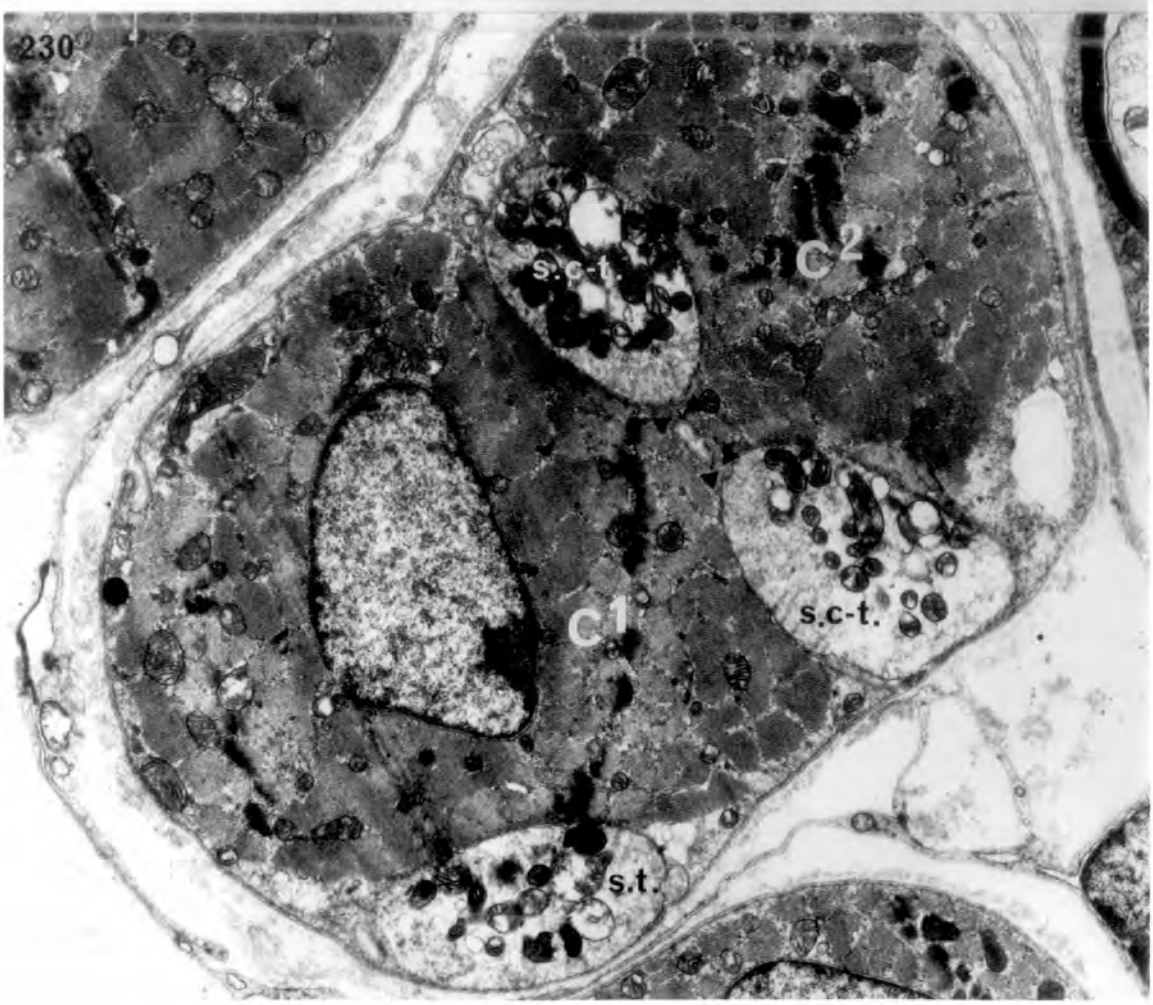
230
s.c-t.
C2
C1
s.c-t.
s.t.

Figures 229 to 230. Close apposition of intrafusal fibres.

Fig. 229. Transverse section through the juxta-equatorial region of a spindle from SR showing two chain fibres (C1 & C2) immediately prior to their close apposition. s.t., sensory terminal.

X 8,000

Fig. 230. Serial transverse section showing C1 & C2 apparently fused. Regions where the plasma membranes are closely apposed are indicated by arrowheads. s.c-t., sensory cross-terminals linking the two chain fibres.

x 8,000

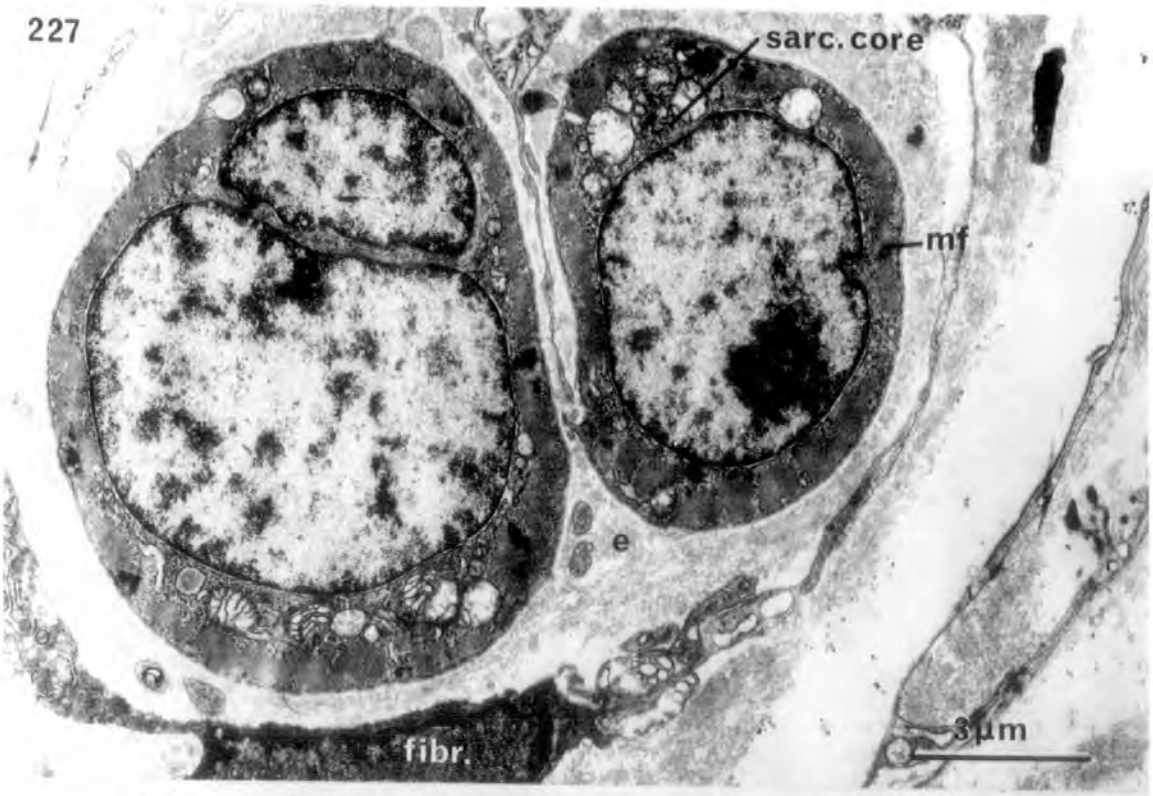
227
sarc. core
mf
e
fibr.
3µm

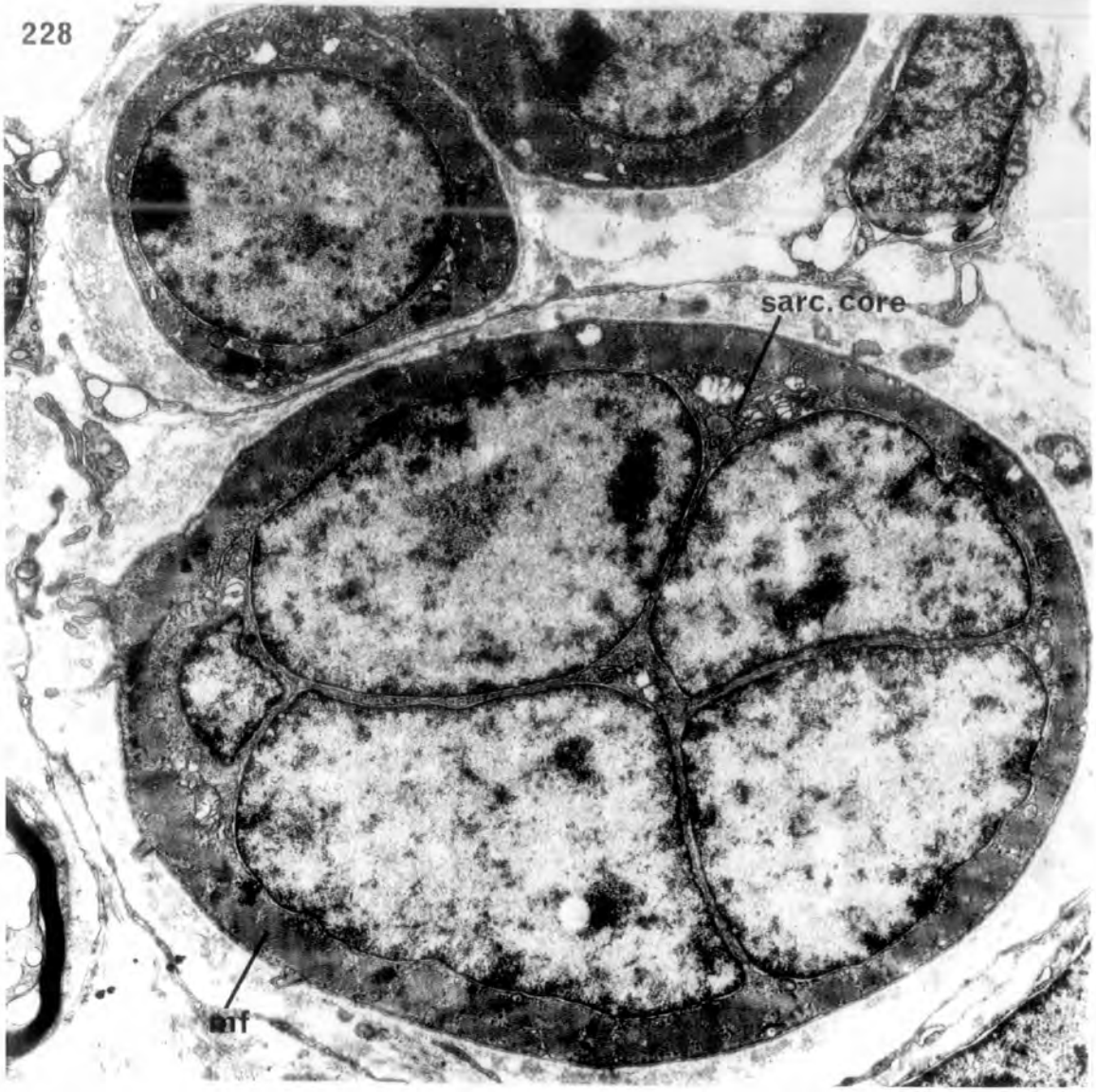
228
sarc. core
mf

Figures 227 to 228. Electron micrographs illustrating the equatorial nucleation of intrafusal fibres in a superior rectus spindle.

Fig. 227. Transverse section through two chain fibres. The fibre on the right shows a single, central nucleus, whereas the fibre on the left has been sectioned through two slightly overlapping nuclei. These lie in a core of sarcoplasm (sarc. core) bounded by a peripheral shell of myofibrils (mf). fibr., fibrocyte forming endomysial envelope; e, elastic fibrils.

x 8,000

Fig. 228. Transverse section through a bag fibre. Note the difference in diameter compared to the chain fibre (both figures are the same magnification) and the difference in the degree of nucleation.

x 8,000

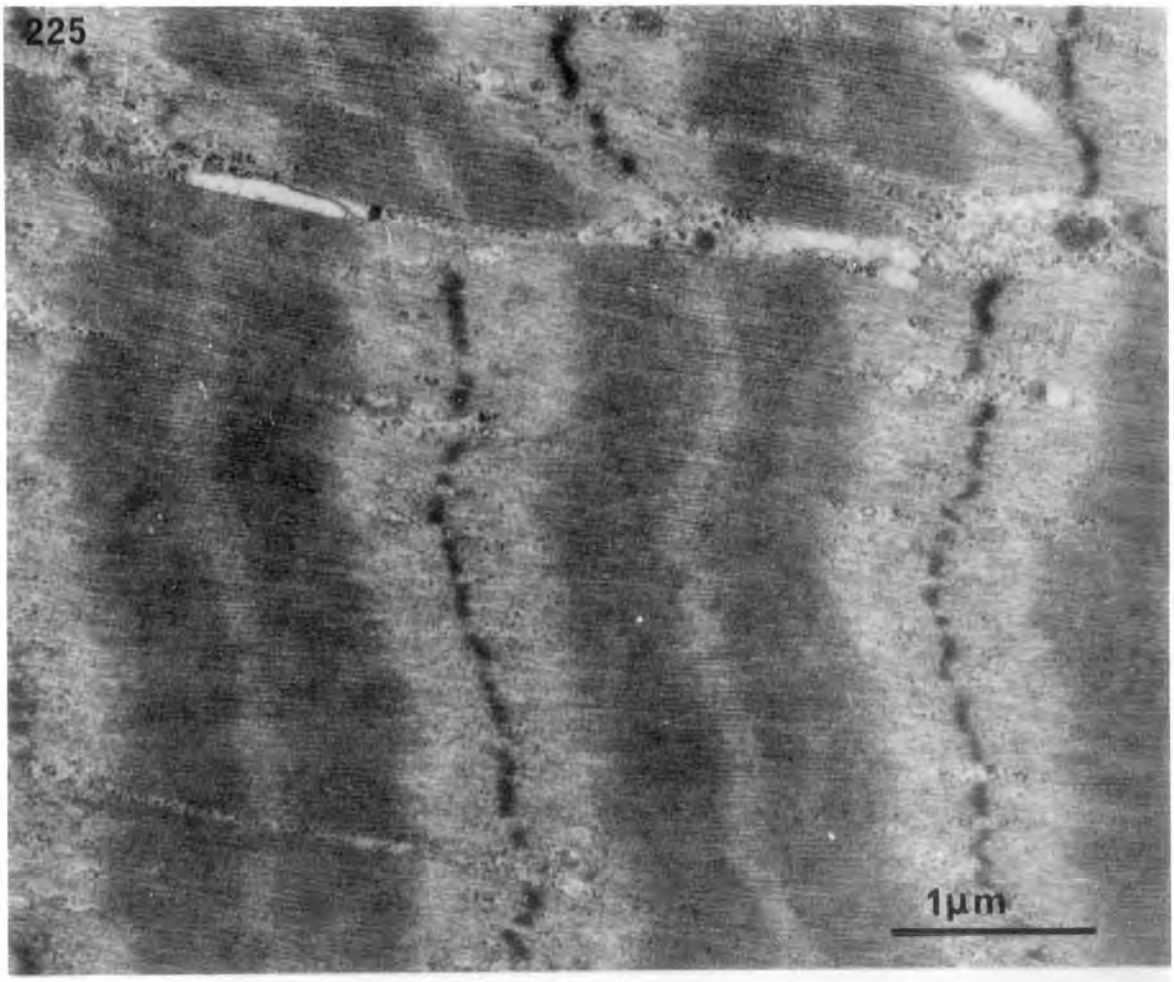
225
1µm


226
tr
m
M
Z

Figures 225 to 226. The ultrastructure of intrafusal fibres in sheep LP.

Fig. 225. Longitudinal section through the polar region of a bag fibre. Note the poor delineation of the myofibrils; the absence of an M line; and the sparsity of sarcotubular system. Compare with fig. 223.

x 24,000

Fig. 226. Longitudinal section through the polar region of a chain fibre. Note the small, well-delineated myofibrils; the distinct M line (M); the elongated mitochondria (m) that form intermyofibrillary chains; and the regular triads (tr). Compare with fig. 221.

x 24,000

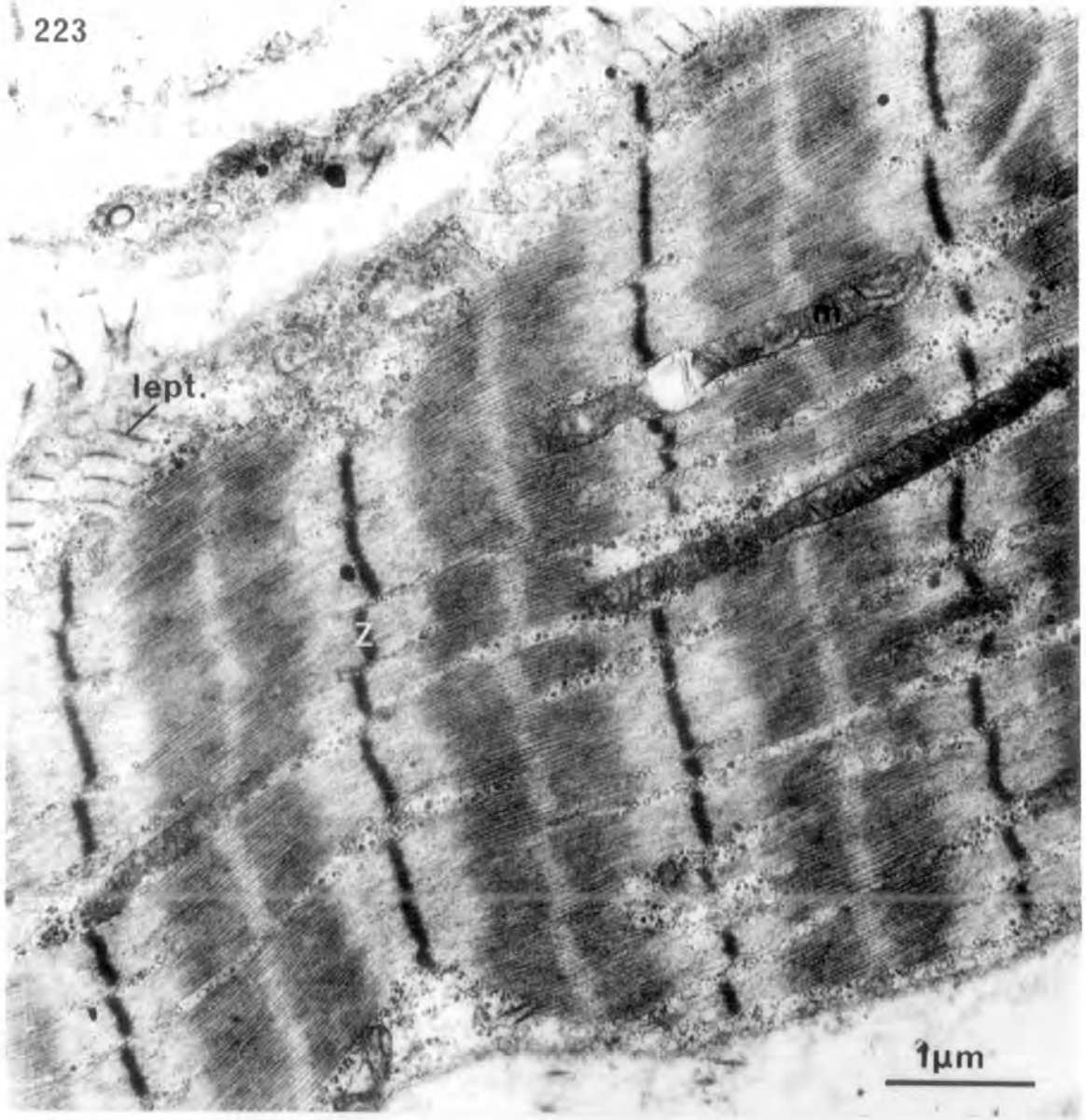
223
lept.
m
Z
1µm

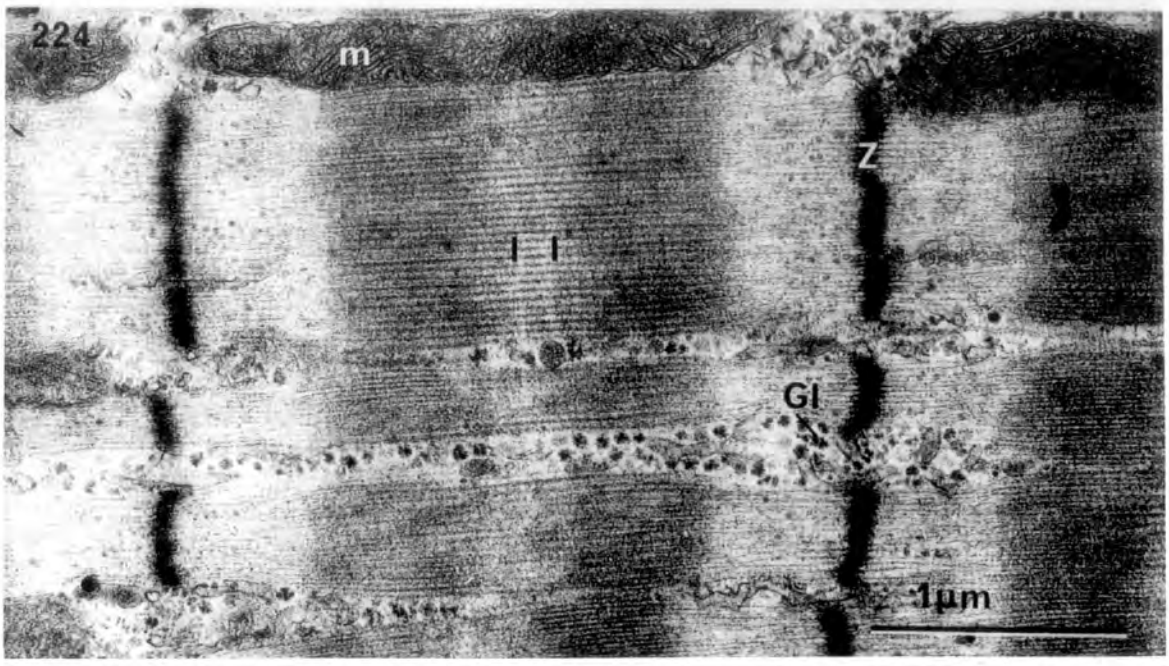
224
m
Z
I I
GI
1µm

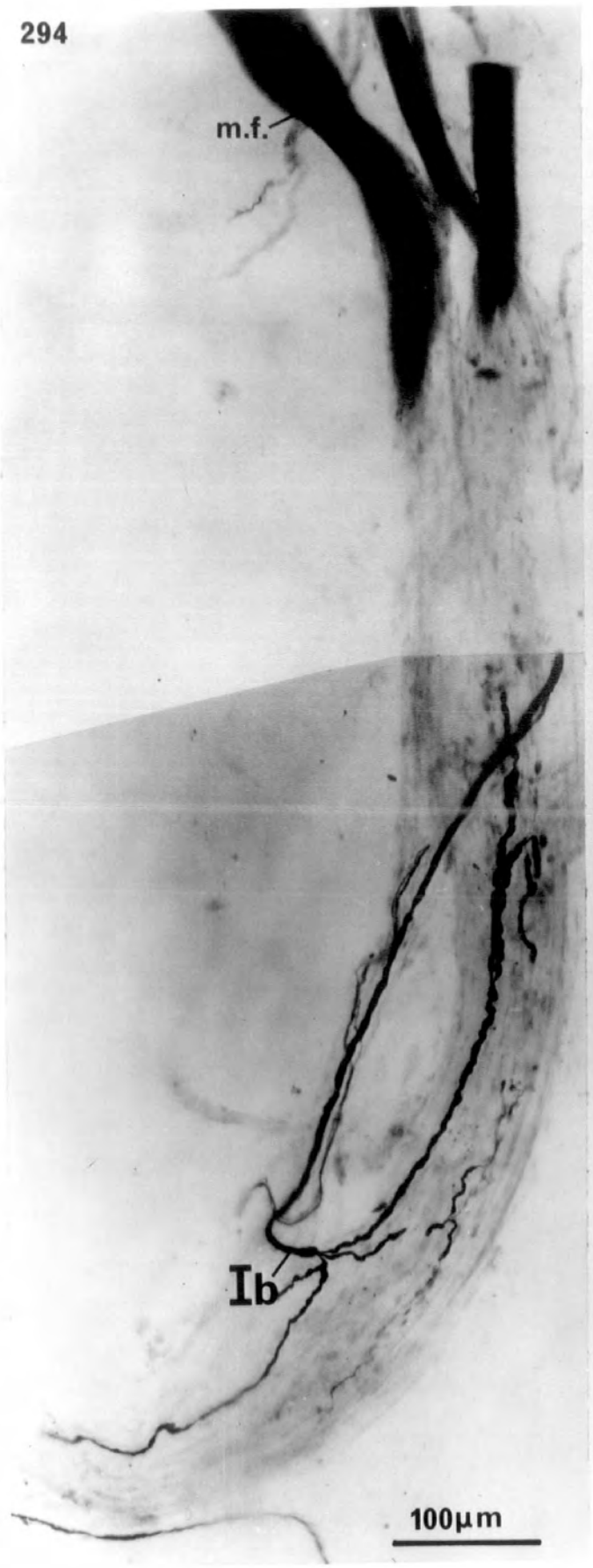
294
m.f.
Ib
100µm

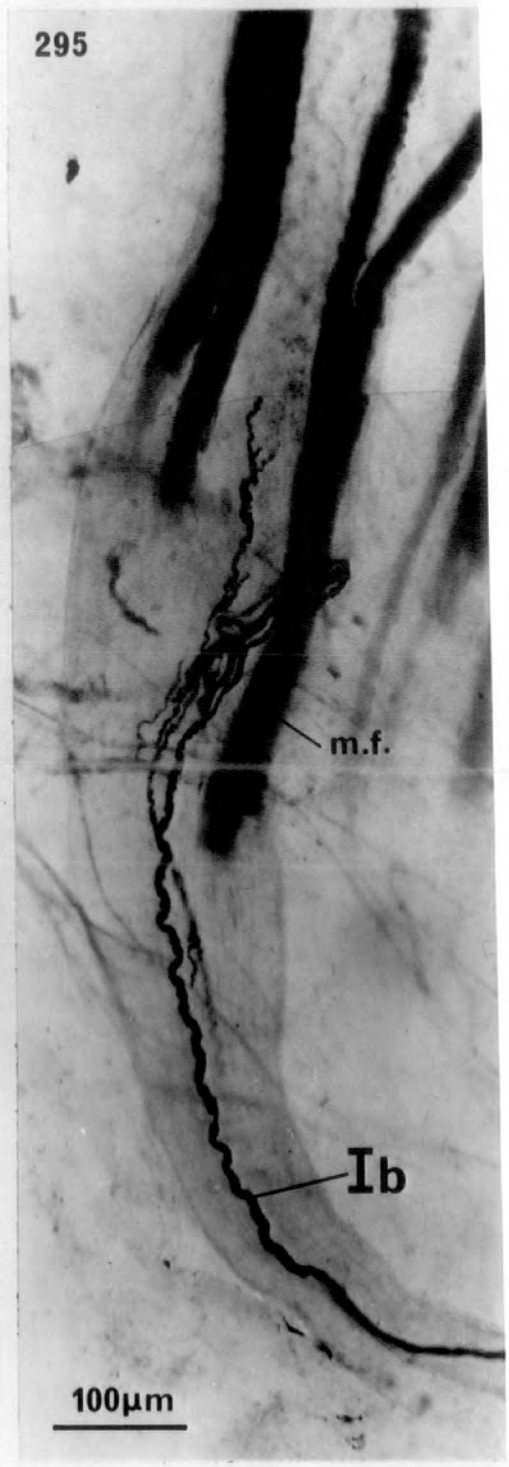
295
m.f.
Ib
100µm

Figures 294 to 295. Teased, silver preparations of tendon organs from the insertion end of superior rectus.

Figs. 294 - 295. Both tendon organs receive a large-diameter afferent nerve fibre (Ib). Usually, as in fig. 294, all the extrafusal muscle fibres (m.f.) are attached at the proximal end of the tendon organ. Occasionally, as in fig. 295, some muscle fibres may attach half way along the capsule.

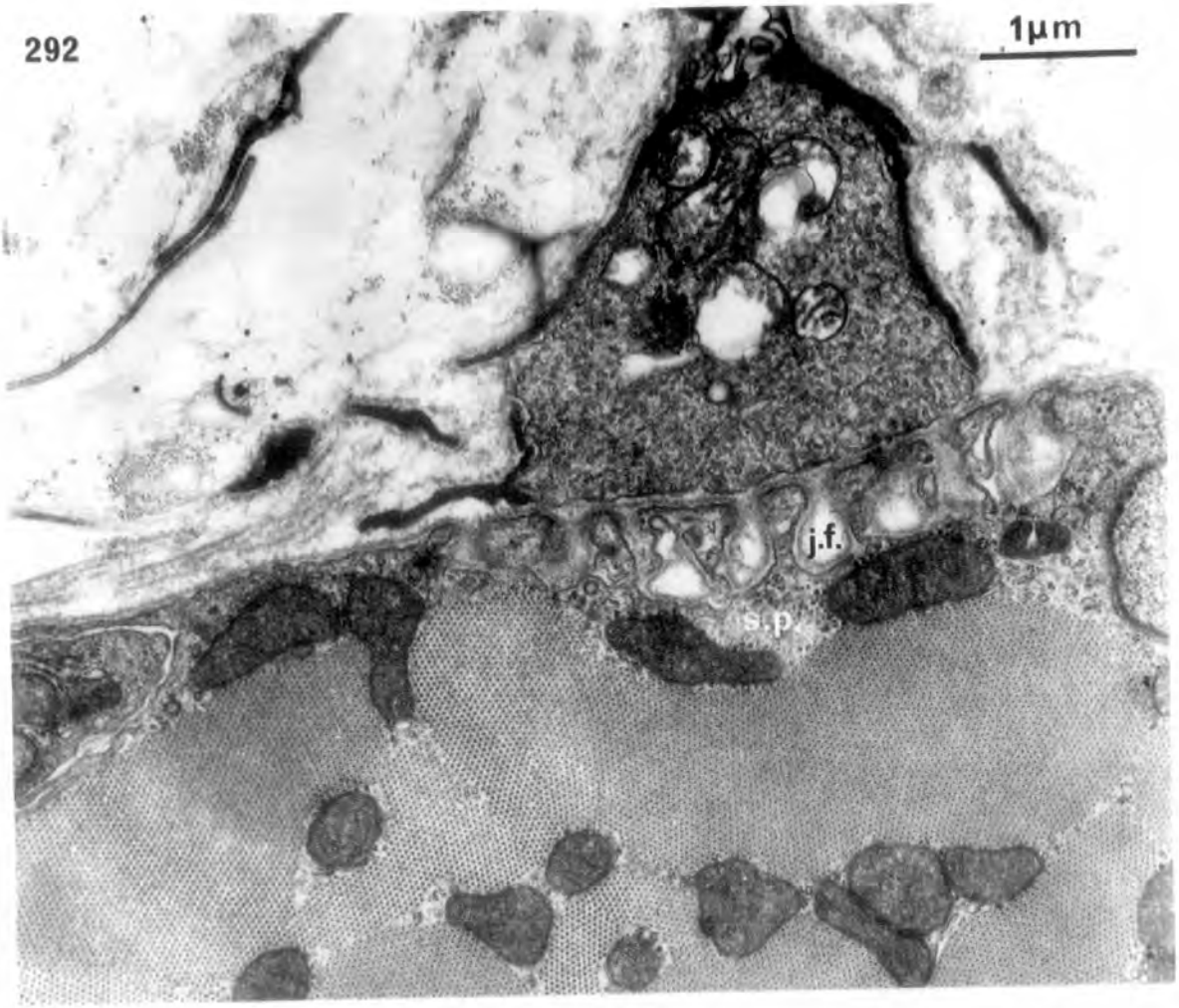
292
1µm
j.f.
s.p.

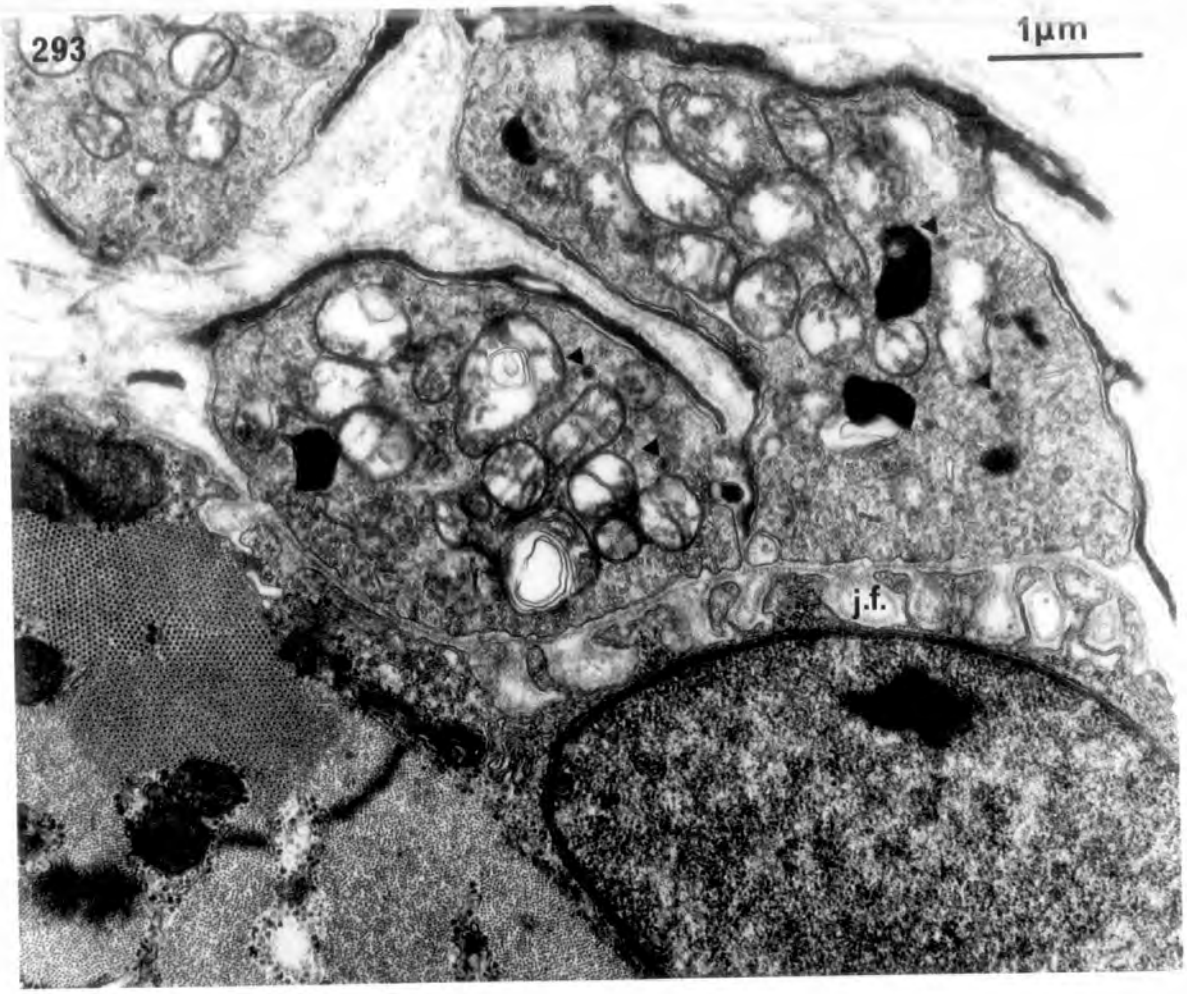
293
1µm
j.f.

Figures 292 to 293. Electron micrographs of mid-polar motor endings in PB spindles.

Figs. 292 - 293. Transverse sections of part of a compact ending located on an intermediate bag fibre. The axon terminals overlie a thin sole plate (s.p.). The post-junctional membrane is thrown into regular folds that are wide, shallow and unbranched (j.f.). These endings may correspond to the p_2 plate endings seen in teased, silver preparations.

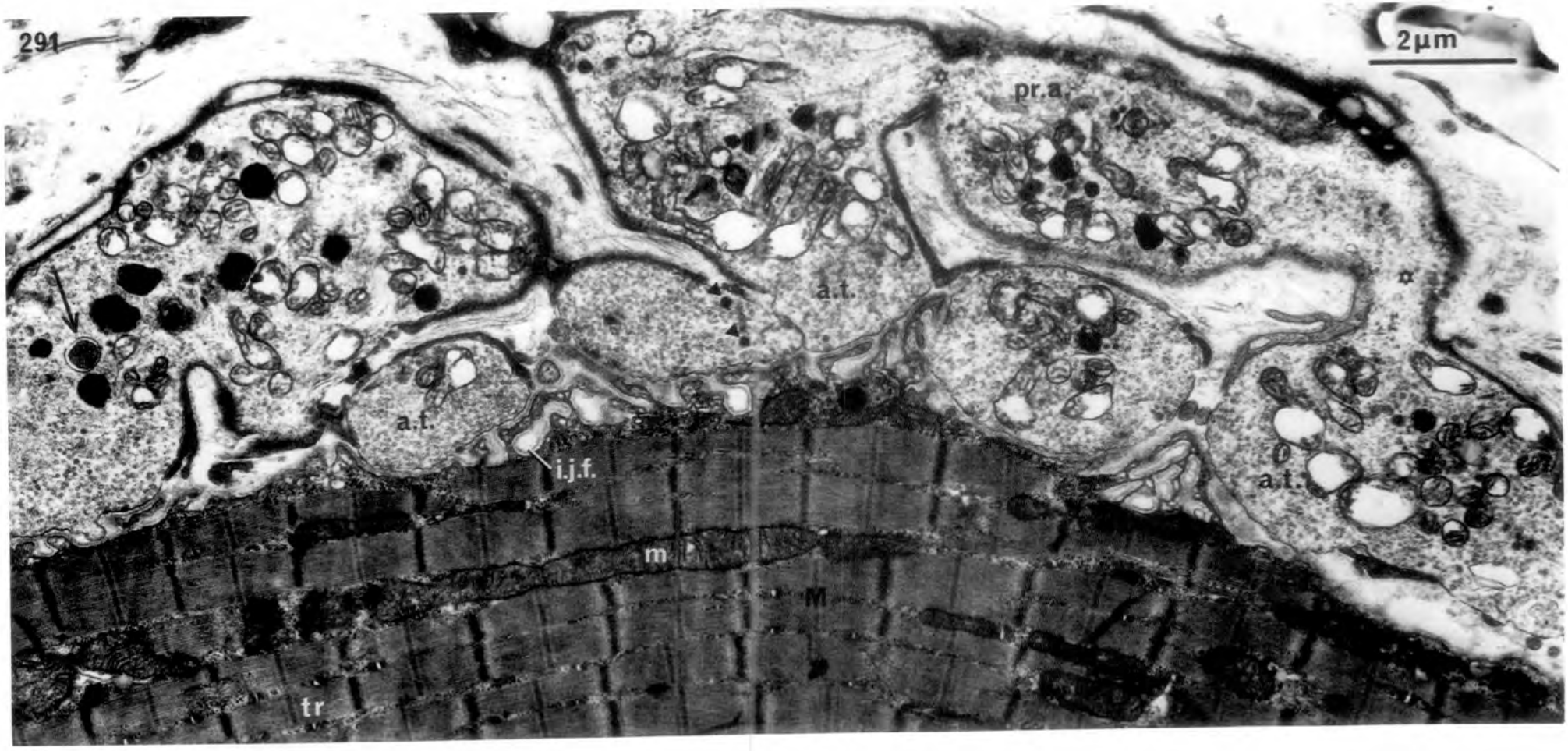
291
2µm
pr.a.
a.t.
a.f.
i.j.f.
a.t.
m
M
tr

Figure 291. Longitudinal section of part of a trail-type termination on a chain fibre in PB.

A non-myelinated preterminal axon bulb (pr.a.) is linked by strands of axoplasm (stars) to two axon terminals (a.t.). The terminals contain the usual organelles including dense-core vesicles (arrowheads) and they also contain densely-packed multivesicular bodies (arrow). The myoneural junction is mainly smooth with only occasional irregular folding (i.j.f.). The underlying chain fibre has large, elongate mitochondria (m); a prominent M line (M); and a regular system of triads (tr).

x 12,600

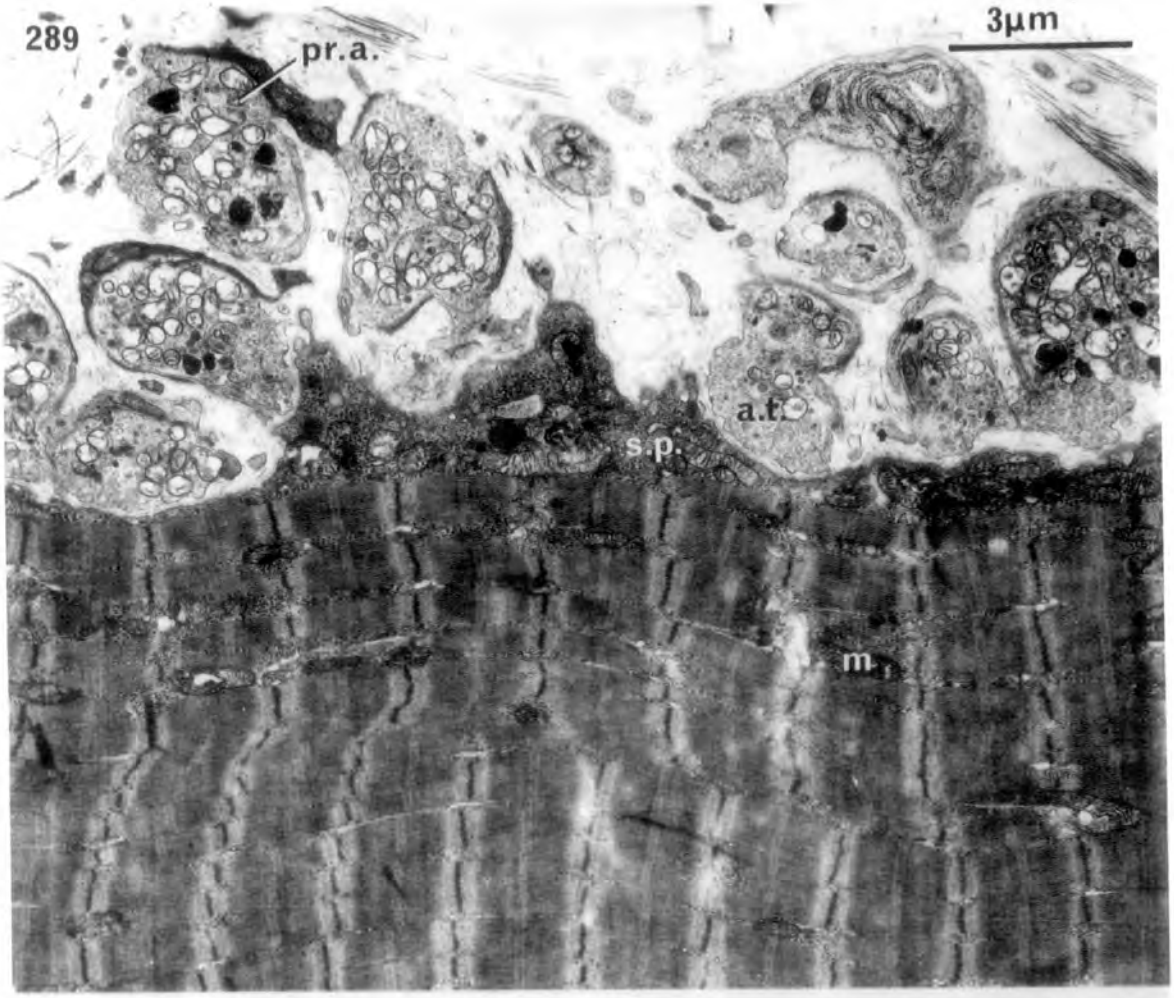
289
pr.a.
3µm
a.t.
s.p.
m

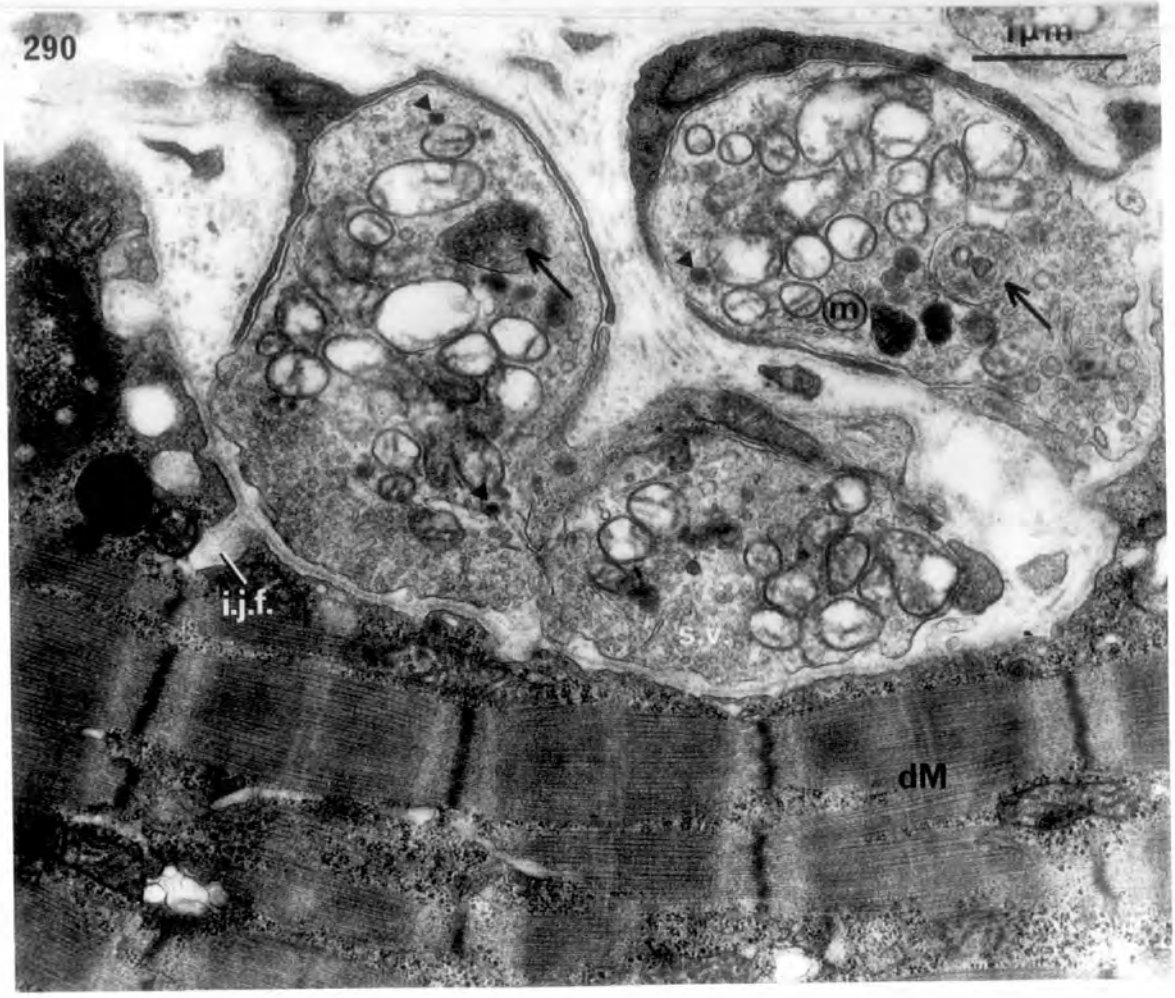
290
1µm
m
i.j.f.
s.v.
dM

Figures 289 to 290. Electron micrographs of juxta-equatorial trail-type motor endings in PB spindles.

Fig. 289. Longitudinal section of part of a trail-type termination on a typical bag fibre. Note the small, infrequent mitochondria (m). The axon terminals (a.t.) are applied to the surface of the typical bag fibre and overlie a thinly-spread sole plate (s.p.). Numerous non-myelinated preterminal axons (pr.a.) lie above the surface of the muscle fibre.

x 8,000

Fig. 290. Part of fig. 289 at high magnification. The axon terminals contain mitochondria (m), synaptic vesicles (s.v.), dense-core vesicles (arrowheads), and densely-packed multivesicular bodies (arrows). Note the occasional irregular junctional folds (i.j.f.) and the 'double' M line (dM) in the form of two faint parallel lines.

x 20,000


285

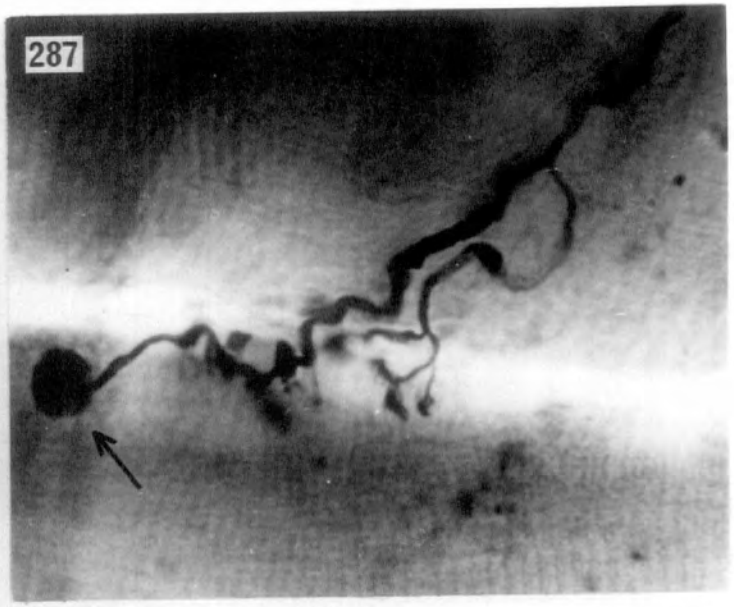
287

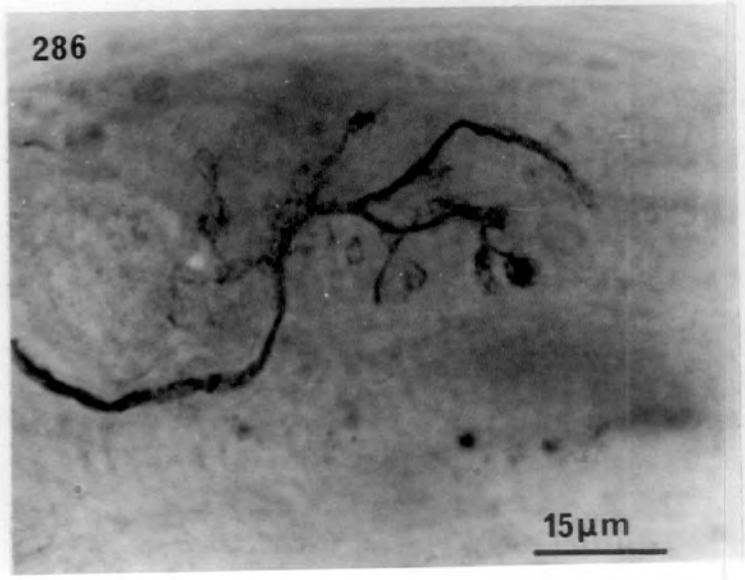
286
15µm

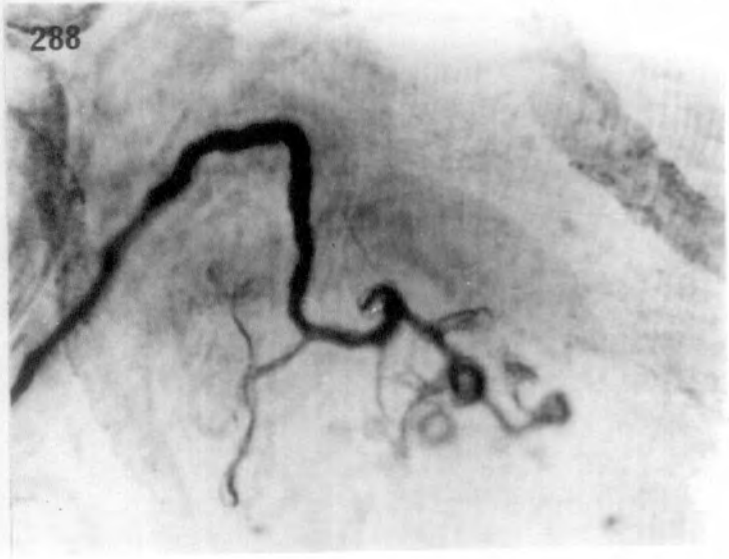
288

Figures 285 to 288. Photographs of teased, silver preparations from peroneus brevis.

Figs. 285 - 286. P_1-type plate endings on bag fibres in the polar region of PB spindles. The two compact plate endings in fig. 285 and the single plate endings in fig. 286 seen in surface view may be compared with extrafusal motor end-plates (figs. 287 & 288) from the same muscle. In fig. 287 note the ultraterminal fibre with a terminal bulb (arrow).
All figs. are the same magnification.

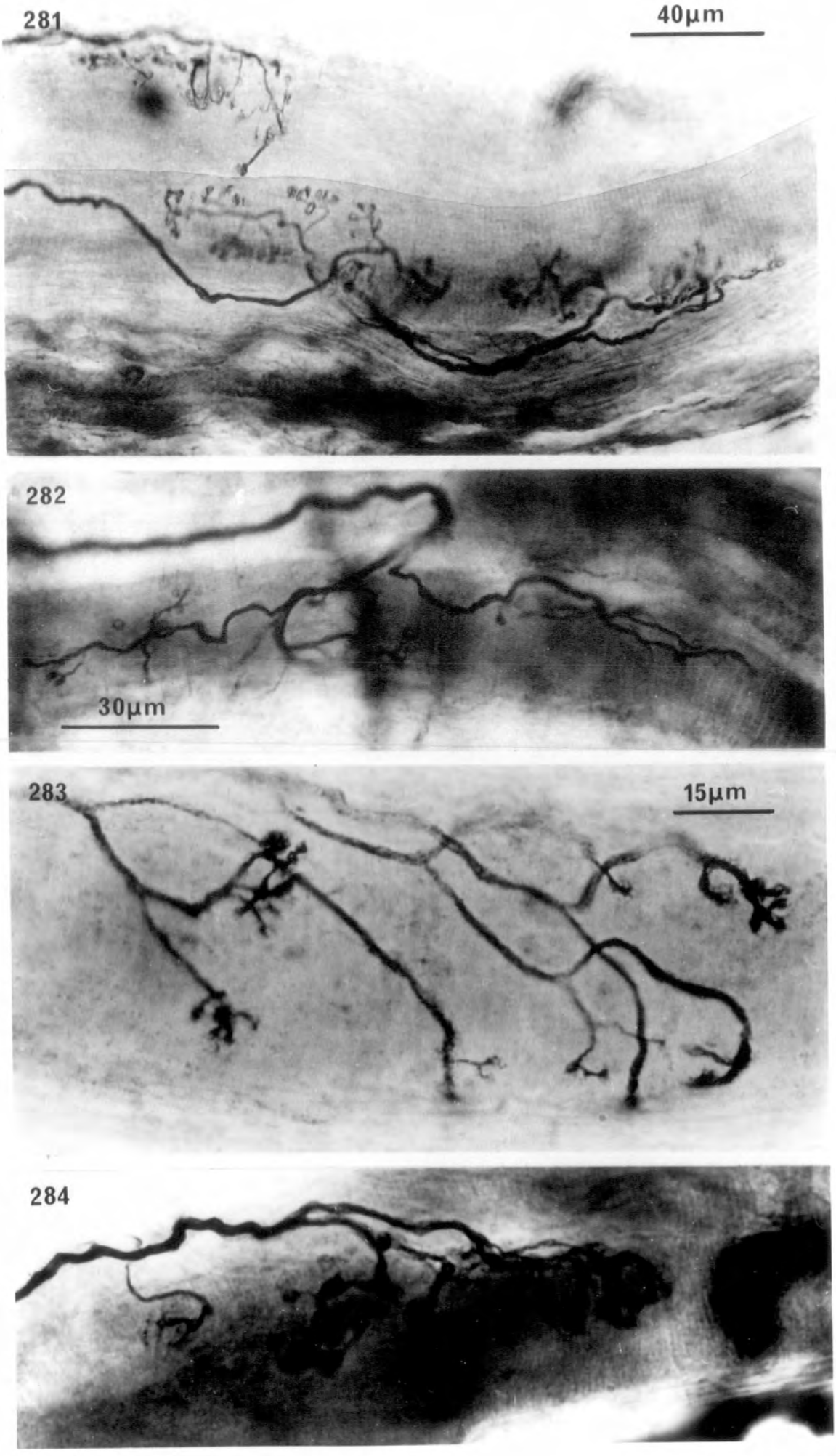
281
40µm
282
30µm
283
15µm
284

Figures 281 to 284. Photographs of teased, silver preparations of spindles from peroneus brevis.

Figs. 282 - 283 are examples of the diffuse and extensively branched terminations in the juxta-equatorial region of the spindles, that are presumed to be homologous with the trail-endings in cat. In fig. 282 the terminations are extended linearly along a bag fibre. In fig. 283 the parent axon branches to give several simple endings, which terminate on both bag and chain fibres.

Figs. 281 & 284 are examples of the more compact mid-polar terminations that resemble the p_2 plate endings found in cat spindles.

The three endings in fig. 281 and the single ending in fig. 284 are located on bag fibres. Note the complex, extended nature of these plate endings compared with the p_1-type plates (figs. 285 - 286).

Figs. 283 and 284 are the same magnification.

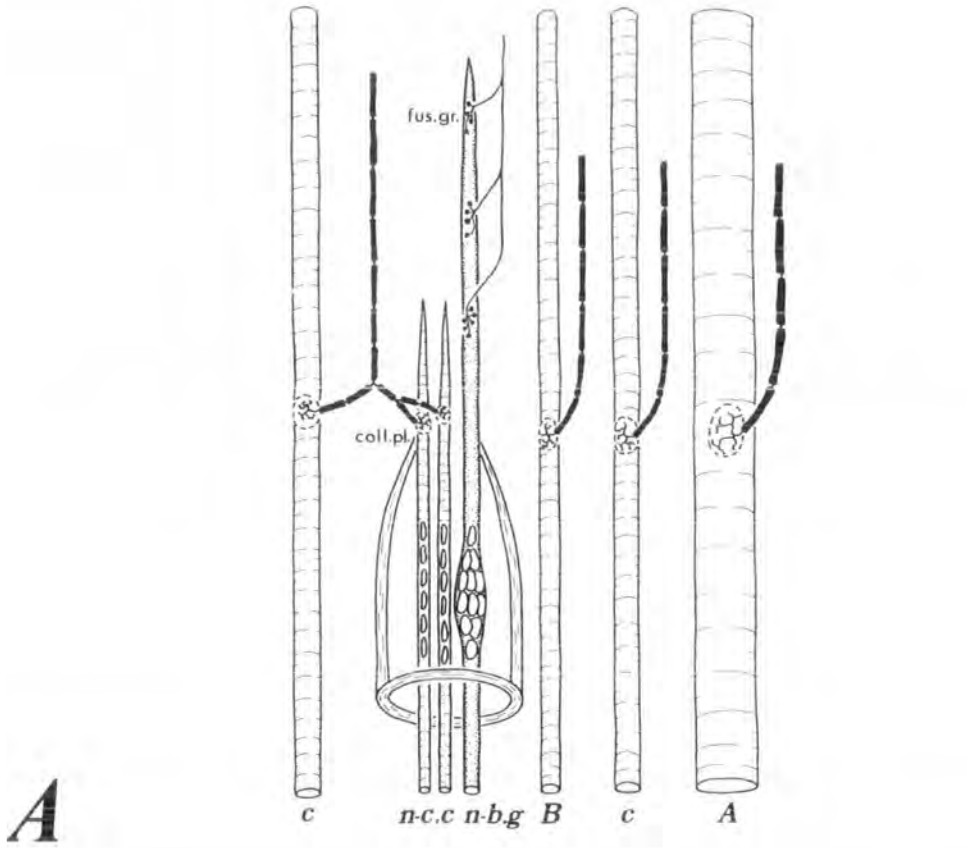
A
fus.gr.
coll.pl.
c
n-c.c
n-b.g
B
c
A

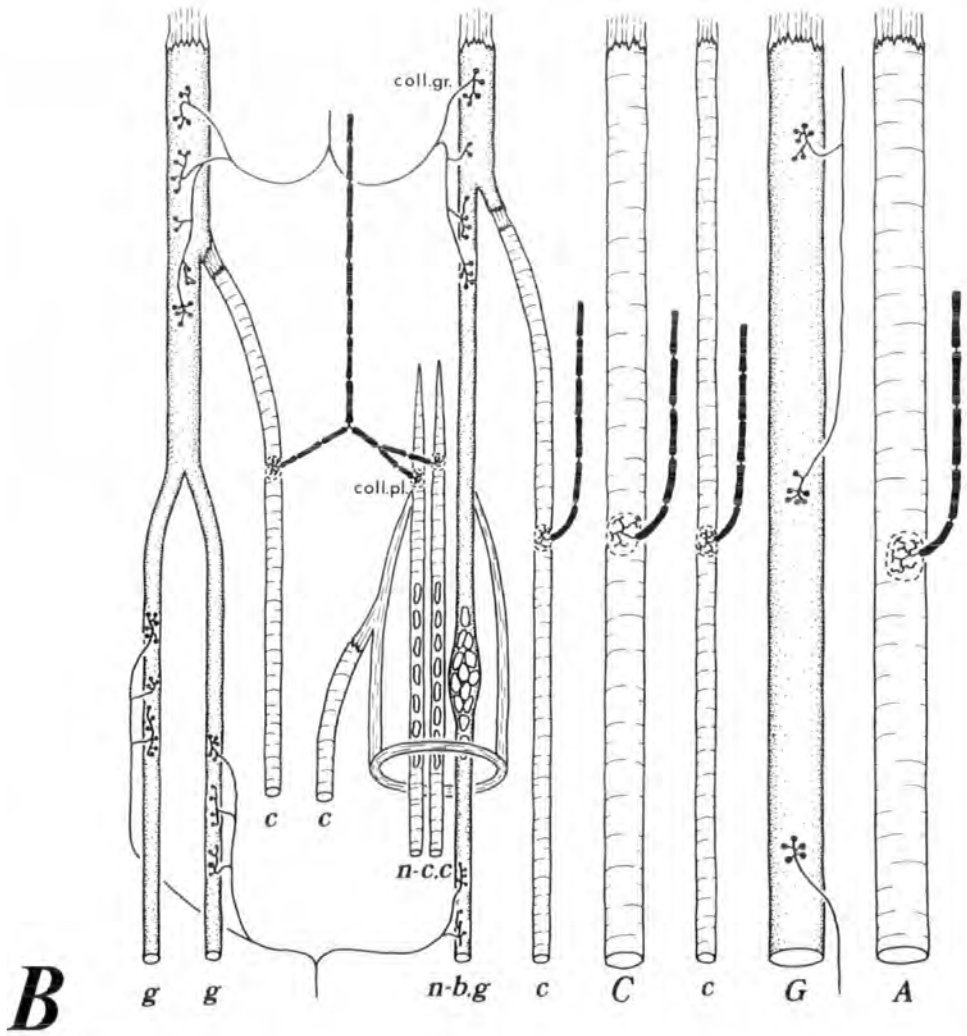
B
coll.gr.
coll.pl.
c
c
n-c.c
g
g
n-b.g
c
C
c
G
A

Figure 280. Schematic diagrams of the pattern of motor innervation in levator palpebrae (A) and superior rectus (B) muscles of the sheep.

The extrafusal muscle fibres are shown as: A., large A fibre; B., small B fibre; C., intermediate C fibre; c., small C fibre; G., large G fibre; g., small G fibre.

The intrafusal muscle fibres are shown as: n-b.g., nuclear-bag G fibre; n-c.c., nuclear-chain C fibre.

The features of the motor innervation are indicated by: coll.gr., collateral grape endings; coll.pl., collateral plate endings; and fus.gr., fusimotor grape endings.

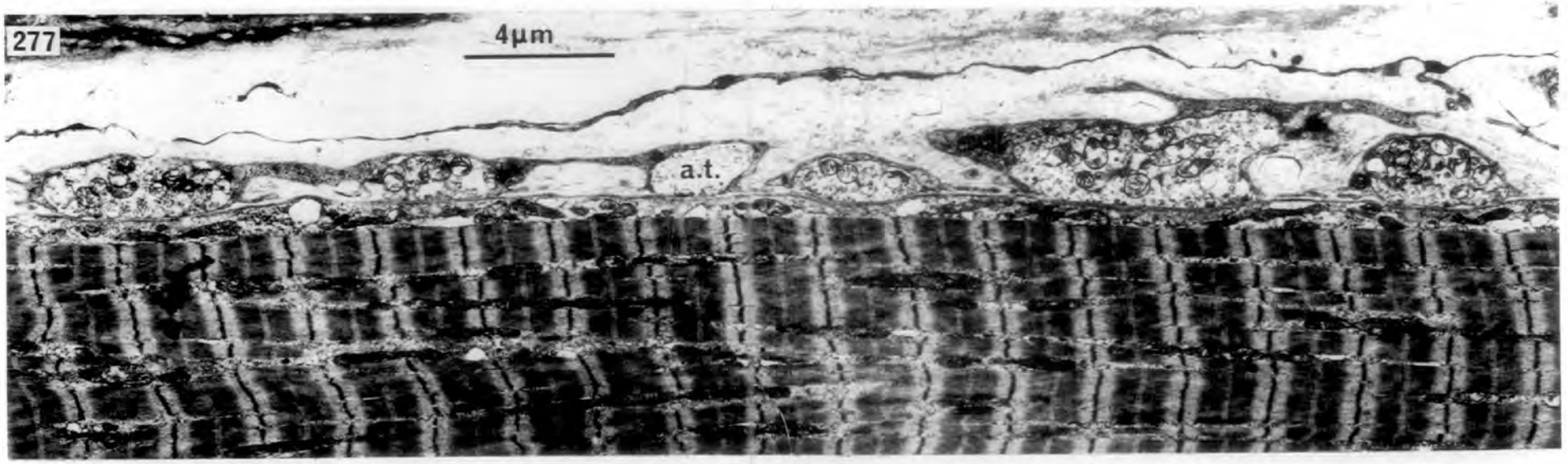
277
4µm
a.t.

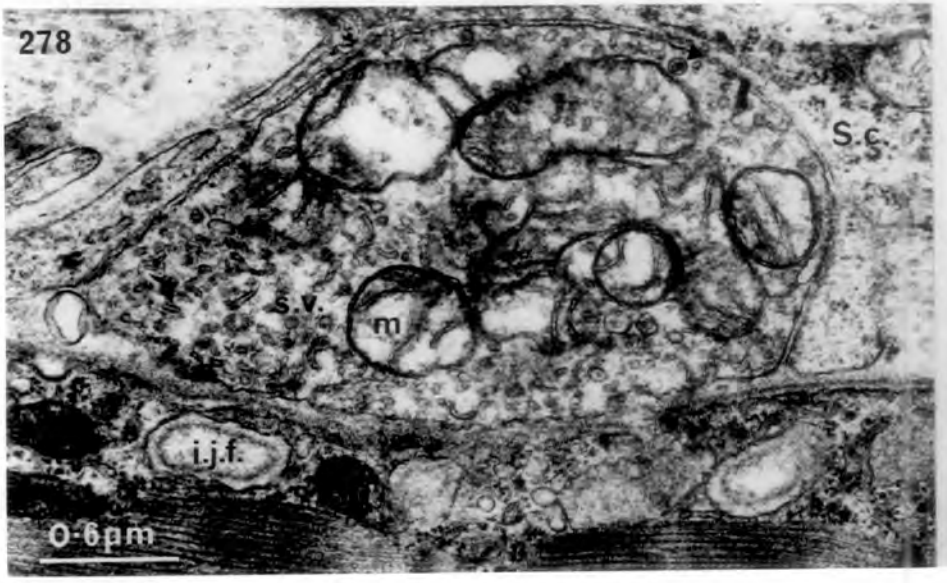
278
S.C.
s.v.
m
i.j.f.
0·6µm

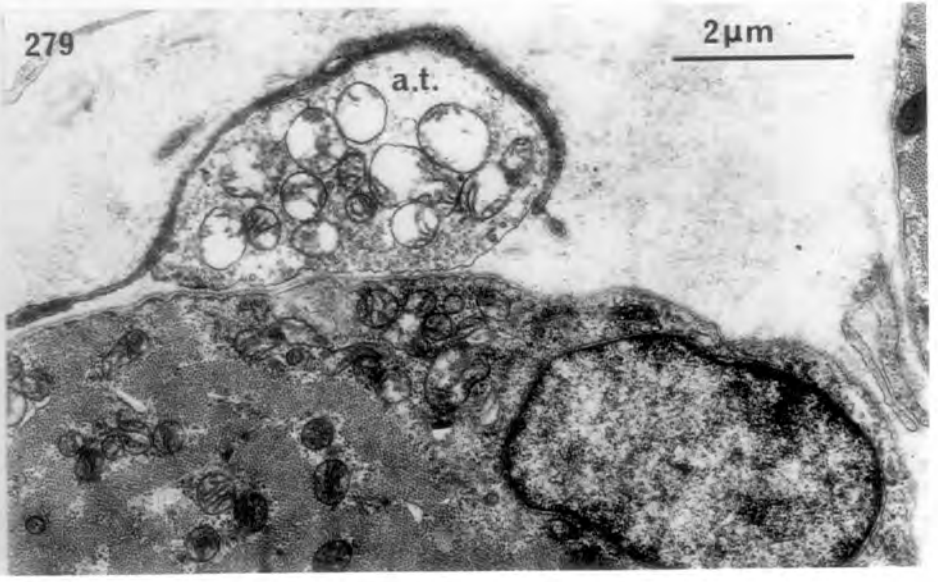
279
2µm
a.t.

Figures 277 to 279. Electron micrographs illustrating the ultrastructure of intrafusal grape endings in SR.

Fig. 277. Longitudinal section through the mid-polar region of a spindle showing six grape axon terminals (a.t.) applied to the surface of a bag fibre, with a very thinly-spread sole plate.

x 6,300

Fig. 278. Longitudinal section through a grape axon terminal that contains mitochondria (m), synaptic vesicles (s.v.) and dense-core vesicles (arrowhead). Note the occasional 'vacuolar' junctional folds (i.j.f.). S.c., Schwann cell.

x 32,000

Fig. 279. Transverse section through a grape axon terminal on a bag fibre. Note the completely smooth myoneural junction.

x 12,600

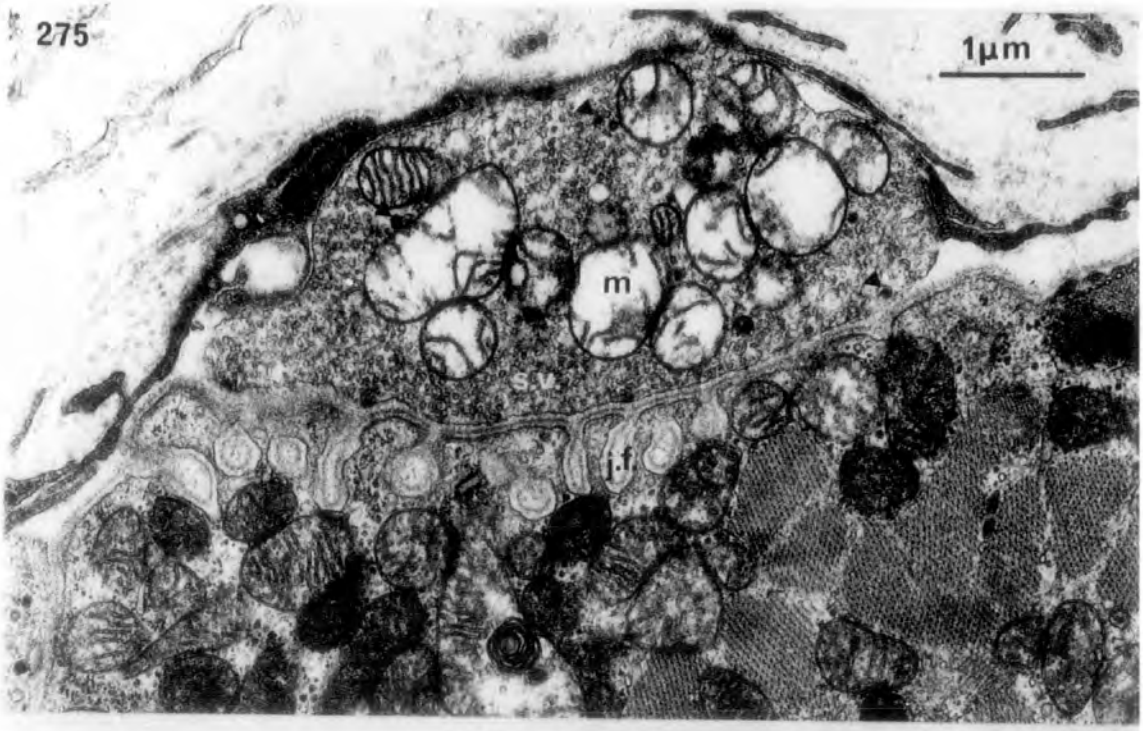
275
1µm
m
s.v.
j.f.

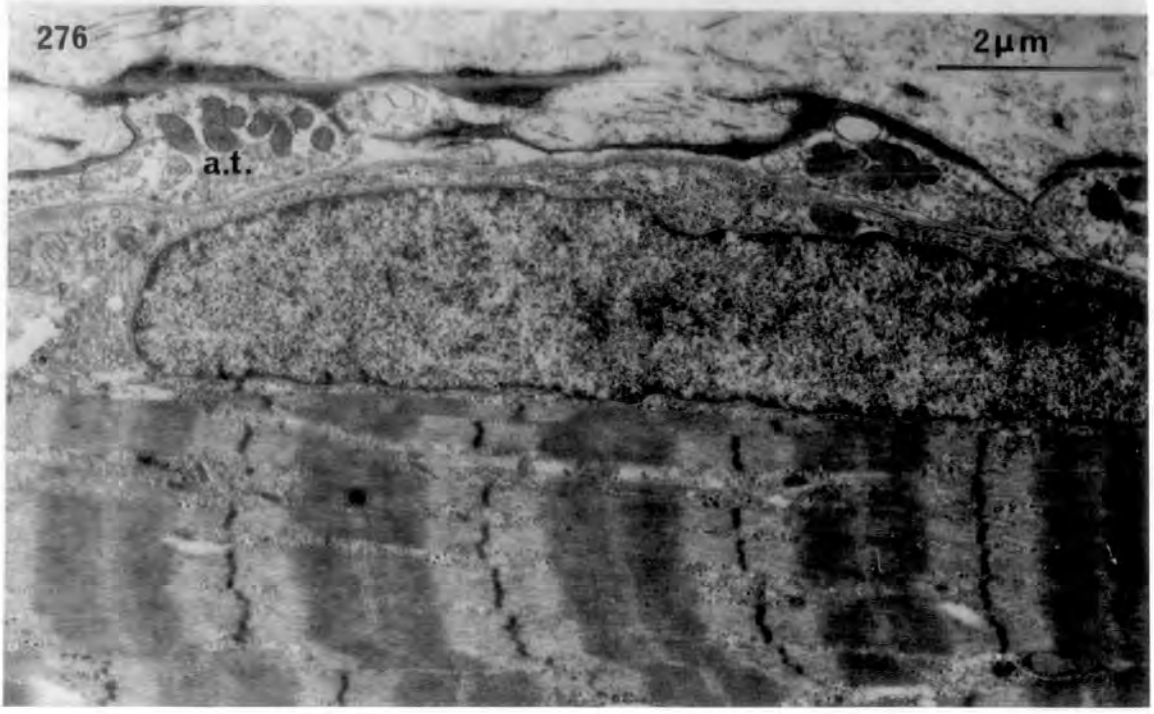
276
2µm
a.t.

Figures 275 to 276. Electron micrographs illustrating the ultrastructure of intrafusal motor endings in LP.

Fig. 275. Transverse section of an axon terminal from a plate ending on a chain fibre. The terminal contains mitochondria (m), synaptic vesicles (s.v.), and dense-core vesicles (arrowheads). The junctional folds (j.f.) are short and bulbous.

x 20,000

Fig. 276. Longitudinal section of grape axon terminals (a.t.) on a bag fibre . Note the smooth myoneural junctions and the absence of an M line from the pseudo-H zone.

x 12,800

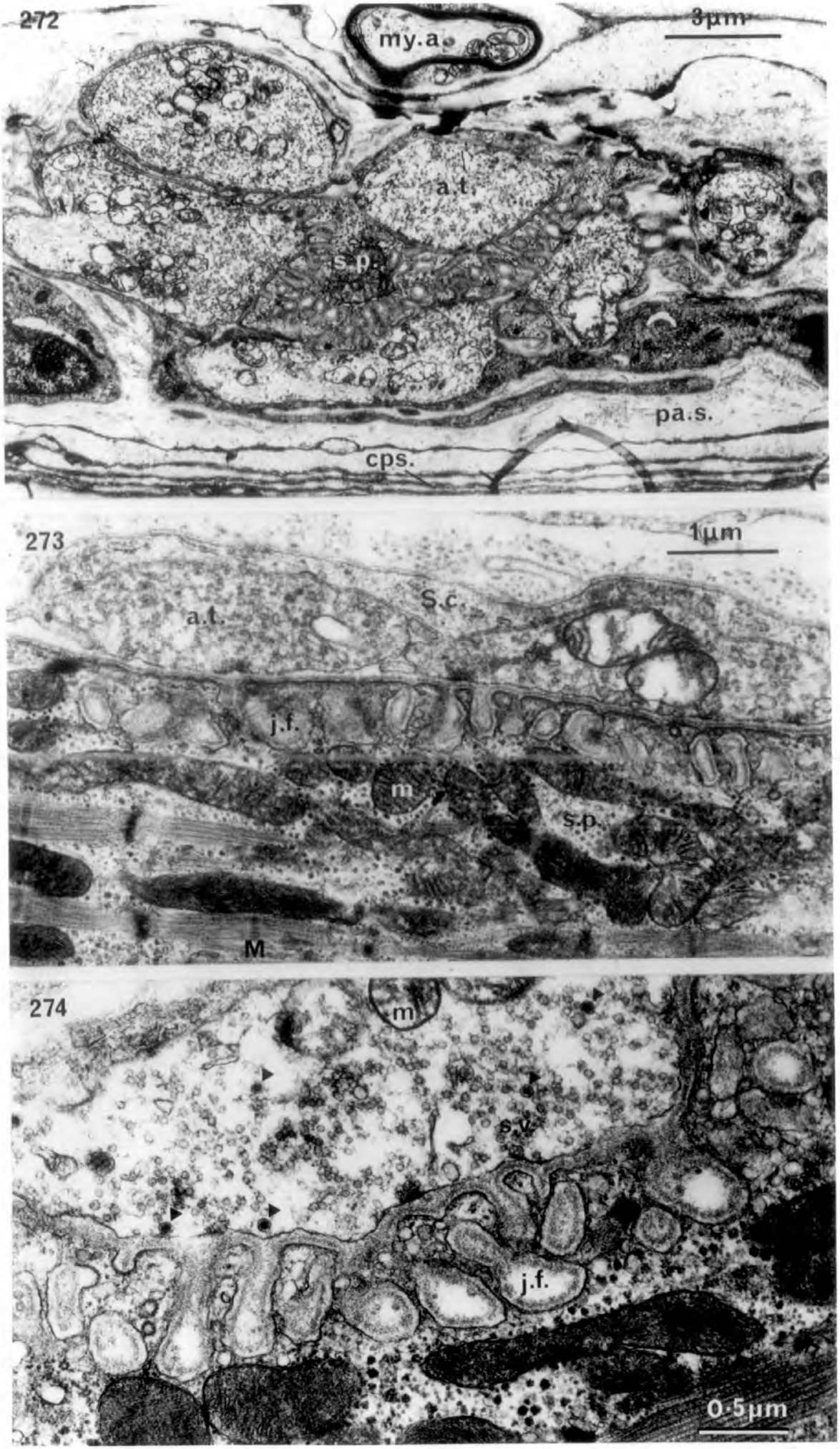
272
3µm
my.a.
a.t.
s.p.
pa.s.
cps.
273
1µm
S.c.
a.t.
j.f.
m
s.p.
M
274
m
s.v.
j.f.
0·5µm

Figures 272 to 274. Electron micrographs illustrating the ultrastructure of intrafusal motor end-plates in SR.

Fig. 272. Longitudinal section through the juxta-equatorial region of a spindle passing through the raised sole plate of a plate ending. The underlying chain fibre is beyond the plane of section. Six axon terminals (a.t.), derived from an adjacent myelinated axon (my.a.), are grouped around a central sole plate (s.p.) cps., capsule; pa.s., periaxial space.
x 7,000

Fig. 273. Longitudinal section showing part of a plate endings on a chain fibre. Note the junctional folds (j.f.) in the sole plate (s.p.) that has accumulations of mitochondria (m); and the M line (M) of the chain fibre. S.c., Schwann cell.
x 20,000

Fig. 274. A single axon terminal of a plate ending containing mitochondria (m), synaptic vesicles (s.v.), and dense-core vesicles (arrowheads). Note the short, wide and unbranched junctional folds (j.f.) lined by basement membrane.
x 32,000

271a

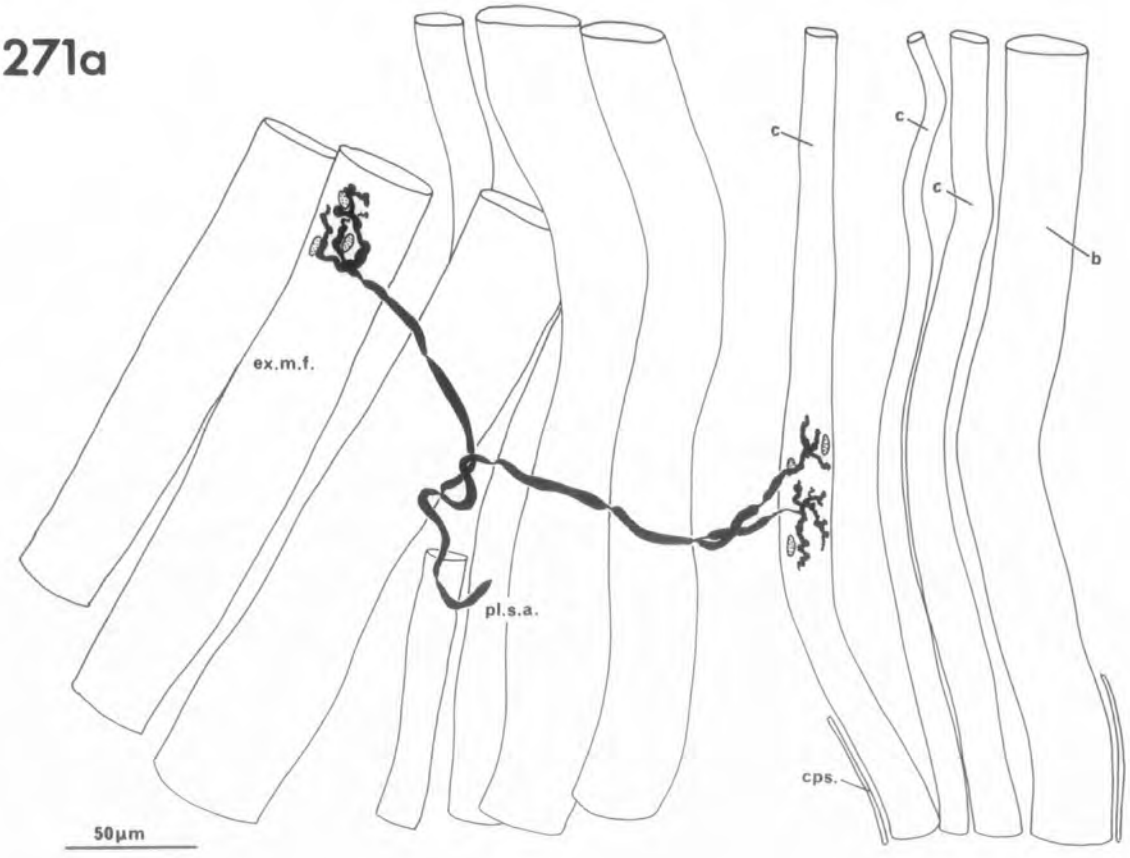

271b

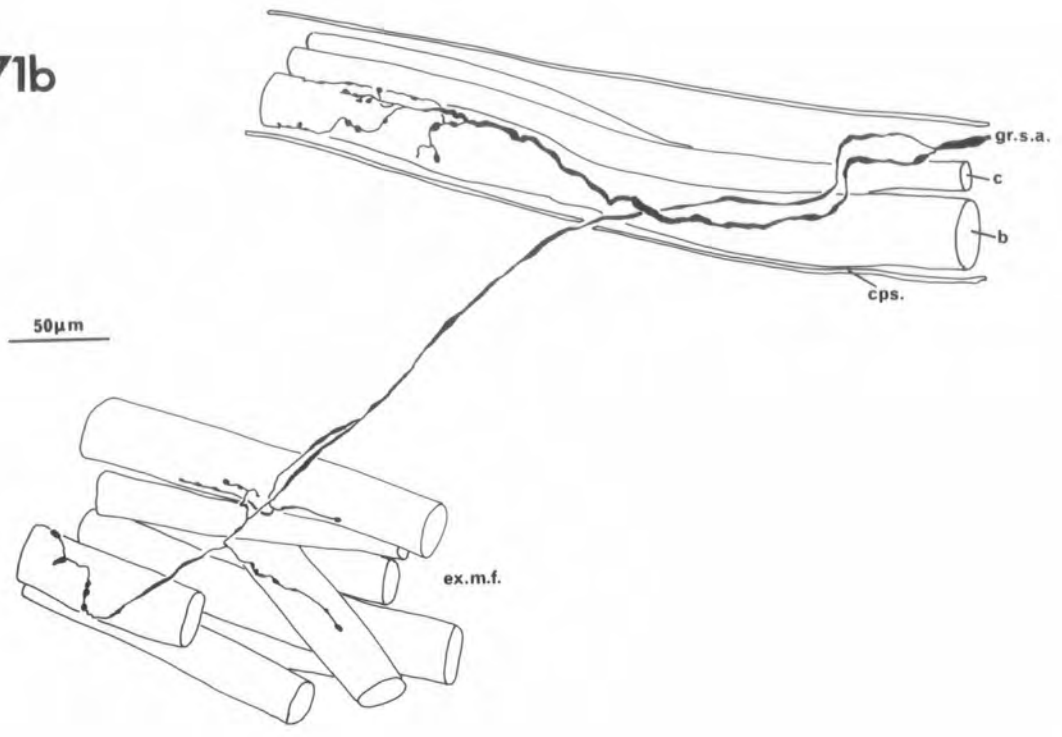

Figure 271. Drawings of motor endings traced from photographs of teased, silver preparations of SR.

Fig. 271 a. Collateral plate innervation.
b, bag fibre; c, chain fibre; cps., capsule; ex.m.f., extrafusal muscle fibre; pl.s.a., stem axon supplying plate endings to the chain fibre of the spindle and also an extrafusal muscle fibre.

Fig. 271 b. Collateral grape innervation.
gr.s.a., stem axon supplying grape endings to the bag fibre of the spindle and also extrafusal muscle fibres. Other labels as above.

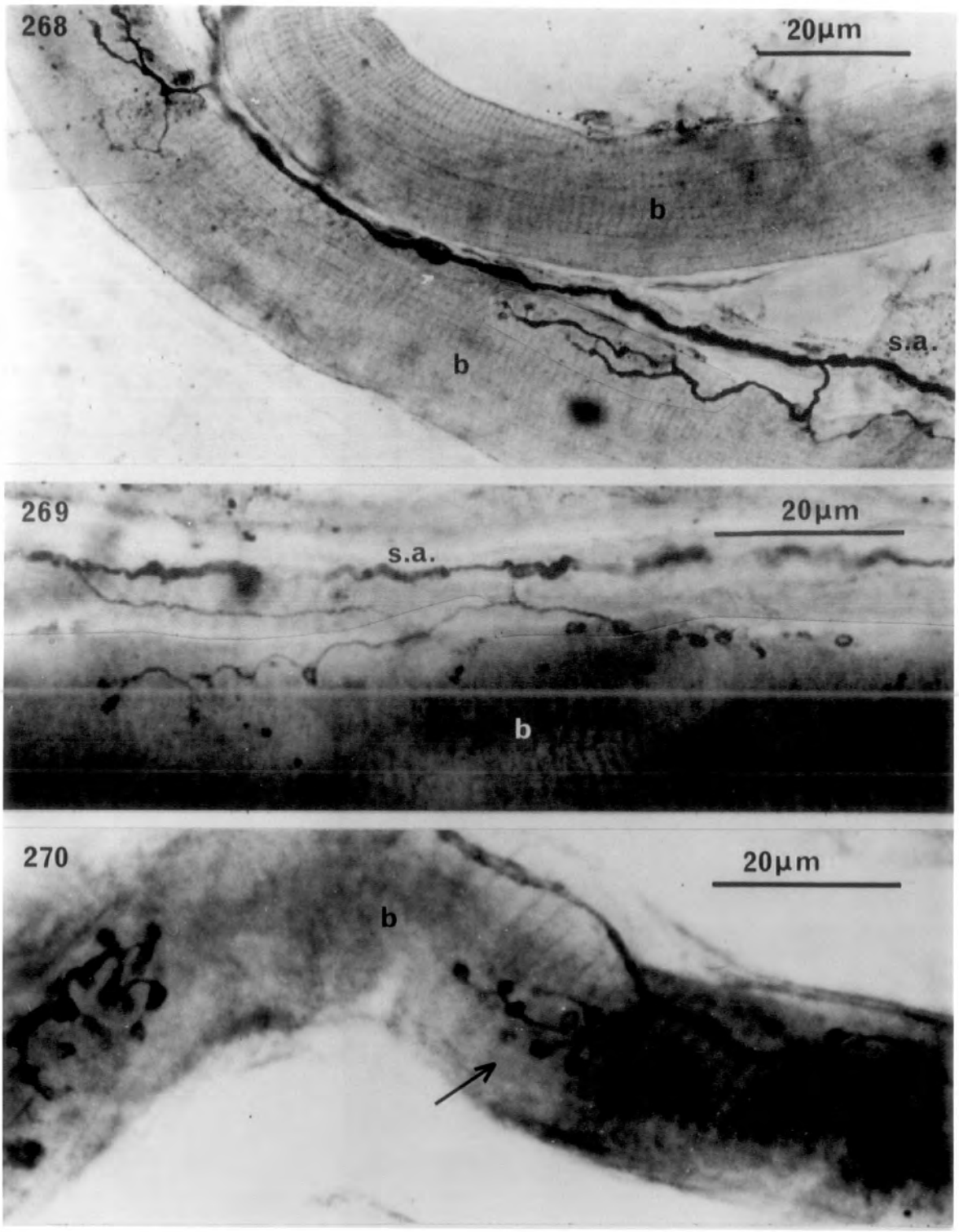
268
20µm
b
b
s.a.
269
20µm
s.a.
b
270
20µm
b

Figures 268 to 270. Photographs of teased, silver preparations of spindles from LP illustrating grape endings.

Figs. 268 & 269 are examples of linear grape terminations on the polar portions of bag fibres (b). The stem axon (s.a.) gives non-myelinated terminal fibrils that end in axoplasmic knobs.

Fig. 270. Grape termination on a bag fibre in the mid-polar region of a spindle showing classic 'bunch of grapes' appearance.

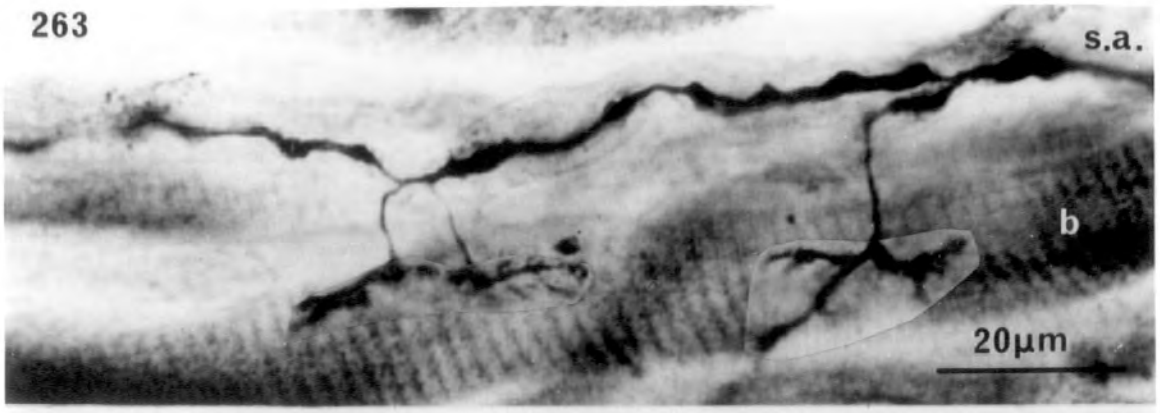
263
s.a.
b
20µm

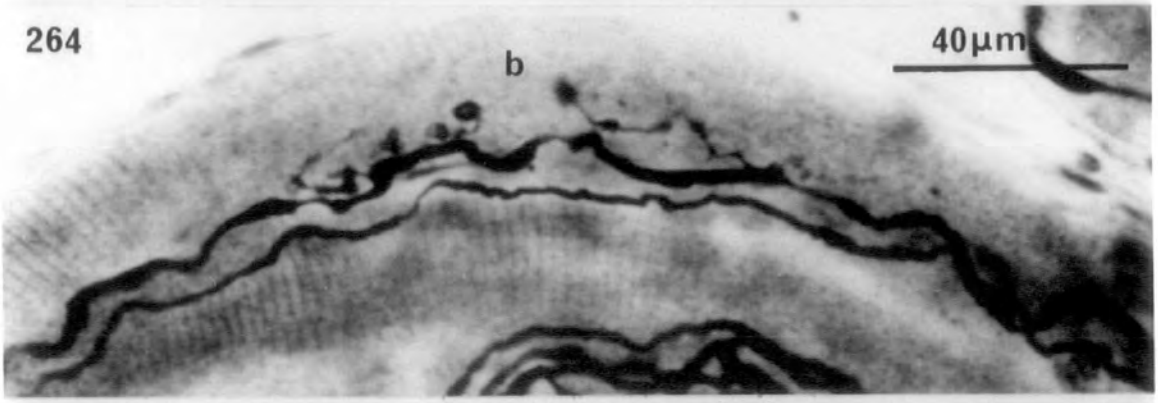
264
b
40µm

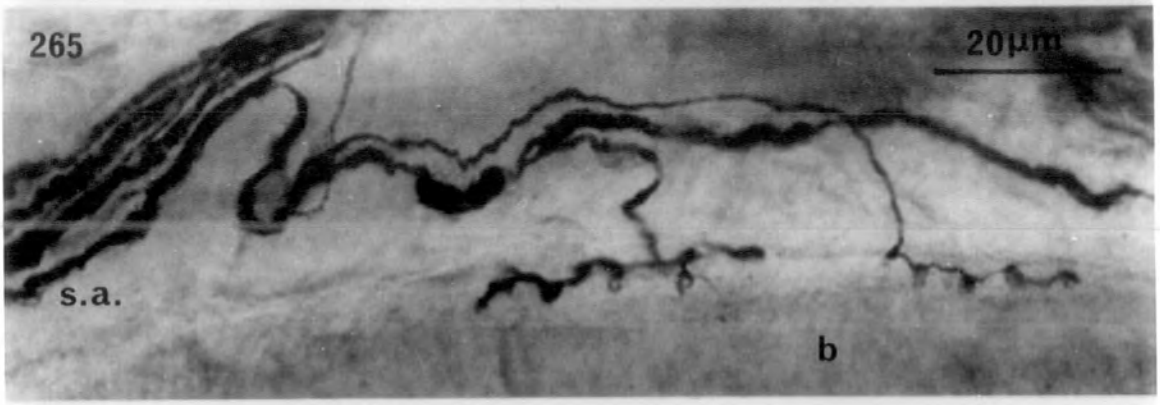
265
20µm
s.a.
b

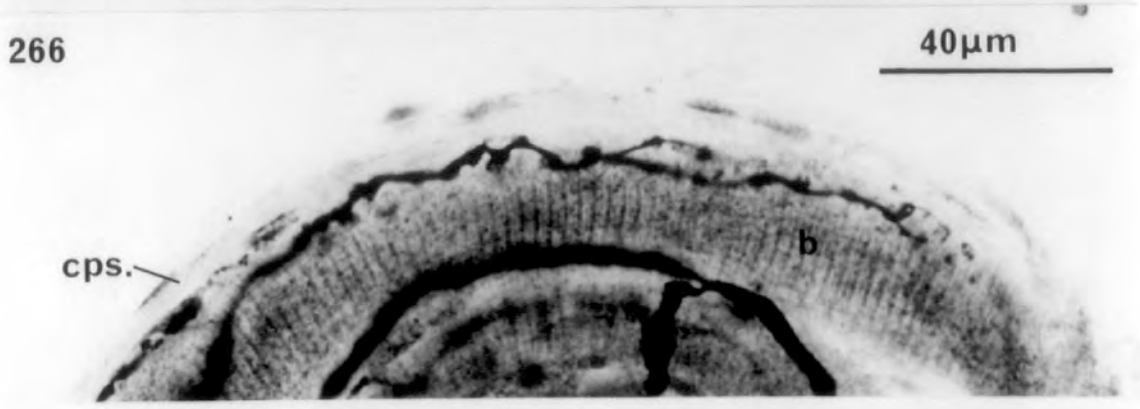
266
40µm
cps.
b

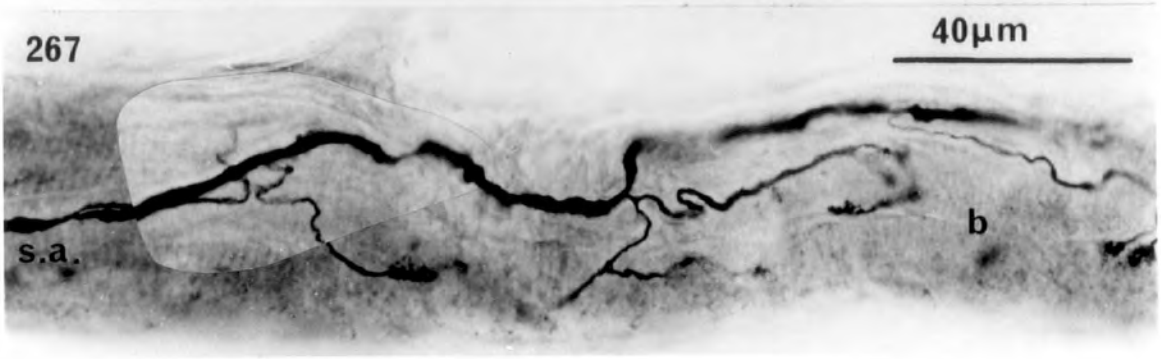
267
40µm
s.a.
b

Figures 263 to 267. Photographs of teased, silver preparations of spindles from SR illustrating grape endings.

Figs. 263, 265 & 267 are examples of linear grape terminations on the polar portions of bag fibres (b). In each case a myelinated stem axon (s.a.) spirals around the bag fibre and branches to give non-myelinated or very thinly-myelinated terminal fibrils that end in axoplasmic knobs and swellings.

Figs. 264 & 266 are examples of grape endings in the juxta-equatorial region of the spindle, where the form of the ending is often more like a 'bunch of grapes'. cps., capsule.


260

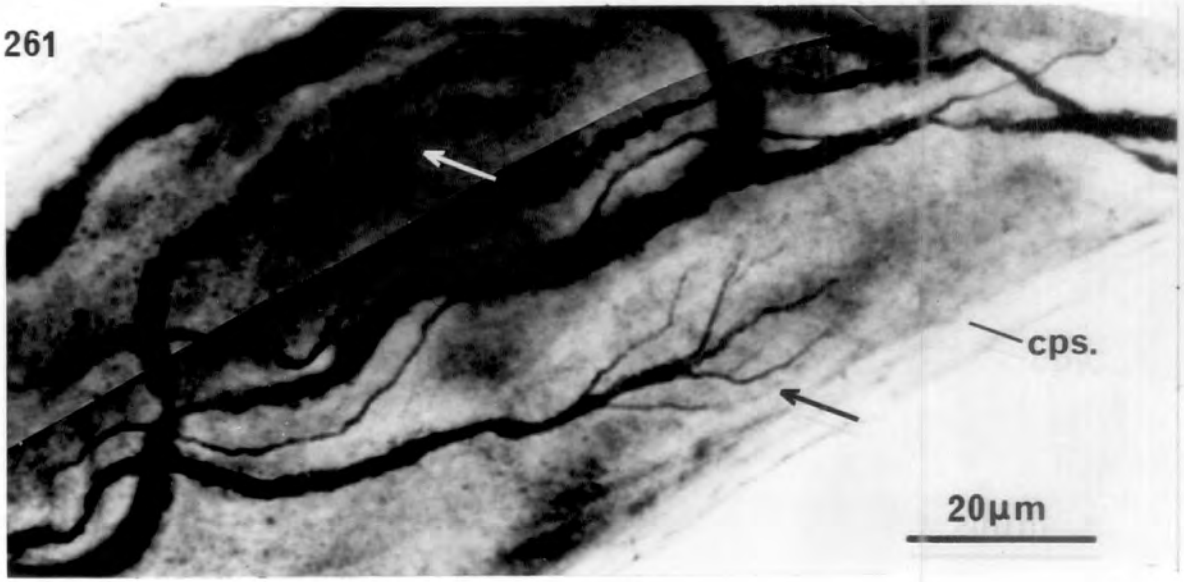
261
cps.
20µm


262
cps.

Figures 260 to 262. Photographs of teased, silver preparations of spindles from LP, illustrating plate endings.

Fig. 260. Photomicrograph montage of the juxta-equatorial region of a spindle showing a group of five plate endings. Two endings (white arrows) are derived from an axon that enters at the right of the figure, and three endings (black arrows) are derived from an axon that enters at the top left of the figure.

Figs. 261 - 262. Montages of the juxta-equatorial region of spindles showing examples of plate endings (arrows). cps., capsule.

All figures are the same magnification.

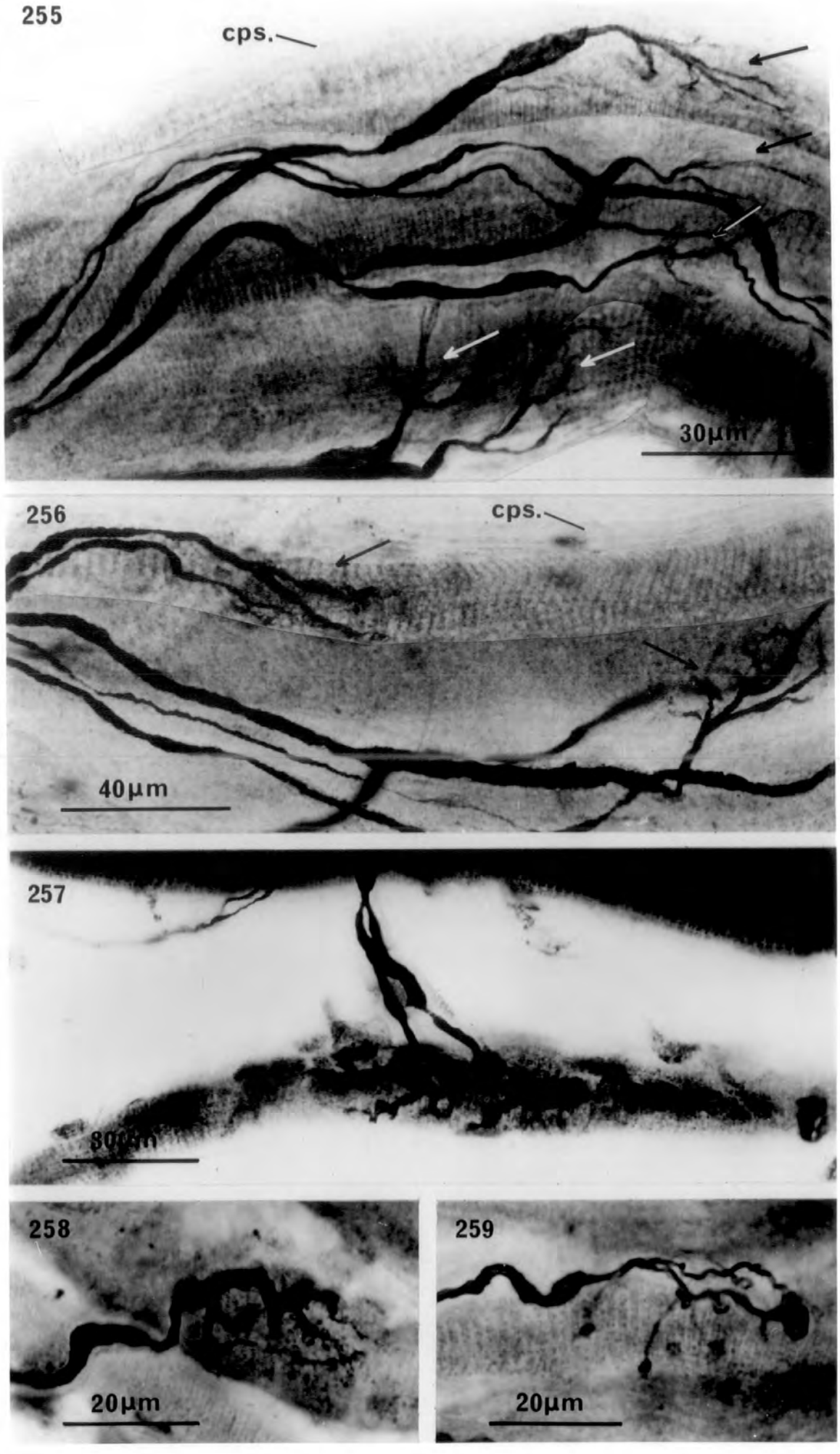
255
cps.
30µm
256
cps.
40µm
257
258
20µm
259
20µm

Figures 255 to 259. Photographs of teased, silver preparations of spindles from SR, illustrating plate endings.

Figs. 255 - 256. Photomicrograph montages of the juxta-equatorial region of spindles showing the "terminal innervation band" of plate endings (arrows) on chain fibres. cps., capsule.

In fig. 255 the three endings marked by black arrows are derived from a single axon that enters at the left of the figure. The other two plate endings (white arrows) are derived from a second axon.

In fig. 256 two plate endings (arrows) that occur at the same polar level are derived from a single axon that enters the spindle with the sensory supply at the equator.

Figs. 257 - 259. Single collateral plate endings on chain fibres in the mid-polar region of SR spindles.

Fig. 257. Surface view of a plate with a T_2 configuration.

Figs. 258 - 259. Surface views of collateral plates with T_1 configurations.